J. Condensed Matter Nucl. Sci. 5 (2011) 1–6

Research Article

Modification of Pd–H_2 and Pd–D_2 Thin Films Processed by He–Ne Laser

V. Nassisi*, G. Caretto and A. Lorusso

Laboratory of Applied Electronics, Department of Physics, I.N.F.N.,University of Lecce, Lecce-I, Italy

D. Manno, L. Famà, G. Buccolieri and A. Buccolieri

Department of Material Science, University of Lecce, Lecce-I, Italy

U. Mastromatteo

STMicroelectronics, via Tolomeo, 1 200010 Cornaredo, Milano-I, Italy

Abstract

In this work, we performed experiments of absorption of hydrogen and deuterium gas by Pd thin films, and we compared the behavior of these samples to unprocessed films. We also employed a continuous wave He–Ne laser to irradiate the samples inside the chamber during the treatment, in order to increase the gas absorption. Using a scanning electron microscope (SEM) and an electron probe micro-analyzer (EDX), we observed structures like spots on the surface of the treated samples. Inside the spots, elements other than Pd were found. Based on these results, we determined that gas loading is an effective way to transmute elements, and the laser action has been a very effective way to increase morphological changes in the treated samples.
© 2011 ISCMNS. All rights reserved.

Keywords: Cold fusion, Laser, Palladium thin film, Silicon, Transmutation

1. Introduction

In March 1989, Fleischmann and Pons [1] reported a large amount of excess enthalpy, and a weak level of radioactivity, from electrolytic cells with Pd cathodes during the electrolysis of D_2O. The effect only occurred when a critical threshold of the stoichiometric ratio $x = [D]/[Pd]$ of deuterium in palladium is achieved. The main point at issue was that the claimed excesses of enthalpy were consistent only with a nuclear process (deuterium fusion) and that such a process at ambient temperature and without the emission of a commensurate number of neutrons was considered to be inconsistent with modern nuclear science.

*E-mail: vincenzo.nassisi@le.infn.it, Tel.: +39-832-297495, Fax.: +39-832-297482

© 2011 ISCMNS. All rights reserved.

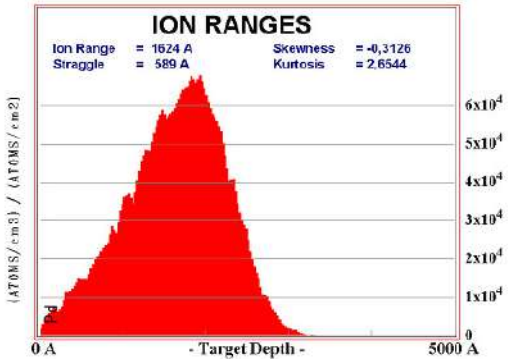

Figure 1. Boron ion distribution vs. target depth.

In the years following the announcement, many replications of excess heat and helium have been published [2,3], and many new methods to improve the stoichiometric ratio x have been studied [4]. Possible theoretical explanations of the reported phenomena were proposed [5,6] but they are still far from explaining all results.

Recently the gas loading method became a very effective tool to obtain high absorption of D or H gases inside Pd metallic lattice, while at the same time keeping the level of contamination low [7]. Important results were achieved by this method and particular attention has been paid to reproducing transmutation effects [8].

In this work, our attention was devoted to the transmutation phenomenon utilizing Pd film samples treated by gas loading. We also implanted B in these samples in order control the nuclear processes the way Iwamura et al. have done. The treatment of the samples was combined with a continuous wave He–Ne laser light to enhance gas loading inside Pd thin films, as in previous studies [9].

2. Experimental Set-up and Results

Using the thermal evaporation technique, we fabricated Pd thin films of 500 nm thickness deposited on Si wafers of about 1 cm^2 surface area. A 50 nm Ti layer was used to improve the adhesion between the substrate and the Pd layer.

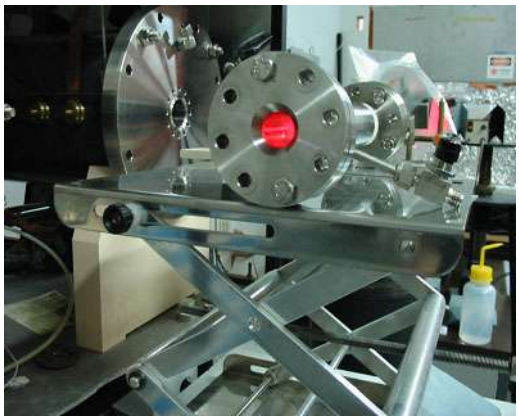

Figure 2. Photo of experimental set-up showing the irradiated chamber.

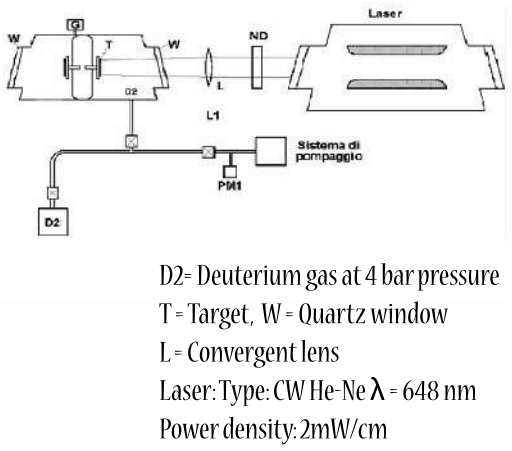

Figure 3. Schematic drawing of the experimental set-up. D_2: Deuterium gas at 4 bar pressure; T: Target; W: Quartz window; L:Convergent lens; Laser: CW He–Ne $\lambda = 648$ nm and Power density = 2 mW/cm^2.

These samples were implanted with B ions; a 150 keV accelerating voltage produced a maximum ion concentration at 158 nm depth in the palladium layer. Figure 1 shows the distribution of B ions versus target depth.

The thin film samples were placed in cylindrical stainless steel chambers of about 250 cm^3 in volume. Figure 2 shows a photo of the experimental set-up.

The chambers were equipped with at least one quartz window to allow the laser beam to irradiate the samples. To avoid contamination, the chambers were carefully cleaned with acetone and dried in nitrogen flux before the experiment. Subsequently a pair of Pd/Si samples has been placed inside the chambers filled with H_2 or D_2 gas to a maximum pressure of 4 bar. In Fig. 3, we have a schematic drawing of a chamber.

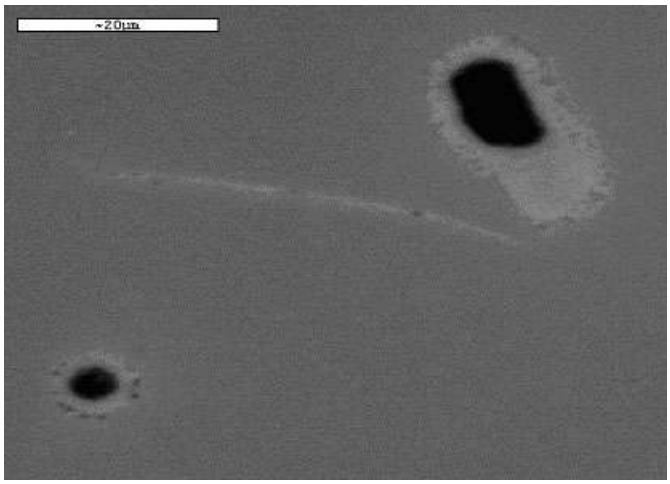

Figure 4. Spots on the surface of a sample with 76 days of treatment (by D_2 gas only).

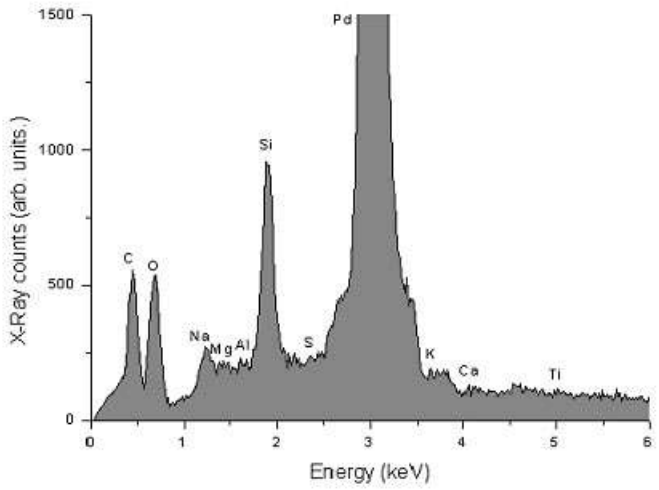

Figure 5. EDX spectrum of a sample with 76 days of treatment (by D_2 gas only). We can observe the presence of the following elements: C, O, Ca, Al, S, Mg, K, Na.

The samples were gas loaded, and one sample for each chamber was irradiated by a CW He–Ne laser ($\lambda = 648$ nm) from 16 July to 29 September 2004, at a laser power density of about 2 mW/cm^2.

After the treatment ending, the samples were analyzed by a Scanning Electron Microscope (SEM) and an EDX micro-analyzer. Different behaviors were revealed for samples kept in air, laser treated and without laser treatment. With the samples kept in air, the film surface was smooth, with a mirror-finish. The

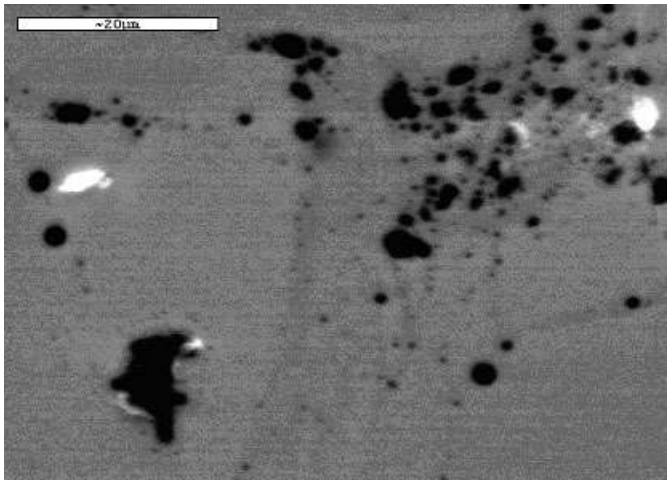

Figure 6. Spots on the surface of a sample with 76 days of treatment (by H_2 gas and by He–Ne laser action).

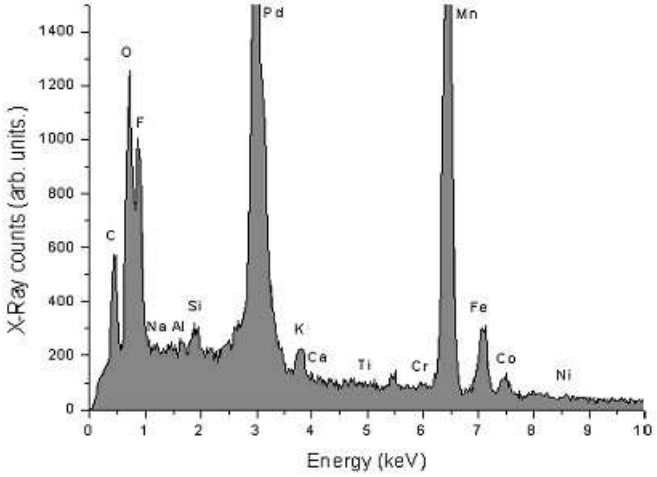

Figure 7. EDX spectrum of a sample with 76 days of treatment (by H_2 gas and He–Ne laser). We can observe the presence of the following elements: C, O, Ca, Fe, Al, S, Mg, K, Na, F, Cr, Mn, Co, Ni.

samples placed in deuterium gas but not treated with lasers showed morphological modifications of the Pd-film due to the gas absorption. Those treated with lasers showed even more morphological modifications. The modifications consisted of the formation of spots with dimension of 1–50 μm after gas loading. Figure 4 shows an example of spots on the surface of a sample of palladium implanted with boron, loaded by D_2 gas, but not laser irradiated.

Table 1. The principal detected elements in every experiment.

H_2		D_2	
Laser	No-laser	Laser	No-laser
Si	Si	Si	Si
Pd	Pd	Pd	Pd
Ti	Ti	Ti	Ti
C		C	C
O		O	O
Ca		Ca	Ca
K		K	K
Na		Na	Na
Al		Al	Al
Cr		Mg	Mg
Fe			S
CO			
Ni			
Mn			
S			
F			

By EDX analyser, we investigated inside the spots and found the presence of new elements such as C, O, Ca, Fe, Al, S, Mg, K and Na. In Fig. 5, an example of the EDX spectrum of a Pd sample with 76 days of treatment is shown. It is possible to observe the presence of many "new" elements which were not present before the treatment.

In addition, by He–Ne laser action, we found a larger number of spots and a larger number of new elements. Figure 6 shows a SEM micrograph of a sample processed by H_2 gas and laser; Fig. 7 shows EDX spectrum obtained from one spots of the sample: the new elements were: C, O, Ca, Fe, Al, S, Mg, K, Na, F, Cr, Mn, Fe, Co, and Ni.

Table 1 shows the new elements reported in the experiments. We observe that the combination between H_2 gas loading and laser action on the treatment of the samples is an effective method of producing many transmutation elements. The results with D_2 gas loading alone, without laser irradiation, also produce new elements, and there are no evident differences between the number and type of elements produced with and without the laser. The laser action increases the spot density on the surface of the treated samples, but it does not change the nature of the reaction. All new elements were found inside the spots. None of them seems to be generated from a particular nuclear reaction between B and D_2 and H_2. These experiments confirm the reproducibility of the transmutation phenomenon but we are still far from clarifying the mechanism inside the crystalline lattice of Pd samples that causes the transmutations.

References

[1] M. Fleischmann, S.J. Pons, *J. Electroanal. Chem.* **261** (1989) 301.
[2] A.B. Karabut, *ICCF9*, Beijing, China, May 19–24, 151 (2002).
[3] F. Celani, A. Spallone, P. Tripodi, A. Petrocchi, D.Di Gioacchino, P. Marini, V. Di Stefano, S. Pace, A. Mancini, *Phys. Lett.* A **214** (1996) 1.
[4] A. De Ninno, A. La Barbera, V. Violante, *Phys. Rev.* B **56** (1997) 2417.
[5] M. Fleischmann, S. Pons, G. Preparata, *Nuovo Cimento* A **105** (1992) 763.
[6] A. Takahashi, *ICCF9*, Beijing, China, May 19–24, 343 (2002).
[7] F. Scaramuzzi, Survey of Gas Loading Experiments, in Second Annual Conference on Cold Fusion, The Science of Cold Fusion, Como, Italy, 1991.
[8] Y. Iwamura, T. Itoh, M. Sakano, S. Sakai, S. Kuribayashi, *ICCF-10*, Cambridge, MA, Aug. 24–29, 68 (2003).
[9] V. Nassisi, *Fusion Technol.* **33** (1998) 468.

J. Condensed Matter Nucl. Sci. 5 (2011) 7–16

Research Article

Study on the Phenomenon Reported "Neutron Generation at Room Temperature in a Cylinder Packed with Titanium Shavings and Pressurized Deuterium Gas"

Takayoshi Asami *

Research Institute of Innovative Technology for the Earth (retired), 9-2 Kizugawadai, Kizu-cho, Soraku-gun, Kyoto 619-0292, Japan

Abstract

This paper describes the analysis and study of the neutron generation experiment performed under pressurized and/or evacuated conditions between room temperature and liquid nitrogen temperature, using titanium shavings and deuterium gas packed in a cylinder. To clarify the mechanism of this phenomenon, the author has studied the experiment taking into account the characteristics of the phase equilibrium, the metal crystal construction, the theory of chemical bond and the first principle molecular orbital calculation. From the result of this study, it seems that the same phenomenon will happen in a similar experiment performed using another electron deficient metal with a suitable crystal construction.
© 2011 ISCMNS. All rights reserved.

Keywords: Crystal lattice, Deuterium, Neutron generation, Octahedron cage, Tetrahedoron cage, Titanium

1. Introduction

There are many reports on deuterium nuclear fusion at room temperature. However, some of them have not had sufficient plausible evidence to prove them and the others are doubtful.

Out of these reports, the experiments performed by ENEA, etc. appear to have been performed by suitable devices and measurement methods [1–3]. Although it is preferable that more reproducible experiments will be executed, we cannot deny the experimental results. It seems that they achieved neutron generation using titanium shavings and deuterium, which is performed in a process similar to that of deuterium adsorption and desorption.

The author has intended to study the behavior of deuterium in each process of the experiment, and has studied the conditions for deuterium atoms or deuterons to collide and the possibility of nuclear fusion occurring at room temperature, applying both the theory of chemical bond and the first principle molecular orbital calculation.

*E-mail: takaysami@yahoo.co.jp

© 2011 ISCMNS. All rights reserved.

2. The Main Process, the Conditions of the Experiment and Explanation of Each Step

According to the experiment performed by ENEA [1] and LANL [2], neutrons are generated during the course of warming the cylinder containing pressurized deuterium and titanium shavings with adsorbed and/or combined deuterium, and at the condition of nonequiliblium such as a change of particular temperature and pressure in the process of adsorption/desorption of deuterium in titanium.

The main process of the experiment and the conditions of the experiment are as follows:

Step 1: It is the generation process of the combined material of titanium and deuterium (from here on we will call it "combined material") by adsorption, etc., under the pressurized condition in the cylinder made of stainless steel. Pressure: 2–5 MPa, Temperature: room temperature

Step 2: It is the process of the cooling of the cylinder (Ca. 80 K) in the liquid nitrogen bath.

Step 3: It is the process of removing the cylinder from the liquid nitrogen bath and leaving the cylinder to warm until it reaches room temperature (we assume it is Ca. 300 K).

3. Generally Predictable Behavior of Deuterium Inside and/or on the Titanium Shavings in Each Step

In Step 1, deuterium will enter and subsequently diffuse throughout the crystal lattice of titanium metal, forming the combined material.

According to other experiments dealing with the characteristics of adsorption and desorption, the deuterium behavior in this process is similar to the graphical curve of pressure-composition isotherm adsorption with the parameter, temperature. In particular, it is similar to the characteristics of substances that also show hysteresis as shown in Fig. 1 [4].

The type of titanium crystal has a hexagonal close-packed (hcp) structure. It is said that there are three locations, where deuterium atoms or deuterons are able to be located in titanium crystal. The locations where deuterium atoms are able to locate under the suitable condition are in the tetrahedral interstice (T-site), in the octahedral interstice (O-site) formed by titanium atoms, and in the location between two titanium atoms in the c-axes of the crystal in Fig. 2 [5].

Figure 2 simply shows the structure of titanium crystal lattice and the inferred location of deuterium.

In Step 2 (the cooling of the cylinder) the saturated region of deuterium in titanium metal that expresses the length of the plateau region in the phase diagram indicated in Fig. 1, will become greater than that of room temperature, by the formation of combined material. In this step, it seems that deuterium atoms will go further into the titanium and diffuse into the lattice of titanium metal.

In Step 3, because of the temperature rise, in accordance with the characteristics of phase equilibrium, some portion of the deuterium must exit from the constrained state in titanium and the length of the plateau region in the phase diagram becomes less than that at liquid nitrogen temperature. It indicates that some portion of deuterium in the combined material is released to the gaseous phase over the course of the temperature rise, relating to adsorption phase change as written standard book.

When we compare the strength of constrained deuterium in T-site and O-site and deuterium in another site, it appears that trapping potential depth in the different sites differs with each other because the combined condition with titanium atoms differs.

According to the experimental results [1,2], it is said that substantial bursts of neutron counts (Ca. 70 and Ca. 100, respectively) were observed after the cylinder was removed from the liquid nitrogen bath. In the one experiment, it says that the average count in the active period run (at desorption phase from liquid nitrogen temperature warming to room temperature) was much higher than the previous run (at pressurized condition with thawing terms and cooling cycles). In the other experiment, the pressurized cylinder had to experience several thermal cycles before neutrons were

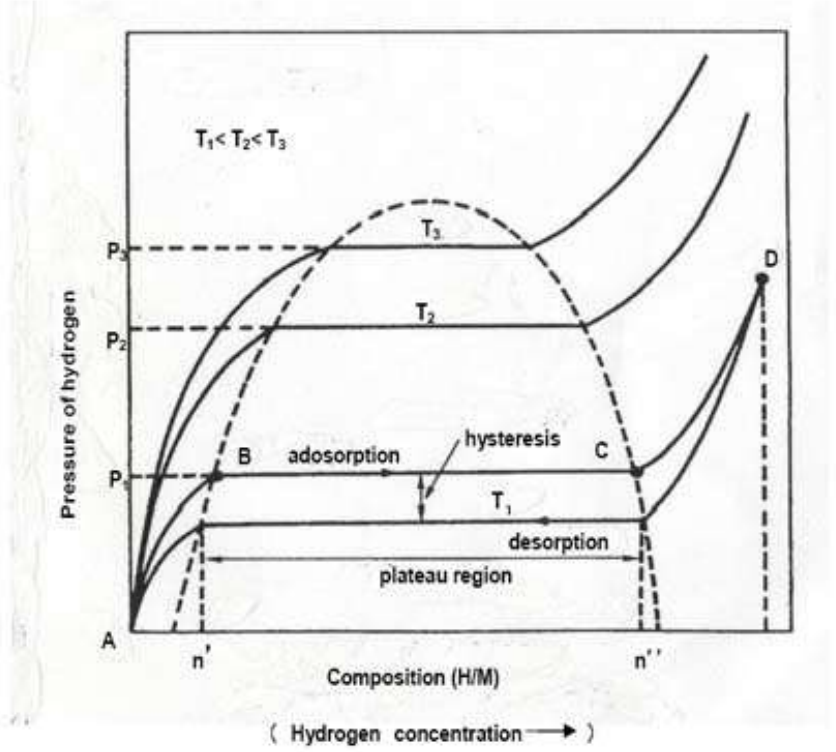

Figure 1. Pressure-composition isotherm adsorption with the parameter, temperature [4].

detected. About 1 h into the warm up cycle, when the pressurized cylinder was at –30°C, high neutron counts (∼85) were observed, followed by smaller bursts.

It is inferred that any reaction must occur in a condition of nonequilibrium, such as a change of pressure and/or temperature.

4. The State and Behavior of Deuterium Atoms in Titanium Crystal

4.1. Analysis of the state of deuterium atoms in titanium crystal based on the theory of chemical bond

4.1.1. *Bonding state of the deuterium atoms and the titanium atoms in the tetrahedron cage*

In the following, the author will study the mechanism of the bonding of deuterium atoms with titanium atoms in accordance with the theory of chemical bond, taking into account the electron orbits of titanium.

The reason why the deuterium atoms are stable in that location must be because they combine with the titanium atoms by a specified chemical bond. As an example of an electron-deficient substance, when boron forms diborane (B_2H_6), the boron atoms cause adjacent hydrogen atoms to have ligancy (number of stable positions (potential well) for H(D)) 2 as indicated in Fig. 3 [6,7].

It seems that a deuterium atom and the titanium atoms jointly own the valence electron located outside the argon shell in the electron orbits of the titanium atom; the deuterium atom and titanium atoms form a coordinate bond. In the

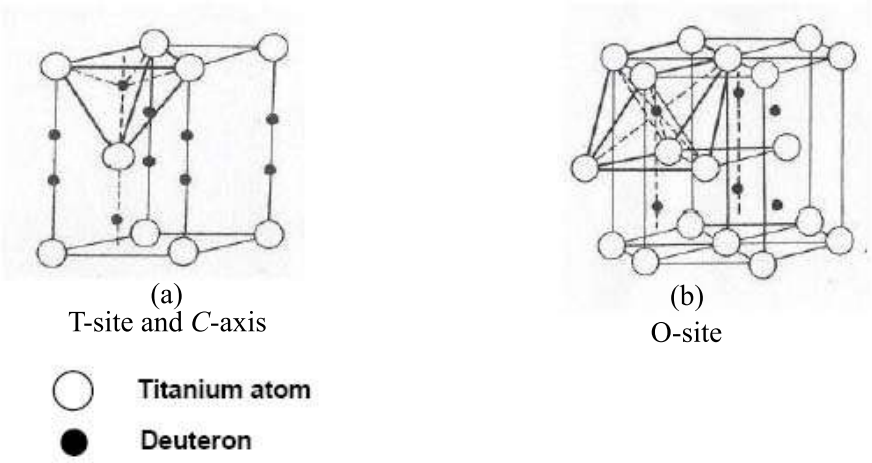

Figure 2. The location of deuterons in the titanium crystal lattice [5].

following, we will study why this combination is formed.

By the same process as the formation of diborane, it seems that the titanium atoms forming the cage can also cause the entering deuterium atom to have ligancy 2. The reason why it is deemed so is because the electron orbits and their respective number of electrons regarding a titanium and argon atom are as follows:

Titanium: $(1s^2\ 2s^2\ 2p^6\ 3s^2\ 3p^6)\ 3d^2\ 4s^2$

Argon: $(1s^2\ 2s^2\ 2p^6\ 3s^2\ 3p^6)$

According to the theory of chemical bond explained by Pauling [8], there are nine stable orbits, $3d^5 4s 4p^3$, outside this shell. Even if these nine orbits are occupied by nine electrons, 0.72 is allocated as metallic orbit, leaving 8.28 for occupancy by bonding electrons and unshared electron pairs.

On the other hand, the titanium atom has four electrons outside the saturated orbits (argon shell). As compared to the number of electrons, four, in the part of the titanium electron orbits outside the argon shell and nine, the total

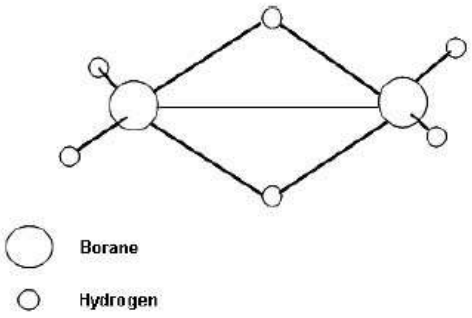

Figure 3. The configuration of atoms in diborane, $B_2\ H_6$ [6, 7].

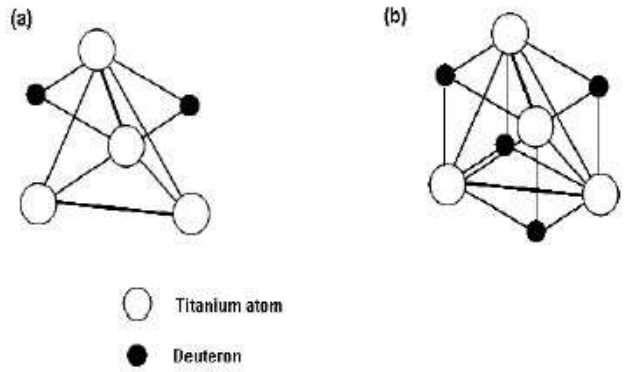

Figure 4. Ti cage models with two bridged deuterium atoms.

number of electrons outside the argon shell is far less than the preferred number of electrons to be stable, which is nine.

As a result, it seems that the electrons left from the deuterium atoms that entered the titanium metal will move toward the titanium orbits side. On the other hand, to get to a stable condition, deuterons will have a tendency to jointly own the electron with the titanium atoms.

As an example of diborane, Ti atom also is electron-deficient substance. So we can easily guess Ti atoms cause two deuterium atoms to have ligancy 2 as in the case of diborane. So it seems the adsorbed two deuterium atoms will also form ligancy 2. In this condition, it seems that two Ti atoms will prepare two bridged deuterium atoms indicated in Fig. 4a. If two orthogonal pairs of two Ti atoms in the T-site will prepare two bridged deuterium atoms per each Ti pair, the classical model will be indicated as in Fig. 4b.

This form is equivalent to the Tetrahedral Symmetric Condensate (TSC) model which is presented by Takahashi [9]. It seems that four electrons that have left from each deuterium atom may form bosonized pair [9] in the outer orbit of each Ti atom forming two orthogonal edges of the tetrahedron cage of which the edge is composed of two Ti atoms. According to hypothesis of Takahashi, it says that strong central squeezing force may happen by TSC plus four spin-regulated (bosonized) electrons. However, the author's model is a form of combined material produced just after deuterium atoms entered into Ti crystal. On the other hand, Takahashi's model is the form with very short life assuming when the reaction happens in transient state under the special condition. So, the author thinks that his model is different from the author's model, and is a model which is a work in progress.

4.1.2. *Geometrical relation of the deuterium atoms in the tetrahedron cage*

In the case of titanium, its crystal is in the form of a hcp structure including cages as mentioned above.

Assuming that one of the cages is a regular tetrahedron and the titanium atoms are sphere like shape, the diameter of the inscribed sphere, between the three spheres of titanium atoms and within the regular triangular surface formed by the centers of three titanium atoms, is approximately 0.502 Å indicated in Fig. 5a. As the diameter of a deuterium atom is approximately 1.06 Å, if the deuterium atom intends to enter the tetrahedron cage, it must not be as a deuterium atom (D) but as a deuteron (d) having lost an electron. In the case of deuterons, it seems that each of them will be able to pass through the inlet of the cage provided that Coulomb repulsion is shielded, as its diameter is approximately 10^{-4} Å.

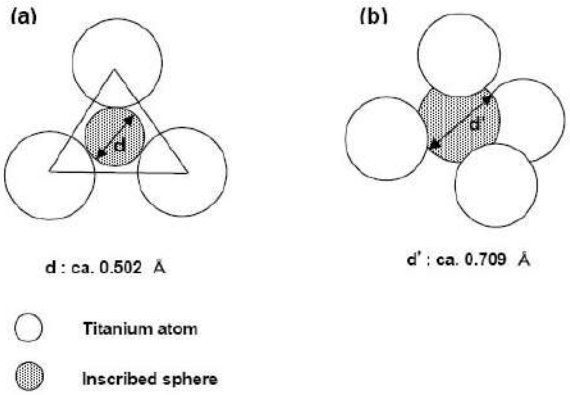

Figure 5. Conceptual figure of the tetrahedron cage in titanium crystal. (a) and (b): the diameter of the inscribed sphere.

4.1.3. *Deuterons able to exist in the tetrahedron cage*

Inside of the tetrahedron cage, the diameter of the inscribed sphere is approximately 0.709 Å indicated in Fig. 5b. So the distance from the center of this inscribed sphere to the center of the titanium atom is approximately 1.81 Å. On the other hand, using the average covalent radius of hydrogen, 0.3 Å [10], the estimated Ti–D distance is approximately 1.78 Å, assuming that both Ti–D and Ti–H distances are equal. Regarding the bridged Ti–D(-Ti) distance, it may slightly be longer than that of a single bond of Ti–D which is similar to the example of the distance of B–H (Ca. 1.19 Å) and bridged B–H(-B) (Ca. 1.33 Å) of diborane [6]. Anyhow, the estimated Ti–D distance coincides well with the distance from the center of the inscribed sphere to the center of the contacting spheres, Ti atoms.

4.1.4. *Plausible behavior and possibility of collision of deuterons in the tetrahedron cage*

As it is said, in the case of the tetrahedron cage, the location where a deuterium atom or deuteron is able to locate is in the cage.

As previously mentioned, we can infer that combined material as indicated in Fig. 4 will be formed. After that, as there is a stable location in the cage, it seems that the deuterium atom or deuteron in the state may intend to get to the stable location as indicated in Fig. 6 if the condition of nonequilibrium state occurs, such as changing of deuterium

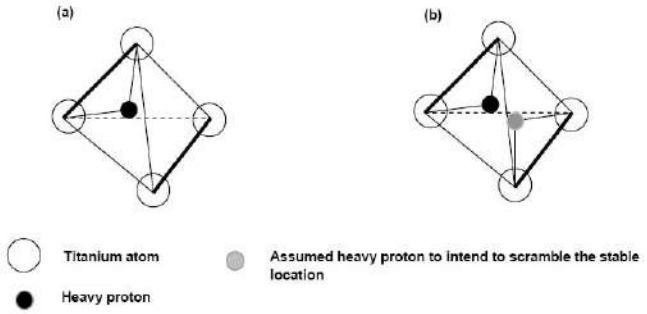

Figure 6. Ti cage models with the bridged deuterium atom in the T-site.

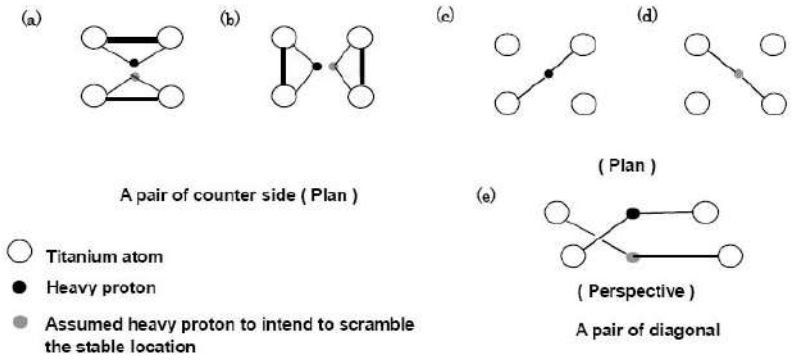

Figure 7. The heavy protons model in the O-site. (a), (b): a pair of counter side (plan), and (c), (d): a pair of diagonal side (plan), (e): a pair of diagonal side (perspective).

pressure and/or temperature in the cylinder.

If plural deuterium atoms or deuterons will enter the cage, collision may occur in the cage.

The constrained two deuterium atoms at the edge of the cage without a strong Coulomb repulsion by the bridging bond of ligancy 2 are electrically neutral. It may be that under this condition, deuterons do not need an enormous amount of energy to collide.

If we estimate the kinetic energy of a free deuterium atom at 80 and 300 K, the energy of each is 6.9 and 25.9 meV, respectively.

4.1.5. *The state of the deuterium atoms combined with the octahedron cage formed by titanium atoms*

As in the case of the tetrahedron cage, it is said that there is a location where a deuterium atom or a deuteron is able to locate in the octahedron cage.

If we take out a quadrilateral pyramid cross section from the octahedron cage that is formed by titanium atoms, and set our eyes to the square part composed of two titanium atoms and a summit atom, both the diameters of the inscribed sphere within the top half pyramid and the inscribed sphere within the square cross section are Ca. 1.27 Å. So if the deuterium or deuteron is located in these locations of O-site, there is more space than in that of the T-site. As it is said, if the heavy proton is located in the center of the O-site, the location is that of the latter of the case mentioned above. In this cross section of the square area formed by four titanium atoms, two titanium atoms must be selected to get to the stable condition of deuterium atoms by forming the bridging bond of ligancy 2. Geometrically, there is a total of six possible independent Ti pairs of chemical combinations with a bridged deuterium atom in this part. These pairs are selected from the side parts and diagonal line parts in the square which is formed by Ti atoms indicated in Fig. 7.

If we assume the two heavy protons are constrained by two diagonally opposite titanium atom pairs indicated in Fig. 7c–e, both heavy protons in the cage will be localized along the centerline of the square, and move near the center point of the square. If the collision of caged heavy protons occurs, chances are that it will occur by the heavy protons constrained by two diagonally opposite titanium atom pairs of the different diagonal. However, the length of the diagonal is Ca. 4.18 Å and it is slightly longer than two times the estimated Ti–d distance, 3.56Å.

It seems that it is difficult to more precisely estimate the condition for the deuterium to locate by only the theory of chemical bond.

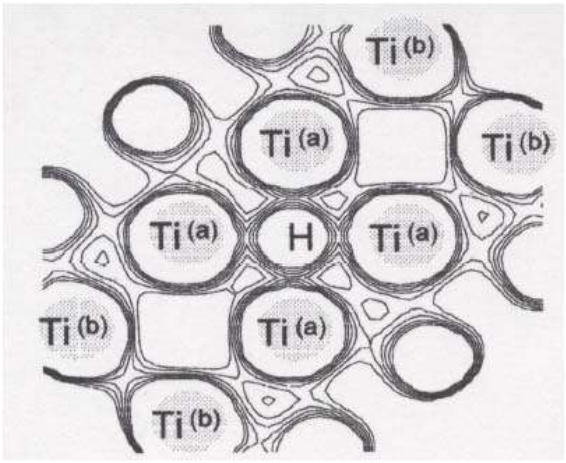

Figure 8. The distribution of charge density for (2–203) plane of Ti H3 (7.69 at.% H) cluster [11].

4.1.6. *The state of the deuterium atoms on the c-axis of titanium crystal*

The *c*-axis length of titanium crystal is Ca. 4.74 Å and it is said that two deuterium atoms can be located on the *c*-axis between titanium atoms [5]. The nearest titanium atom from the deuterium atom is at the end of this axis. If a deuterium atom combines with a titanium atom, it will be the titanium atom located at the end of the *c*-axis. Under this condition, we cannot find special condition for deuterium atoms to collide.

4.2. Analysis based on the first principle molecular orbital calculation

At present, there are not only the analysis based on the theory of chemical bond but on the first principles calculations. By comparison an analysis basing on a different stand point, it seems that we will be able to deduce a more precise state of deuterium in titanium crystal.

As there is the research of electronic structure of the Ti–H solid solution by a first principle molecular orbital calculation, the author cites in Figs. 8 and 9 [11]. Figure 8 shows the distribution of charge density around a hydrogen atom on Ti–H solid solution cluster.

Essentially, both the distance and the bonding force between Ti atom and H atom in the symmetrical location can be the same as each other. The bond between the second nearest Ti atoms ($Ti^{(b)}$) from the H atom in the center is strongly formed with each other. However, there is clear difference in the bond between the first nearest Ti atoms ($Ti^{(a)}$) and $Ti^{(b)}$. In diagonally face side Ti atom pairs surrounding H atom, there is a slight difference in the distribution of charge density between vertical and horizontal bonds of Ti and H atom in Fig. 8. It seems that there is a possibility the horizontal 2 face side Ti atoms pair may cause the hydrogen to have ligancy 2, although, of course, the resonance will occur between these pairs .

Figure 9 [11] shows the density of states of solid solution. In Fig. 9, density of state of 3d orbital of titanium decreases with increasing of hydrogen content and that of 4s orbital of titanium also slightly decreases with increasing of hydrogen content. It means that the electrons of 3d orbital of metallic bond is used for bonding between Ti atoms and the hydrogen atom.

In a regular octahedron cage, each orthogonal plane including the center line and the diagonal line of the square to (2–203) plane also has two diagonally face side Ti atom pairs. So it means that another Ti pair in the other planes

can cause hydrogen to have ligancy 2 if there is a hydrogen atom between them. On the other hand, there is only one location where H is stable is in the octahedron cage.

So, in a condition of nonequilibrium state inside and/or outside Ti metal, such as changing deuterium pressure and/or temperature, if deuterium atoms or deuterons scramble the location of each other, collision may occur near the center of octahedron cage.

As another inference of this analysis, in Ti metal composed of dense crystal, it seems that it may be difficult for two deuterium atoms in ligancy 2 to exist as indicated in Fig. 4. except Ti atom pair at cleavage plane and/or metal surface.

In other chance, the author would like to also analyze the tetrahedron cage, from both the theory of chemical bond and the first principles calculations.

5. Discussion and Conclusion

To clarify the mechanism of neutron generation experiment, the author analyzed the site and state of adsorbed deuterium into titanium metal, basing on both the theory of chemical bond and the first principle molecular orbital calculation.

As a result, it seems that the titanium atoms forming the cage cause the deuterium atom to have ligancy 2, especially at diagonally 2 face side Ti atoms in octahedron cage, from both the theory of chemical bond and the first principle molecular orbital calculation.

If two bridged deuterium atoms combine with two Ti atoms as "combined material", as same as that of diborane and bosonized electrons are produced in the orthogonal Ti pairs of the tetrahedron cage, its form is equivalent to TSC form presented by Takahashi. However, their images of each concept are different from each other.

On the other hand, taking into account of the result of the first principle molecular orbital calculation, it seems that the driving force for deuterium to collide may be scrambling force to get to the stable location by the deuterium atoms between different diagonally two face side Ti atom pairs in the octahedron cage. This situation may occur in a condition of nonequilibrium state, such as the change of temperature and/or pressure.

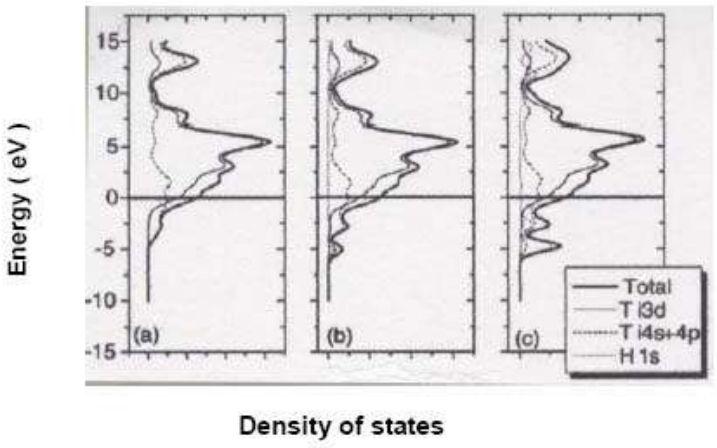

Figure 9. Density of states from (a) Ti, (b) TiH1 (2.70 at.% H), and (c) TiH2 (5.26 at.% H) cluster [11].

If the above-mentioned concept on the room temperature nuclear fusion is right, the observed phenomenon may also occur in an experiment under the condition of nonequilibrium state, such as changing pressure and/or temperature even with another element which is electron deficient, has suitable crystal construction and adsorbs the deuterium.

Acknowledgement

The author wishes to express sincere thanks to Dr. Takahashi, emeritus Professor of Osaka University, for the valuable suggestions and discussions on the manuscript.

References

[1] A. De Ninno, A. Frattolillo, G. Lollobattista, L. Martinis, M. Martone, L. Mori, S. Podda, F. Scaramuzzi, Evidence of emission of neutrons from a titanium–deuterium system, *Europhys. Let.* **9** (1) (1989) 221, ENEA, Dipartimento TIB, U.S. Fisica Applicata, Centro Ricerche Energia Frascati, C.P. 65-00044 Frascati, Rome, Italy, 1 May, 1989.

[2] H.O. Menlove, M.M. Fowler, E. Garcia, A. Mayer, M.C. Miller, R.R. Ryan (Los Alamos National Laboratory), S.E. Jones (Bringham Young University), Highlights of papers presented at the workshop on cold fusion phenomena , *The Measurement of Neutron Emissions from Ti plus D_2 Gas"*, Santa Fe, New Mexico, May 23–25, pp. 13, 1989.

[3] A. De Ninno, F. Scaramuzzi, ENEA- Area Energia e Innovazione, Dip. Sviluppo Tecnologie di Punta, Centro Ricerche Energia Frascati, CP 65, I-00044 Frascati, Italy, *AIP Conference Proceedings*, Vol. 228, Anomalous Nucear Effects in Deuterium/Solid Systems, PROVO, UT 1990, Emission of Neutron Bursts from a Titanium–deuterium Gas System in a High-efficiency Low-background Eeperimental Setup, p. 122.

[4] Y. Ohsumi, *Hydrogen Adsorption Alloy (Suiso Kyuzo Gokin)*, Chapter 2 (Agune Gijutu Senta Corp. Ltd., Tokyo, 2000), p. 33.

[5] Y. Hukai, *Bull. Japan Inst. Metals* **24** (8) (1985) 671.

[6] L. Pauling, The nature of the chemical bond and the structure of molecules and crystals, *An Introduction to Modern Structural Chemistry,* 3rd edn., Cornell University Press, Ithaca, NY, 1960, p. 368.

[7] L. Pauling, The nature of the chemical bond and the structure of molecules and crystals, *An Introduction to Modern Structural Chemistry*, 3rd edn., Cornell University Press, Ithaca, NY, 1960, p. 363.

[8] L. Pauling, The nature of the chemical bond and the structure of molecules and crystals, *An Introduction to Modern Structural Chemistry*, 3rd edn., Cornell University Press, Ithaca, NY, 1960, pp. 398–401.

[9] A. Takahashi, N. Yabuuchi, On condensation force of TSC, *J. Condensed Matter Nucl. Sci.* **1** (2007) 97–105.

[10] L. Pauling, The nature of the chemical bond and the structure of molecules and crystals, *An Introduction to Modern Structural Chemistry*, 3rd edn., Cornell University Press, Ithaca, NY, 1960, p. 227.

[11] D. Setoyama, J. Matsunaga, H. Muta, M. Uno, S. Yamanaka, *J. Alloys and Compounds* **385** (2004) 156–159.

J. Condensed Matter Nucl. Sci. 5 (2011) 17–33

Research Article

Role of PdO Surface-coating in CMNE D(H)-Gas Loading Experiments *

A.Takahashi,† R. Seto and Y. Fujita

Technova Inc., 1-1-1 Uchisaiwai-cho, Chiyodaku, Tokyo 1000011, Japan

A. Kitamura, Y. Sasaki, Y. Miyoshi and A. Taniike

Graduate School of Maritime Sciences, Kobe University, 5-1-1 Fukaeminami-machi, Higashinada-ku, Kobe 6580022, Japan

Abstract

The PdO-coated layer of Pd-nano-particle may arrange fractal nano-dips on its surface when D(H)-gas is charged and de-oxidation molecules (D_2O or H_2O) are released. Fractal nano-dips may make local deep adsorption potentials, through which rapid penetration of D-atoms (ions) into deeper Pd-local lattice (Bloch potential) O-sites of nano-particle may be induced, to realize full or over-full D(H) loaded state ($x > 1.0$) of PdDx in a short time of the Phase-I process. Formation of D-clusters, such as 4D/TSC on surface may be enhanced at nano-dips. A phenomenological model of quasi-free D-motion under constraint of the Bloch potential within a global mesoscopic potential well is proposed for the Phase-II phenomena, where nuclear heating by 4D fusion reactions may rather steadily take place. Generation of collective mesoscopic potential well (CMPW) will make a Pd nano-particle with PdO working as "mesoscopic catalyst" which realizes very large D(H)-loading ratios and anomalously large chemical heat releases both for H-gas and D-gas loading.
© 2011 ISCMNS. All rights reserved.

Keywords: Anomalous heat, Collective mesoscopic potential, D-gas loading, Mesoscopic catalyst, Over-full D/Pd loading, Pd nano-particle, Phenomenological model, Role of PdO, Sub-nano dip

1. Introduction

We of the Kobe Group have reported newer results on anomalous D(H) absorption and excess heat by nano-Pd/Metal-Oxide dispersed samples in the JCF10 meeting 1,2 , 5–6 March 2010, Tokyo, and also in the ACS-2010 NET Symposium7, 21–22 March 2010, San Francisco.

*Note: This paper is submittal to the 9th International Workshop on Anomalies in Hydrogen/Deuterium Gas Loaded Metals, 17–19 September 2010, Siena, Italy.

†E-mail: akito@sutv.zaq.ne.jp

© 2011 ISCMNS. All rights reserved.

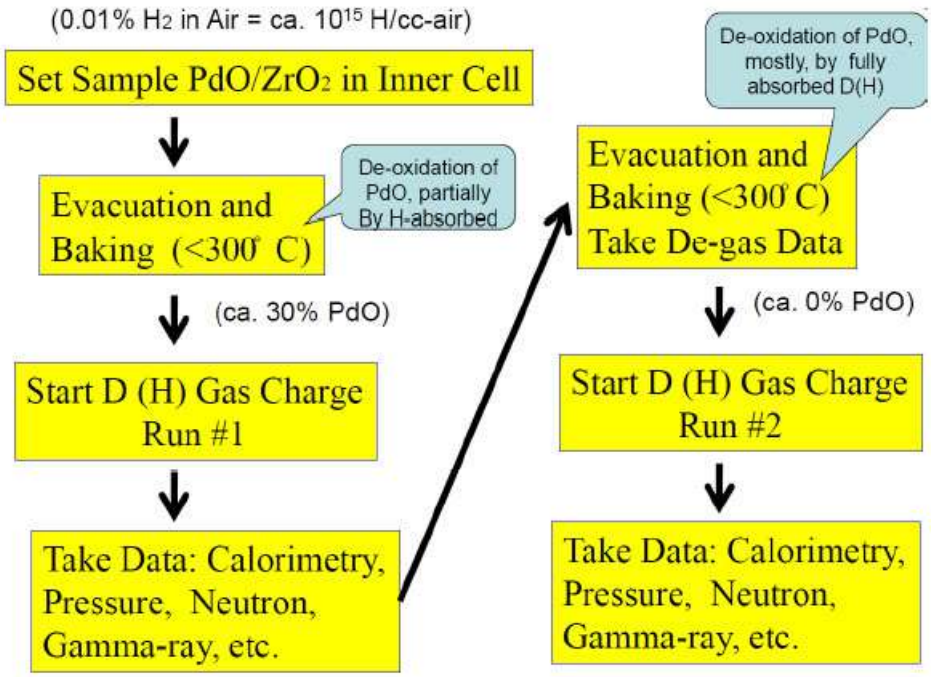

Figure 1. Experimental procedure of D(H)-gas charging to Pd/ZrO_2 powder samples and reduction of PdO.

Two new findings were reported there: (1) Forced oxidation of used Pd/ZrO_2 samples showed remarkable recovery effects on D(H)-loading ratios and heat release rates in the Phase-I interval of D(H)-charging experiments. (2) By time-resolved (time-dependent) measurements of D(H)-loading ratios, we have found the "new second phase" after the Phase-I. At the end of Phase-I, D(H)/Pd ratios became 1.1–1.2 with integrated specific heat-energy 0.83–2.0 eV/atom-Pd. At the end of new second phase (Phase-II) with slower change of D(H)-absorption, additional low level heats were recorded. The third phase (Phase-III) was redefined for the time-period after D(H)/Pd ratios were saturated in Phase-II. We discuss on what kind of underlying physics is there, by proposing a phenomenological model which may relates to the TSC theory [3–5], for the emerging condensed matter nuclear effects (CMNE).

Reduction process of PdO in samples under D(H) charging is first discussed briefly in this paper. Secondly and mainly, the role of PdO surface coating of Pd nano-particle is discussed using a phenomenological (speculative) model on what happens under D(H) charging to induce a mesoscopic catalyst potential and the D-cluster formation and 4D/TSC fusion. We summarize discussions as;

(1) The de-oxidation of PdO may be made mostly during the baking processes between D(H)-loading runs, because of high level D(H)-density under degassing process at relatively high (473 K) temperature which may enhance D_2O (H_2O) chemical formation.
(2) The PdO-coated layer of Pd-nano-particle may arrange fractal sub-nano-dips (sub-nano-holes; SNH) on its

surface when D(H)-gas is charged and de-oxidation molecules (D_2O or H_2O) are released to vacuum.

(3) Fractal sub-nano-dips may make local deep adsorption potentials, through which rapid penetration of D-atoms (ions) into deeper Pd-local lattice (Bloch potential) O-sites of nano-particle may be induced, to realize full or over-full D(H) loaded state ($x > 1.0$) of PdDx in a short time of the Phase-I process.

(4) Formation of D-clusters, such as predicted by the TSC theory [3–5] on surface may be enhanced at sub-nano-dips already in the beginning of Phase-I D(H)-loading process and 4D/TSC fusion may take place with considerable probability.

(5) D-motion in a "mesoscopic deep collective potential" of the nano-PdDx system may be quasi-free to enhance transient D-cluster (4D/TSC [3–5]) formation probability around tetrahedral sites of local Bloch (periodical-lattice) potential inside a PdD nano-particle. This state can be modeled by the non-linear combination of two oscillations, i.e., one (longer pendulum in approximation) by the deep (about 1.5 eV deep) well-type collective potential and the other (shorter pendulum) by the lattice-type periodical three dimensional Bloch potential (about 0.22 eV deep). The shorter pendulum may have "high excited energy" to realize very mobile D-motion under the constraint of three-dimensional local PdD lattice arrangement, within the mesoscopic global deep potential well.

(6) Generation of collective mesoscopic potential well (CMPW) will make a Pd nano-particle working as "meso-

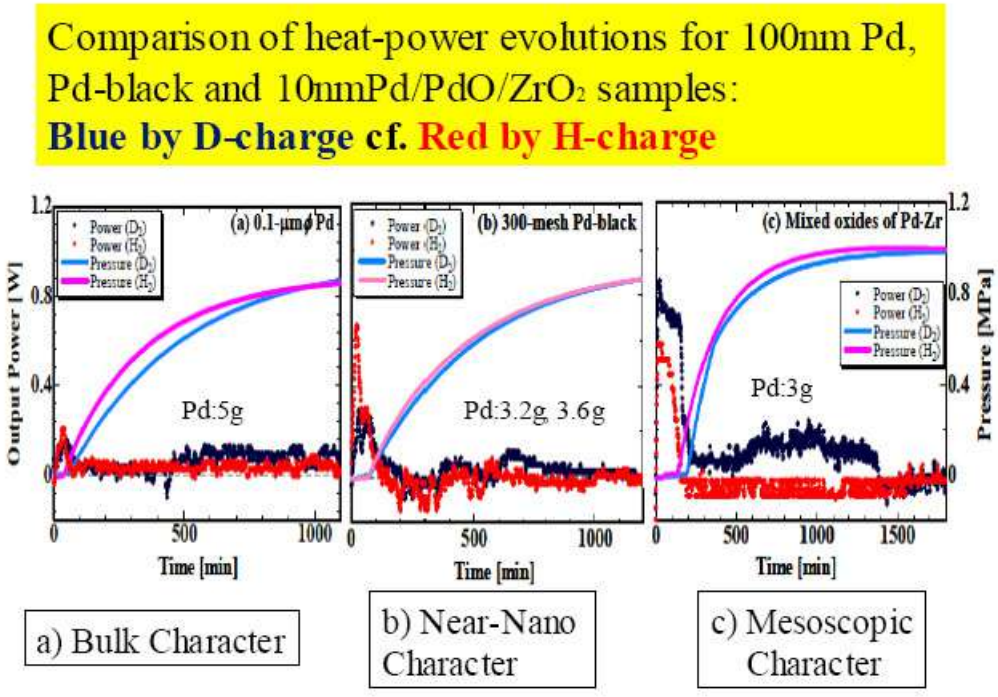

Figure 2. Comparison of typical heat evolution data for PP (0.1 μm diam. Pd powder), PB (300 mesh Pd-black powder) and PZ(10 nm-Pd-nano-powder dispersed in ZrO_2 flakes).

scopic catalyst" which realizes very large D(H)-loading ratios and anomalously large chemical heat releases both for H-gas and D-gas loading.

2. Formation and Reduction of PdO Surface Layer of Pd-nano-particles

Virgin samples of Pd/ZrO_2 (PZ in abbreviation) as provided from the maker (Santoku Co., Kobe, Japan) contained oxygen in the form of PdO/ZrO_2 with 100% PdO and ZrO_2.

Before the first D(H)-charging runs (by the twin system [1,2,7]), we set up PZ samples in reaction chambers of the twin system, evacuated the chambers and baked samples at 200°C to remove "already absorbed" impurity gases. Since samples have been reserved in air for a few months, Pd-particles (PdO) would have absorbed a considerable amount of hydrogen in air (0.01% of air is H_2 gas, 10^{15} H_2 molecules per cc air). During a baking process, significant portion of PdO would have been de-oxidized by forming D_2O (H_2O) vapors to be evacuated. PZ samples may be a composite of $(PdO)_yPd_x/ZrO_2$ with $x + y = 1.0$. We have then made the first D(H)-charging runs to observe D(H)/Pd loading ratios and heat–power evolution in Phases I–III. Before the second D(H)-charging runs for used PZ samples, we have made evacuation and baking. In this second baking stage, we speculate that almost 100% reduction of PdO would have been done by "water-formation" reactions between out-going D(H) atoms and oxygen atoms in PZ sample under the elevated temperature (200°C) which enhanced chemical reaction rates. Such an experimental procedure as above mentioned is flow-charted in Fig. 1.

We refer an essential results of Kitamura et al. PLA 2009 paper [6], for heat–power evolution data under D(H)-gas charging to three kinds of Pd powder samples (PP, PB and PZ), as shown in Fig. 2.

How can we explain the results of anomalously enhanced heat–power evolutions for PZ samples both for D- and

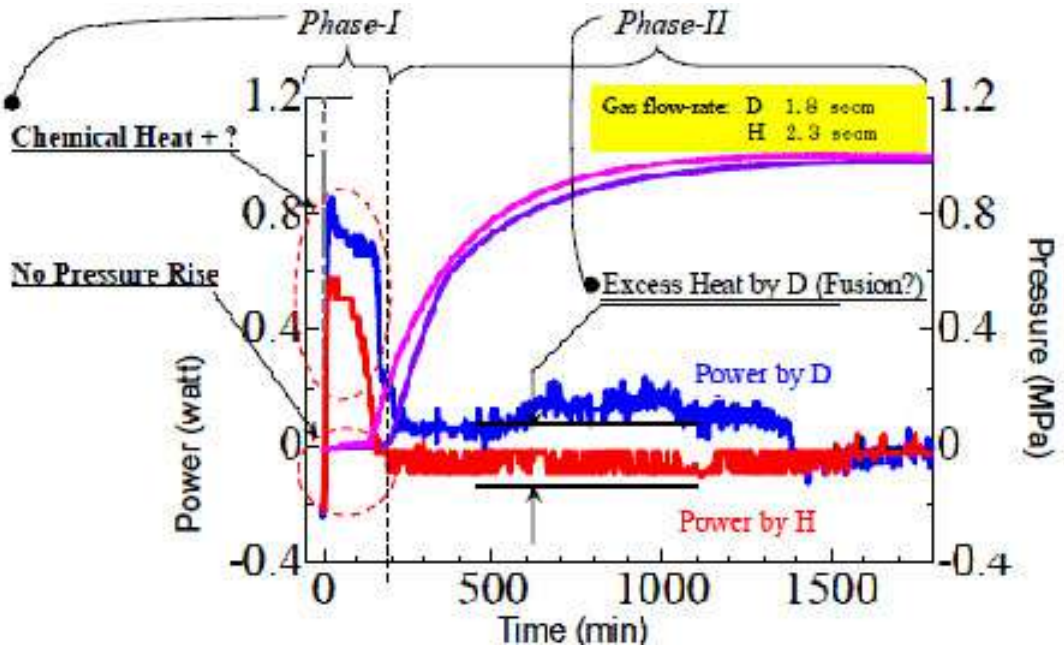

Figure 3. Definition of phases I and II intervals for the D(H)-gas loading experiment [6,7]).

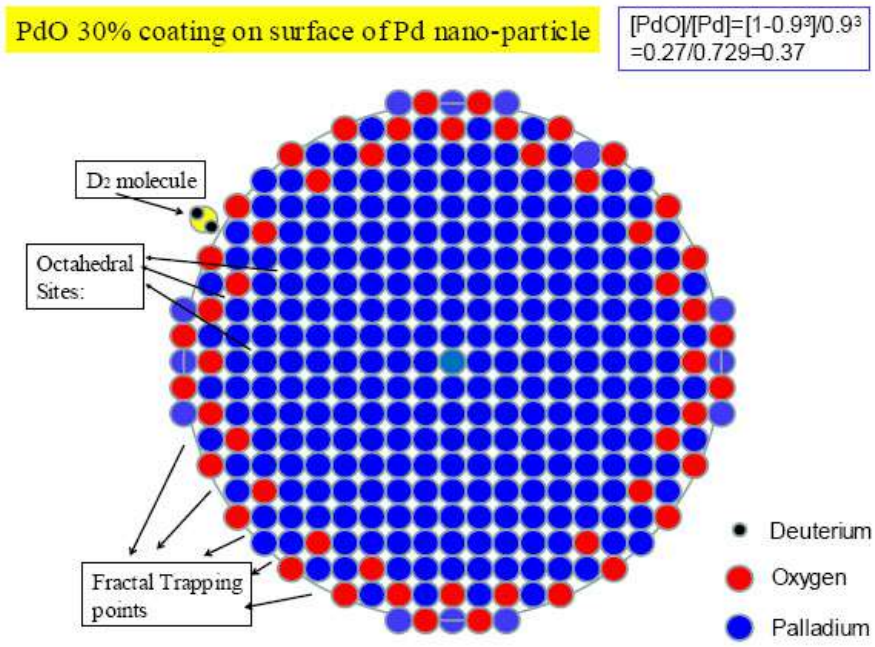

Figure 4. An atomic scale cross sectional image of PdO-layer coated (30%, $y = 0.3$) Pd nano-particle (5 nm diameter); here we used relative sizes of ionic radii and D_2 molecule, and fractal surface structure is supposed to make a role enhancing deeper adsorption potential for D(H)-gas.

H-charging, and why D-charging gave significantly larger heat–power in Phase-I and only gave positive heat–power level in Phase-II? What is a role of PdO component, since the second D(H)-charging runs with used samples (without PdO component) gave very reduced D(H)/Pd-loading ratios and heat? Experiments with forced oxidation [1,2] (4–8% of total Pd amounts) to used PZ and PNZ (Pd/Ni/ZrO_2) samples showed remarkable recovery for D(H)/Pd ratios (up to 1.1–1.8) and heat levels (0.8–2.0 eV) in Phase-I. What is the mechanism for that? Are these phenomena related to the proposed mechanisms of Takahashi's TSC formation models and D-cluster (4D, typically) fusion reactions?

3. A Phenomenological Model of D(H)-Adsorption/Absorption with PdO Layer

We propose phenomenological models in Sections 3 and 4 for the phase-I and phase-II phenomena as defined in [6]. We show a modified figure for helping this purpose in Fig. 3.

From our analysis of forced-oxidization experiments [7], we have speculated that a portion of PdO at the beginning of first (virgin) D(H)-charging run maybe around 30% ($y = 0.3$ or so). Assuming a formation of PdO surface layer (coating with $y = 0.3$) of Pd nano-particle, an image of atomic scale cross section of PdO/Pd nano-particle (5 nm diameter, for instance) is shown in Fig. 4. By TEM image of used sample (as to be reported by Kitamura ICCF 16 paper, and also we reported [7,17] at ACSNET 2010), 2–10 nm PdO/Pd particles are dispersed in/on ZrO_2 flakes with several micro-meter size. We assume here PdO/Pd particles are kept as isolated each other in a supporter ZrO_2 flake. Position of oxygen-atom can be interstitial or substitute for Pd-atom, but we draw here simply as substitute of Pd-atom.

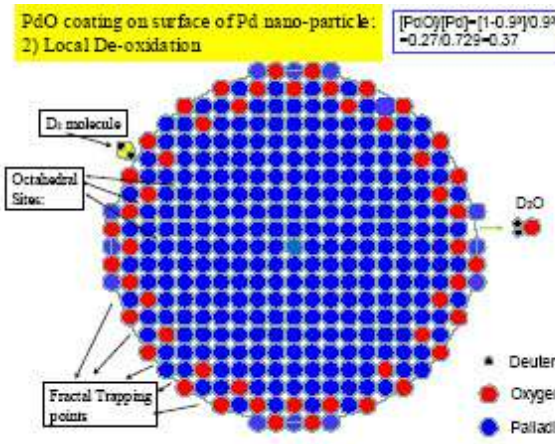

Figure 5. D_2O molecule going out.

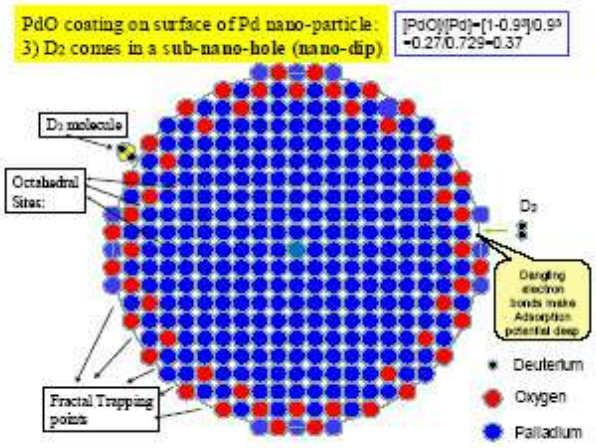

Figure 6. SNH traps D_2 incoming.

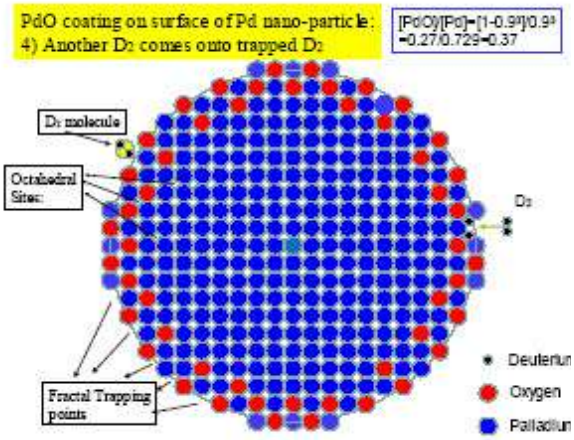

Figure 7. Eventual double D_2 trapping.

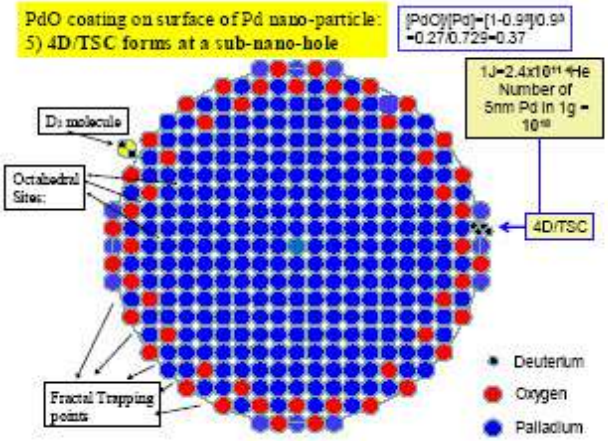

Figure 8. Eventual 4D/TSC fusion on surface.

We are going to propose a mechanism that oxygen of PdO layer will serve as a "seed" for generating a "sub-nano-hole" (SNH) when D(H)-gas will be started to charge and formation of D_2O (H_2O) by incoming D_2(H_2) gas molecule to combine (de-oxidize PdO) with oxygen. Formed D_2O (H_2O) molecule will go out to vacuum, and a SNH with chemical electron dangling bonds will be generated. As the trapping potential of SNH will be "very" deep (strong sticking force by electron-dangling bonds), incoming D_2 molecules will be doubly (or more) trapped there to form a transient TSC (*transitory Bose–Einstein condensate*) with certain probability. The image of such TSC formation is speculative at this

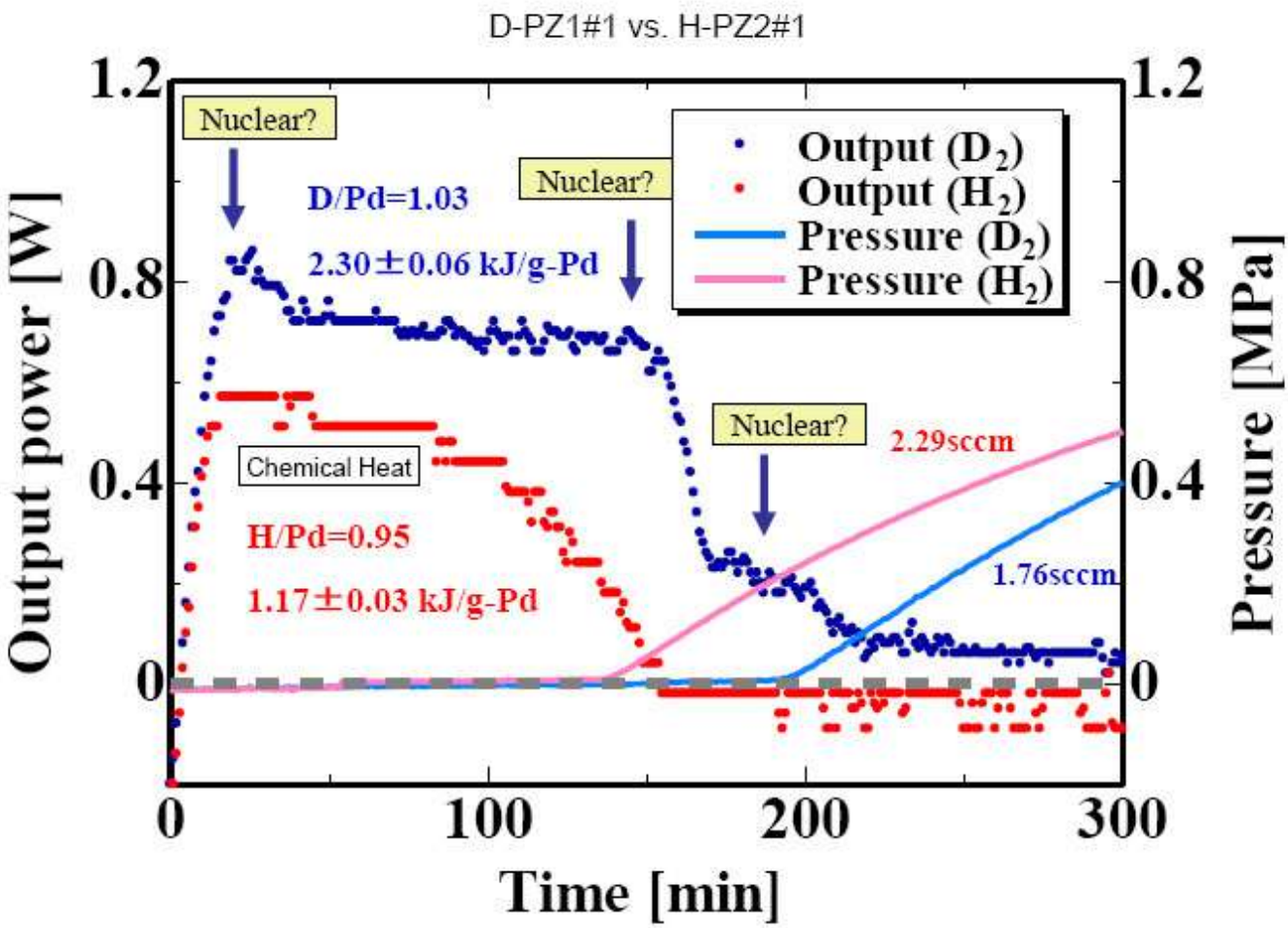

Figure 9. Expanded view of heat–power evolution data by Kitamura et al. [7] for PZ samples.

stage, and we need a further deepened study based on the first principle type quantum-mechanical calculations using time-dependent coupled Schroedinger equations for the SNH composition of three dimensional Pd-atoms arrangement and in-coming D_2 molecules. However, this is not so easy task.

Once a TSC ($t = 0$) is formed, very fast (in 1.4 fs) condensation happens to make a very small (in 10–20 fm diam.) charge neutral entity (TSC-min) which will cause 100% 4d-simultaneous fusion to produce two ^{4}He products with heat (23.8 MeV/^{4}He) [3–5]. Image of such a process is illustrated in Figs. 5–8. After such an event of D_2 trapping at SNHs, remained surface fractal nano-holes will trap more incoming D(H)-gas and enhance "rapid diffusion" into inner PdDx lattice points (namely O-sites of local PdD lattice), as we speculate existence of "D(H)-pressure" from backside where trapping of D_2 molecules is taking place one after another and accumulating "surface D-clusters".

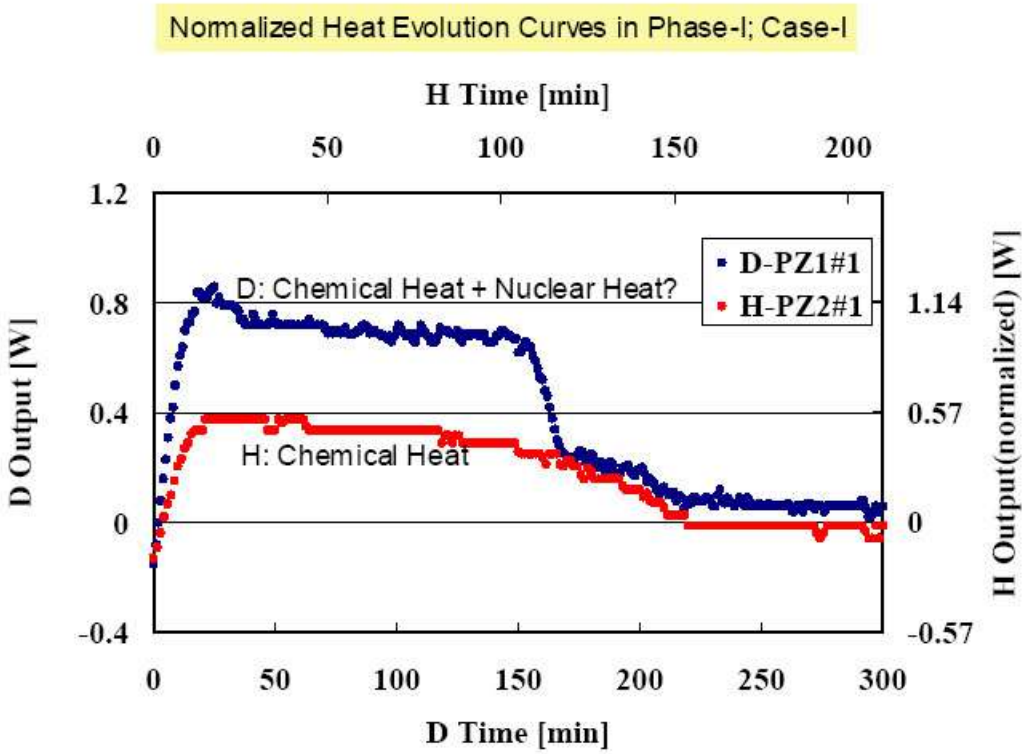

Figure 10. Normalized heat evolution curves in Phase-I for PZ-1(2)#1 runs [7].

As shown in an inset (right top) of Fig. 7, 1 g of Pd nano-powder contains 5 nm-diam. nano-partilces of 10^{18} (of the order). Since 10^{11} 4d/TSC fusion events corresponds to 1 J, one watt heat-level is maintained by a TSC formation rate of "one over 10 million Pd nano-particles per sec" for PZ sample containing 1 g net Pd atoms. This condition looks feasible, in reference to observed heat–power evolution levels by Kitamura et al. [1,2,7].

A typical data reported by Kitamura et al. [7] for Phase-I is expanded and is shown in Fig. 9. We can consider that the heat–power evolution curve for H-charging is purely by chemical heat producing reactions, while the curve for D-charging may have component of some isotope effect, probably "nuclear heating" as shown with specific patterns (see arrows). Data by the twin system [7] gave different end-points of Phase-I for the H-charging and D-charging, respectively, and D(H)/Pd loading ratios are slightly different. We can draw normalized curves by adjusting time-intervals of Phase-I and loading ratios, as shown in Fig. 10.

From Fig. 10, we can have impression that a beginning peak and a later bump of heat-power evolution in the D-charging run look like "nuclear heating components", while bumps around 200 min are due to a pure chemical heat-power evolution. We have observed and deduced similar normalized heat-power evolution curves, three times, for PZ virgin samples (10 g each) in 2008-2009. Hioki, et al (Toyota Central Research Laboratory) reported8 similar heat-power evolution curve having a very clear peak (sharp spike) in the beginning and a broad bump later for a PZ

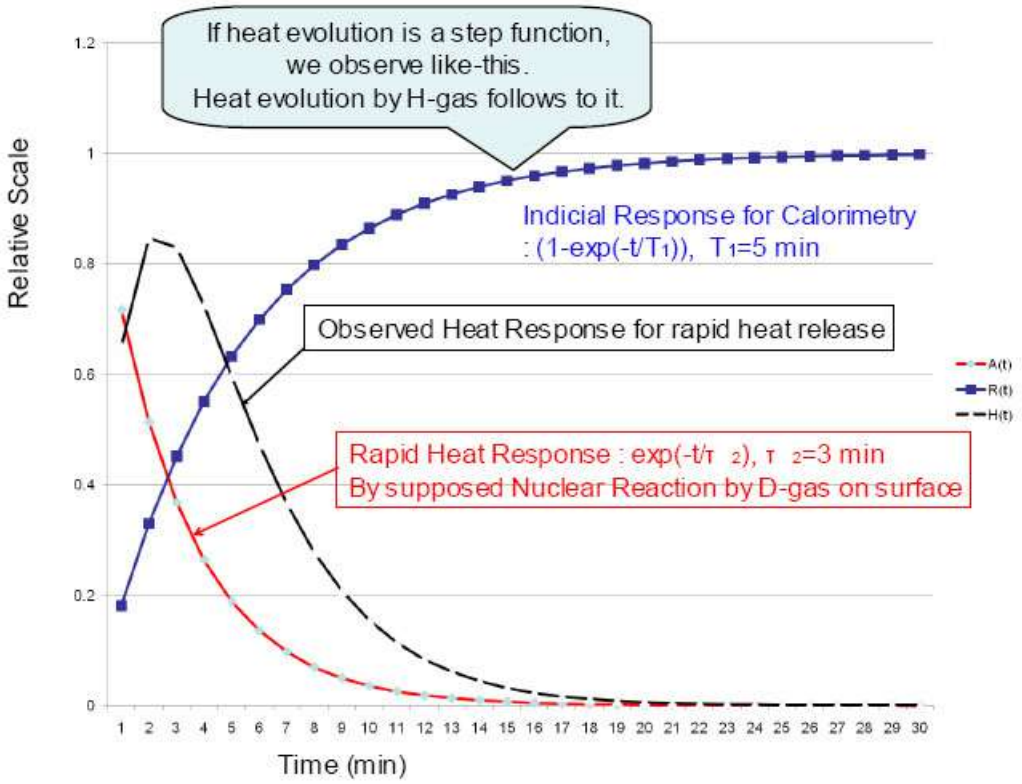

Figure 11. Observed "rapid" heat response is broadened by indicial response of calorimetry, assuming a single exponential "nuclear heat evolution by D-absorption in Phase-I. Such a "nuclear response" may be a superposed component in observed heat evolution data for D-gas, in comparison with rather smooth response by H-gas.

sample (from Santoku Co.) of 54 g. To assure that this is really due to nuclear (fusion) heat, we have of course to detect correlated ash (maybe alpha particles, other minor charged particles, secondary X-rays, EUV and visible lights) on line and/or off-line. This is our future task.

From Fig. 10, we can have impression that a beginning peak and a later bump of heat–power evolution in the D-charging run look like "nuclear heating components", while bumps around 200 min are due to a pure chemical heat–power evolution. We have observed and deduced similar normalized heat–power evolution curves, three times, for PZ virgin samples (10 g each) in 2008–2009. Hioki et al. (Toyota Central Research Laboratory) reported [8] similar heat–power evolution curve having a very clear peak (sharp spike) in the beginning and a broad bump later for a PZ sample (from Santoku Co.) of 54 g. To assure that this is really due to nuclear (fusion) heat, we have of course to detect correlated ash (maybe alpha particles, other minor charged particles, secondary X-rays, EUV and visible lights) on line and/or off-line. This is our future task.

On the other way of precisely observing time-dependent behaviors of heat evolution in the beginning just after D(H)-charging, we may obtain anomalously large isotopic effect, namely too large difference of heat–power levels

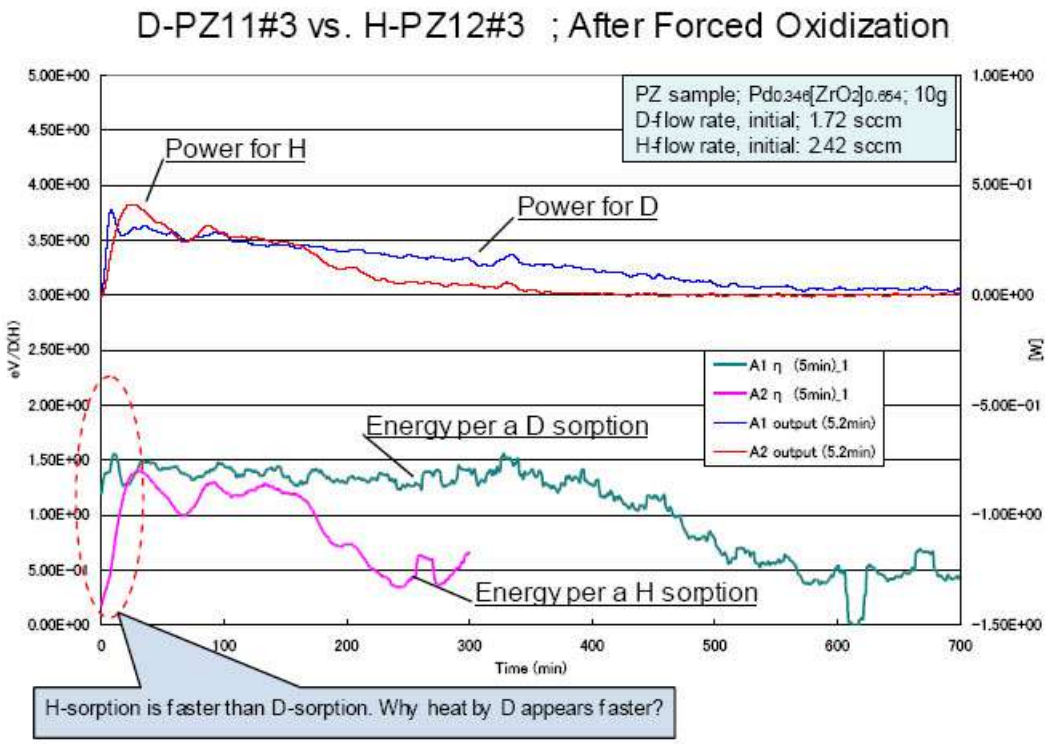

Figure 12. Heat evolution curves and η-values for PZ-11(12)#3 runs; nuclear heating looks appearing in the early stage circled by a red broken elliptic line, for D-gas charging. Amounts of PdO components in PZ-11(12)#3 runs, by forced oxidization, are 8.5 % (5.4 %) for D (H), respectively.

between D-gas and H-gas runs. By exploring such a phenomenon, we may have dynamic information of heat release mechanisms by "new kind of D-related nuclear reactions" such as 4D/TSC cluster fusion.

We can feel now vividly, by such normalized heat–power evolution runs taken by a twin system, that released heat–power by D-charging has a significant component of "some D-related fusion" reactions, due to its time-dependent shapes very different from those for H-charging.

The mechanism of D(H)-absorption in Phase-I is independent of that in Phase-II (the new second phase [2]). The former is a rapid process of absorption with relatively large heat–power level, while the latter looks a slow adsorption/absorption process with relatively weak (about 1/10 of that in Phase-I) heat power level albeit having similar integrated D(H)/Pd loading ratio components (0.5–1.0). Time-dependent D(H)-absorption rate in Phase-I drew decay curves of almost same rates both for D- and H-charging. This fact is another background that the heat–power evolution for D-charging (Fig. 10) looks like containing component by nuclear origin.

Our calorimetry system had a time resolution (time constant) of 5 min and observed heat evolution curve became a convolution with its indicial response and exponential absorption rate. If heat release rate is constant (a step function),

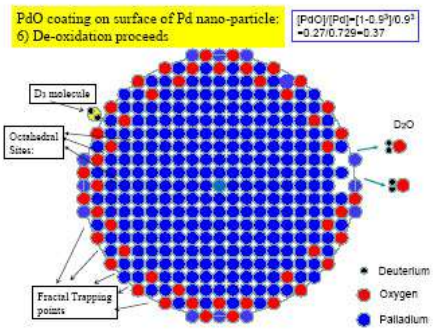

Figure 13. Extended sub-nano dips by D_2O formation.

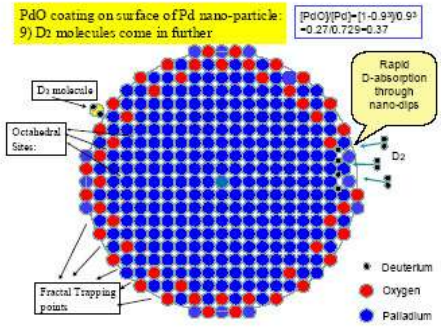

Figure 14. Incoming D_2 molecules are trapped one after another, by dangling bonds of SNH.

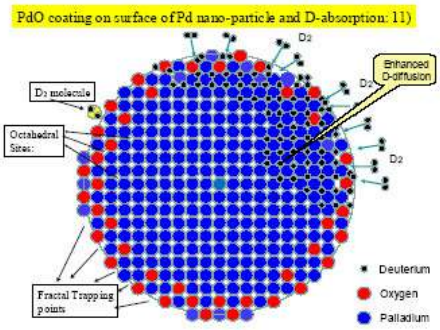

Figure 15. Trapped deuterons diffuse inside with enhanced speed by "D-pressure" from backside.

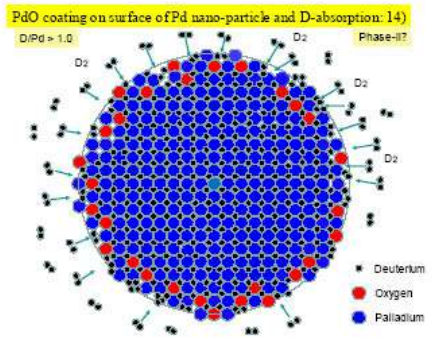

Figure 16. Feature at the end of Phase-I, full D(H)-loading in O-sites plus surface D-clusters component.

we need to wait about 20 min to get saturated (real) power level. However, if we have rapid heat release, as supposed as some surface nuclear reaction, we may have a local peak of heat–power evolution, as shown by simulation in Fig. 11.

Actually observed example of heat responses by H-charging, namely "pure" chemical heat–power evolution curve and energy per an H sorption (adsorption/absorption), η value (13), is shown in Fig. 12, where data by D-charging are drastically different. These runs after the forced oxidization realized significant recovery of heat–power levels and D(H)-loading ratios, in reference to the virgin runs. Heat evolution just after the D-charging has a peak, (see arrows) while that by the H-charging slowly rises without a "corresponding peak", which is considered (speculated) due to the surface 4D/TSC fusion as shown in Fig. 5. The secondly interesting point is that the D-charging gave more than twice longer-lasting (about 10 hours) heat power than that (about 3 hours) of the H-charging. Evolutions of time-dependent η values are compared between the D-gas charging and the H-gas charging to show "drastic isotopic effect". Such a big "isotopic effect" is difficult to be explained by usual chemical (electrons-interaction) effects, and needed to explore

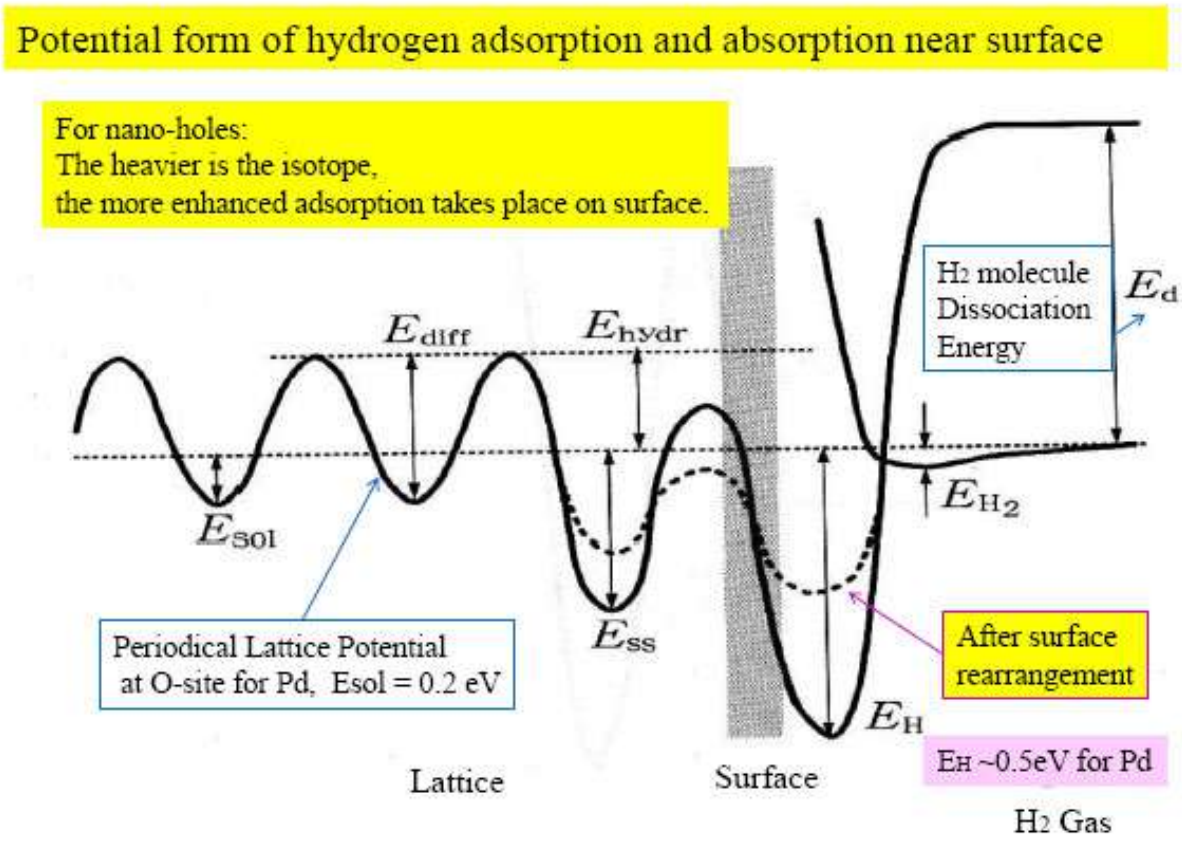

Figure 17. Surface and inner D(H)-trapping potential for a bulk-character Pd metal [9].

some "nuclear origin". Ratio of η values (η-D/η-H) are very large (more than 10) in the beginning few minutes after D(H)-charging. Such a big isotopic effect infers the need of explanation by a rapid heat release mechanism of some nuclear reaction as 4D/TSC fusion on surface.

Now we come back to follow the simulation after Fig. 8 for D(H)-absorption into Pd nano-particle. Double D_2 trapping in an SNH does not always make a TSC, but does make reaction with near-by oxygen to form D_2O molecules and extended SNH as shown in Fig. 13. Through the extended SNH, deuterons trapped diffuse to inner O-sites as shown in Fig. 14.

In Fig. 15, we draw an image of D-diffusion enhanced by pressure of incoming deuterons from behind through the extended SNH. Finally, at the end of Phase-I, Pd nano-particle is fully loaded (PdD, $x = 1.0$), but we have additional trapped deuterons on surface (in SNHs) and apparent x-value becomes more than unity, typically as we can roughly calculate from the drawing, $x = 1.1$–1.5 which agrees well with observed Phase-I D(H)/Pd ratios [1,2,7]. This feature is drawn in Fig. 16.

4. A Phenomenological Model in Phase-II

As shown in Fig. 16, PdD local lattice may be formed inside a Pd nano-particle in Phase-II. We have in addition trapped deuterons (possibly making D-clusters) on surface SNH. For a known characteristics of bulk Pd metal for D(H) absorption, we have potential forms as shown in Fig. 17 for the surface adsorption and trapping (absorption) in inner lattice O-sites [9].

The surface adsorption energy (depth of potential) is 0.5 eV and lattice absorption energy is 0.2 eV, as evaluated in a standard text book [9]. Therefore heat release level for a bulk Pd sample is around 0.2 eV per D(H)-absorption, since number of trapped deuterons on surface is negligible. In contrast, observed specific absorption energy by PZ (and PNZ) samples are very large, namely around 2.0 eV per D(H), about 10-fold of the bulk value (0.2 eV). To explain observed anomalous values of D(H) loading under as "rapid loading process as observed" and such high specific "chemical" heat-energy level, we need to propose some new mechanism. We speculate and model that surface adsorption potential becomes very deep as 1.5–1.8 eV for a nano-Pd particle and local periodical Bloch potential should be in "shrunken state as shown in right figure of Fig. 18. Here anomalously high chemical heat releases are considered both for D-gas and H-gas charging procedures.

Existence of PdO surface "barrier" and formed SNHs would make very deep D(H) adsorption potential on surface (1.5–1.8 eV deep, speculated by our experiments [9]), which is categorized as an *collective mesoscopic potential well*

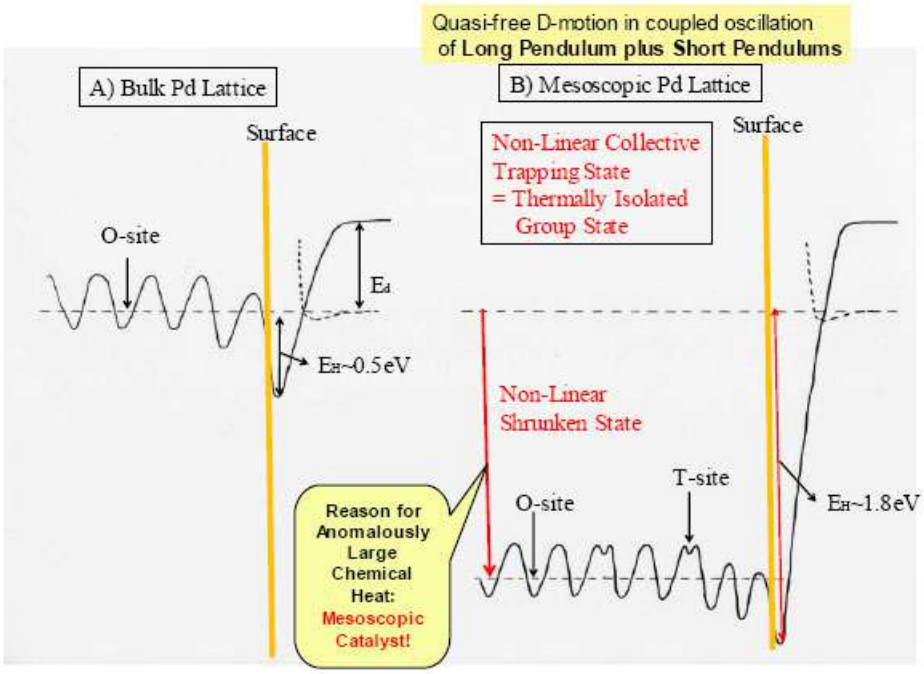

Figure 18. Collective shrunken state potential of Pd nano-particle for D(H) trapping, right figure, compared with a bulk metal trapping potential, left figure.

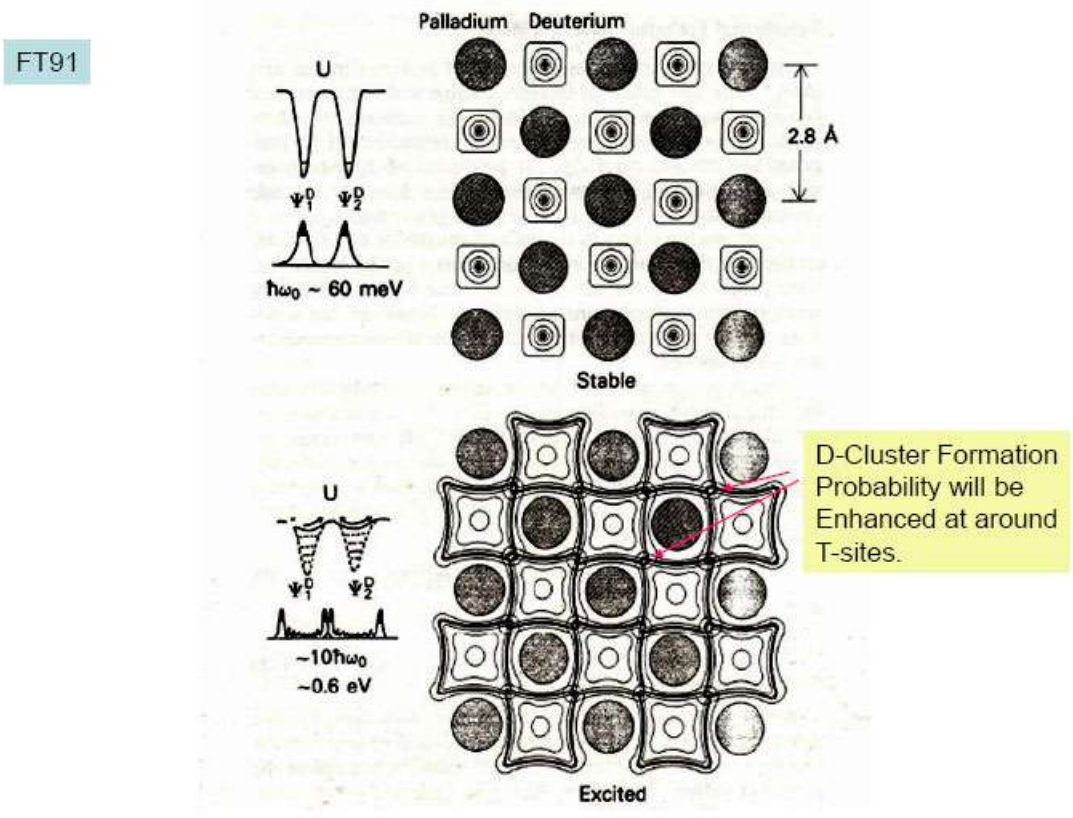

Figure 19. Quasi-free motion of deuterons inside CMPW potential enhances TSC formation around T-sites of local PdD lattice of Pd nano-particle which has formed a collective mesoscopic potential well (CMPW).

(CMPW, or a global potential for a nano-particle). Inside a CMPW confinement, three-dimensional PdD lattice (Bloch) potential exists as local fine structure in "shrunken state".

The CMPW potential induces a QM non-harmonic oscillation, and the local Bloch potential induces a QM harmonic oscillation (wave function becomes a Hermite function, of which ground state is Gaussian and highly excited state has a U-shape wave-function). Two QM oscillations combine non-linearly [14] to make D-motion in a nano-Pd particle highly free (quasi-free) under the three dimensional constraint of PdD Bloch structure. This quasi-free motion of deuterons inside a mesoscopic nano-particle enhances very much probability of TSC (tetrahedral symmetric condensate [3–5]) formation as we give an image of QM wave superposition in Fig. 19 [10].

Generation of CMPW will basically make a Pd nano-particle working as "mesoscopic catalyst" which realizes very large D(H)-loading ratios and anomalously large chemical heat releases both for H-gas and D-gas loading. If anomalously large heat observed for H-gas run is by this process, some endothermic (slow heat sink) process should exist before we made de-sorption runs for which we observed [13] only about 1/10 levels of heat absorption, compared with released heat levels for the sorption runs, both for D- and H-absorbed samples.

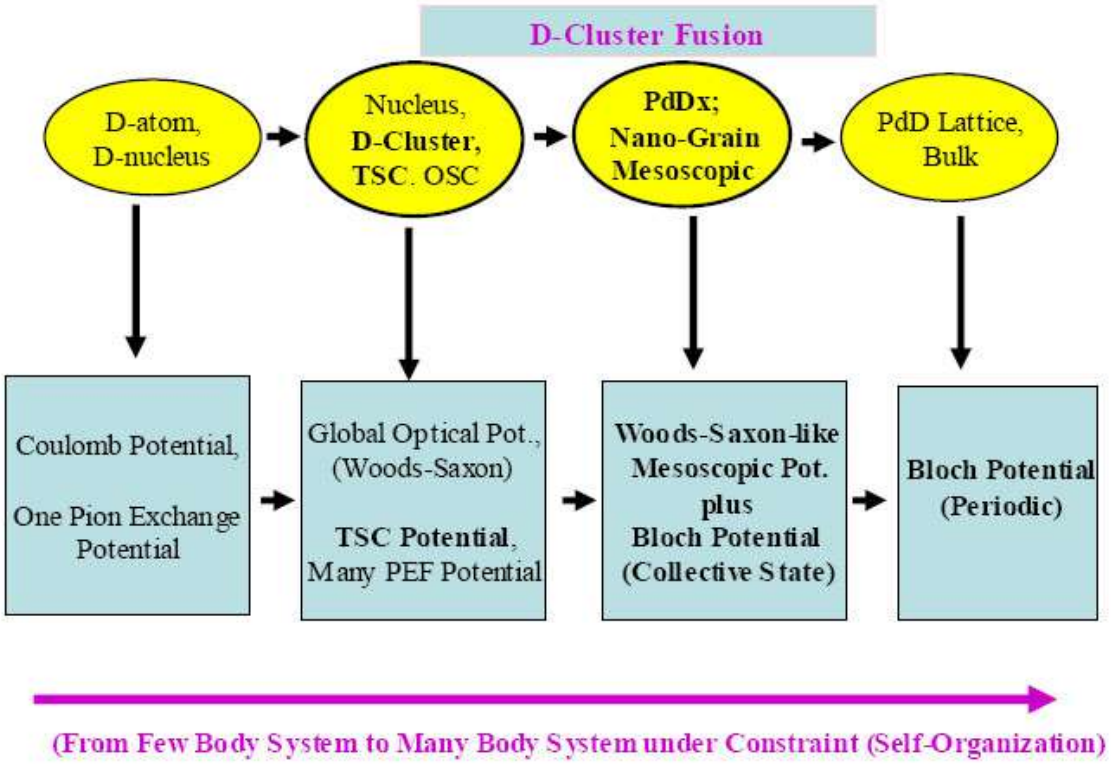

Figure 20. Speculation of useful potential forms to be applied for QM calculations to estimate fusion reaction rates from a simple system to many body, mesoscopic and bulk condensed matter systems.

In Fig. 20, we show a flow-chart drawing of considered useful potential forms in Coulombic (electro-magnetic) and nuclear strong interaction, starting from a simple system of atom and two nucleons to more complex systems as D-cluster, mesoscopic nano-particle and bulk material. By defining useful potentials for interactions in every step, we can extend quantum-mechanical (QM) analysis by using many body Schroedinger equations (or dynamic equations as QM-Langevin equation [3–5]). Fusion reactions in microscopic random systems (gas and plasma) can be treated by using a simple Coulombic potential and a one pion exchange potential (OPEP) [11]. For D-cluster systems, we can apply special trapping potential-forms for Coulombic interactions based on Platonic symmetry (orthogonal coupling) between electron wave functions and deuteron wave functions. For multi-body strong interactions of 4D, 6D, 8D, etc. cluster fusion reactions, we can use an empirical formula of PEF (pion exchange force) [12].

The specific nature of condensed matter is of constraint (ordering or self-organization) motion of particles with lattice regularity or surface fractals. A global shrunken state potential well for trapping D(H) atoms in deep hole will realize a non-linear oscillation mode coupled with harmonic oscillation in PdD lattice, which makes deuteron motion inside a nano-particle quasi-free under ordered constraint to induce enhanced cluster (TSC) formation probability. A bulk Bloch potential (periodical) is useful for established states of D(H) absorption. We speculate that D-cluster fusion is induced in the states of D-cluster and D-mesoscopic systems.

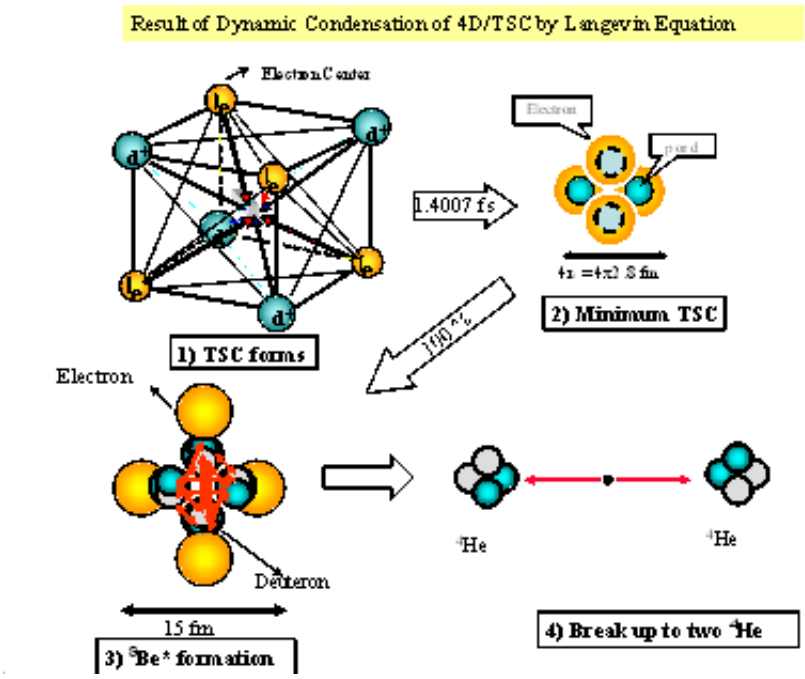

Figure 21. Typical four steps for TSC condensation and simultaneous 4d fusion.

We copy lastly typical four steps of TSC motion and 4d fusion in Fig. 21.

5. Concluding Remarks

(1) With a PdO surface layer, sub-nano-holes (SNH) are formed in the beginning of D(H)-gas charging. This SNH would become a seed of "anomalous phenomena" in D(H)-loaded Pd nano-particle samples.
(2) PdO layer also helps to make up a global deep mesoscopic trapping potential well which is a shrunken state of local PdD lattice Bloch potentials inside a nano-particle.
(3) In SNHs, formation of 4D/TSC is largely enhanced in the Phase-I interval of D(H)-gas loading. 4D fusion thus induced may be a main nuclear component of heat release in Phase-I.
(4) Within a global mesoscopic potential with local Bloch potentials, quasi-free D-motion is induced by non-linearly coupled oscillations for the global QM state (long pendulum) and a local harmonic oscillator (short pendulum). Anomalous heat by D-charging in Phase-II may be by 4D/TSC fusion of this process.
(5) Generation of CMPW will basically make a Pd nano-particle working as "mesoscopic catalyst" which realizes very large D(H)-loading ratios and anomalously large chemical heat releases both for H-gas and D-gas loading.

References

[1] Y. Sasaki, Y. Miyoshi, A. Taniike, A. Kitamura, A. Takahashi, R. Seto, Y. Fujita, Measurements of heat and radiation from Pd nano-powders during absorption of hydrogen isotopes, *Proc. JCF10*, 2010, to be published.
[2] Y. Miyoshi, Y. Sasaki, A. Taniike, A. Kitamura, A. Takahashi, R. Seto, Y. Fujita, Two absorption/adsorption processes of hydrogen isotopes observed for Pd nano-powders, *Proc. JCF-10*, 2010, to be published.

[3] A. Takahashi, N. Yabuuchi, Study on 4D/TSC condensation motion by non-linear Langevin equation, In *ACS Symposium Series 998*; Low Energy Nuclear Reactions Source Book, J. Marwan, S. Krivit (eds.), American Chemical Society, Oxford University Press, Washington, DC, 2008, pp. 57–83.
[4] A. Takahashi, The basics of deuteron cluster dynamics as shown by a Langevin equation, in LENR Source-Book 2, J. Marwan, S. Krivit (eds.), Washington, DC, American Chemical Society, 2009, pp. 193–217.
[5] A. Takahashi, *J. Condensed Matter Nucl. Sci.* **2** (2009) 33–44.
[6] A. Kitamura, T. Nohmi, Y. Sasaki, A. Taniike, A. Takahashi, R. Seto, Y. Fujita, *Phys. Lett*. A, **373** (2009) 3109–3112.
[7] A. Kitamura, A. Takahashi, Yu Sasaki, Y. Miyoshi, A. Taniike, R. Seto, Y. Fujita, Heat evolution from Pd nanopowders exposed to high-pressure hydrogen isotopes and associated radiation measurements, J. Marwan (ed.), *LENR Sorcebook*, vol. 3, American Institute of Physics, to be published in 2010.
[8] T. Hioki, H. Azuma, T. Nishi, A. Itoh, S. Hibi, J. Gao, T. Motohiro, J. Kasagi, Hydrogen/deuterium absorption capacity of Pd nanomaterials and its relation with heat generated upon loading of hydrogen isotope gases, *Proc. JCF10*, 2010, to be published.
[9] 9) Y. Fukai, K. Tanaka, H. Uchida, Hydrogen and Metal (in Japanese), ISBN4-7536-5608-x C3042, Material Series, Uchida Rokakuho Publ., Tokyo, 2002.
[10] A. Takahashi, T. Iida, F. Maekawa, H. Sugimoto, Y. Yoshida, *Fusion Technol.* **19** (1991) 380–390.
[11] 11) T. Hamada, I. Johnston, *Nucl. Phys.* **34** (1962) 382.
[12] A. Takahashi, N. Yabuuchi, *J. Condensed Matter Nucl. Sci.* **1** (2007) 106–128.
[13] A. Kitamura, A. Takahashi, Y. Sasaki, Y. Miyoshi, A. Taniike, R. Seto, Y. Fujita, Anomalous heat evolution in charging of pd powders with hydrogen isotopes, J. Marwan (ed.), *LENR NET Sourcebook*, vol. 3, American Chemical Society, to be published in 2010.
[14] B. Ahern, Private communication, 2009.

J. Condensed Matter Nucl. Sci. 5 (2011) 34–41

Research Article

Issues Related to Reproducibility in a CMNS Experiment

Jeff Driscoll
254 Shaw Avenue, Abington, MA 02351, USA

Mike Horton
26451 Trancas Ct., Sun City, CA 92586, USA

Ludwik Kowalski *
Montclair State University, Montclair, NJ 07043, USA

Pete Lohstreter
The Hockaday School, 11600 Welch Road, Dallas, TX 75229 , USA

Abstract

Unexplained emission of charged nuclear projectiles due to electrolysis has been reported by Richard Oriani. Experimental results were said to be highly reproducible. Working independently, we were not able to observe emission of charged nuclear particles (in a chemical process similar to Oriani's) and therefore are unable to provide supporting evidence that the effect is reproducible.
© 2011 ISCMNS. All rights reserved.

Keywords: Cold Fusion, CMNS, LENR, Nuclear Reactions

1. Introduction

Radioactivity, such as emission of alpha particles, has long been thought to be independent of chemical processes, such as electrolysis. The same is true for nuclear reactions including fusion and fission. The reason for this is that the kinetic energies of molecules in a typical chemical process are too small to overcome the Coulomb repulsion between positively charged nuclear particles [1]. This expectation was challenged by Pons and Fleischman [2], Oriani [3, 4], and other scientists, as described by Storms [5]. We were attracted by Oriani's work because his findings were impressive

*E-mail: kowalskil@mail.montclair.edu

© 2011 ISCMNS. All rights reserved.

(a nuclear process taking place during electrolysis) and his methodology was simple. Our goal was to either confirm or refute the claimed reproducibility of the effect.

The electrolyte in Oriani's cell, Li_2SO_4, is usually dissolved in light water at the concentration of 0.022 g per cubic centimeter. The cathode electrode is usually nickel while the anode electrode is usually platinum. To detect charged nuclear particles, Oriani uses CR-39 chips. This method of detection is widely used in personal neutron dosimeters as well as in other fields of research [6] such as measuring the amount of radon in the air and studying thermonuclear reactions. In Oriani's 2003 experiment, described in [3], the detector was suspended in the electrolyte between the anode and the cathode. The mean track density on the experimental chips was 470 tr/cm^2 while the mean track density on control chips was 168 tr/cm^2. The corresponding standard deviations were 384 and 99 tr/cm^2, respectively.

Referring to such results, Oriani et al. concluded in 2003 that: "a nuclear reaction of as-yet unknown nature can accompany the electrolysis." Experimental results, according to Oriani's more recent 2008 paper [4], are now highly reproducible. The purpose of the present study was to verify this assertion.

2. Oriani's Cell and New Experimental Results

The cell used in Oriani's new study [4] is shown in Fig. 1. It was similar to the cell used in [3]. The essential difference was the addition of a thin Mylar film (6 μm) placed between the CR-39 detector and the nickel cathode. That film was chosen to protect the CR-39 detector from the electrolyte without interfering with detection of expected nuclear particles.

Twenty-one experiments were performed and 42 CR-39 surfaces were examined, as described in his 2008 paper [6]. The track density on one of these surfaces was reported as "too large to count." Track densities on the remaining 41 experimental surfaces ranged from 9 to 498 tr/cm^2, as illustrated in Fig. 2. The histogram was drawn without making a distinction between surfaces facing the cathode and surfaces facing away from the cathode. Note that the distribution of densities is not bell-shaped. Track densities on control CR-39 chips were usually much lower (mean 21 tr/cm^2 and standard deviation 9.7 tr/cm^2) than on most experimental chips (mean 122 tr/cm^2 and standard deviation 124 tr/cm^2). Mean track densities on surfaces facing the cathode, according to data published in [4], were essentially the same as mean track densities on surfaces facing away from the cathode.

On the basis of these observations Oriani concluded that "the present technique has consistently produced evidence that a nuclear reaction of some sort has been generated in the course of electrolysis." Investigations described in this paper were undertaken to determine if Oriani's results could be reproduced in another laboratory.

3. Our Cells and Experimental Results

Our experiments, done in four separate laboratories, were performed using cells that were similar to Oriani's cell. Figure 3 displays a generic diagram of our cells. We used the same electrolyte (Li_2SO_4 in distilled H_2O, at the initial concentration of 0.022 g/cm^3) as Oriani; our electrodes were also made from Ni and Pt. Oriani's nickel cathode wire and our nickel cathode wires were from the same spool. All of us used the 6 μm Mylar which is capable of transmitting alpha particles with energies higher than 2 MeV. Distances between the cathodes and the anodes were approximately 3 cm, which is approximately the same as Oriani's. The essential cell parameters of Oriani's and our experiments were the same.

Differences between Oriani's experiment and our experiment are the following: Platinum wires for the anodes did not come from the same manufacturer. Oriani's cathode was spot-welded to a vertical titanium rod, placed inside a glass tube. Vertical parts of our electrodes, on the other hand, were placed into long heat shrink tubes (not shown in Fig. 3). Lower parts of our shrink tubes were thermally compressed, to prevent capillary creep of the electrolyte. Also note that Oriani's cell exposes the bottom surface (the side away from the electrolyte) of the CR-39 detector to air while our

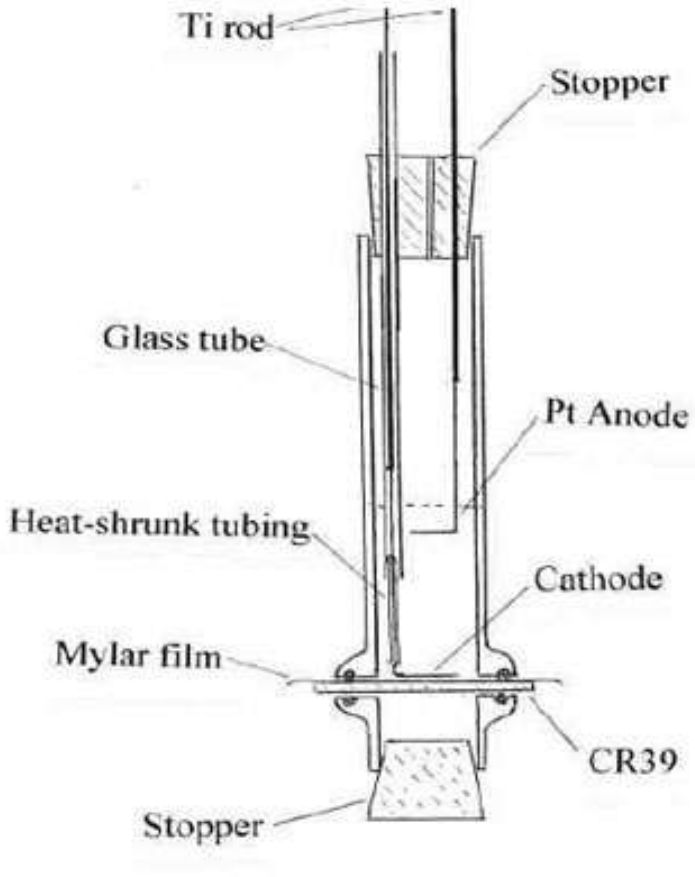

Figure 1. A diagram of an Oriani cell from his 2008 paper [4]. Small circles are cross sections of O-rings placed between the two sections of the cell. A clamp (*not shown*) is used to press the sections toward the CR-39 detector.

cells do not. In our cells, the bottom surface of the CR-39 is in contact with a 25" layer of polyethylene. That layer was clamped to the cell. The leakage of the electrolyte was prevented by squeezing the CR-39, Mylar and O-ring between the polyethylene and the cell.

Both we and Oriani used Fukuvi CR-39 material purchased from Landauer. The delivered sheets of that material are protected from scratches and alpha particles in air by a thin layer of polypropylene plastic. That layer usually peels off when the sheet is cut into small chips. Our unprotected chips were kept in salty distilled water (NaCl concentration of about 10 mg/cm^3). Furthermore, all control chips were kept in unused electrolyte during electrolysis. Salty water prevents potential accumulation of electric charges on CR-39 surfaces kept in air. This precaution was taken to reduce the possibility that electric charges on CR-39 surface in air might attract or repel radioactive ions. No chips were exposed to air for more than one hour. One author (P.L.) compared track densities on two CR-39 chips, one kept in

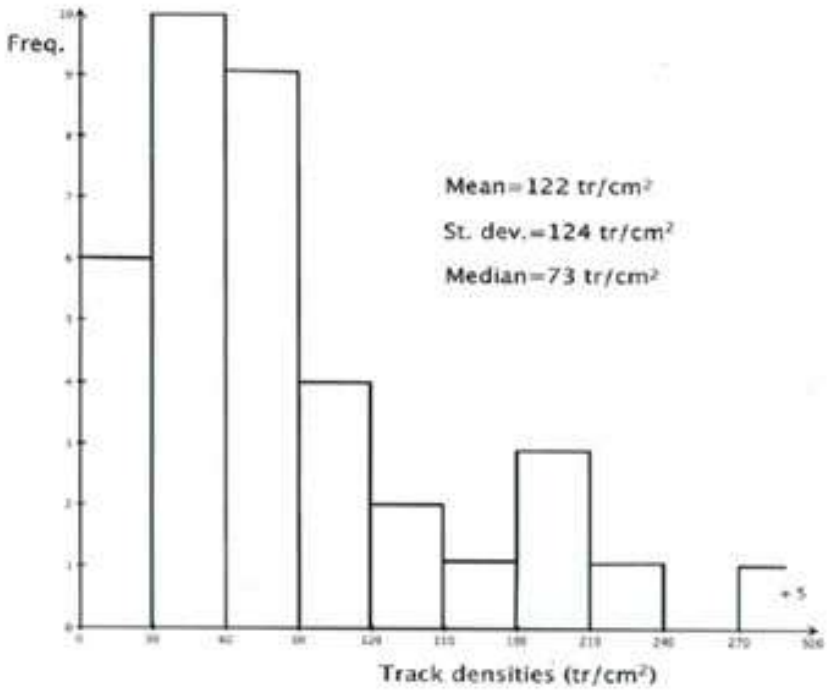

Figure 2. Oriani's distribution of track densities from his 2008 paper [4]. The +5 and 500, near the lower right corner, refer to five surfaces where track densities were between 300 and 500.

distilled salty water and in air, for 15 days. The track density turned out to be 30 tr/cm^2 on the chip kept in salty water and 505 tr/cm^2 on the chip kept in air. This can be explained by the big difference between ranges of alpha particles in air (centimeters) and in water (microns). Oriani did not use salty water; he wrapped the chips in aluminum foil and kept them in air. All of our "control" chips were kept in unused electrolyte during the time that the "experimental" chips were exposed to electrolysis.

Like in [4], we typically exposed the experimental chips to electrolysis for three days. During this time the electric current was changing slowly from 60 to about 90 mA, due to the loss of water. The corresponding voltage across the electrodes was typically 7– 8 V and was kept constant during the experiment. The cell was dismounted after each experiment and the CR-39 chip was removed. It was then etched for 12 h in the stirred water solution of NaOH (concentration 6.5 M, temperature 72°C). The pits on CR-39 surfaces, identified as tracks of nuclear particles, were subsequently counted under the microscope. The uncertainty of up to plus or minus 5% (in reported track densities) was common due to difficulties in distinguishing tracks from certain surface defects. Each experimenter was given a CR-39 chip with one corner that was exposed to alpha particles from an ^{241}Am source. This helped the experimenter learn the difference between pits and defects. Pits due to particles from that source are shown in Fig. 4. They had the same size as pits found on control and experimental chips.

The mean and standard deviation on eight of P.L.'s experimental surfaces were 87 and 46 tr/cm^2. The mean and standard deviation on his five control surfaces were 59 and 38 tr/cm^2. This information, as illustrated in the Appendix, can be used to justify the statement that the reported difference between mean track densities on experimental and

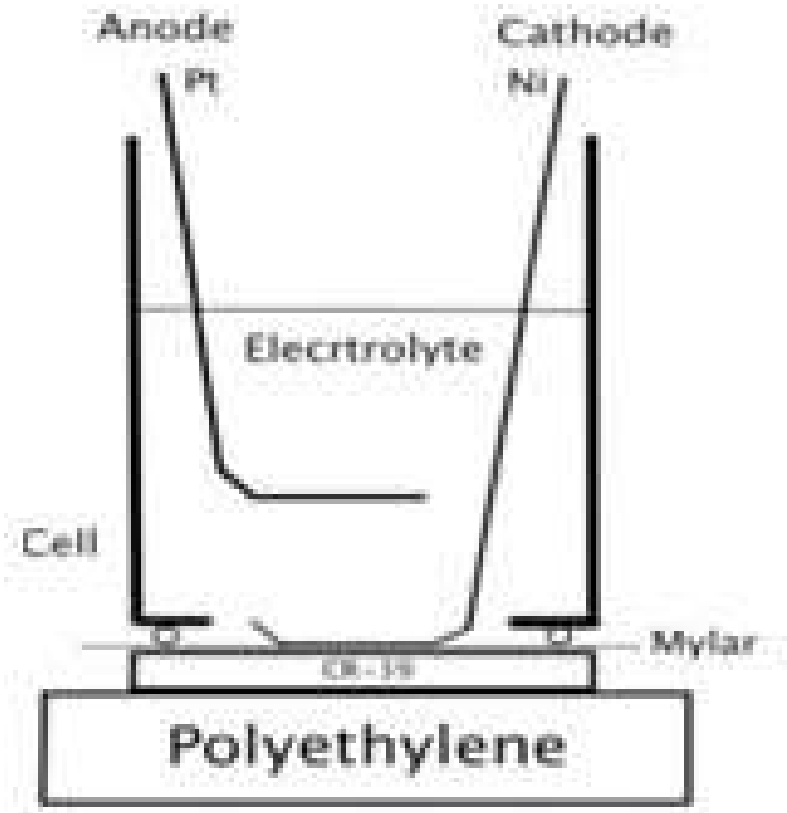

Figure 3. A generic diagram for our electrolytic cells. Small circles are cross sections of the compressed O-ring.

control surfaces, 87–59 = 28 tr/cm^2 was not statistically significant, considering small numbers of examined surfaces.

The mean and standard deviation on six of M.H.'s experimental surfaces were185 and 73 tr/cm^2. The mean and standard deviation on his eight control surfaces were 192 and 72 tr/cm^2. This information was also used to justify the statement that the reported difference between mean track densities on experimental and control surfaces, 185–192 = –7 tr/cm^2 was not statistically significant.

The mean and standard deviation on eight of J.D.'s experimental surfaces were 98 and 17 tr/cm^2. The mean and standard deviation on his six control surfaces were 125 and 29 tr/cm^2, respectively. This information was used to justify the statement that the reported difference between mean track densities on experimental and control surfaces, 98–125 = –27 tr/cm^2 was not statistically significant.

The mean and standard deviation on nineteen of L.K.'s experimental surfaces (excluding three exceptional surfaces from experiments 13, 14 and 15 — see below) were 16 and 8 tr/cm^2. The mean and standard deviation on his 16 control surfaces were 14 and 5 tr/cm^2, respectively. This information was used to justify the statement that the reported

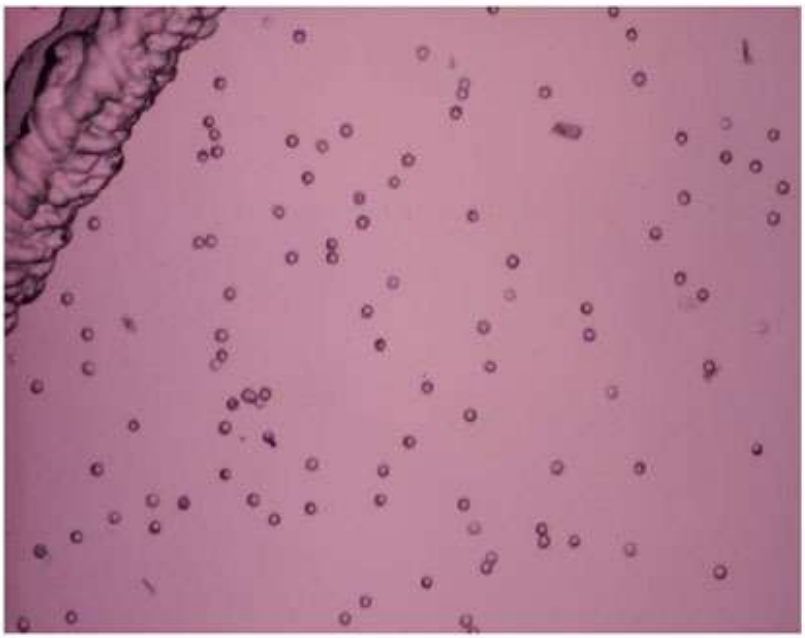

Figure 4. A CR-39 surface seen under the magnification of 40, after 12 h of etching. Small circles are pits due to alpha particles from an Americium source. The upper left corner shows a mechanically damaged area.

difference between mean track densities on experimental and control surfaces, 16–14 = 2 tr/cm^2 was not statistically significant. In other words, experimental results from our four sets of experiments are consistent with each other. But they are not consistent with the results reported by Oriani.

Let us address the issue of extremely high track densities on three surfaces from experiments 13, 14 and 15. The estimated track density on the up-facing surface of the CR-39 chip from Experiment No. 13 were around 15,000 tr/cm^2. This is two orders of magnitude higher than typical densities reported by Oriani [6]. The other side of the chip had nothing but the usual background. The area covered by copious tracks, nearly two square centimeters, matched the circle delimited by the O-ring. Distribution of tracks in that area was more or less uniform, except near the boundaries, where the track density decreased progressively.

Copious tracks from Experiment Nos. 14 and 15 were very different from Experiment No. 13. On these two surfaces, tracks were concentrated in small areas, near a hole drilled in each CR-39 chip. The holes were drilled to facilitate etching; each CR-39 chip was suspended in the etching solution by means of a thin copper wire threaded through the hole. These copper wires were from a telephone cable of unknown origin. The area covered by copious tracks from Experiment No. 14 was about 10 mm^2; the estimated track density was 200,000 tr/cm^2. The area covered by copious tracks from Experiment No. 15 was approximately 3 mm^2; the estimated track density was close to 12,000 tr/cm^2. Track densities outside of the small affected areas were about the same as on control chips.

It is remarkable that in each of the three cases of high track density, the mean density on the other side of the chip was essentially the same as on the control chips. That is very different from what was reported in [4]. The most likely cause of copious tracks was migrating radioactive contamination. Attempts made to identify it were unsuccessful. Alpha

radioactive substances such as uranium, thorium and radium are known to be present in our environment. One nanogram of radium, for example, emits 37 alpha particles per second. Testing of nuclear weapons in the 1960s contributed to contamination of our environment with long-lasting radioactive isotopes, tritium and uranium for example. Note that track densities on our three exceptional surfaces were much higher than those reported in [4].

Project participants worked independently of each other in four different states. Collective results, shown in Table 1, became available to participants only after their own results were submitted to L.K. He collected results after counting tracks on his own CR-39 surfaces. Note that Experiment No. 12 was performed without using the Mylar film. Low track densities resulting from this experiment seem to indicate that all experiments could have been performed without Mylar. Oriani used Mylar to protect the CR-39 from potential chemical effects. Most tracks on control chips were probably due to natural background, most likely due to radon, radium, etc. Concentrations of such substances are known to be location dependent. That fact was probably responsible for differences between mean track densities on the control chips of individual researchers.

4. Conclusion: Facts and Interpretations

The purpose of our four independent investigations was to find evidence for reproducible emission of nuclear particles described in Oriani's 2008 paper [4]. No such evidence was found. We examined 40 CR-39 surfaces and found only three cases of excessive tracks. No excessive tracks were found on the remaining 37 surfaces.

We do not know why we were not able to observe emission of charged nuclear particles (in a chemical process similar to Oriani's). There could have been a setup or procedural difference between the experiments. Further experimentation is needed to confirm the existence of nuclear particle emission in light water electrolysis, understand the causes of such

Table 1. Track densities on 34 surfaces of our experimental chips. No Mylar was used in Experiment No. 12.

Exp. No. ID	Experimental chip (upper side) tr/cm^2	Experimental chip (lower side) tr/cm^2	Control chip averages tr/cm^2
1 P.L.	20	28	
2 P.L.	125	148	59 (from five surfaces)
3 P.L.	89	94	
4 P.L.	99	91	
5 M.H.	128	118	
6 M.H.	128	192	192 (from eight surfaces)
7 M.H.	278	267	
8 J.D.	121	113	125 (from six surfaces)
9 J.D.	87	85	
10 L.K.	21	23	
11 L.K.	24	24	
12 L.K.	18	8	
13 L.K.	> 10000	11	
14 L.K.	10	> 10000	
15 L.K.	> 10000	17	14 (from 16 surfaces)
16 L.K.	31	20	
17 L.K.	23	8	
18 L.K.	12	24	
19 L.K.	10	8	
cr 20 L.K.	11	3	

emission and determine the conditions required for reproducibility.

Appendix: An Example of Statistical Analysis

The mean and standard deviation on eight of P.L.'s experimental surfaces were 87 and 46 tr/cm^2. The mean and standard deviation on his five control surfaces were 59 and 38 tr/cm^2. Is the difference between mean track densities on experimental and control surfaces, 87–59 = 28 tr/cm^2 statistically significant? To answer this question one must estimate uncertainties associated with actually measured track densities (87 and 59). The uncertainty about 87 is 46/2.8 = 16, where 46 is the reported standard deviation while 2.8 is the square root of 8 (the sample size consisted of eight surfaces). Likewise, the uncertainty about 59 was 38/2.23 = 17 tr/cm^2, where 2.23 is the square root of 5 (the sample size consisted of five surfaces).

The difference of 28 tr/cm^2 is too small to be significant, considering large uncertainties associated with the reported mean densities (59 and 38 tr/cm^2).

The same approach was used to show that differences between mean values on experimental and control chips of –7, –27, and 2 tr/cm^2, as reported by M.H., J.D., and L.K. respectively, were also statistically insignificant.

Acknowledgement

Dr. Richard Oriani helped us to design experimental set-ups; Dr. Helen Roberts helped us to perform statistical analysis of experimental data. Constructive criticism from two anonymous referees was also highly appreciated.

References

[1] K.S. Krane, *Introductory Nuclear Physics*; Wiley, New York, 1987.
[2] M. Fleischmann, S. Pons and M. Hawkins, Electrochemically induced nuclear fusion of deuterium, *J. Electroanal. Chem.* **261** (1989) 301–308.
[3] R. A. Oriani and J.C. Fisher, Detection of energetic charged particles during electrolysis, in *Condensed Matter Nuclear Science,* edited by P. Hagelstein and S. Chubb, *Tenth International Conference on Cold Fusion Conference Proceedings*, Cambridge, MA 2003, pp. 577–584.
[4] R.A. Oriani, Reproducible Evidence for the Generation of a Nuclear Reaction During Electrolysis, *Proceedings of the 14th International Conference on Condensed Matter Nuclear Science*, Washington, DC, 2008 (in press).
[5] E. Storms, *The Science of Low Energy Nuclear Reaction,* World Scientific, Singapore, 2007
[6] F.M.F. Ng et al., *Nucl. Instrum. Meth. Phys. Res*. B **263** (2007) 266.

J. Condensed Matter Nucl. Sci. 5 (2011) 42–51

Research Article

Time-resolved Measurements of Loading Ratios and Heat Evolution in D_2 (and H_2)-Pd·Zr Mixed-oxide Systems

Akira Kitamura,* Yuki Miyoshi, Hideyuki Sakoh and Akira Taniike

Graduate School of Maritime Sciences, Kobe University, 5-1-1 Fukaeminani-machi, Higashinada-ku, Kobe 658-0022, Japan

Akito Takahashi, Reiko Seto and Yushi Fujita

Technova Inc., Uchisaiwaicho 1-1-1, Chiyodaku, Tokyo 100-0011, Japan

Abstract

Using a twin system for hydrogen absorption, we have studied heat evolution and high-energy particle generation by D_2 and H_2 gas absorption into nano-sized mixed oxide powders of palladium and zirconium. We have found very large energy of hydrogen absorption by Pd·Zr oxide compounds exceeding 1.0 eV/D (or H) together with a very high D/Pd loading ratio, exceeding 1.0. The system has been improved to enable time-dependent measurements of the gas flow rate and loading ratio simultaneously with the output heat. It has been revealed that the first phase is divided into two sub-phases; the 1a-phase, where most of the anomalously large output energy is produced with a very high loading, D/Pd $\approx$ 1.2, and the 1b-phase, where much smaller power is produced as loading increases further by a ratio of about 0.5 with a difference in pressure between deuterium and hydrogen.
© 2011 ISCMNS. All rights reserved.

Keywords: D/Pd loading ratio, Heat output, Pd·Zr oxide compounds, Time-resolved measurements, Two sub-phases

1. Introduction

The present work describes experiments on deuterium gas charging of palladium nano-powders in the form of Pd/ZrO_2 nano-composite. This work is a replication of Arata and Zhang [1], which was in turn a sophisticated, yet simplified, version of the Arata and Zhang's previous-generation experiments with double-structured reactors [2]. With the new configuration, Arata and Zhang report anomalous heat and helium-4 generation. If confirmed, this would be an extremely important phenomenon, so it is crucial that it be replicated if possible. Although successful replications using systems similar to the original double-structured reactor with Pd-black have been reported [3,4], few reports of replications of heat and helium-4 with the new configuration have been published.

We constructed an experimental system to replicate the phenomenon and to investigate the underlying physics [5,6]. The system is composed of two identical reaction chambers, what we call a "twin system" where the chambers

*E-mail: kitamura@maritime.kobe-u.ac.jp

© 2011 ISCMNS. All rights reserved.

are designated A_1 and A_2. Both chambers are equipped for calorimetry. A third chamber, designated B, is equipped for nuclear diagnostics. We have performed heat measurements as well as charged particle measurements under D_2 or H_2 absorption by a variety of palladium nano-powders [5–16] including: 0.1-μmϕ Pd powder (PP); 300-mesh Pd-black (PB); oxide composites of Pd·Zr (PZ); oxide composites of Pd·Ni·Zr (PNZ) and oxide composites of Ni·Zr (NZ). We have recently reevaluated the loading ratios D/Pd (or H/Pd) and E_1 based on a revised value for the volume of the of the reaction chamber, which we now estimate is 120 ml. The revised results are as follows:

(a) The loading ratio D/Pd $\approx$ 0.44 (H/Pd is also $\sim$0.44) and the first phase absorption energy $E_1 \approx 0.26$ eV/atom-D (or 0.20 for H) for the PP samples. These figures are in good agreement with those found in the literature [17–22]. The figures for both deuterium and hydrogen increase as a function of the fineness of the sample surface, where the PP samples have the roughest surface, followed by PB, and PZ is the finest.

(b) For the virgin PB samples, the loading ratios for both D/Pd and H/Pd = 1.3 ± 0.04 and the output energies in the first phase, $E_1 = 0.42 \pm 0.07$ eV/atom-D (or 0.39 for H). These values are 2–3 times larger than for the PP sample.

(c) The virgin PZ samples have shown outstanding performance with very high loading ratios D/Pd = 1.8 ± 0.3 (or 1.7 H/Pd) together with the high absorption energies E_1, or the deuteride (hydride) formation energy $Q_{D(H)}$ ranging from 0.92 to 1.4 eV/D (and 0.92–1.2 eV/H) depending on how much fraction of PdO_x reduction contributes to the measured values of D(H)/Pd and E_1.

(d) The PB and PZ samples have given substantially smaller D/Pd (and H/Pd) ratios and E_1 values in their recycled use. These are smaller than or nearly equal to those for the PP samples. We inferred that these are due to a clumping-together (aggregation) effect of palladium nano-particles.

(e) The outstanding performances of the PZ sample have been significantly restored by oxidizing a small amount (less than 10%) of the sample. The runs after forced oxidization allowed us to measure the hydridation energy, $Q_{D(H)} = 1.11 \pm 0.04$ eV/D (0.93 ± 0.09 eV/H), which is about 2 times larger than the adsorption energy, and 5 times larger than the absorption energy of a bulk-Pd-metal.

(f) In the second phase, we observed positive output, $E_2 \sim 2.5$ kJ/g-Pd for the deuterium runs employing both the virgin PZ and the used-PZ samples and the PNZ sample. However, this was only slightly above the margin of error, so it will have to be confirmed in further investigation.

In these experiments, we determined the amount of hydrogen isotopes absorbed/adsorbed by the samples of palladium from the gas flow rate multiplied by the duration of the first phase, with the gas flow rate being calculated from a rate of the pressure increase in the reaction chamber at the beginning of the second phase. This determination is reasonable if absorption ends completely when the second phase begins. Otherwise, D(H)/Pd will be underestimated.

In recent tests we have improved the experimental setup by equipping the sub-tanks with pressure gauges to directly measure the flow rate and the loading ratio [16]. Deuterium (or hydrogen) gas is stored in this sub-tank beforehand, and then absorption runs are initiated after closing the gas supply-valve on the head of the gas cylinder to close the system. With this improvement, we can make accurate time-resolved measurements of absorbed amount of gas as well as the flow rate. This enables a measurement of time-dependent sorption energy for each hydrogen isotope (differential heat of hydrogen uptake), which we describe in the present paper.

2. Experimental Procedure

The D_2/H_2 absorption system is composed of two identical chambers (A_1·A_2 twin system): one for a D_2 gas foreground run, and the other for an H_2 gas background run. As shown in Fig. 1, each of the twin systems has an inner reaction chamber containing palladium powder and an outer chamber that is evacuated to provide thermal insulation for calorimetry. The detailed description of the system is given in refs. [14,16]. The statistical error in the output power is

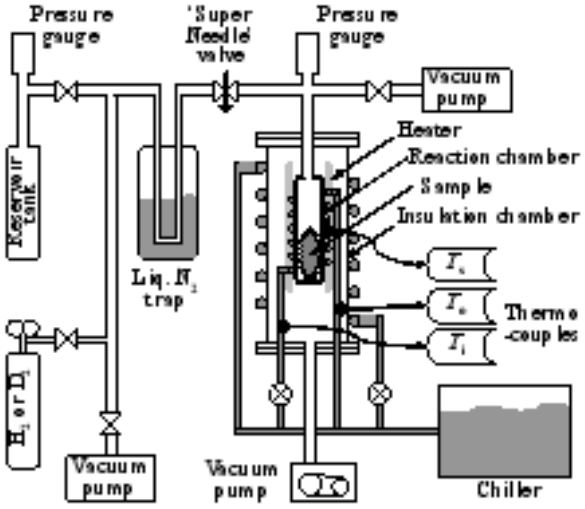

Figure 1. Schematic of one of the twin absorption systems.

evaluated based on the standard deviation of the longitudinal data, and is 0.67 mW. This is multiplied by the duration of the first phase to give the statistical error in the time-integrated output energy, e.g., 4.0 kJ for a 100-min run.

The data nomenclature is as follows. The run number is designated G-PN#M(A)(d), where G is the gas species (D or H); P the type of powder (PP, PB, PZ); N the powder identification number; and M the number of times the powder has been used. The number M is incremented when a sample is baked and then used in another absorption run. When the sample is reused without baking it, in what might be considered a continuation of the same run, the number M is not incremented. The letter A, B, or C is appended to the number instead. Thus, D-PZ11#3B indicates a run with deuterium, a PZ powder, powder identification number 11, which has been baked and run 3 times, and then run again without baking (run 3B).

Every absorption run is followed by a desorption run, which is carried out by evacuating the reaction chamber. This is an endothermic process. The thermal data has occasionally been processed and presented in the data tables with the run designation lower-case "d." For the example above, data from a desorption run following the 3B absorption run would be labeled DPZ11#3Bd.

The powder species used in the present paper are mixed oxides of Pd·Zr (PZ) fabricated by Santoku Corporation, Kobe, Japan.

To analyze the heat evolution, we assume that the chemical reaction that occurs during loading is described in Eq. (1) or Eq.. (2). These describe a combination of an oxygen pickup reaction during the formation of D_2O (or H_2O) with a reduction energy of Q_{red} (expressed as eV/atom-Pd) and a hydridation reaction during the formation of hydride atoms PdD(H) and surface adatoms with a reaction energy of $Q_{\mathrm{D(H)}}$ (eV/atom-D(H)).

$$\mathrm{PdO}_x + \left(x + \frac{y}{2}\right)\mathrm{D}_2 = x\mathrm{D}_2\mathrm{O} + \mathrm{PdD}_y, \tag{1}$$

$$\mathrm{PdO}_x + \left(x + \frac{y}{2}\right)\mathrm{H}_2 = x\mathrm{H}_2\mathrm{O} + \mathrm{PdH}_y. \tag{2}$$

Here a fraction x of Pd is assumed to have been oxidized and reduced by introduction of D_2 (H_2), while a fraction y of Pd is deuterized (or hydrized).

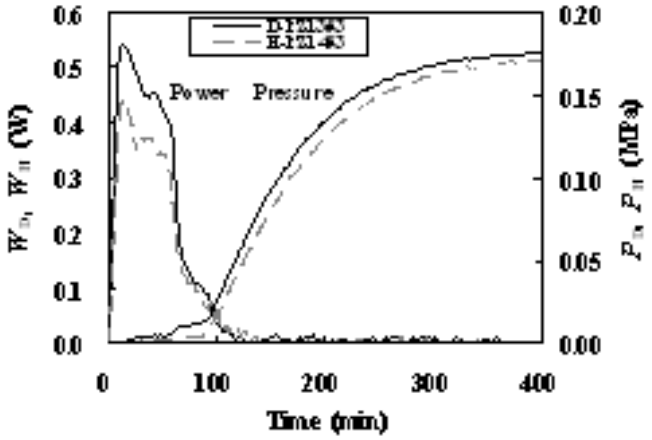

Figure 2. Typical variation of output power, W_D and W_H, and pressure in the reaction chamber, P_D and P_H.

The specific output energy, E_1 either in units of (kJ/g-Pd) or (eV/atom-Pd) is expressed as

$$E_1 = x\,Q_{\mathrm{red}} + y\,Q_{\mathrm{D(H)}}. \tag{3}$$

The fraction y and the energy $Q_{\mathrm{D(H)}}$ may include those of bulk hydride formation and adsorption to the palladium particle surface as well as other possible reactions. We take the value of Q_{red} = 1.85 eV/atom-Pd (or 1.68 for H) from the literature.

The value of y is calculated from the mass conservation law during the gas introduction through the Super Needle:

$$\frac{P_{\mathrm{R0}}V_{\mathrm{R}}}{N_{\mathrm{A}}kT_{\mathrm{R}}} = \frac{P_{\mathrm{R}}V_{\mathrm{R}}}{N_{\mathrm{A}}kT_{\mathrm{R}}} + \frac{PV}{N_{\mathrm{A}}kT} + \left(\ell x + \frac{y}{2}\right), \tag{4}$$

where (V_{R}, P_{R}) and (V, P) are the (volume, pressure) of the upstream (reservoir) tank and the downstream (reaction) chamber subdivided by the Super Needle, respectively, both including the connecting pipes. The left-hand side of Eq. (4) represents the amount (in mol) of D_2 (H_2) molecules in the reservoir tank before opening the Super Needle, and λ represents the fraction of liquid D_2O (H_2O), if any, generated as a result of the reduction. The third term on the right-hand side of Eq. (4) then represents the volume (in mol) of D_2 (H_2) molecules lost to liquefaction or absorption/adsorption. In the present experimental conditions it is assumed that the water molecules produced through the reaction (1) will remain in the gas phase, i.e., $\lambda = 0$.

To see the effect of oxygen, the sample was occasionally oxidized or deoxidized deliberately [14,16]. The value of x is calculated from the pressure decrease during the oxidization process.

3. Experimental Results and Discussion

3.1. Time integrated parameters in absorption/desorption runs for PZ samples

Typical variations of the output power, W_D and W_H, after the introduction of D_2 and H_2 gas are shown in Fig. 2 together with the pressure, P_D and P_H, in each reaction chamber for the PZ13 and PZ14 samples. As seen in the other runs described above, the pressure remains low during the main heat generation period, which we call the first phase.

In the absence of an apparent anomaly, the first phase heat is dominated by the chemical reaction of absorption and adsorption. In some cases, we have observed positive output in the second phase. In the runs described here, however, we observed no significant output, even when the reservoir pressure was increased to 1 MPa.

Table 1 and Fig. 3, which show the same results described in [16], summarize the parameters integrated over the first phase of the runs using PZ11 through PZ14; the specific output energy E_1 in units of both kJ/g-Pd and eV/atom-Pd, which is the time-integrated output power per palladium atom; the loading ratio y_D (y_H) at the end of the first phase, which is calculated from Eq. (4); and the hydridation energy calculated with Eq. (3). Here it is assumed that the water molecules produced through the reaction (1) will remain in the gas phase, i.e., $\lambda = 0$.

The results are briefly summarized as follows. The virgin PZ samples (No. 1 runs) have very large specific output energy, $E_1 = 2.28 \pm 0.42$ eV/atom-Pd for D-runs or $E_1 = 2.28 \pm 0.29$ eV/atom-Pd for H-runs on average, as well as very high loading ratios, D/Pd =2.31 ± 0.06 or H/Pd = 2.29 ± 0.03.

The specific energy E_1 for these "recycle" runs is more than one order of magnitude smaller than the virgin runs. The loading ratios, D/Pd and H/Pd, also decrease for the recycle runs to average values of 0.60 ± 0.10 and 0.49 ± 0.14 (by a factor of about 4), respectively. Accordingly, the hydridation energy $Q_{D(H)}$ also decreases for the recycle runs to average values of 0.27 ± 0.02 eV/D (0.30 ± 0.08 eV/H) (by a factor of about 3), respectively. These are consistent with those for the bulk (PP) samples.

We see essentially the same values for E_1, D/Pd (or H/Pd) and Q_D (or Q_H) in the No. 2 (deoxidized sample) runs as those in the recycle runs. However, the performance characteristics are largely recovered in the No. 3 runs by oxidizing the sample palladium to a small extent (a few percent). The averaged values are: E_1 =1.97 ± 0.1 eV/Pd, D/Pd = 1.72 ± 0.09 and Q_D =1.11 ± 0.04 eV/D for D-runs, and $E_1 = 1.37 \pm 0.06$ eV/Pd, H/Pd = 1.44 ± 0.16 and $Q_H = 0.93 \pm 0.09$ eV/H for H-runs. A detailed discussion of these results is found in [16].

3.2. Time-resolved parameters; loading ratio and specific absorption energy

Since we were monitoring the time-dependent pressure both in the reaction chamber and the reservoir tank constituting a closed system, we can calculate time-resolved loading ratio D(H)/Pd, defined as $L_{D(H)}(t)$, which is equal to the parameter $y_{D(H)}$ defined in Eq. (1), when we can assume that the water molecules, if any, have negligible volume, i.e., $\lambda = 0$.

Figure 4 shows $L_{D(H)}(t)$ as a function of pressure $P_{D(H)}$ in the first phase for D(H)-PZ13(14)No. 1, D(H)-PZ13(14)No. 2 and D(H)-PZ13(14)No. 3 runs. This relationship between the pressure and the loading ratio corresponds roughly to the absorption isotherm, since the temperature change during the run is smaller than a few degrees Celsius. We find a similarity between the traces for the No. 1 run (a) and the No. 3 run (c). In both cases there are two distinct phases, phase 1a and phase 1b. In phase 1a the choice of isotopes, deuterium or hydrogen, has no effect, while in phase 1b deuterium produces higher pressure.

The transition from the 1a-phase to the 1b-phase occurs at about 60 min for the No. 3 run, which is readily apparent in Fig. 2. The effect of the isotopes (deuterium or hydrogen) appears to be of the same nature as that in [24]. The pressure during the 1b-phase for the D-runs is about 10 kPa, while that for the H-runs it is about 5 kPa. Note that the No. 2 run has only the 1b-phase. The hydrogen uptake in the 1b-phase is $\Delta L_{D(H)} \approx 0.5$ in all cases. These values of the pressure and the hydrogen uptake are consistent with those extrapolated from the values found in ref. [24] which used 10-μm-thick palladium foils. From this we infer that the 1b-phase is characteristic of the bulk palladium absorption, and not of the surface adsorption. On the other hand, the 1a-phase is considered to be characteristic of the sample containing PdO, since the samples for the No. 2 runs have no oxygen.

From the above results we can exclude the possibility that the anomalously large D(H)/Pd might be due to condensation of D_2O (or H_2O) atoms into the liquid phase with negligible volume, i.e., an overestimation of D(H)/Pd (= y) due to a nonzero λ (cf. Eq. (4)). Condensation, if it could occur, would be in the 1b-phase at higher pressure. However, the

Table 1. Summary of the first phase parameters in absorption/desorption runs for PZ11 through PZ14 samples. Contribution of deoxidization (oxygen pick-up and water formation) to the output energy is not subtracted in calculating $Q_{D(H)}$ in the case of the virgin sample runs indicated with asterisks*.

Run No.	O/Pd (= x)	Specific output energy E_1 (kJ/g-Pd)	Specific output energy E_1 (eV/atom-Pd)	D/Pd(= y)	Q_D (eV/D)	Remarks
D-PZ11						
No. 1	Unknown	1.69 ± 0.05	1.86	2.37	0.79*	Virgin
No. 2	0	0.14± 0.01	0.16	0.56	0.28	Deoxidized
No. 3	0.086	1.88 ± 0.07	2.08	1.81	1.15	Oxidized
No. 3d	0	–0.13 ± 0.01	–0.14	–	–	
No. 3A	0	0.14 ± 0.01	0.15	0.56	0.27	
No. 3Ad	0	–0.11 ± 0.01	–0.12	–	-	
No. 3B	0	0.12 ± 0.01	0.14	0.49	0.28	
No. 3Bd	0	–0.11 ± 0.01	–0.13	–	–	
D-PZ13						
No. 1	Unknown	2.44 ± 0.13	2.69	2.25	1.20*	Virgin
No. 1d	0	–0.27 ± 0.03	–0.30	–	–	
No. 1A	0	0.16 ± 0.02	0.18	0.63	0.28	
No. 1Ad	0	–0.16 ± 0.02	–0.18	–	–	
No. 1B	0	0.15 ± 0.01	0.16	0.70	0.23	
No. 1Bd	0	–0.14 ± 0.01	–0.16	–	–	
No. 2	0	0.26 ± 0.06	0.23	0.59	0.39	Deoxidized
No. 2d	0	–0.17 ± 0.02	–0.18	–	–	
No. 3	0.073	1.69 ± 0.17	1.87	1.63	1.06	Oxidized
H-PZ12						
No. 1	Unknown	1.80 ± 0.13	1.99	2.26	0.88*	Virgin
No. 2	0	0.14 ± 0.01	0.16	0.45	0.35	Deoxidized
No. 3	0.054	1.18 ± 0.05	1.31	1.28	1.02	Oxidized
No. 3d	0	–0.10 ± 0.01	–0.11	–	–	
No. 3A	0	0.11 ± 0.01	0.12	0.41	0.29	
No. 3Ad	0	–0.10 ± 0.01	–0.11	–	–	
No. 3B	0	0.10 ± 0.01	0.11	0.44	0.25	
No. 3Bd	0	–0.09 ± 0.01	–0.10	–	–	
H-PZ14						
No. 1	Unknown	2.32 ± 0.12	2.56	2.31	1.11*	Virgin
No. 1d	0	–0.42 ± 0.05	–0.46	–	–	
No. 1A	0	0.13 ± 0.01	0.15	0.35	0.42	
No. 1Ad	0	–0.16 ± 0.02	–0.18	–	–	
No. 1B	0	0.16 ± 0.02	0.18	0.73	0.25	
No. 1Bd	0	–0.16 ± 0.02	–0.18	–	–	
No. 2	0	0.19 ± 0.04	0.21	0.65	0.33	Deoxidized
No. 2d	0	–0.14 ± 0.01	–0.22	–	–	
No. 3	0.061	1.29 ± 0.13	1.43	1.59	0.83	Oxidized

1b-phase is observed also in the No. 2 runs with no oxygen involved. Therefore, it is unlikely we have overestimated D(H)/Pd because of condensation.

We can define time-resolved specific sorption energy, or differential heat of hydrogen uptake, $\eta_{D(H)}(t)$, as the output energy per hydrogen isotope atom absorbed/adsorbed, which is calculated as the output energy during a time interval

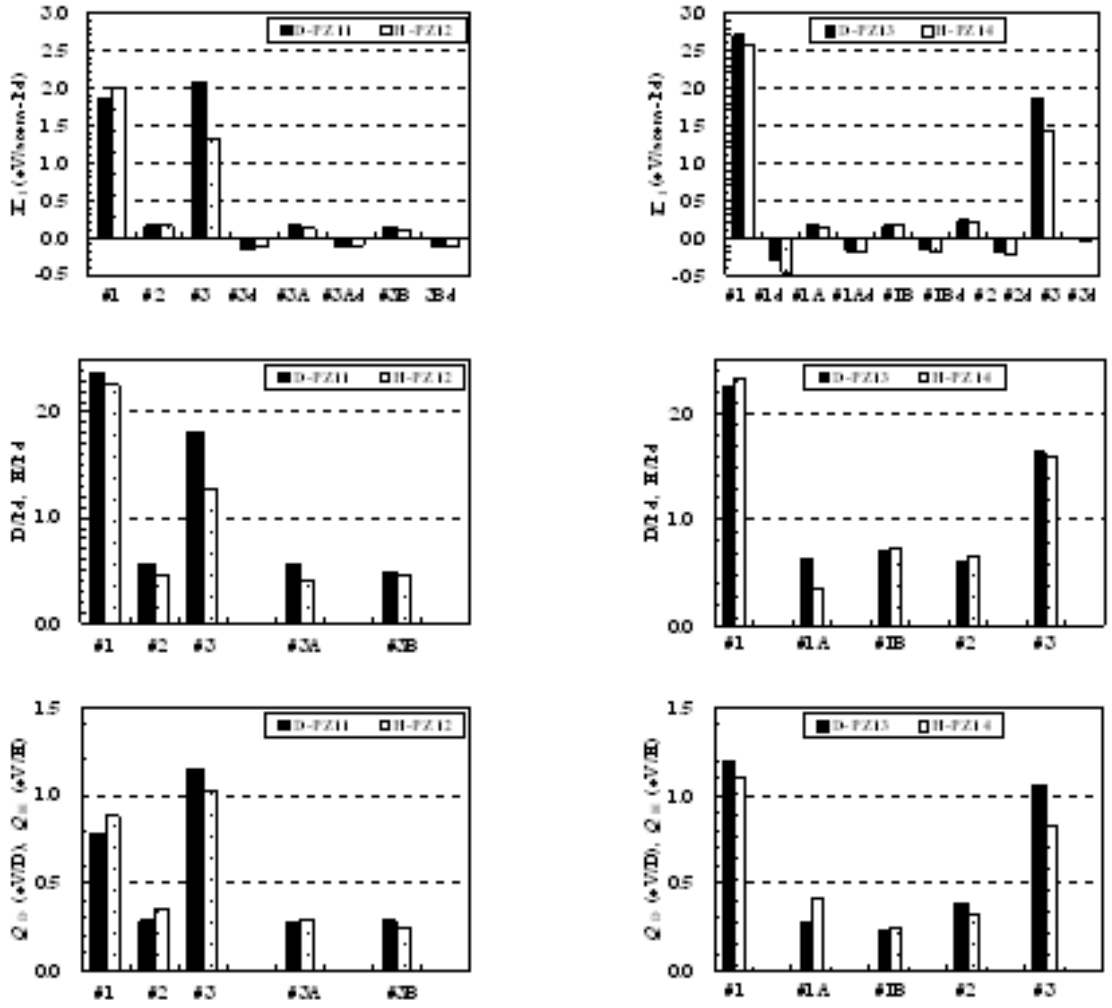

Figure 3. First phase parameters in comparison with D-runs and H-runs; specific output energy E_1, loading ratio D(H)/Pd, and hydridation energy $Q_{\mathrm{D(H)}}$.

τ divided by the increment of $L(t)$ in the same interval;

$$\eta(t) \equiv \frac{\int_t^{t+\tau} W_{\mathrm{s}}(t)\mathrm{d}t}{L(t+\tau) - L(t)}, \tag{5}$$

where $W_{\mathrm{s}}(t)$ is in unit of power per palladium atom including the contribution from the oxygen pickup reaction. The interval τ is arbitrary, and chosen here to be the time constant of the calorimetry system. For the samples with no oxygen involved, the hydridation energy $Q_{\mathrm{D(H)}}$ introduced above is equal to time-averaged value of $\eta_{\mathrm{D(H)}}(t)$ with τ being the first phase duration and $t = 0$. Since both $W_{\mathrm{s}}(t)$ and $L(t)$ are values per palladium (absorber) atom, $\eta_{\mathrm{D(H)}}(t)$ is independent of sample constituent, namely whether we use PZ or PNZ or other mixed samples.

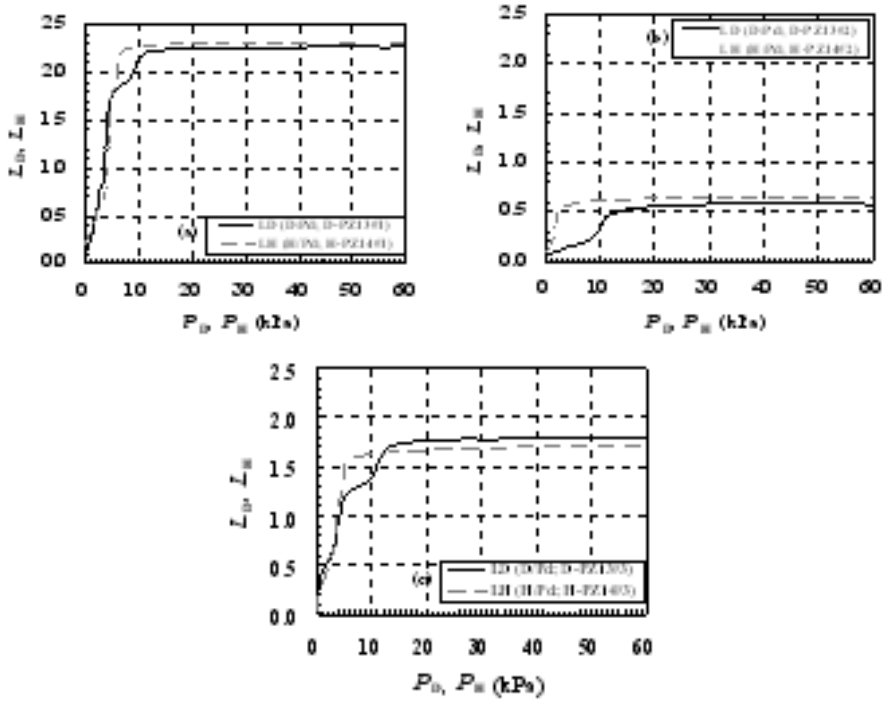

Figure 4. Time-resolved loading ratio, L_D and L_H, expressed as a function of pressure in PZ13(14)No. 1–3 runs. The first phase appears to be divided into 1a-phase and 1b-phase.

Figure 5 shows examples of time-resolved sorption energy $\eta_{D(H)}$ and loading ratio $L_{D(H)}$ compared with the output power $W_{D(H)}$ in the run D(H)–PZ13(14)No. 3. We notice here again that the evolution of heat has two phases divided at t = 60 min. The heat evolution associated with hydrogen isotope absorption/adsorption proceeds mainly in the low-pressure 1a-phase below ∼4 kPa. In a difference from $L_{D(H)}(t)$, a not-inconsiderable difference in the effect of the isotopes (deuterium or hydrogen) is observed for the heat evolution in the 1a-phase: $\eta_D \approx 1.33$ eV/D, while $\eta_H \approx 1.15$ eV/H. On the other hand, a relatively small amount of heat is generated in the 1b-phase from 60 to 100 min; $\eta_D \approx 0.47$ eV/D and $\eta_H \approx 0.41$ eV/H with a moderate isotope effect compared with that in the pressure mentioned above.

It has been found that most of the heat evolution from the samples in the 1a-phase only occurs when oxygen atoms are involved, and the 1b-phase with no oxygen produces much less heat. From this we might infer that the main heat source is the oxygen pickup reaction. However, it must be emphasized that $Q_{D(H)}$ obtained after the contribution of the deoxidization subtracted from E_1 is still anomalously large, being 1.11 ± 0.04 eV/D (or 0.93 ± 0.09 eV/H), as was shown in Table 1 and Fig. 3. Therefore, the main heat source in the 1a-phase is related to the presence of oxygen, but it is independent of the deoxidization reaction. From the fact that the 1a-phase proceeds at low pressure with little difference in the effect of the isotopes (deuterium or hydrogen) on pressure, we conclude that the heat source is on or near the surface of palladium nanoparticles, or that the reaction is triggered on or near the surface.

What is important is that the hydridation energy $Q_{D(H)}$ = 1.11 ± 0.04 (0.93 ± 0.09) eV/D(H) is much larger than the bulk hydride formation energy (≅ 0.2 eV) and the surface adsorption energy (≅ 0.5 eV). Huang et al. [23] have reported that differential heat of hydrogen uptake for hydrogen chemisorption reaches or even exceeds 1 eV/H for a

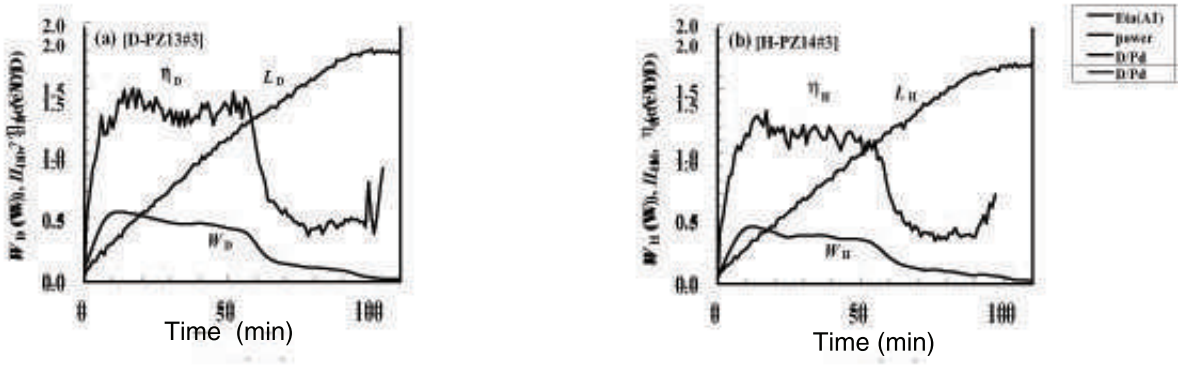

Figure 5. Time-resolved sorption energy $\eta_{D(H)}$, loading ratio $L_{D(H)}$ compared with the output power $W_{D(H)}$ in the run D(H)-PZ13(14)No. 3.

dispersed 2-nm-diameter palladium particles. In the present case of our Santoku samples, however, the mean diameter of the palladium nanoparticles is 10 nm, and oxygen incorporation is necessary for the large hydridation energy.

A phenomenological modeling and discussions on the role of the PdO layer of the Pd-nano-particle and possible mechanisms relating the anomalous heat component found in the present work to a nuclear origin are given in the separate papers [15, 25]

4. Conclusion

The hydrogen isotope absorption/adsorption system has been improved to enable time-dependent measurements of the gas flow rate and the D (or H) loading ratio simultaneously with the thermal output power. Runs using the samples after forced deoxidization and forced oxidization, as well as the virgin runs at room temperature, have revealed interesting facts. The first phase, in which chemical heat is produced, is divided into two subphases, after which the chemical heat is completed. In the 1a-phase, the predominant heat evolution is associated with hydrogen isotope absorption/adsorption, and proceeds under relatively low pressure below about 4 kPa with the specific sorption energy being $\eta_D \approx 1.33$ eV/D and $\eta_H \approx 1.15$ eV/H. In the 1b-phase, a relatively small amount of heat is generated under an isotope-dependent pressure of several to 10 kPa with $\eta_D \approx 0.47$ eV/D and $\eta_H \approx 0.41$ eV/H. It should be noted that samples tested after forced deoxidization exhibited only the 1b-phase. The 1a-phase only appears with samples incorporating oxygen.

References

[1] Y. Arata, Y. Zhang, The establishment of solid nuclear fusion reactor, *J. High Temperature Soc*. **34**(2) (2008) 85–93.
[2] Y. Arata, Y. Zhang, *Condensed Matter Nuclear Science*, *Proc. 12th Int. Conf. on Cold Fusion*, A. Takahashi, Y. Iwamura, K. Ota (eds.), World Scientific, Singapore, 2006, pp. 44–54.
[3] V.A. Kirkinskii, A.I. Kumelnikov, *Proc. ICCF13, Sochi,* Publisher Center MATI, Moscow, ISBN 978-5-93271-428-7, 2007, pp. 43–46.
[4] J.P. Biberian, N. Armanet, *ibid*. pp. 170–180.
[5] T. Nohmi, Y. Sasaki, T. Yamaguchi, A. Taniike, A. Kitamura, A. Takahashi, R. Seto, Y. Fujita, http://www.ler-canr.org; to be published in *Proc. 14th Int. Conf. Condensed Matter Nuclear Science (ICCF14)*, Washington, DC, 2008.
[6] Y. Sasaki, A. Kitamura, T. Nohmi, Y. Miyoshi, A. Taniike, A. Takahashi, R. Seto, Y. Fujita, *Proc. 9th Meeting of Japan CF-Research Society*, 2009, pp. 29–34; http://www.lenr-canr.org/acrobat/SasakiYdeuteriumg.pdf.
[7] A. Takahashi, A. Kitamura, T. Nohmi, Y. Sasaki, Y. Miyoshi, A. Taniike, R. Seto, Y. Fujita, *ibid.* pp. 35–41; http://www.lenr-canr.org/acrobat/TakahashiAdeuteriumg.pdf.

[8] A. Kitamura, T. Nohmi, Y. Sasaki, A. Taniike, A. Takahashi, R. Seto, Y. Fujita, *Phys. Lett.* A **373** (2009) 3109–3112.
[9] Y. Sasaki, A. Kitamura, Y. Miyoshi, T. Nohmi, A. Taniike, A. Takahashi, R. Seto, Y. Fujita, to be published in *Proc. 15th Int. Conf. Condensed Matter Nuclear Science (ICCF15)*, Rome, 2009; http://iccf15.frascati.enea.it/ICCF15-PRESENTATIONS/S7_O5_Sasaki.pdf.
[10] A. Takahashi, A. Kitamura, Y. Sasaki, T. Miyoshi, T. Nohmi, A. Taniike, Y. Furuyama, R. Seto, Y. Fujita, *ibid*., */S2_O4_Takahashi.pdf*.
[11] A. Kitamura, Y. Sasaki, Y. Miyoshi, T. Nohmi, T. Yamaguchi, A. Taniike, Y. Furuyama, A. Takahashi, R. Seto, Y. Fujita, *ibid*., */S3_O2_Kitamura.pdf*.
[12] A. Kitamura, A. Takahashi, Y. Sasaki, Y. Miyoshi, A. Taniike, R. Seto, Y. Fujita, to be published in *J. Condensed Matter Nucl. Sci.*
[13] Y. Sasaki, Y. Miyoshi, A. Taniike, A. Kitamura, A. Takahashi, R. Seto, Y. Fujita, Measurements of heat and radiation from Pd nano-powders during absorption of hydrogen isotopes, *Proceedings of JCF10 Meeting*, Japan CF-Research Society, 2010, paper JCF10-3.
[14] Y. Miyoshi, Y. Sasaki, A. Taniike, A. Kitamura, A. Takahashi, R. Seto, Y. Fujita, Absorption/adsorption processes of hydrogen isotopes observed for Pd nano-powders, *ibid*., paper JCF10-4.
[15] A. Takahashi, A. Kitamura, Y. Sasaki, Y. Miyoshi, A. Taniike, R. Seto, Y. Fujita, Role of PdO Surface-Coating of Pd Nano-Particle for D(H) Charging and Cluster Fusion, *ibid*., paper JCF10-5.
[16] A. Kitamura, Y. Miyoshi, H. Sakoh, A. Taniike, A. Takahashi, R. Seto, Y. Fujita, Anomalous heat evolution in charging of Pd nano-powders with hydrogen isotopes, submitted to *LENR-NET Source book 3, ACS*, J. Marwan (ed.)
[17] G. Alefeld, J. Voelkl (eds.), *Hydrogen in Metals II–Topics in Applied Physics*, vol. 29, Springer, Berlin, 1978.
[18] A Koiwai, A. Itoh, T. Hioki, Japan Patent 2005-21860 (P2005-21860A).
[19] C.P. Chang et al., *Int. J. Hydrogen Energy* **16** (1991) 491.
[20] M.M. Antonova, *Sboistva Gidriedov Metallov (Properties of Metal-hydrides)*, Naukova Dumka, Kiev, 1975; translated by NissoTsushinsha, Wakayama, 1976 [in Japanese].
[21] Y. Fukai, K. Tanaka, H. Uchida, *Hydrogen and Metals*, Uchida Rokakuho, Tokyo, 1998 [in Japanese].
[22] P. Chou, M.A. Vannice, *J. Catalysis* **104** (1987) 1–16.
[23] S.-Y. Huang, C.-D. Huang, B.-T. Chang, C.-T. Yeh, *J. Phys. Chem.* B **110** (2006) 21783–21787.
[24] R. Laesser, K.-H. Klatt, *Phys. Rev.* B **28** (1983) 748–758.
[25] A. Takahashi, A. Kitamura, Y. Sasaki, Y. Miyoshi, A. Taniike, R. Seto, Y. Fujita, Phenomenological Model on the Role of PdO Surface-Coating in CMNE D(H)-Gas Loading Experiments, to be published in *J. Condensed Matter Nucl. Sci.*.

J. Condensed Matter Nucl. Sci. 5 (2011) 52-71

Research Article

Energy Exchange In The Lossy Spin-Boson Model

Peter L. Hagelstein *

Research Laboratory of Electronics, Massachusetts Institute of Technology, Cambridge, MA 02139, USA

Irfan U. Chaudhary

Department of Computer Science and Engineering, University of Engineering and Technology. Lahore, Pakistan

Abstract

Excess heat in the Fleischmann–Pons experiment is observed without commensurate energetic particles, which is inconsistent with known nuclear reactions. Any proposed model must address this at the outset. At present, we recognize are two general approaches to the problem: mechanisms which transfer the reaction energy directly to a condensed matter mode, which requires the fractionation of a large quantum into many small quanta; mechanisms in which the large energy quantum is converted to kinetic energy over a very large number of neighboring nuclei. We have focused on the first approach, and we have found a model that seems to accomplish this. Here we introduce the model, which we call the "lossy spin-boson model". We find that energy exchange in the lossless spin-boson model is hindered due to destructive interference effects. Augmenting the model with loss removes the destructive interference, and we use perturbation theory on a specific example for illustration. Feshbach projection operators and the Brillouin–Wigner formalism which we adopt to describe loss in the model are reviewed in Appendix A.
© 2011 ISCMNS. All rights reserved.

Keywords: Coherent energy exchange, Excess heat, Fleischmann–Pons experiment, Lossy spin-boson model, Theory

1. Introduction

Over the past several years, we have been thinking about models relevant to excess heat in the Fleischmann–Pons experiment [1,2]. In these experiments, a prodigious amount of energy is observed, and ^{4}He is seen in the gas phase in amounts correlated quantitatively with the energy produced [3–5]; essentially no energetic particles are observed correlated with the energy [6]. This latter aspect of the experiments has drawn our attention over the years as being of particular importance.

To understand why, we consider briefly the situation in a "normal" nuclear reaction. In a Rutherford picture, the incident nuclei might be taken to be as classical particles, and similarly the product nuclei might also be thought about

*E-mail: plh@mit.edu

© 2011 ISCMNS. All rights reserved.

classically. Both energy and momentum are conserved in such a picture, so that the basic kinematic relations for the final state products can be determined from a knowledge of the reaction energy and initial state momenta and energies. A consequence of this is that the reaction energy in the case of deuteron-deuteron fusion ends up as kinetic energy of the proton and triton, or neutron and ^{3}He nucleus, in the final state. In the quantum mechanical description of the reaction, energy and momentum conservation similarly requires that the reaction energy appears as kinetic energy of the product nuclei.

In the Fleischmann–Pons experiment, there are no energetic particles commensurate with the energy produced. In light of the comments above, one might reasonably conclude that no nuclear reactions take place. But if so, then what is the source of the energy, and where does the ^{4}He come from? In the early days following the initial announcement of 1989, arguments were put forth that the energy was a result of chemical reactions, or experimental error [7]. The arguments against chemical reactions include the absence of observable commensurate chemical reaction products, and that the amount of energy is much greater in some cases than a chemical level of energy associated with all the atoms of the cathode and electrolyte. The primary argument against experimental error at this time is that the effect has been reported in a very large number of experiments [8,9], where different calorimeters and different types of calorimetry have been used.

So, what can be the resolution? Energy at the nuclear level is seen in many experiments, ^{4}He seems to be present as a product that is correlated with the energy produced, and yet there are no commensurate energetic particles as would be required in a Rutherford-type picture of a nuclear reaction. We are by now sure that energy is produced as an experimental fact; we are pretty sure that ^{4}He is produced as an experimental fact; and we are sure that commensurate energetic particles are not present as an experimental fact. In essence, some new kind of reaction seems to be taking place in a way inconsistent with the Rutherford picture of how a nuclear reaction is supposed to work.

If so, then where does the energy go? From experiment, we measure it as thermal energy; but whatever intermediate forms the energy might appear in prior to thermalization so far is hidden.

There is indirect evidence in the Letts two-laser experiment that the energy goes into optical phonon modes (in this experiment in particular) stimulated at the beat frequency, since excess heat persists after the lasers are turned off [10,11]. The theoretical question as to how such a thing might happen is at present an open one.

In our efforts to understand the effect, we have been interested in the possibility of the fractionation of a large energy quantum into a very large number of smaller energy quanta [12]. The basic idea is that the initial nuclear reaction energy will be measured in units of MeV, while the characteristic energy of an optical phonon mode as an oscillator is measured in units of meV. This suggests that perhaps the large nuclear quanta is somehow being split up into on the order of 10^8 smaller energy quanta. If a mechanism exists to accomplish this, then we might be able to understand how excess heat is produced in the Fleischmann–Pons experiment.

Although this approach has seemed perhaps the most plausible one to us, there is no precedent, and the majority of our colleagues favor various other approaches. Among the schemes that are presently being considered there are aneutronic fusion schemes in which the reaction products are hidden [13]; there is the approach of Kim wherein the reaction energy is somehow partitioned as kinetic energy among a very large number of deuterium atoms [14]; and there is the general approach of Widom and coworkers [15] where the reaction products are again hidden. There have been a great many proposals for reaction mechanisms put forth over the years, some of which are based on aneutronic mechanisms that are otherwise largely conventional. The intuition associated with such proposals is that a reasonably unreactive energetic product (such as an alpha) would be able to slow down and thermalize inside the cathode so as to be "hidden". The measurements described in [6] can be interpreted, based on direct calculations of the associated secondary yields, as placing an upper limit on the energy of a product alpha to be conservatively less than 20 keV. In essence, energetic alphas produced at the watt level cannot be "hidden" in a PdD cathode. Since ^{4}He appears as a primary product of the new process, this upper limit on the kinetic energy is a very severe constraint, and rules out the majority of proposed mechanisms involving ^{4}He that have been proposed. We do not think that it is possible to "hide"

commensurate energetic reaction products [6], and we do not understand what kind of direct physical mechanism is capable of distributing a large reaction energy (for example, 24 MeV) over more than 10^4 deuterium atoms as proposed by Kim.

In the case of direct coupling of the reaction energy into condensed matter modes, there is no real precedent for such an effect. The results outlined here follow from our recent studies of basic models involving two-level systems and harmonic oscillators that began around 2000. The thinking behind this kind of model was that the two-level system would stand in for two nuclear states with an MeV energy difference, and the oscillator would stand in for a vibrational mode of the lattice. The question of interest was whether there was any way to exchange energy coherently between the two systems; our earlier results (from the previous decade) suggested that that it would be extremely difficult to couple a relevant number of quanta directly from two-level systems to the oscillator. Computations of coupled systems were done under a variety of assumptions: weak coupling, strong coupling, linear interactions and nonlinear interactions. In these computations, energy exchange seemed to be restricted to less than 100 oscillator quanta at a time.

The situation changed qualitatively when we recognized that energy exchange in these systems was inhibited by massive destructive interference, which could be removed in lossy systems. We presented calculations at ICCF9 in 2002 which showed the basic effect [16]. We used a quantum flow formulation at that time, and carried out calculations which showed that coherence was maintained under conditions where up to 10^4 oscillator quanta were exchanged. This result seemed to us to be quite significant, since it showed that coherent energy exchange could occur between two-level systems and an oscillator with incommensurate quanta. Following the initial presentation at ICCF9, there seems to have been little outside interest in the result.

Subsequently, we devoted significant effort to better understand the new models. In the absence of loss, the early models that we had explored are equivalent to the spin-boson model which has received considerable attention in the literature [17–19] (but much less attention in regard to the issue of energy exchange in the multiphoton regime). We developed a rotation that allowed us to treat coherent multiphoton energy exchange in the spin-boson model in the same way as one would analyze linear coupling [20,21]. In this approach, we were able to isolate dressed states which were nearly degenerate, but "distant" with regard to the linear coupling of the model, and estimate the indirect coupling between them analytically.

The lossy problem is much harder, and to date we have not identified an analogous rotation that would allow a similar treatment of the problem. However, we have over the years applied a number of different techniques which have allowed us to characterize the model and establish important limits. In this manuscript, we begin our discussion of the lossy spin-boson model. We start with a brief consideration of the spin-boson model, and then augment the spin-boson model with loss using a Brillouin–Wigner loss operator. Since the projection operators of Feshbach and infinite-order Brillouin–Wigner theory were used more often in decades past, we provide a brief review in Appendix A. Finally, we demonstrate explicitly that indirect coupling between distant states is hindered by destructive interference in the spin-boson model using perturbation theory (which provides for the cleanest demonstration of the effect), and that the indirect coupling is not hindered in the lossy model (by considering the limit where the loss becomes infinite for states with an energy excess).

In the course of the review process, a great many criticisms were put forth by a reviewer, who wanted them to be addressed systematically in this paper. The issues of interest cover a lot of topics, and we chose to focus our attention on a subset of the problems so that papers of manageable size might result. Nevertheless, some of our colleagues thought that the associated discussion might be useful, so we have added selections of the reviewer's criticisms along with some responses in Appendix B.

2. Spin-boson Model Augmented with Loss

The spin-boson model is a popular model which includes two-level systems and an oscillator with linear coupling. Earlier versions of the model were investigated in association with NMR research about 70 years ago [17], and extended to problems involving atoms and electromagnetic fields about 35 years ago [18]. From our perspective, this Hamiltonian is interesting because it describes the most basic interaction between two fundamental quantum models (two-level systems and a harmonic oscillator), and more particularly, it sheds light on coherent energy exchange between the two systems when the two-level transition energy is a large multiple of the oscillator energy.

2.1. Spin-boson model

The Hamiltonian for the spin-boson model is [19]

$$\hat{H} = \frac{\Delta E}{\hbar}\hat{S}_z + \hbar\omega_0\hat{a}^\dagger\hat{a} + V(\hat{a}^\dagger + \hat{a})\frac{2\hat{S}_x}{\hbar}. \quad (1)$$

In this model, ΔE is the transition energy of the two-level systems, $\hbar\omega_0$ is the characteristic energy of the oscillator, and V is a coupling strength.

Our intuition might lead us to anticipate that energy exchange between the two systems should occur when the transition energy of the two-level systems is matched to the characteristic energy of the oscillator. This is so when the coupling is weak. If the coupling is stronger, and if there is a near resonance between the two-level transition energy and three oscillator quanta, then once again energy can be exchanged coherently. The reason that this works is that the system is able to maintain coherence over the time that several interactions occur, so that a nonlinear response is possible even though the coupling is linear.

We have explored energy exchange in this model in the multiphoton regime, with much larger numbers of oscillator quanta exchanged for a single two-level system quantum [20,21]. Unfortunately, coherent energy exchange in the multiphoton regime is a weak effect that requires very precise level matching. Coherent energy exchange at finite rates in this model is possible under moderately strong coupling for up to about 50 quanta at a time; for the exchange of even more quanta, the constraints on the degree of resonance becomes prohibitive, and the energy exchange rates become very small [23].

2.2. Lossy spin-boson model

If we augment the spin-boson model with loss, things change qualitatively in regard to energy exchange in the multiphoton limit as we will show later on in this paper. We write such a model as [22–24]

$$\hat{H} = \frac{\Delta E}{\hbar}\hat{S}_z + \hbar\omega_0\hat{a}^\dagger\hat{a} + V(\hat{a}^\dagger + \hat{a})\frac{2\hat{S}_x}{\hbar} - i\frac{\hbar\hat{\Gamma}(E)}{2}. \quad (2)$$

The loss term in this model is an operator that comes about from an infinite-order Brillouin–Wigner model as discussed in Appendix A. As written, this loss term is completely general, but we are thinking of it as being referenced to the oscillator so as to provide strong loss at energies in the vicinity of the two-level system transition energy.

In regard to the Fleischmann–Pons model, the oscillator here stands in for an optical phonon mode, so that $\hbar\omega_0$ is tens of meV. The transition energy ΔE for the two-level system is assumed to be associated with nuclear energy levels, on the order of MeV. The thought regarding the loss term here is that loss channels for the phonon mode open if the system has available several MeV of energy through the disintegration of nuclei that make up the phonon mode.

3. Indirect Coupling in Perturbation Theory

We have argued previously that the introduction of loss into the model leads to an enormous enhancement of indirect coupling between distant states that are nearly degenerate. To understand this better, if we consider a product basis state of the form

$$|S, m\rangle|n\rangle,$$

then the Hamiltonian leads to coupling between neighboring states of the form

$$|S, m \pm 1\rangle|n \pm 1\rangle.$$

If the two-level transition energy ΔE were matched to the characteristic energy $\hbar\omega_0$ of the oscillator, then this direct coupling would lead to coherent energy exchange on or near resonance. However, in the multiphoton regime of the model, we require the exchange of more oscillator quanta to bring the system back into energy balance. As a result, the closest states which are nearly degenerate are the distant states

$$|S, m-1\rangle|n+\Delta n\rangle,\ |S, m+1\rangle|n-\Delta n\rangle,$$

where Δn is the number of oscillator quanta exchanged. There is no direct coupling between $|S, m\rangle|n\rangle$ and these states; when the coupling constant is sufficiently large there can be a weak indirect coupling. It is this weak indirect coupling that we are interested in here.

3.1. Indirect coupling in perturbation theory with no loss

Indirect coupling is very weak in the lossless spin-boson model because of destructive interference. We can see this most readily in a perturbation theory calculation. As an example, we consider indirect coupling in the case where 5 oscillator quanta are exchanged between the nearly degenerate basis states $|S, m\rangle|n\rangle$ and $|S, m+1\rangle|n-5\rangle$.

We can develop the perturbative result that we are interested in starting from a finite basis expansion of the form

$$\begin{aligned}\Psi &= \sum_j c_j \Phi_j \\ &= c_1|S, m\rangle|n\rangle + c_2|S, m-1\rangle|n-1\rangle + c_3|S, m+1\rangle|n-1\rangle + c_4|S, m-2\rangle|n-2\rangle \\ &+ c_5|S, m\rangle|n-2\rangle + c_6|S, m+2\rangle|n-2\rangle + c_7|S, m-1\rangle|n-3\rangle + c_8|S, m+1\rangle|n-3\rangle \\ &+ c_9|S, m+3\rangle|n-3\rangle + c_{10}|S, m\rangle|n-4\rangle + c_{11}|S, m+2\rangle|n-4\rangle + c_{12}|S, m+1\rangle|n-5\rangle. \end{aligned} \quad (3)$$

The numbering here corresponds to the state definitions indicated in Fig. 1.

The finite basis equations for the coefficients can be written as

$$Ec_1 = m\Delta E + n\hbar\omega_0 + V_{1,2}c_2 + V_{1,3}c_3,$$

$$Ec_2 = (m-1)\Delta E + (n-1)\hbar\omega_0 + V_{2,1}c_1 + V_{2,4}c_4 + V_{2,5}c_5,$$

$$\vdots$$

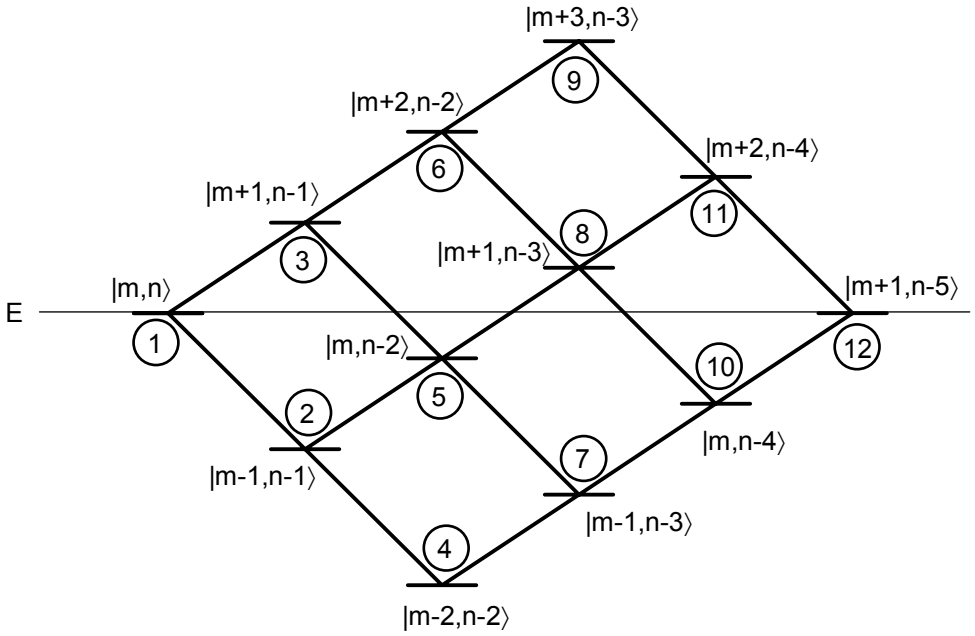

Figure 1. Basis states involved at lowest order in perturbation theory for indirect coupling with the exchange of five oscillator quanta.

$$Ec_{12} \;=\; (m+1)\Delta E + (n-5)\hbar\omega_0 + V_{12,10}c_{10} + V_{12,11}c_{11}. \tag{4}$$

To develop these equations, we require the diagonal and off-diagonal matrix elements of the spin-boson Hamiltonian. The nonzero matrix elements are

$$\begin{aligned}
\langle n|\langle S,m|\hat{H}|S,m\rangle|n\rangle \;&=\; M\Delta E + n\hbar\omega_0,\\
\langle n+1|\langle S,m+1|\hat{H}|S,m\rangle|n\rangle \;&=\; V\sqrt{n+1}\sqrt{(S-m)(S+m+1)},\\
\langle n-1|\langle S,m+1|\hat{H}|S,m\rangle|n\rangle \;&=\; V\sqrt{n}\sqrt{(S-m)(S+m+1)},\\
\langle n+1|\langle S,m-1|\hat{H}|S,m\rangle|n\rangle \;&=\; V\sqrt{n+1}\sqrt{(S+m)(S-m+1)},\\
\langle n-1|\langle S,m-1|\hat{H}|S,m\rangle|n\rangle \;&=\; V\sqrt{n}\sqrt{(S+m)(S-m+1)}.
\end{aligned} \tag{5}$$

Since our focus is on the indirect coupling between $|S,m\rangle|n\rangle$ and $|S,m+1\rangle|n-5\rangle$, we can keep the corresponding coefficients c_1 and c_{12}, and eliminate the others algebraically. This leads to coupled equations of the form

$$\begin{aligned}
Ec_1 \;&=\; m\Delta E + n\hbar\omega_0 + \Sigma_1(E)c_1 + V_{1,12}(E)c_{12},\\
Ec_{12} \;&=\; (m+1)\Delta E + (n-5)\hbar\omega_0 + \Sigma_{12}(E)c_{12} + V_{12,1}(E)c_1.
\end{aligned} \tag{6}$$

Here $\Sigma_1(E)$ and $\Sigma_{12}(E)$ are self-energies, and $V_{1,12}(E)$ and $V_{12,1}(E)$ are indirect coupling coefficients. The lowest-order contribution to the indirect coupling coefficient $V_{1,12}(E)$ is obtained by summing over the different paths

$$V_{1,12}(E) = \frac{V_{1,2}V_{2,4}V_{4,7}V_{7,10}V_{10,12}}{(E-H_2)(E-H_4)(E-H_7)(E-H_{10})}$$

$$+\frac{V_{1,2}V_{2,5}V_{5,7}V_{7,10}V_{10,12}}{(E-H_2)(E-H_5)(E-H_7)(E-H_{10})}+\cdots, \tag{7}$$

where H_j is the diagonal matrix element of basis state j. There are 10 terms altogether in this summation. Assuming resonance $H_1 = H_{12}$, this sum can be evaluated in closed form to yield

$$V_{1,12}(E) = \frac{625}{64}\frac{V^5\sqrt{n(n-1)(n-2)(n-3)(n-4)}}{\Delta E^4}\sqrt{(S-m)(S+m+1)}. \tag{8}$$

3.2. Destructive interference

The indirect coupling term in the lossless case is very small due to destructive interference. This can be seen from a comparison of the summed indirect coupling coefficient $V_{1,12}(E)$ with the first term of the series of Eq. (7). We may write

$$\frac{V_{1,2}V_{2,4}V_{4,7}V_{7,10}V_{10,12}}{(E-H_2)(E-H_4)(E-H_7)(E-H_{10})} = \frac{625}{64}\frac{V^5\sqrt{n(n-1)(n-2)(n-3)(n-4)}}{\Delta E^4}$$

$$\sqrt{(S-m)(S+m+1)}\frac{(S+m)(S+m-1)(S-m+1)(S-m+2)}{36} \tag{9}$$

If the number of two-level systems is large, then S will be large. This term can be larger than the sum by a factor that can be on the order of $S^4/36$, which gives an indication of how effective destructive interference is for this case.

3.3. Indirect coupling in the lossy model

In the augmented version of the problem with loss, the destructive interference can be removed if the loss terms are sufficiently large. We can begin to see this in perturbation theory by using a finite basis approximation with the same basis states as we used above. This time, the first three expansion coefficients satisfy coupled equations of the form

$$Ec_1 = H_1c_1 + V_{1,2}c_2 + V_{1,3}c_3,$$

$$Ec_2 = (H_2 - i\hbar\Gamma_2/2)c_2 + V_{2,1}c_1 + V_{2,4}c_4 + V_{2,5}c_5,$$

$$Ec_3 = H_3c_3 + V_{3,1}c_1 + V_{3,5}c_5 + V_{3,6}c_6. \tag{10}$$

Intermediate states (such as Φ_2) which have energies less than E have decay modes available in this model, since the system can decay to such states if energy is lost through the decay processes modeled by the loss operator. Other states (such as Φ_3) which are in energy deficit as intermediate states do not have analogous decay modes available, and are

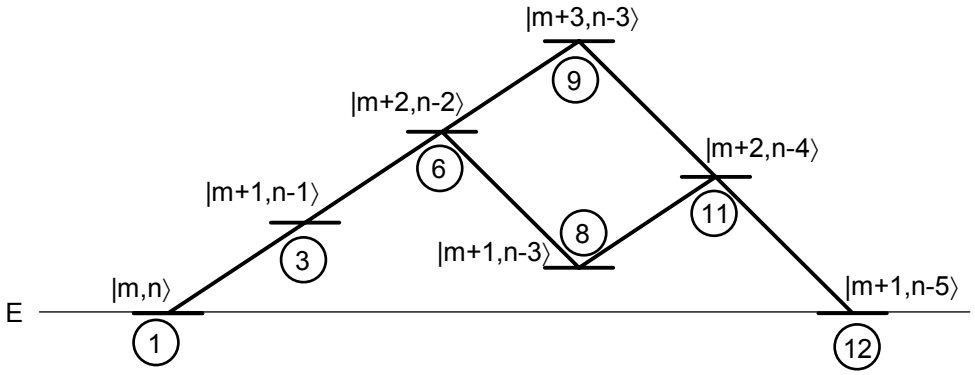

Figure 2. Basis states involved at lowest order in perturbation theory for indirect coupling with the exchange of five oscillator quanta in the limit of infinite loss.

free of loss in this model. States that are resonant (such as Φ_1 and Φ_{12}) are assumed to be stable against zero-energy decay processes.

The expression one obtains in such a model for the indirect coupling coefficient is very complicated, and not particularly enlightening. As we are interested in the issue of destructive interference between different pathways, we can eliminate the destructive interference completely by considering a model in which the loss terms are much greater than other terms that appear in the denominator. In the limit that the associated loss is infinite, then only pathways which include intermediate states in energy deficit contribute (see Fig. 2). In this limit we sum to obtain

$$V_{1,12}(E) \;\rightarrow\; \left[V_{1,12}(E)\right]_{\Gamma_j=0} F(S,M) \qquad (\Gamma_j \rightarrow \infty), \tag{11}$$

where the $\Gamma_j = 0$ result is given in Eq. (8), and where the factor $F(S, M)$ evaluates to

$$F(S,M) \;=\; \frac{(S-m-1)(S+m+2)(7S^2+7S-7m^2-23m-18)}{36}. \tag{12}$$

We see from this calculation that destructive interference greatly reduces the indirect coupling between distant resonant states in the original Dicke model, leading to a much larger indirect coupling matrix element.

4. Discussion and Conclusions

We are interested in the possibility that a large nuclear quantum of energy can be fractionated and exchanged with a condensed matter mode. To investigate this possibility, we have focused on the simplest basic physics model which exhibits coherent energy exchange between relevant quantum systems – the spin-boson model augmented with loss. This model is interesting in that it describes coherent energy exchange at usefully large rates under conditions where a large two-level system energy quantum is divided into a great many small energy quanta. In our most recent studies with more realistic and more sophisticated models, the indirect coupling appears to be strong enough to allow for coherent energy transfer at rates relevant to excess heat production in the Fleischmann–Pons experiment. This provides us with motivation for pursuing this model and its generalizations.

We presented the spin-boson Hamiltonian along with the generalization to the lossy version of the problem. Although one can find in the literature versions of the spin-boson model augmented with loss, these generalizations of the model

are usually concerned with oscillator loss near the characteristic frequency of the oscillator (so that the oscillator is damped). These models are qualitatively different from the one we have given, since we are interested in oscillator loss generally at higher frequency which produces a different physical effect.

We used perturbation theory to argue that indirect coupling between distant nearly degenerate states is hindered by destructive interference in the spin-boson model (without loss), and that this destructive interference is removed in the lossy problem when the loss is large. This establishes the most important property of the new model in a clean and obvious way, that it allows for very much enhanced indirect coupling.

The new model is moderately complicated despite its deceptively simple sector Hamiltonian, so it seemed helpful to provide a review of projection operators and infinite-order Brillouin–Wigner theory in Appendix A. This seems appropriate given that the version of the model that we have been studying is expressed using this formalism, and such a review may be helpful for our colleagues in the field.

It remains to establish the scaling of the new model with respect to its dimensionless coupling constant, to develop a formalism that allows us to understand it using a formalism based on indirectly coupled nearly degenerate states, and to establish formulas for the indirect coupling in the limit that a very large number of quanta are exchanged. These issues will be dealt with in following manuscripts.

Appendix A. Second-order Loss Models

From the earliest days of quantum mechanics, the inclusion of loss into models has been of interest. Over the years a variety of different approaches have been introduced of varying degrees of complexity. In our work, we have made use of an approach which is sometimes called infinite order Brillouin–Wigner theory. While this approach was at one time a very standard approach, in recent years it has not been as popular as other methods. This motivates us to provide a brief review in this section.

Appendix A.1. Sectors

We consider a simple example of a system which has a set of states that we can identify readily in which the system resides prior to decaying, which we will refer to as $\{\Psi_a\}$; and a second set of states that we can readily associate with the system after it has decayed, which we will refer to as $\{\Psi_b\}$. By identifying these two distinct sets of states in this way, we divide the associated Hilbert space, or Fock space, into two different sectors.

We assume that there is a Hamiltonian $\hat{H}$ that is valid for all of the states of the system, and that eigenstates satisfy

$$E\Psi \;=\; \hat{H}\Psi. \tag{A.1}$$

We can divide the wavefunction Ψ into different pieces corresponding to the different sectors. One way to do this is to use projection operators ($\hat{P}$ and $\hat{Q}$) [25] so that

$$\Psi_a \;=\; \hat{P}\Psi, \qquad \Psi_b \;=\; \hat{Q}\Psi. \tag{A.2}$$

The first projection operator $\hat{P}$ separates out the part of the wavefunction Ψ that belongs in the first sector; and the second operator $\hat{Q}$ does the same for the second sector. If we assume that there are only two sectors of interest, then we may write

$$\hat{P} + \hat{Q} \;=\; 1. \tag{A.3}$$

Appendix A.2. Sector equations

We can take advantage of these operators to isolate the parts of the Hamiltonian $\hat{H}$ which refer to the different sectors, which leads to sector equations. We may write

$$E\hat{P}\Psi \;=\; \hat{P}(\hat{H}\Psi) \tag{A.4}$$

to project into the a sector. Since

$$\hat{H}\Psi \;=\; \hat{H}(\hat{P}+\hat{Q})\Psi, \tag{A.5}$$

we can expand and write

$$E\Psi_a \;=\; (\hat{P}\hat{H}\hat{P})\Psi_a + (\hat{P}\hat{H}\hat{Q})\Psi_b, \tag{A.6}$$

where we have used the identities

$$\hat{P}^2 \;=\; \hat{P}, \quad \hat{Q}^2 \;=\; \hat{Q}. \tag{A.7}$$

Similarly, we may write

$$E\Psi_b \;=\; (\hat{Q}\hat{H}\hat{Q})\Psi_b + (\hat{Q}\hat{H}\hat{P})\Psi_a. \tag{A.8}$$

Appendix A.3. Sector Hamiltonian with loss

The projection operators have allowed us to separate cleanly the problem into two pieces, but now we have a situation in which the coupling terms between the different sectors are not Hermitian. This is important, and also useful, since when there is loss we expect to lose probability from the first sector.

It is possible to eliminate Ψ_b algebraically from the a sector equation, which will produce a second-order Hamiltonian for the a sector that includes simple loss effects. We can do this by first writing

$$\Psi_b \;=\; [E-(\hat{Q}\hat{H}\hat{Q})]^{-1}(\hat{Q}\hat{H}\hat{P})\Psi_a, \tag{A.9}$$

which allows us to obtain the second-order equation for the a sector

$$E\Psi_a \;=\; (\hat{P}\hat{H}\hat{P})\Psi_a + (\hat{P}\hat{H}\hat{Q})[E-(\hat{Q}\hat{H}\hat{Q})]^{-1}(\hat{Q}\hat{H}\hat{P})\Psi_a. \tag{A.10}$$

The second-order term in general is complex; the real part is an effective potential, and the imaginary part gives rise to loss. We might express this as

$$\hat{\Sigma}(E) \;=\; \mathrm{Re}\Big[(\hat{P}\hat{H}\hat{Q})[E-(\hat{Q}\hat{H}\hat{Q})]^{-1}(\hat{Q}\hat{H}\hat{P})\Big], \tag{A.11}$$

$$-\frac{\hbar\hat{\Gamma}(E)}{2} \;=\; \mathrm{Im}\Big[(\hat{P}\hat{H}\hat{Q})[E-(\hat{Q}\hat{H}\hat{Q})]^{-1}(\hat{Q}\hat{H}\hat{P})\Big]. \tag{A.12}$$

Our sector Hamiltonian $\hat{H}_a$ might be written as

$$\hat{H}_a(E) \;=\; (\hat{P}\hat{H}\hat{P}) + \hat{\Sigma}(E) - i\frac{\hbar\hat{\Gamma}(E)}{2}. \tag{A.13}$$

Appendix A.4. Connection with Golden Rule decay

On the one hand, this might seem to be a rather strange Hamiltonian, since it depends explicitly on the energy eigenvalue E, and since it is not Hermitian if loss is present. On the other hand, this formalism can be very useful since it includes decay very simply, and since the loss term in the Hamiltonian is consistent with the Golden Rule decay rate [26]

$$\gamma \;=\; \frac{2}{\hbar}\left\langle \mathrm{Im}\left[(\hat{P}\hat{H}\hat{Q})[E-(\hat{Q}\hat{H}\hat{Q})]^{-1}(\hat{Q}\hat{H}\hat{P})\right]\right\rangle \;=\; \frac{2\pi}{\hbar}|\langle\Psi_b|\hat{Q}\hat{H}\hat{P}|\Psi_a\rangle|^2\rho(E_f). \tag{A.14}$$

The eigenvalues of this second-order a sector Hamiltonian are complex, so that if we solve

$$E\psi_a \;=\; \hat{H}_a(E)\psi_a \tag{A.15}$$

then we can find the associated decay rate for a state from

$$\gamma \;=\; -\frac{2}{\hbar}\mathrm{Im}\{E\}. \tag{A.16}$$

Appendix B. Reviewer Comments and Responses

T he first reviewer for this and the following paper had a great many criticisms. To address all of the issues raised by the reviewer in the main text did not seem to be a reasonable thing to do, as it would have greatly extended the length and complexity of the paper. Our approach has been to recognize at the outset that the problem of interest is complicated, and made up of a great many pieces, so that we might make progress best by focusing on a small number of issues at a time.

Some of our colleagues thought that the associated discussion was helpful. As a result, we have decided to include a subset of the comments (which we have in some cases restated or revised), along with some associated comments. In some cases these comments were those in our response, in other cases we have summarized comments from our response, and in yet others we have provided different and hopefully better comments.

Appendix B.1. On the need for many step-wise levels

As ^{4}He(E_x) nuclear excited states are known to be limited for E_x = 23.8, 23.35, 23.04, 21.04, 21.01, 20.21 MeV after the d+d reaction, possible electromagnetic transitions from the E_x = 23.8 MeV state are limited for step-wise emitting photon quanta of 0.45, 0.31, 0.03, 0.8, 20.21, 0.76, 0.83, 2.7, 3.6 and 23.8 MeV; even neglecting the spin-parity selection rule (as spin-parity of 23.8 MeV state is unknown). These are all easily measurable gamma-rays by an HPGe detector, but they are never observed. Therefore the proposed transition with very small quanta (30 meV; 3×10^{-2} eV) stepwise is not possible as the corresponding ^{4}He excited states do not exist step-wise.*

To avoid this difficulty, one must show that very fine (30 meV step, for instance) new levels with defined spin-parities are possible by the third interaction field. This is not done in the present paper (once Talbot Chubb proposed such an idea, but has never proved it by his theory).

This comment is the one most relevant to the technical content of our papers. From our perspective, we are grateful that the reviewer has spelled out this argument, since it very much helps to clarify a very pervasive misunderstanding about the models we have studied.

In the conventional spin-boson model, significant rates for coherent energy exchange occur when several tens of oscillator quanta make up a single two-level system quantum. There are no intermediate states available for a step-wise excitation as the reviewer has mentioned in the associated model. I note that there are reports of experimental results in which this kind of energy exchange has been observed directly, in agreement with the theoretical models.

I agree that many people have intuition that suggests that the only way to exchange a lot of quanta with an oscillator is by having a lot of equi-spaced levels. Many years ago, I started from the same place, and at one time I used this very argument to dismiss the possibility of energy exchange with a low energy oscillator. However, the argument is simply wrong. One does not need equi-spaced levels in order to exchange a large number of quanta with an oscillator. In the case of the spin-boson model, this was known at least as early as 1965 when Shirley's paper [18] appeared; there is now a sub-field that focuses on this regime (which is called the multi-photon regime in the literature). In our paper, we show that this is true for the lossy version of the spin-boson model, and obtain an analytic result in the simplifying case when the loss is infinite.

Appendix B.2. The Coulomb barrier problem

At the end of reading through the paper, the reviewer noticed a big problem. The paper does not describe about how to overcome the Coulomb barrier, for two deuterons to make their relative distance very close for inducing nuclear fusion reaction by the strong interaction under mutual very short range interaction (nuclear confinement) potential. Did they solve the problem in their past works? Probably not. The paper does not use the relative distance between two deuterons as key variable for solving wave functions of quantum-mechanical equations with defined Hamiltonians. As a consequence, the solution, how very close d–d pairs are realized in the assumed nuclear-lattice-phonon coupled-particle confining potential, is not shown.

The first two papers introduce the lossy spin-boson model; make clear that destructive interference is the reason that coherent energy exchange is hindered in the normal spin-boson model; demonstrates a strongly enhanced coherent energy exchange effect under conditions where a modest number of oscillator quanta are exchanged; and then presents a tool with which the we can analyze this kind of model. However, the reviewer wants to see a solution to the problem of tunneling through the Coulomb barrier, a discussion of excited states of ^{4}He, confining potentials, and many other topics as well. All of this is well out of the scope of the papers under consideration. The inclusion of material to deal with these issues would greatly lengthen the papers, and make them incomprehensible to readers.

Nevertheless, the Coulomb barrier appears in more sophisticated versions of the model, and we have worried a great deal about the associated tunneling contribution to the matrix element. We note that in a coherent reaction theory, the reaction rate can be linear in the matrix element, where the reaction rate goes as the square of the matrix element in incoherent reaction models [so the Gamow factor can come in as $\exp(-G)$ rather than as $\exp(-2G)$]. This provides a natural way within the theory to obtain a dramatic enhancement of the associated reaction rate while taking into account tunneling through the Coulomb barrier.

In early versions of our models from many years ago, we made use of the molecular D_2 potential to estimate the Gamow factor numerically. In recent years, we have found that the coherent reaction rate that results from such an assumption ends up being much too small to account for experimental observations. The inclusion of screening effects at the level of U_e near 100 eV greatly improves the agreement between model predictions and experiment. Such values for the screening energy U_e are close the those estimated in the Thomas–Fermi approximation by Czerski and coworkers [27], who obtain $U_e = 133.8$ eV for $PdD_{0.2}$.

Appendix B.3. Derivation of nuclear-phonon coupling

The imagined "direct coupling mechanism between nuclear excited states and solid-state lattice optical phonons (10^4 *quanta)" is not plausible in view of EM-nuclear-force coupling. First we need to treat nuclear-EM coupling and next we may treat succeeding coupling between EM-waves (virtual photons) and lattice optical phonons. The present paper does not consider such necessary path; hence, the proposed spin-boson model is in question.*

We have not included a derivation of the model in these papers in order to restrict our focus to a manageable set of issues.

So far, there does not seem to exist a theory in the literature that allows such computations to be done in the case of a D_2 to ^{4}He transition. We have in fact worked out a theory along the lines of what the reviewer suggests, and presented it at ICCF14 [28]. This approach can be used for coupling between molecular D_2 states and the ^{4}He ground state.

For transitions involving ground state nuclei as might be relevant to receiver systems in more complicated versions of the model, we are exploring phonon exchange associated with nuclear transitions that are dipole and quadrupole coupled to atomic electrons in the context of three- or more-level models.

The inclusion of associated discussions and derivations is out of the scope of the present set of papers. If we included such material here, the resulting modified papers would become very long, and would be difficult to read.

Appendix B.4. Magnitude of the coupling matrix element

The formalism of the "spin-boson model" seem OK, but only if the DIRECT and significant-magnitude coupling between the nuclear strong interaction (to MeV level intermediate compound state) and the lattice optical phonons exists. However, this is surely in doubt. Extending the elegant mathematics looks off-centered. The authors should explain the supporting logic of it. If not, the treated transition between two levels seems to be forbidden by itself; and it is nonsense to develop the mathematics associated with the coherent dynamics between the two levels.

We are not aware of a way to develop the effects of interest by pursuing transitions to intermediate compound states as seems to be required by the reviewer. We are also not aware of any general result that argues that phonon exchange is forbidden in association with transitions between different nuclear states.

We are able to derive the relevant phonon exchange matrix elements (as noted above), and the associated transitions are not forbidden as proposed by the reviewer.

Implicit in the reviewer's comment seems to be the notion that the reviewer would be able to tell if the coupling matrix element were sufficiently large to be relevant. This seems unlikely. From our perspective, one needs to analyze the models in order to figure out how large the coupling matrix elements need to be. It is only relatively recently that we have been able to establish such criteria for simplified versions of our models.

Appendix B.5. Adoption of a solution prior to solving the problem

It seems that they assumed that a d–d nuclear admixture or ^{4}*He* (probably its excited energy 23.8 MeV, or something else) intermediate excited state happened to appear abruptly (or a priori) without any proper reasons of substantially shown confining mechanisms. They assume superposition of two deuteron's wave functions are 100% both in the complex EM (electro-magnetic field) potential for many particles (palladium atoms, deuterons, electrons, lattice phonons, virtual photons for EM interaction) and in the strong interaction confining potential. Such an initial assumption is, unfortunately, common to other "theories" as Y. Kim's BECNF. Isn't the adoption of a solution before solving the*

problem a forbidden methodology in theory? Anyway, they started with the desired condition that a close deuteron–deuteron pair or $^4He^*$ (probably its excited energy 23.8 MeV) with very long life time (also unimaginable in nuclear physics) exists in the assumed nuclear-lattice-phonon coupled particle confining potential. The reviewer requires for the authors to explain how such a priori conditions can have consistent capability (proper logics in physics) to deduce proper solutions of the F-P excess heat problem or phenomenon if existing.

From our perspective, the biggest theoretical issue that must be addressed in response to the Fleischmann–Pons excess heat effect is coherent energy exchange under conditions where a large quantum is fractionated into a very large number of smaller quanta. As a result, we have studied very general models involving two-level systems and an oscillator, seeking a basic understanding of this new coherent energy exchange mechanism. This is the subject of the first two papers, and the three that follow.

If we had found that these general models were not capable of the coherent energy exchange effect of interest, then there would be no reason to pursue the identification of specific states and coupling mechanisms. So, the big question of interest initially is whether the effect can be demonstrated under any conditions or set of assumptions. Once this has been done, then possible reactions scenarios can be analyzed using results from the more general models.

In any event, the reviewer seems to want to focus on the specific states and pathways first, before developing the associated coherent dynamics models. From our perspective, had we been analyzing a much simpler incoherent reaction mechanism, then we would use the Golden Rule to evaluate the reaction rates, so that all that would be needed would be a specification of the initial, intermediate, and final state reaction channels (much as the reviewer would like to see specified here). However, coherent reaction dynamics are much more difficult to analyze. There is no simple general formula analogous to the Golden Rule for coherent reaction dynamics. For the idealized lossy spin-boson model under discussion in our papers, it has taken us five papers to develop tools and results sufficient to associate the model reaction rate to the relevant matrix elements. We need all of these results, and more, in order to begin to understand how coherent reactions involving specific reaction pathways might work.

Appendix B.6. Impossibility of describing d + d + particle reactions

The present paper never treats the nuclear excited state after the deuteron–deuteron reaction; the spin, parity, and isospin, with excited energy value, after "some external force interaction" (lattice optical phonons are out of this scope, in principle). Therefore the "spin-boson model" of the paper has no capability to tell the final state interaction of the (d + d) + "something" reaction going out to the ^4He ground state only, if at all, killing known break-up channels (p+t and n+^3He). Thus whole story becomes a desired scenario, a-priori chosen, in imaginary thought.

The reviewer appears to assume here that an additional particle is needed, as in d + d +"something". We know that in vacuum, ^{4}He when it occurs (with low probability) is accompanied by a 23.85 MeV gamma. Energy and momentum conservation in vacuum requires an additional particle, so that if another particle is present then it could result in another final state channel with ^{4}He and no gamma.

However, if we accept that experiments have been done where excess heat is observed, and where no significant neutron emission is correlated with the excess heat (with an upper limit near 0.01 n/J) [6], then we are forced to conclude that no reaction of this kind is going to be consistent with experiment. Let us consider systematically the possibilities in the case that d + d + something is in the input channel, and ^{4}He + something is in the output channel, with a 24 MeV reaction energy:

- ^{4}He + Pd (an example where the alpha energy is maximized), with the alpha particle ending up with about 23 MeV. Although fast alphas are not penetrating, they cause α(d,n+p)α deuteron break-up reactions with a

high yield, with fast neutrons that are penetrating. We calculated an expected yield of 10^7 n/J, which is nine orders of magnitude above the neutron per unit energy upper limit from experiment.

- ^{4}He +d (since there are deuterons in the system), so that the alpha particle ends up with about 8 MeV. We would expect about 10^4 n/J from the same alpha-induced deuteron break up reaction, which is now six orders of magnitude above experiment. However, the deuteron will have 16 MeV, which would make dd-fusion neutrons with a yield of just under 10^8 n/J, which is a bit less than 10 orders of magnitude above the upper limit from experiment.
- ^{4}He+p, so that we get the minimum alpha particle recoil for any nucleus, and the alpha ends up with 4.8 MeV. The number of secondary neutrons produced as a result of primary collisions between the alphas and deuterons in the lattice now is reduced to about 200 n/J, which is about four orders of magnitude above the experimental limit. The energetic protons in this case would cause deuteron break up reactions with a yield near 10^7 n/J, which is nine orders of magnitude above the experimental limit.
- ^{4}He+e, which gives close to the minimum alpha recoil for any single particle, and the alpha ends up with about 76 keV. Now the secondary neutron emission due to the alphas is down to 10 n/J, only three orders of magnitude above experiment. However, penetrating 24 MeV electrons produced at the watt level would again constitute a significant health hazard for any experimentalists nearby. For an experimentalist within a meter of an experiment producing a watt of 24 MeV betas, the radiation dose would be on the order of 1 rem/s (assuming a 10 cm range) which would be lethal in about 1 min.
- ^{4}He+γ, again giving 76 keV recoil energy for the alpha, and again 10 n/J which is again three orders of magnitude above experiment. Penetrating 24 MeV gammas at the watt level would be a major health hazard for any human beings in the general vicinity. As in the case of fast electrons, 24 MeV gammas at the watt level would be lethal for an exposure of about 1 min at a meter distance.
- ^{4}He + neutrino (as advocated by Li), also gives 76 keV recoil energy for the alpha, so we would expect three orders of magnitude more neutrons than the experimental upper limit. The neutrinos in this case are not a health hazard, and we would not know from direct measurements if they were there. However, most of the reaction energy would go into the neutrinos, so that the observed reaction Q-value would be about 76 keV, which differs from the experimental value by about 300.

We can conclude from this that no reaction scheme based on d + d + particle is capable of being consistent with the experimental upper limit on neutron emission in association with energy production, with the observed Q-value (energy produced per ^{4}He observed), and with the absence of lethal amounts of electrons, gammas or other light particles.

Appendix B.7. Impossibility of killing off 3+1 channels

... Therefore the "spin-boson model" of the paper has no capability to tell the final state interaction of the (d + d) + "something" reaction going out to the ^{4}He ground state only, if at all, killing known break-up channels (p + t and n + ^{3}He) ...

The reviewer seems to require some particle and associated mechanism to "kill off" the n + ^{3}He and p + t exit channels, and faults the two-level system description as not being able to deal with this. If we focus on the two-level system part of the problem alone (since the optical phonon modes are associated with the oscillator), then there is no ability to describe in detail the microscopic physics that the reviewer believes is required in the final state to "suppress" the primary deuteron–deuteron fusion channels, and hence favor ^{4}He.

In our view, there is no way to suppress the fast n + ^{3}He or p+t decay channels; with, or without, an additional particle present. When two deuterons approach each other sufficiently close for conventional fusion reactions to occur,

the 2+2 to 3+1 reactions proceed about as fast as the laws of physics allow, and there is not much that is going to stop them from happening. The reviewer seems to suggest that these channels need to be killed off somehow, perhaps through the introduction of a third body. Now, if one were to pursue such an approach, and if one were to start from the conventional fusion branching ratios, then one would need to kill off the 3+1 channels by about 11 + 7 = 18 orders of magnitude relative to the ^{4}He channel to be consistent with experiment (11 orders of magnitude for the observed branching ratio, and 7 since the ^{4}He branch occurs at a rate much slower than the 3+1 channels). From our perspective, this is simply impossible.

Our approach has been instead to focus on coherent dynamics mechanisms, which work differently. So, instead of trying to change the existing incoherent reaction pathways (which we don't think can be changed significantly anyway), our view is to focus on new coherent mechanisms that might be able to happen in addition to the existing incoherent reactions. In the end, to determine relative reaction rates, one need compare a coherent rate to an incoherent rate. There seems to be no fundamental problem in having a coherent rate be orders of magnitude larger than an incoherent rate.

We have pursued more sophisticated models in which there are more sets of two-level systems. In these models, one set of two-level systems is responsible for converting a large quantum into many small quanta. Since matrix elements between the D_2 and ^{4}He system is hindered by Coulomb repulsion, the associated coupling is very small, which means that there is no way to exchange significant energy with the lattice in the simple lossy spin-boson model. In these more sophisticated models, the energy from the D_2/^{4}He system is transferred to other transitions, which then convert it to phonon mode excitation. In this case, all that we require is a single phonon exchange to convert molecular D_2 to ^{4}He. We can compute the incoherent reaction rate for decay to 3+1 channels on the same footing as for the coherent reaction pathway, and we can find conditions under which the coherent pathway is many orders of magnitude greater.

Appendix B.8. Neutron detection not done with calorimetry

The authors mixed up various measurements for independent items under different conditions to conclude as if all the measured data took place simultaneously in one experiment.

In our Naturwissenschaften paper (Ref. [6]), we cited five experiments in which neutron detection was operating when excess heat bursts were seen.

- In the case of the Oak Ridge result (Scott et al. [29]), a graph showing the level of neutron emission during the time at which excess heat was seen is presented in Fig. 6 of a preliminary version of their conference proceeding paper for ICCF1 [30].
- In the case of the OSU result (Klein et al. [31]), one can see plotted temperature excursions and neutron emission levels on the same graphs as a function of time in Figs. 2–4 in their AIP conference proceedings paper.
- In the *J. Fusion Energy* paper of Wolf et al. [32], one finds written: "The correlation of the results on neutrons, tritium, and heat production has proved to be negative. Obvious heat generation (ignition) by a Srinivasan cell was not accompanied by neutron emission, and none of these cells show tritium production despite an indication of 5–15% excess heat."
- In the ICCF3 paper by Takahashi et al. [33], results for excess heat measurements and neutron measurements using the L-H current protocol are given in Fig. 7.
- In the ICCF4 paper by Gozzi et al. [34], Fig. 9 shows excess heat results for cell #10, and Fig. 12 shows neutron counts for various neutron detectors for the same acquisition period, where detector #1 is reasonably close to cell #10.

In these references, experiments were discussed in which neutron detection ran monitoring cells that produced

excess power. In all of these cases, one of the points of the experiments reported was to determine whether the neutron emission was correlated with excess heat production. There are additional experiments that have been done in which excess heat was reported also with neutron detection operational; however, only in the references we used were we able to develop quantitative estimates in terms of source neutrons per unit energy. From the information reported in the papers cited in Ref. [6], it seems clear that neutron measurements were done on cells that produced excess heat, when they produced excess heat, in contrast to the claim of the reviewer.

Appendix B.9. Absence of energetic particles not yet proven

An experimental proof showing noncorrelation of energetic out-going particles and claimed (not reproducible) excess heat in Fleischmann-Pons type electrolysis experiments is not clear at all. Accurate experimental works accurately measuring time-dependent correlations between excess heat, helium, alpha-particles with their energies, neutrons with their energies, gamma-rays, X-rays, and low energy photons has not been given. Some experiments measured once-through excess heat without accurate nuclear radiation detection; others measured nuclear radiation somehow accurately, but the calorimetry was poor, or else there was no calorimetry. Therefore the argument in Ref. [6], which is the starting assumption of paper is not certain, or wrong.

The very restricted view of choosing only one scenario out of Takahashi's four scenarios ([3]) is in question. The true status is that we do not have enough experimental evidences showing on-line correlations between excess heat (irreproducible), neutrons (unknown energy), alpha-particles or helium (unknown energy), gamma-rays (unknown energy), X-rays (unknown energy), EUV, EV, visible light, etc. data. Nobody has made successfully such experiments. Due to the irreproducibility of Fleischmann-Pons excess heat experiments, we do not have definite logics to make such a narrow-focus conclusion as done by Hagelstein [6]. It is premature and dangerous.

I will be the first to agree with the reviewer that more experimental results are needed generally in the field. The controversy that has plagued the field has resulted in funding difficulties, so that a great many experiments that we would like to be done have not managed to get done. As a result, in our considerations today we are forced to deal with the experimental data set that is available today, imperfect as it may be. If new experiments are done in the future, we can revisit the associated issues.

Perhaps the most significant issue in response to what the reviewer has written concerns a misconception that you need to diagnose for all kinds of emissions ("helium, alpha-particles with their energies, neutrons with their energies, gamma-rays, X-rays, low energy photons") in order to be able to say something about whether there are energetic particles in the exit channel. In this, the reviewer is simply incorrect. The point of the discussion of Ref. [6] (and also of related papers [35–37] that appeared last year in the CMNS journal) is that if you think ^{4}He is a reaction product, then you can say something about how much energy it has, since energetic alphas make primary or secondary neutrons very efficiently in PdD.

You do not need to detect the alphas directly, or measure their energies, for the purpose of this argument. If there are no commensurate neutrons produced, then you can be sure that there are not a corresponding number of energetic alphas as determined by the yield functions given in [6] (and in the other papers published in the CMNS journal). If the neutrons aren't there, you do not need to measure gamma-rays or X-rays to answer the question of whether there are a lot of fast alphas – there aren't, or else you would have known from the neutron measurements.

The reviewer argues that inaccurate calorimetry impacts the issue of whether commensurate energetic alphas are present. Now, let us suppose that the calorimetric errors are as large as a factor of 2 (which is substantially larger than the claimed accuracy in the different papers used in [6]). In this case, we might take the excess power to be less by 2x, which would increase the upper limits for neutrons per Joule by 2x. So, an upper limit in this case might go from 0.01 to 0.02 n/J. This does not help very much since from the examples given above, we would need on the order of 9 or

10 orders of magnitude more in order to have consistency between the number of neutrons expected and the number of neutrons seen for the different proposed incoherent reaction mechanisms with a two-body exit channel (that are not fatal to the experimentalists, and have roughly the right ratio between energy and amount of helium).

Results from reproducible experiments are preferred. But the reviewer seems to be suggesting that observations taken in the case of experiments where the reproducibility of the excess heat effect is less than 100% should be ignored. From our perspective, the issue as to whether there are energetic alphas involves a very large numbers of neutrons, so that having five published reports of observations of excess heat bursts, where each of which reports neutron emission at levels more than a factor of a million below what would be seen if energetic alphas were present in commensurate amounts, is very significant.

Both the reviewer, and the authors, would like for the associated heat bursts in these experiments to be reproducible, and even better if the measurements were more accurate. However, for us, these and other papers provide good confirmation that large numbers of neutrons simply aren't there; while this reviewer rejects all of the measurements (of these five papers, as well as all other papers – of which there are at least five more reporting similar results, but without giving sufficient numbers so that a value of neutrons per Joule could be extracted) that give similar results. Moreover, this reviewer seems unwilling to accept any relevant experiment until the excess heat effect is completely reproducible, until the calorimetry is very accurate, until the neutrons are measured with energy resolution at the same time, until energetic alphas are measured at the same time, and until also gammas, X-rays, EUV, and optical photons are measured as well. This reviewer has exceptionally high standards in what measurements will be accepted. But in our view, this matter is settled already with orders of magnitude to spare in the difference between the level of neutron emission observed, and that needed for energetic alphas to be present.

I do not think that such conclusions are either premature, dangerous, or narrowly focused. The real issue here is that energetic alphas in amounts commensurate with the energy observed produce secondary neutrons with a surprisingly high yield, so that if they were there it would be very easy to tell. They simply aren't there.

Appendix B.10. Chemical origin of energy in the Letts experiment

The excess energy observed by Letts et al. [10,11] has no evidence that it is nuclear reaction energy, but may be chemical energy. So, the possibility of chemical reactions should be considered as candidate explanation of the observed results.

The original argument that the excess energy in the Fleischmann–Pons experiment is nuclear was based on the very large amount of energy observed, combined with the relative absence of observed chemical products. A similar argument can be made for the two-laser experiment. In run 669Z, Letts observed 118 kJ of excess energy produced in about 36 h following initiation by two-laser stimulation. The cathode in these experiments have a volume of about 0.0012 cm^3, which corresponds to about 7.2×10^{19} Pd atoms. The observed energy per Pd atom is then over 9300 eV. As in the Fleischmann–Pons experiment, there were no observed commensurate chemical reaction products.

The energy produced in the two-laser experiments used to develop the spectrum of Ref. [11] was less (closer to 10 kJ). The corresponding energy per Pd atom in this case is less (about 800 eV/Pd atom), but still well outside of what can be accounted for by chemistry.

References

[1] M. Fleischmann, S. Pons and M. Hawkins, *J. Electroanal Chem.* **201** (1989) 301; errata, **263** (1990) 187.
[2] M. Fleischmann, S. Pons, M.W. Anderson, L.J. Li and M. Hawkins, *J. Electroanal. Chem.* **287** (1990) 293.

[3] M.H. Miles, R.A. Hollins, B.F. Bush, J.J. Lagowski, R.E. Miles, *J. Electroanal. Chem.* **346** (1993) 99.
[4] M.H. Miles, B.F. Bush, and J.J. Lagowski, *Fusion Technol.* **25** (1994) 478.
[5] M.H. Miles, "Correlation of excess enthalpy and helium-4 production: A review," *Proc. ICCF10* p. 123 (2004).
[6] P.L. Hagelstein, *Naturwissenschaften* **97** (2010) 345.
[7] J.R. Huizenga, *Cold Fusion, the Scientific Fiasco of the Century*, University of Rochester Press, Rochester, NY, 1992.
[8] M.C.H. McKubre, S. Crouch-Baker, R.C. Rocha-Filho, S.I. Smedley, F.L. Tanzella, T.O. Passell, J. Santucci, *J. Electroanal. Chem.* **368** (1994) 55.
[9] E. Storms, *Science of Low Energy Nuclear Reaction: A comprehensive compilation of evidence and explanations about cold fusion*, World Scientific, Singapore, 2007.
[10] D. Letts, D. Cravens and P.L. Hagelstein, Dual laser stimulation of optical phonons in palladium deuteride, *Low-energy Nuclear Reactions Sourcebook* , J. Marwan and S. Krivit (eds.), 2009.
[11] P. L. Hagelstein, D. Letts, and D. Cravens, *J. Cond. Mat. Nucl. Sci.* **3** (2010) 59.
[12] P.L. Hagelstein and I.U. Chaudhary, Excitation transfer and energy exchange processes for modeling the Fleischmann-Pons excess heat effect, *Proc. ICCF14* (2008) 579.
[13] A. Takahashi, *J. Cond. Mat. Nucl. Sci* **1** (2007) 62.
[14] Y. Kim, *Naturwissenschaften* **96** (2009) 803.
[15] A. Widom and L. Larsen, *Eur. Phys. J. C* **46** (2006) 107.
[16] P.L. Hagelstein, A unified model for anomalies in metal deuterides, *Proc. ICCF9* (2002) 121.
[17] F. Bloch and A. Siegert, *Phys. Rev.* **57** (1940) 522.
[18] J. Shirley, *Phys. Rev.* **138** (1965) B979.
[19] C. Cohen-Tannoudji, J. Dupont-Roc and C. Fabre, *J. Phys. B: Atom. Molec. Phys.* **6** (1973) L214.
[20] P.L. Hagelstein and I.U. Chaudhary, *J. Phys. B: Atom. Molec. Phys.* **41** (2008) 035601.
[21] P.L. Hagelstein and I.U. Chaudhary, *J. Phys. B: Atom. Molec. Phys.* **41** (2008) 035602.
[22] P.L. Hagelstein and I.U. Chaudhary, Progress on phonon exchange models for excess heat in metal deuterides, *Proc. 13th Int. Conf. Cold Fusion*, (2007) 590.
[23] P.L. Hagelstein and I.U. Chaudhary, Models relevant to excess heat production in Fleischmann-Pons experiments, *Low-energy Nuclear Reactions Sourcebook*, ACS Symposium Series 998 (2008) 249.
[24] P.L. Hagelstein and I.U. Chaudhary, Excitation transfer and energy exchange processes for modeling the Fleischmann–Pons excess heat effect, *Proc. 14th Int. Conf. Cold Fusion*, 2008, p. 579.
[25] H. Feshbach, *Rev. Mod. Phys.* **36** (1964) 1076.
[26] P.L. Hagelstein, S.D. Senturia and T.P. Orlando, *Introductory Applied Quantum and Statistical Mechanics*, Wiley, 2004.
[27] K. Czerski, A. Huke and G. Ruprecht, *Eur. Phys. Lett.* **68** (2004) 363.
[28] P.L. Hagelstein, I.U. Chaudhary, M. Melich and R. Johnson, A theoretical formulation for problems in condensed matter nuclear science, *Proc. 14th Int. Conf. Cold Fusion*, 2008, p. 596.
[29] C.D. Scott, J.E. Mrochek, T.C. Scott, G.E. Michaels, E. Newman and M. Petek, Measurement of excess heat and apparent coincident increases in the neutron and gamma-ray count rates during the electrolysis of heavy water, *Fusion Technol.* **18** (1990) 103.
[30] C.D. Scott, J.E. Mrochek, T.C. Scott, G.E. Michaels, E. Newman and M. Petek, The initiation of excess power and possible products of nuclear interactions during the electrolysis of heavy water, a preliminary version of their ICCF1 proceedings paper that is posted on the OSTI website, http://www.osti.gov/bridge/servlets/purl/6964062-aNiBsw/ (1990).
[31] A.C. Klein, L.L. Zahm, S.E. Binney, J.N. Reyes, J.F. Higgeinbotham, A.H. Robinson, M. Daniels, R.B. Peterson, Anomalous heat output from Pd cathodes without detectable nuclear products, *American Institute of Phys. Conf. Proc. 228* (1990) 247.
[32] K.L. Wolf, N.J.C. Packham, D. Lawson, J. Shoemaker, F. Cheng, J.C. Wass, Neutron emission and the tritium content associated with deuterium-loaded palladium and titanium metals, *J. Fusion Energy* **9** (1990) 105.
[33] A. Takahashi, A. Mega and T. Takeuchi, Anomalous excess heat by D_2O/Pd cell under L-H mode electrolysis, *Frontiers of Cold Fusion, Frontier Science Series* **4** (1993) 79.

[34] D. Gozzi, R. Caputo, P.L. Cignini, M. Tomellini, G. Gigli, G. Balducci, E. Cisbani, S. Frullani, F. Garibaldi, M. Jodice and G.M. Urciuoli, Excess heat and nuclear product measurements in cold fusion electrochemical cells, *Proc. Fourth Int. Conf. Cold Fusion* **1** (1994) (2–1).
[35] P.L. Hagelstein, *J. Cond. Mat. Nucl. Sci.* **3** (2010) 35.
[36] P.L. Hagelstein, *J. Cond. Mat. Nucl. Sci.* **3** (2010) 41.
[37] P.L. Hagelstein, *J. Cond. Mat. Nucl. Sci.* **3** (2010) 50.

J. Condensed Matter Nucl. Sci. 5 (2011) 72–86

Research Article

Dynamics in the Case of Coupled Degenerate States

Peter L. Hagelstein *

Research Laboratory of Electronics, Massachusetts Institute of Technology, Cambridge, MA 02139, USA

Irfan U. Chaudhary

Department of Computer Science and Engineering, University of Engineering and Technology. Lahore, Pakistan

Abstract

Excess heat in the Fleischmann–Pons experiment has been observed in a great many experiments, and we have been working toward the development of a theoretical model to account for it. In the experiments, excess heat is correlated with ^{4}He, but there are no commensurate energetic particles. This has motivated us to consider models in which the excess energy is communicated directly to low energy degrees of freedom associated with the solid state environment. We have found relatively simple models which are capable of splitting up a large energy quantum into a very large number of much smaller energy quanta. In order to analyze these new models, we are motivated to consider the dynamics associated with a set of ordered degenerate states with nearest neighbor coupling.
© 2011 ISCMNS. All rights reserved.

Keywords: Coherent dynamics, Degenerate states, Excess heat, Fleischmann–Pons experiment, Lossy spin-boson model

1. Introduction

There has been a keen interest in the elucidation of the underlying mechanism associated with excess heat in the Fleischmann–Pons experiment [1,2] over the past two decades, and there have been a great many papers put forth over the years suggesting how it might work. Some years ago Takahashi and coworkers gave a simple overview of the situation, wherein was described four scenarios [3]. These included aneutronic fusion with hidden reaction products, fusion with the energy coupled directly to the lattice, chemical or mechanical explanations, or experimental error. Enough experimental confirmations of the effect have been reported that it seems unlikely that we are dealing with experimental error [4,5]. The amount of energy observed is sufficiently large that chemical or mechanical explanations seem impossible, and there is no indication of chemical reaction products or mechanical changes commensurate with the energy produced. Recently we were able to make strong arguments against the possibility of hidden energetic products from proposed aneutronic fusion reactions, since they would produce secondary neutrons in sufficient quantities to have

*E-mail: plh@mit.edu

© 2011 ISCMNS. All rights reserved.

been readily observed [6]. Among Takahashi's scenarios, the one that remains (coupling the nuclear energy directly to the lattice) has been the focus of our efforts for many years now.

Of course, the theorists have been busy since publication of the different scenarios by Takahashi et al (for example, see [5,7]), and it is likely that at present a revised list of scenarios is appropriate. From our perspective, the constraints imposed from the upper limits of energetic reaction products [6] are sufficiently severe that the majority of mechanisms that have been proposed since 1989 can be ruled out as inconsistent with experiment. At this point there seem to be two kinds of candidates that remain. One of these are schemes which involve direct coupling of energy to the lattice, or to other condensed matter degrees of freedom (such as plasmon modes [8], or hybrid plasmon–phonon modes). The other are schemes in which an extreme fractionation of the nuclear energy occurs into kinetic energy of a very large number of nuclei, as argued for by Kim [9]. Our concern with this approach is that a mechanism through which this might occur has not yet been clarified.

We have been interested for some time in the problem of how a large quantum can be split up into a very large number of small quanta. To study this problem, we first focused on the spin-boson model [10–12] and variants. In the spin-boson model, two-level systems and an oscillator are coupled, with an interaction that is linear in the sense that one transition of the two-level systems occurs with the exchange of a single oscillator quantum. It has been understood for many years that this model described coherent energy exchange in the multiphoton regime, in which many oscillator quanta are exchanged for a single two-level system quantum [13,14]. The transition rates in this model are slow because of destructive interference effects. We found that the destructive interference could be removed in part if loss terms are included, resulting in an enhancement by many orders of magnitude of the associated rate for coherent energy exchange [15].

In this work we are interested in the dynamics of coherent energy exchange in this and related models. We might think of coherent energy exchange in the limit where many oscillator quanta are exchanged as occurring as a result of nearly degenerate states which are weakly coupled through off-resonant transitions through intermediate states. We would expect the resulting system dynamics when the indirect coupling is strong to be similar to that of a chain of degenerate states with nearest neighbor coupling. This leads to a quantum mechanical problem that we can analyze relatively simply. In the event that there is a small systematic mismatch between the nearly degenerate levels, we are also able to recover useful evolution equations.

We note that the first reviewer for this paper had numerous criticisms. With encouragement from colleagues, we have included selected criticisms with responses in Appendix C.

2. A Basic Model for Coupling between Degenerate States

We begin by considering a highly idealized model for a quantum system that evolves through coupling between ordered degenerate states. We assume that the dynamics are governed by a Hamiltonian $\hat{H}$ so that

$$i\hbar\frac{\partial}{\partial t}\Psi \;=\; \hat{H}\Psi, \tag{1}$$

We assume the wavefunction Ψ can be expanded in terms of a set of degenerate basis states

$$\Psi \;=\; \sum_m c_m(t)|\Phi_m\rangle. \tag{2}$$

We assume that the dynamics of the system can be reasonably approximated by coupling only between nearest neighbors (see Fig. 1), so that

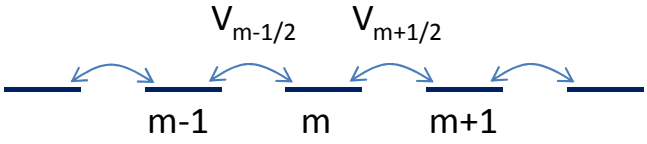

Figure 1. Schematic of ordered degenerate states with nearest neighbor coupling.

$$i\hbar\frac{\mathrm{d}}{\mathrm{d}t}c_m(t) \;=\; V_{m+\frac{1}{2}}c_{m+1}(t) + V_{m-\frac{1}{2}}c_{m-1}(t). \tag{3}$$

This presumes that the energies are degenerate

$$\langle\Phi_m|\hat{H}|\Phi_m\rangle \;=\; 0, \tag{4}$$

where we have removed any finite offset from our model Hamiltonian for simplicity. The coupling coefficients $V_{m\pm1/2}$ are the matrix elements

$$V_{m\pm\frac{1}{2}} \;=\; \langle\Phi_m|\hat{H}|\Phi_{m\pm1}\rangle, \tag{5}$$

which we take to be real in our model.

Equation (3) defines the basic model of interest to us here. One might argue that the assumptions of the model are restrictive, so that there are only a few quantum systems that work this way. However, it may be the case that the simplified model under discussion here is one that has been extracted from a much more complicated model, that the focus is on a small subset of the states which are degenerate, and the effect of all the other states has been included through indirect coupling in the model Hamiltonian $\hat{H}$. This will be our point of view, although it will not be required in the discussion which follows in this work.

In the particular case of two-level systems coupled to an oscillator (a case that we will analyze later on in this paper), the degenerate states are those in which energy is kept constant by maintaining constant $m\Delta E + n\hbar\omega_0$, where ΔE is the two-level system transition energy and where $\hbar\omega_0$ is the characteristic energy of the oscillator. In this case, the degenerate states are indirectly coupled since many oscillator quanta need to be exchanged in order to make up for the change of a single two-level system.

3. Evolution Equation for $\langle m\rangle$

Let us define the average $\langle m\rangle$ according to

$$\langle m\rangle \;=\; \sum_m m|c_m|^2. \tag{6}$$

To understand the dynamics of the system, we would like to know how $\langle m\rangle$ changes with time. As a result, we are interested in the calculation of the derivative. As a first step we may write

$$\frac{\mathrm{d}}{\mathrm{d}t}\langle m\rangle \;=\; \sum_m m\left(\frac{\mathrm{d}c_m^*}{\mathrm{d}t}c_m + c_m^*\frac{\mathrm{d}c_m}{\mathrm{d}t}\right). \tag{7}$$

We evaluate to obtain

$$\begin{aligned}\frac{\mathrm{d}}{\mathrm{d}t}\langle m\rangle \;&=\; -\frac{1}{i\hbar}\sum_m m(V_{m-1/2}c_{m-1}^* + V_{m+1/2}c_{m+1}^*)c_m \\ &\quad + \frac{1}{i\hbar}\sum_m m c_m^*(V_{m-1/2}c_{m-1} + V_{m+1/2}c_{m+1}).\end{aligned} \tag{8}$$

We can recast this as

$$\begin{aligned}\frac{\mathrm{d}}{\mathrm{d}t}\langle m\rangle \;&= \frac{1}{i\hbar}\sum_m m(c_m^*c_{m+1} - c_{m+1}^*c_m)V_{m+\frac{1}{2}} \\ &\quad + \frac{1}{i\hbar}\sum_m m(c_m^*c_{m-1} - c_{m-1}^*c_m)V_{m-\frac{1}{2}},\end{aligned} \tag{9}$$

which simplifies to

$$\frac{\mathrm{d}}{\mathrm{d}t}\langle m\rangle \;=\; -\frac{1}{i\hbar}\sum_m V_{m+1/2}(c_m^*c_{m+1} - c_{m+1}^*c_m). \tag{10}$$

It is convenient to define the average velocity $\langle\hat{v}\rangle$ according to

$$\langle\hat{v}\rangle \;=\; -\frac{1}{i\hbar}\sum_m V_{m+1/2}(c_m^*c_{m+1} - c_{m+1}^*c_m). \tag{11}$$

This allows us to write

$$\frac{\mathrm{d}}{\mathrm{d}t}\langle m\rangle \;=\; \langle\hat{v}\rangle. \tag{12}$$

In general we can identify $\langle\hat{v}\rangle$ with the rate for transitions between the different nearly degenerate states.

4. Evolution Equation for $\langle\hat{v}\rangle$

Next, we require an evolution equation for the average velocity. We write

$$\frac{\mathrm{d}}{\mathrm{d}t}\langle\hat{v}\rangle \;=\; -\frac{1}{i\hbar}\sum_m V_{m+1/2}\left(\frac{\mathrm{d}c_m^*}{\mathrm{d}t}c_{m+1} + c_m^*\frac{\mathrm{d}c_{m+1}}{\mathrm{d}t} - \frac{\mathrm{d}c_{m+1}^*}{dt}c_m - c_{m+1}^*\frac{\mathrm{d}c_m}{\mathrm{d}t}\right). \tag{13}$$

We substitute to obtain

$$\frac{\mathrm{d}}{\mathrm{d}t}\langle\hat{v}\rangle = \frac{2}{(i\hbar)^2}\sum_m V^2_{m+\frac{1}{2}}(|c_{m+1}|^2 - |c_m|^2) + \frac{1}{(i\hbar)^2}\sum_m V_{m+\frac{1}{2}}V_{m-\frac{1}{2}}(c^*_{m-1}c_{m+1} + c^*_{m+1}c_{m-1}) - \frac{1}{(i\hbar)^2}\sum_m V_{m+\frac{1}{2}}V_{m+\frac{3}{2}}(c^*_m c_{m+2} + c^*_{m+2}c_m). \quad (14)$$

We can collect terms and rearrange to obtain

$$\frac{\mathrm{d}}{\mathrm{d}t}\langle\hat{v}\rangle = -\frac{2}{(i\hbar)^2}\sum_m (V^2_{m+1/2} - V^2_{m-1/2})|c_m|^2. \quad (15)$$

It seems reasonable to introduce the notation

$$\left\langle\frac{\mathrm{d}V^2}{\mathrm{d}m}\right\rangle = \sum_m (V^2_{m+1/2} - V^2_{m-1/2})|c_m|^2. \quad (16)$$

The resulting evolution equation takes the form

$$\frac{\mathrm{d}}{\mathrm{d}t}\langle\hat{v}\rangle = \frac{2}{\hbar^2}\left\langle\frac{\mathrm{d}V^2}{\mathrm{d}m}\right\rangle. \quad (17)$$

Note that the velocity increases towards regions where the magnitude of the coupling constant is larger.

4.1. Discussion

We are familiar with the evolution equations for the closely related problem of the dynamics of spin systems (which is discussed in Appendix A). The evolution equations that we developed in this section and in the previous section constitute an interesting and nontrivial generalization of this model.

Several interesting features of this generalization can be observed. One feature is that we have obtained only two independent evolution equations, which is significant since had we chosen a somewhat more complicated model we could have easily generated an infinite set. Another is that the resulting equations are of the general form of Newton's laws in one dimension, which allows us to apply our intuition about classical particle dynamics in one dimension to this new problem involving coupling between ordered degenerate basis states. Finally we see that the coupling matrix elements $V_{m+1/2}$ determine the dynamics in a fundamental way. Hence when we analyze new models that involve a set of coupled degenerate basis states, our attention should properly be focused on these coupling matrix elements. With an understanding of these coupling matrix elements, we can predict the associated dynamics simply.

5. Analogy with Kinetic and Potential Energy

Since the evolution equations are of the same form as classical Newton's laws in one dimension, we can develop an effective energy equation for the classical version of the problem. To proceed, we identify the classical position $m(t)$ and velocity $v(t)$ with the average values

$$\langle m \rangle \rightarrow m(t), \qquad \langle \hat{v} \rangle \rightarrow v(t). \tag{18}$$

The classical equations are

$$\frac{\mathrm{d}}{\mathrm{d}t} m(t) = v(t),$$

$$\frac{\mathrm{d}}{\mathrm{d}t} v(t) = \frac{2}{\hbar^2} \frac{\mathrm{d}V^2}{\mathrm{d}m}. \tag{19}$$

The associated energy equation is then approximately

$$C = \frac{1}{2} v^2 - \frac{2}{\hbar^2} V^2(m). \tag{20}$$

From this it is possible to determine the velocity as a function of position as

$$v = \pm \sqrt{2C + \frac{4}{\hbar^2} V^2(m)}. \tag{21}$$

This is analogous to the situation in classical dynamics where we can specify the momentum at each position from a knowledge of the potential and total energy.

In some cases, the coupling becomes weaker for the outer values of m. If so, then for a trajectory that starts at these outer values it should be a reasonable approximation that C is small (since the velocity is small where the coupling is very weak). For zero C we obtain

$$v(m) = \pm \frac{2}{\hbar} V(m). \tag{22}$$

This formula is important since we can specify the velocity v (which is the rate for transitions between the different nearly degenerate states) directly in terms of the coupling matrix elements as a function of m. If the velocity is a sufficiently simple function of m, then we might be able to integrate to obtain an explicit expression for $m(t)$.

The maximum rate in this approximation occurs where the coupling matrix element is maximum, with a value of

$$\max(v) = \frac{2}{\hbar} \max |V(m)|. \tag{23}$$

6. Dynamics of Coherent Energy Exchange in the Perturbative Limit

In a previous work [15] we analyzed indirect coupling matrix elements for the spin-boson model augmented with loss using perturbation theory. We can make use of these results to calculate the associated system dynamics. In the event that there are a very large number of two-level systems, then it is possible to arrange for a version of the problem in which the indirectly coupled states are very nearly degenerate. In this case we can make use of the equivalent classical evolution equations from the section above

$$\frac{\mathrm{d}^2}{\mathrm{d}t^2}m(t) \;=\; \frac{2}{\hbar^2}\frac{\mathrm{d}}{\mathrm{d}m}V^2(m). \tag{24}$$

It seems reasonable to take as an example the perturbation theory model where one two-level system quantum is exchanged for five oscillator quanta. In this case we developed explicit formulas for the indirect coupling matrix elements which can be used directly to evaluate the evolution.

6.1. Large S and n approximation

The explicit expressions for the indirect coupling constants are complicated, so that the equation that results from taking the difference of the squares to determine the acceleration will be more complicated. We seek a simplification of the problem relevant to the large S limit. A common approximation is to neglect terms of order unity in the Dicke factors, so that

$$\sqrt{(S\mp m)(S\pm m+1)} \;\rightarrow\; \sqrt{(S^2-m^2)}. \tag{25}$$

Using this kind of approximation, we can write

$$F(S,M) \;\rightarrow\; \frac{7}{36}(S^2-m^2)^2 \tag{26}$$

$$V_{1,12}(E) \;\rightarrow\; \frac{625}{64}\frac{(V\sqrt{n})^5}{\Delta E^4}\sqrt{(S^2-m^2)} \quad (\Gamma=0), \tag{27}$$

where we have assumed that n is large. The indirect coupling in the lossy limit is then approximated by

$$V_{1,12}(E) \;\rightarrow\; \frac{4375}{2304}\frac{(V\sqrt{n})^5}{\Delta E^4}(S^2-m^2)^{\frac{5}{2}} \quad (\Gamma=\infty). \tag{28}$$

6.2. Approximation for the force

We can use the estimate for the indirect coupling in order to estimate the force. We may write

$$\begin{aligned}\frac{\mathrm{d}}{\mathrm{d}m}V^2(m) \;&=\; \left(\frac{4375}{2304}\right)^2\frac{(V\sqrt{n})^{10}}{\Delta E^8}\frac{\mathrm{d}}{\mathrm{d}m}(S^2-m^2)^5 \\ &=\; -10\left(\frac{4375}{2304}\right)^2\frac{(V\sqrt{n})^{10}}{\Delta E^8}m(S^2-m^2)^4.\end{aligned} \tag{29}$$

The dynamics for the classical version of the problem is then described by

$$\frac{\mathrm{d}^2}{\mathrm{d}t^2}m(t) \;=\; -20\left(\frac{4375}{2304}\right)^2\frac{(V\sqrt{n})^{10}}{\hbar^2\Delta E^8}m(t)[S^2-m^2(t)]^4. \tag{30}$$

6.3. Simplification

It is convenient to recast the problem in terms of a normalized version of $m(t)$

$$y(t) \;=\; \frac{m(t)}{S}, \tag{31}$$

which allows us to write

$$\frac{\mathrm{d}^2}{\mathrm{d}t^2}y(t) \;=\; -\,\Omega_0^2 y(t)[1-y^2(t)]^4, \tag{32}$$

where the characteristic frequency Ω_0 is defined through

$$\Omega_0^2 \;=\; 20\left(\frac{4375}{2304}\right)^2 \frac{(V\sqrt{n})^{10}}{\hbar^2 \Delta E^8} S^8. \tag{33}$$

6.4. Solutions

The nonlinear second-order classical equation (Eq. (32)) has oscillatory solutions (which correspond to a ball rolling back and forth confined in a nonlinear well) and a non-oscillatory solution (corresponding to a ball with an energy matched to the top of the well). The latter solution is illustrated in Fig. 2. This function can be fit well according to

$$y(t) \;=\; -\,\frac{ax+bx^3}{1+bx^2\sqrt{c+x^2}} \tag{34}$$

with

$$a \;=\; 0.381902, \qquad b = 0.00708607, \qquad c = 161.393. \tag{35}$$

7. Summary and Conclusions

We are interested in developing models for excess heat in the Fleischmann–Pons experiment, as outlined in the Introduction. The key problem from our perspective in the development of relevant models is that of coherent energy exchange under conditions where a large energy quantum is split up into a very large number of smaller energy quanta. We have proposed models that accomplish this, and which begin to be relevant to the new effect. However, these new models are not so easy to analyze in general. To make progress on them, we have found that some understanding is possible by considering a subset of the states which are nearly degenerate, and then developing models which account for the indirect coupling between these nearly degenerate states. Once this is done, then we are able to understand what the new models do, and we are able to extract estimates for the reaction rates from them. From this point of view, it seems that the place to start in our discussion of the new models is by examining the dynamics associated with a set of ordered degenerate states with nearest neighbor coupling. This is the simple model we have introduced in Section 2.

We find that the resulting evolution equations for this model are simple, and are of the form of Newton's laws in one dimension. We find that the dynamics are determined ultimately by the coupling matrix elements between the different nearly degenerate basis states, hence in studying such models our attention will naturally be drawn to these coupling

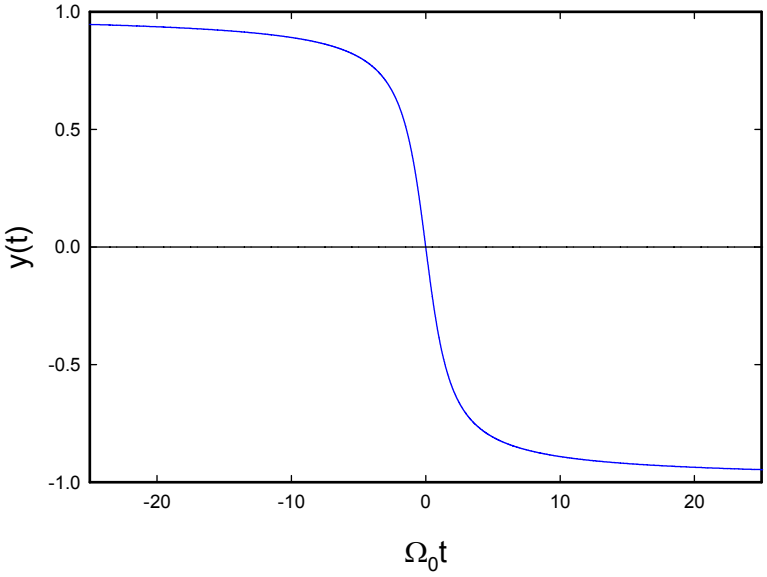

Figure 2. Schematic of ordered states with constant energy separation, and with nearest neighbor coupling..

matrix elements. We have tested them against a well-known problem involving spin dynamics in Appendix A, and we have verified that we get the right answer. Since the evolution equations are similar to Newton's laws, we can construct an energy expression for the equivalent classical problem. This allows us to specify the velocity, or coherent reaction rate, as a function of the index given an equivalent energy. Explicit results were given for the dynamics of a spin-boson model augmented with loss, where we made use of the indirect coupling matrix elements calculated in an earlier work. This provides an example which shows how the approach under discussion can be used to describe the dynamics of coherent energy exchange in the multiphonon regime.

The requirement of precise energy degeneracy is restrictive. In general, if the states are not degenerate, then the dynamics become very complicated. However, in the special case where the basis state energies are linear in the index, it is possible to develop somewhat more general evolution equations which are similar in form to those found in the dynamics of a spin system (see Appendix B). The absence of degeneracy in this model results in the presence of a reactive term which impacts the velocity.

Appendix A. Spin Dynamics Example

To see whether the simple model developed above works, we would like to try it out on a test problem for which the answer is known.

Appendix A.1. Test problem

In this case, an obvious test problem is the dynamics of a system of many equivalent spins governed by a simple Hamiltonian. For the test problem, we take the Hamiltonian to be

$$\hat{H}_T \;=\; 2\Omega \hat{S}_x. \tag{A.1}$$

We can make use of the commutation relations of the spin operators to write

$$\frac{\mathrm{d}}{\mathrm{d}t}\langle \hat{S}_z\rangle \;=\; \frac{2\Omega}{i\hbar}\langle [\hat{S}_z,\, \hat{S}_x]\rangle \;=\; \Omega\langle \hat{S}_y\rangle. \tag{A.2}$$

Similarly, we may write

$$\frac{\mathrm{d}}{\mathrm{d}t}\langle \hat{S}_y\rangle \;=\; \frac{2\Omega}{i\hbar}\langle [\hat{S}_y,\, \hat{S}_x]\rangle \;=\; -\,\Omega\langle \hat{S}_z\rangle. \tag{A.3}$$

Appendix A.2. Dynamics from the spin operators

To make a connection with our test problem, we can identify

$$\langle m\rangle \;=\; \frac{\langle \hat{S}_z\rangle}{\hbar}, \qquad \langle \hat{v}\rangle \;=\; \frac{\Omega\langle \hat{S}_y\rangle}{\hbar}. \tag{A.4}$$

With these definitions we obtain the exact equations

$$\frac{\mathrm{d}}{\mathrm{d}t}\langle m\rangle \;=\; \langle \hat{v}\rangle,$$

$$\frac{\mathrm{d}}{\mathrm{d}t}\langle \hat{v}\rangle \;=\; -\,\Omega^2\langle m\rangle. \tag{A.5}$$

Appendix A.3. Dynamics from coupled degenerate states

To make use of the approach from above based on degenerate states, we first require evaluation of the spin matrix element

$$V_{m+\frac{1}{2}} \;=\; \langle S, m|2\Omega\hat{S}_x|S, m+1\rangle \;=\; \hbar\Omega\sqrt{(S-m)(S+m+1)}, \tag{A.6}$$

$$V_{m-\frac{1}{2}} \;=\; \langle S, m|2\Omega\hat{S}_x|S, m-1\rangle \;=\; \hbar\Omega\sqrt{(S+m)(S-m+1)}. \tag{A.7}$$

We can use these to compute

$$\begin{aligned} V^2_{m+\frac{1}{2}} - V^2_{m-\frac{1}{2}} \;&=\; (\hbar\Omega)^2\Big[(S-m)(S+m+1) - (S+m)(S-m+1)\Big] \\ &=\; -\,2(\hbar\Omega)^2 m. \end{aligned} \tag{A.8}$$

The spin dynamics computed using from the dynamics above is then

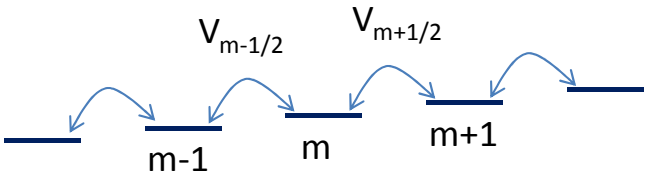

Figure 3. Schematic of ordered states with constant energy separation, and with nearest neighbor coupling.

$$\frac{\mathrm{d}}{\mathrm{d}t}\langle m\rangle = \langle\hat{v}\rangle,$$
$$\frac{\mathrm{d}}{\mathrm{d}t}\langle\hat{v}\rangle = -\Omega^2\langle m\rangle \tag{A.9}$$

in agreement with the dynamics obtained from the spin commutation relations.

Appendix B. Generalization to a Non-degenerate Set of States

For more sophisticated models it may be that the levels are not strictly degenerate, in which case the dynamics quickly becomes much more complicated. It is possible to provide an extension of the dynamical equations for the simplest generalization to the non-degenerate case where the basis state energy increases linearly in the index (see Fig. 3). The associated model is described by

$$i\hbar\frac{\mathrm{d}}{\mathrm{d}t}c_m(t) = \delta E m c_m(t) + V_{m+\frac{1}{2}}c_{m+1}(t) + V_{m-\frac{1}{2}}c_{m-1}(t). \tag{B.1}$$

The evolution equations now become

$$\frac{\mathrm{d}}{\mathrm{d}t}\langle m\rangle = \langle\hat{v}\rangle,$$
$$\frac{\mathrm{d}}{\mathrm{d}t}\langle\hat{v}\rangle = \frac{2}{\hbar^2}\left\langle\frac{\mathrm{d}V^2}{\mathrm{d}m}\right\rangle + \langle\hat{w}\rangle,$$
$$\frac{d}{\mathrm{d}t}\langle\hat{w}\rangle = -2\left(\frac{\delta E}{\hbar}\right)^2\langle\hat{v}\rangle. \tag{B.2}$$

The average value $\langle\hat{w}\rangle$ is defined by

$$\langle\hat{w}\rangle = \frac{2\Delta E}{\hbar^2}\sum_m V_{m+\frac{1}{2}}(c_m^* c_{m+1} + c_{m+1}^* c_m). \tag{B.3}$$

These equations are closely related to the evolution equations obtained for spin systems, but they can provide estimates for the dynamics for more complicated models.

Appendix C. Responses to Reviewer Comments

The first reviewer put forth a great many criticisms of this paper and the preceding one [15]. Our colleagues provided encouragement to include some of the associated criticisms and responses in the papers. In response, we have provided a selection of the reviewer's criticisms, modified where appropriate to be more understandable, as well as some discussion of the associated issues.

Appendix C.1. No reason to focus on degenerate states

There is no reason to have degenerate states, which seems merely a "desired assumption" by the authors.

What we mean by degenerate states in the context of the lossy spin-boson model are basis states with constant energy

$$E = m\Delta E + \Delta n\hbar\omega_0.$$

For example, suppose that we start with a state with m two-level systems excited, and n oscillator quanta. To go to a degenerate state with $m - 1$ two-level systems excited, we are going to have to have an increase in the oscillator energy by Δn oscillator quanta, where Δn is the ratio the two-level transition energy and the characteristic oscillator energy. More simply, if the two-level transition energy is matched to five oscillator quanta, then you need to increase the oscillator energy by five quanta every time you lose one excited state of the two-level systems.

Hence, the "desired" assumption in this case is that we would like to conserve energy overall between the two-level systems and the oscillator.

Appendix C.2. No reason to focus on indirect coupling

There is no reason to have indirect coupling, which also seems merely a "desired assumption".

In the spin-boson model, there is no direct coupling between these degenerate states in the multiphoton regime, which we are working in. As a result, the coupling is indirect. This is explained in the papers, and we have presented an explicit perturbation theory calculation as a concrete example. The coupling under discussion in the spin-boson model is due to phonon exchange, and we are able to derive this directly from more general Hamiltonians.

Appendix C.3. Nuclear reactions are irreversible

Nuclear reactions are irreversible (one-way for out-going channel with significant mass-energy defect) and are stochastic processes (namely one-way or never-return for going out to final interaction products with big entropy increase). So the assumed oscillatory dynamics between the two states (where energy is transferred from the nuclear system to the oscillator) cannot exist, due to the stochastic one-way nuclear decay.

In the simple models discussed in this paper, the dynamics can be oscillatory in the sense that the energy can go from the two-level systems to the oscillator and back again, coherently. This is consistent generally with how coherent dynamics tend to work.

The reviewer has decided that one cannot apply models with this kind of dynamics to a nuclear transition, seemingly because conventional (incoherent) nuclear reactions are directional. As we have argued, because of the absence of commensurate energetic particles, conventional incoherent nuclear reactions cannot account for excess heat in the Fleischmann-Pons experiment, which is why we are interested in coherent processes. Coherent models in many cases show oscillatory behavior as does the example considered in this paper. We would have no problem in principle with a coherent process producing energy that shows oscillations.

However, in more sophisticated versions of the coherent models that we have studied, phonon loss in the vicinity of ω_0 must be included. In these models, the energy that is exchanged coherently with the oscillator thermalizes, which makes it unavailable for transferring back. So, even though the simple models that we focus on to begin the discussion do show oscillations, we agree with the reviewer that such oscillations should not occur in a realistic model for excess heat production. In the more sophisticated models that will be considered in later papers, thermalization of optical phonons results in unidirectional dynamics. for models describing excess heat. Some transfer of energy from the lattice (oscillator) to nuclear transitions however is predicted by our models, and has the potential to result in a lattice-induced X-ray or gamma-ray emission effect, independent of the Fleischmann–Pons experiment.

Appendix C.4. Limitations due to relativity

The authors have not discussed issues associated with speed of light limitations in nuclear fusion, since the process is very fast (less than a femtosecond) once the deuterons get sufficiently close.

Back in 1989, the notion was put forth that deuteron-deuteron fusion might be occurring in some new way, such that the reaction energy was somehow going directly into the lattice. Critics responded with the argument that once the deuterons got close enough to interact, the reaction itself was over long before there was time for communication with the nearest atoms.

We can quantify this argument starting with the reaction rate for molecular D_2 written in the form

$$\gamma \;=\; A|\Psi(0)|^2,$$

where $\Psi(r)$ is the molecular wavefunction for the relative deuteron separation; A is a reaction constant that is derived from the astrophysical S factor, and has a numerical value estimated to be [16]

$$A \;=\; 1.5\times 10^{-16}\ \mathrm{cm}^3/\mathrm{s}.$$

Hence, if we take the two deuterons to be localized within a spherical volume with maximum separation of r =10 fm

$$V \;=\; \frac{4\pi}{3}r^3 \;=\; 4.2\times 10^{-36}\ \mathrm{cm}^3.$$

The associated reaction timescale given this localization could be estimated as

$$\tau = \frac{V}{A} \;=\; 2.8\times 10^{-20}\ \mathrm{s}.$$

The associated speed of light limitation for this time interval is

$$c\tau \;=\; 8.4 \times 10^{-10}\ \text{cm},$$

which is less than a tenth of an Angstrom. Critics used this argument effectively to convince others that it was impossible to couple energy to the lattice, since there was not sufficient time to communicate to the nearest atom that the reaction had occurred given the speed of light constraint.

We generally agree with this argument in connection with the incoherent fusion reaction process. The argument might be criticized in that there is some energy exchange with the lattice nonetheless since the lattice structure is changed instantaneously. We could compute the associated phonon exchange from existing theory; however, the effect is not large, and is unlikely to be measurable.

In the models that we have studied, the coherent energy exchange associated with the fractionation of a large nuclear quantum to optical phonons cannot be accomplished in the D_2/^{4}He system, since Coulomb repulsion makes the associated coupling strength much too small. Consequently, the picture that might be associated with this criticism is not one relevant to the models of interest to us.

Appendix C.5. Excitation transfer

However, some further discussion of the issue is worthwhile. In our earlier studies, we have considered D_2 to ^{4}He transitions mediated by phonon exchange, where the reaction energy is transferred elsewhere.

What we have termed excitation transfer as a physical effect has not been considered previously (outside of our work) in connection with nuclear reactions or MeV-level nuclear transitions. It is known in biophysics as the Förster effect, or as resonant energy transfer. An excited molecule can transfer its excitation to a nearby molecule through Coulomb dipole–dipole interactions. The effect is observed experimentally, and the theoretical explanation was given by Förster more than 60 years ago [17].

What we have proposed is that nuclear de-excitation can occur mediated by phonon exchange (rather than by Coulomb interactions), with the excitation energy being transferred to another nucleus (and subsequently coherently exchanged with the lattice). In this scenario, the issue raised by the reviewer then concerns whether this kind of de-excitation can occur in the presence of fast incoherent reaction rates. Since the coherent and incoherent processes are basically separate processes, one would address this by computing the rates for both processes; and if the rate associated with excitation transfer happens to be faster, then the answer would be yes. The situation in our models is made somewhat more complicated in that we need to consider the incoherent process as a loss mechanism in the coherent dynamics associated with the D_2 to ^{4}He transitions, but the essential argument is basically the same.

References

[1] M. Fleischmann, S. Pons and M. Hawkins, *J. Electroanal. Chem.* **201** (1989) 301; errata, **263** (1990) 187.
[2] M. Fleischmann, S. Pons, M.W. Anderson, L.J. Li and M. Hawkins, *J. Electroanal. Chem.* **287** (1990) 293.
[3] A. Takahashi, T. Inokuchi, Y. Chimi, T. Ikegawa, N. Kaji, Y. Nitta, K. Kobayashi and M. Taniguchi, *Proc. ICCF5*, 1995, p. 69.
[4] M.C.H. McKubre, S. Crouch-Baker, R.C. Rocha-Filho, S.I. Smedley, F.L. Tanzella, T.O. Passell, J. Santucci, *J. Electroanal. Chem.* **368** (1994) 55.
[5] E. Storms, *Science of Low Energy Nuclear Reaction: A comprehensive compilation of evidence and explanations about cold fusion*, World Scientific, Singapore, 2007.
[6] P.L. Hagelstein, *Naturwissenschaften* **97** (2010) 345.

[7] E. Storms, How to explain cold fusion, *Low-energy Nuclear Reactions Sourcebook*, ACS Symposium Series 998, 2008, p. 85.
[8] G. Preparata, Cold fusion '93: Some theoretical ideas, *Proc. ICCF4*, Vol. 1, 1994, pp. 12–1.
[9] Y. Kim, *Naturwissenschaften* **96** (2009) 803.
[10] F. Bloch and A. Siegert, *Phys. Rev.* **57** (1940) 522.
[11] J. Shirley, *Phys. Rev.* **138** (1965) B979.
[12] C. Cohen-Tannoudji, J. Dupont-Roc and C. Fabre, *J. Phys. B: Atom. Molec. Phys.* **6** (1973) L214.
[13] P.L. Hagelstein and I.U. Chaudhary, *J. Phys. B: Atom. Mol. Phys.* **41** (2008) 035601.
[14] P.L. Hagelstein and I.U. Chaudhary, *J. Phys. B: Atom. Mol. Phys.* **41** (2008) 035602.
[15] P.L. Hagelstein and I.U. Chaudhary, Energy exchange in the lossy spin-boson model, *J. Cond. Mat. Nucl. Sci.* **5** (2011) 52.
[16] S.E. Koonin and M. Nauenberg, *Nature* **339** (1989) 690.
[17] T.Förster, *Z. Elektrochem.* **53** (1949) 93.

J. Condensed Matter Nucl. Sci. 5 (2011) 87–101

Research Article

Second-order Formulation and Scaling in the Lossy Spin-Boson Model

Peter L. Hagelstein *

Research Laboratory of Electronics, Massachusetts Institute of Technology, Cambridge, MA 02139, USA

Irfan U. Chaudhary

Department of Computer Science and Engineering, University of Engineering and Technology. Lahore, Pakistan

Abstract

In the Fleischmann–Pons experiment, energy is produced without commensurate energetic reaction products. To account for this we have proposed new models in which coherent energy exchange occurs between two-level systems with a large energy quantum, and an oscillator with a much smaller characteristic energy. In earlier work we demonstrated using perturbation theory that the lossy spin-boson model is capable of efficient coherent energy exchange when many oscillator quanta are exchanged for a two-level system quanta on resonance. Here we introduce a formulation that isolates nearly degenerate states in the lossy spin-boson model, and allows the computation of the self-energy and indirect coupling matrix elements. From calculations of simple lossy spin boson models we establish a scaling law and define the dimensionless coupling constant g for the system. Direct calculations using this approach is not possible for large models in which a great many oscillator quanta are exchanged, but the formulation provides a foundation for understanding this kind of model, and will allow us to develop more powerful approximate methods.
© 2011 ISCMNS. All rights reserved.

Keywords: Coherent energy exchange, Excess heat, Fleischmann–Pons experiment, Lossy spin-boson model, Theory

1. Introduction

We have been interested over the past decade or more in developing models [1–4] to account for excess heat in the Fleischmann–Pons experiment [5–8]. From our perspective, the key feature of these experiments which makes the development of a model difficult is the absence of energetic particles commensurate with the energy observed.

The only product which has been identified so far to be commensurate with the energy produced is ^{4}He, which is seen in the off-gas from the cathode [9–11]. We have used the results from experiment in which excess power is seen under conditions where an attempt was made to measure neutron emission in order to obtain an upper limit on the energy of the ^{4}He. We found that energetic alpha particles can collide with deuterons, resulting in secondary neutrons

*E-mail: plh@mit.edu

© 2011 ISCMNS. All rights reserved.

from subsequent deuteron–deuteron fusion reactions. The upper limit on the alpha energy estimated in this way is below 20 keV [12]. The experimental reaction energy per ^{4}He observed is close to 24 MeV [13].

These constraints tell us that no matter what process is responsible, it does not work in the same way as a Rutherford-type of reaction familiar in nuclear physics. Local conservation of energy and momentum in such reactions requires that the reaction energy must be expressed primarily as kinetic energy of the products. If two deuterons react to produce ^{4}He with most of the energy carried away by a gamma or electron, the resulting alpha particle would have an energy near 75 keV, which by itself is inconsistent with experiment (and there are no commensurate fast electrons or gammas observed).

This has motivated us to pursue new models in which the nuclear energy is transferred directly to low energy condensed matter degrees of freedom, such as vibrational modes [1–4]. There is no precedence for this in nuclear physics or condensed matter physics. Coherent many quantum exchange between an oscillator and two-level systems is known in NMR and in problems involving atomic states and an electromagnetic field [14–16]. However, in these models, the number of quanta exchanged is less than 10^2, where on the order of 10^8 would be required to account for the Fleischmann–Pons experiment.

Some years ago, we found new models which are much more efficient at exchanging a large number of quanta [1]. In two recent papers, we began a program of laying out the new models systematically. In the first, we introduced the lossy spin-boson model more properly than in earlier work, we reviewed the sector formalism that underlies loss in a second-order Hamiltonian, and we showed that coherent energy exchange is enhanced dramatically using lowest-order perturbation theory [17]. In the second, we considered the dynamics of a set of nearly degenerate states that have nearest neighbor coupling, and developed reasonably general evolution formula for the dynamics of number and velocity expectation values [18].

Here, we extend the discussion to a second-order formulation which isolates the nearly degenerate states. In previous work on the (lossless) spin-boson model, we studied a rotation which isolated the nearly degenerate states, and allowed us to model the indirect coupling between them simply [19,20]. We have not found an analogous rotation for the lossy version of the problem, but the second-order formulation accomplishes a similar function.

Perhaps the biggest advantage of this formulation is that it allows us to reduce a complicated problem (the lossy spin-boson model) into a much simpler one (a set of nearly degenerate states where the nearest neighbor coupling is dominant). We can use this formulation to compute the self-energies of the nearly degenerate states (which can remove the approximate degeneracy when the coupling is strong), and also the indirect coupling matrix elements. In the latter case, we can compare with perturbation theory in order to verify that the approach is correct in the weak coupling limit. We are able to use this approach to begin to understand how scaling works in the lossy spin-boson model, and to define a relevant dimensionless coupling coefficient.

A disadvantage of the approach is that the matrix calculations that result do not scale well as the number of states increase. So, if we focus on models that involve the exchange of only a few quanta (three, five, or seven), then we can perform calculations effectively even when the coupling is beginning to be strong. However, if we attempt computations for models with tens or hundreds of quanta exchanged, this approach is too slow to give us results in a reasonable time.

Even though the second-order formulation is not capable of handling the problems that we are ultimately interested in, it does provide us with a foundation that we can use for the development of approximation schemes which greatly extend our ability to analyze these models. A discussion of these approximation schemes is deferred to a following paper.

2. Coupling Between Nearly Degenerate States

We begin with the lossy spin-boson model, which is described by the Hamiltonian [17]

$$\hat{H} \;=\; \Delta E \frac{\hat{S}_z}{\hbar} + \hbar\omega_0 \hat{a}^\dagger \hat{a} + V(\hat{a}^\dagger + \hat{a}) \frac{2\hat{S}_x}{\hbar} - i\frac{\hbar\hat{\Gamma}(E)}{2}. \tag{1}$$

Here ΔE is the transition energy between the two-level systems, $\hbar\omega_0$ is the characteristic energy of the oscillator, and V describes the strength of the interaction. We have used many-spin operators $\hat{S}_z$ and $\hat{S}_x$ to describe the two-level systems. The model assumes identical two-level systems with identical linear interactions with the oscillator.

Loss is included using a Brillouin–Wigner formulation as we have reviewed previously [17]. In the case of a general loss model, the model that results is very complicated, and it becomes difficult to analyze. In this paper we will make an assumption about the loss in order to simplify things. In the infinite loss version of the model, we would assume that the loss is infinitely fast (resulting in zero occupation of the lossy states) when the basis state energy is less than E. Although this drastically reduces the complexity of the model, we find that even this simplified version of the model has technical issues associated with it due to the self-energy when the coupling is not weak. Instead, our focus will be on the closely related fixed basis version of the model, where we exclude all basis states with an energy less than the basis state energy of the nearly degenerate set initially selected.

2.1. Nearly degenerate states

We expand in terms of two sets of basis states

$$\Psi \;=\; \sum_j c_j \Phi_j^a + \sum_k d_k \Phi_k^b, \tag{2}$$

where the Φ_j^a states are of the form

$$|S, m\rangle|n\rangle, \quad |S, m-1\rangle|n+\Delta n\rangle, \quad \ldots,$$

which are nearly degenerate at the energy E of interest. Here Δn is the number of oscillator quanta exchanged per unit change in the excitation of the two-level systems. The Φ_k^b states include all of the other basis states with higher energy.

2.2. Isolation of the nearly degenerate states

Our goal is the development of a formulation that allows us to describe the slow evolution of the system between the nearly degenerate states. To accomplish this, we would like to focus on the c_j expansion coefficients of the degenerate basis states, and eliminate the other coefficients. To proceed, we start with the algebraic eigenvalue coefficients for the two sets of expansion coefficients (which we write in vector and matrix form)

$$\begin{aligned} E\mathbf{c} \;&=\; \mathbf{H}_a \cdot \mathbf{c} + \mathbf{V}_{ab} \cdot \mathbf{d}, \\ E\mathbf{d} \;&=\; \mathbf{H}_b \cdot \mathbf{d} + \mathbf{V}_{ba} \cdot \mathbf{c}. \end{aligned} \tag{3}$$

Since the b states are not degenerate at energy E, we can write the $\mathbf{d}$ vector in terms of the $\mathbf{c}$ vector as

$$\mathbf{d} \;=\; (E - \mathbf{H}_b)^{-1} \cdot (\mathbf{V}_{ba} \cdot \mathbf{c}). \tag{4}$$

This allows us to obtain a reduced implicit eigenvalue problem

$$E\mathbf{c} \;=\; \mathbf{H}_a \cdot \mathbf{c} + \mathbf{V}_{ab} \cdot (E - \mathbf{H}_b)^{-1} \cdot \mathbf{V}_{ba} \cdot \mathbf{c}. \tag{5}$$

2.3. Hamiltonian matrix for the nearly degenerate states

The associated second-order Hamiltonian matrix can be written as

$$\mathbf{H}(E) \;=\; \mathbf{H}_a + \mathbf{V}_{ab} \cdot (E - \mathbf{H}_b)^{-1} \cdot \mathbf{V}_{ba}. \tag{6}$$

This new second-order matrix $\mathbf{H}(E)$ is much smaller than the total matrix made up of $\mathbf{H}_a$, $\mathbf{H}_b$, $\mathbf{V}_{ab}$, and $\mathbf{V}_{ba}$, and we can use it for computations specifically on the c_j coefficients. Since the energy eigenvalue appears explicitly in the denominator, this Hamiltonian matrix is more complicated to work with than more standard Hamiltonians. Nevertheless, we can use iterative numerical methods to achieve self-consistency between a specific eigenvalue and the eigenvalue in the denominator.

3. Three-phonon Exchange and Scaling

One of our goals is the demonstration of a scaling law for the lossy spin-boson model. It seem reasonable to make use of the formulation outlined in the previous section to explore scaling for a specific example. The simplest example which shows enhanced coupling between nearly degenerate states is a problem in which a single two-level system quantum is matched to three oscillator quanta

$$\Delta E \;=\; 3\hbar\omega_0. \tag{7}$$

Since the numerical computations outlined increase rapidly when there are a very large number of states involved, we can minimize the number of states for a set of computations by reducing the number of oscillator quanta that are exchanged.

The notion of scaling is familiar to those working on various physics models, such as the spin-boson problem. If we were writing for those working on the this problem, probably a single line and scaling formula would suffice. However, the intended audience for this paper includes researchers who may not be familiar with the idea in the context of this kind of model. As a result, we are interested in clarifying the issue through the examination of a set of specific calculations.

3.1. Energy levels and scaling

The simplest way to understand what a scaling law does is by considering solutions for different examples which satisfy the scaling law. We consider two solutions with different numbers of two-level systems, under conditions where the maximum off-diagonal coupling matrix element for the original lossy spin-boson model are the same.

The largest matrix element has a magnitude of approximately

$$\max\{\langle S, m, n|\hat{H}|S, m \pm 1, n \pm 1\rangle\} \;=\; V\sqrt{n}S. \tag{8}$$

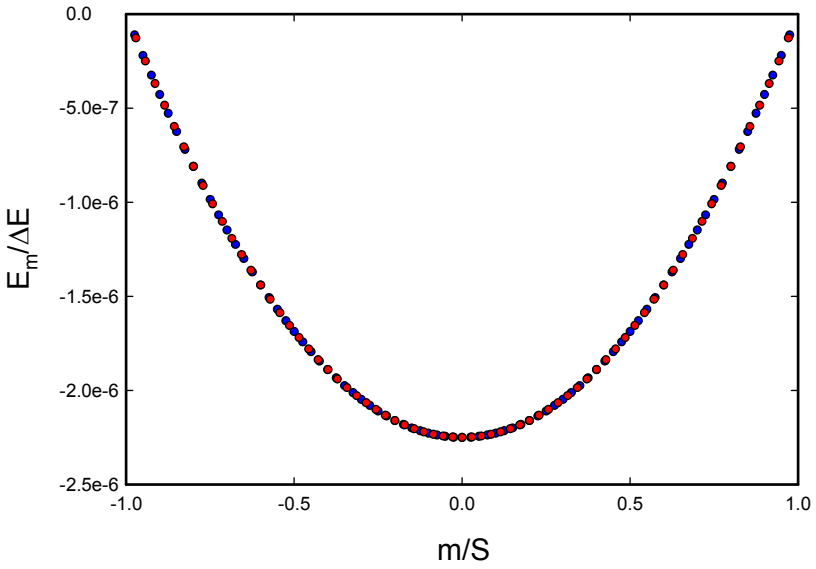

Figure 1. Reduced basis energies for 69 (red) and 79 (blue) two-level systems.

In Fig. 1, we show results for the diagonal matrix elements for $\mathbf{H}(E)$ in the case of 69 ($S = 34$) and 79 ($S = 39$) two-level systems. The product $V\sqrt{n}S$ is the same ($9.75 \times 10^{-3}\ \Delta E$) in both calculations. We have taken $n = 10^{12}$, and used different values for V to match the largest matrix element. We see that the diagonal energies line up together when plotted this way.

3.2. Dimensionless coupling strength

It is customary to define a dimensionless coupling strength g for this kind of problem. In this case, we would take the ratio of the magnitude of the coupling matrix element to the two-level transition energy, so that the maximum coupling strength is

$$\max\{g\} \ = \ \frac{V\sqrt{n}S}{\Delta E}. \tag{9}$$

The intuition that we seek to develop in what follows is that the local dimensionless coupling strength g determines the important parameters of the model, such as the self-energy and the indirect coupling matrix element between nearest neighbors.

3.3. Indirect coupling matrix elements

The indirect coupling matrix elements between nearest nearly degenerate neighbors are shown in Fig. 2 for the same calculations as for Fig. 1. We can make use of perturbation theory to compute the effective coupling matrix element for a transition from $|n, S, m\rangle$ to $|n-3, S, m+1\rangle$, which leads to

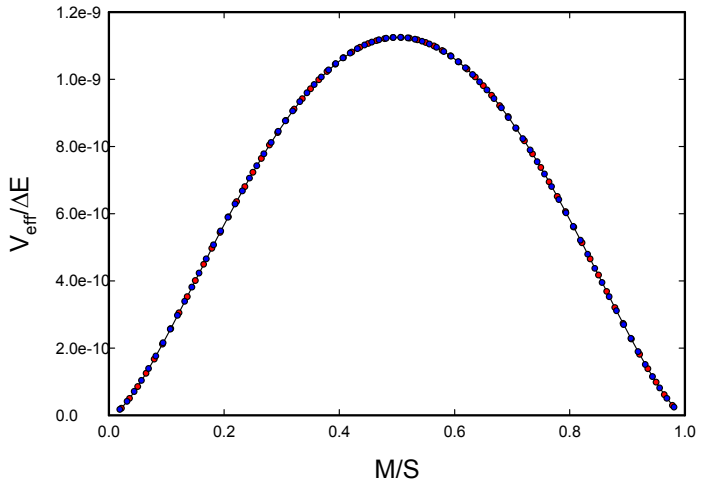

Figure 2. Indirect matrix element between nearly degenerate states for 69 (red) and 79 (blue) two-level systems.

$$V_{eff} \;=\; \frac{9}{8}\frac{V^3}{\Delta E^2}(S^2+S-m^2-3m-2)\sqrt{S^2+S-m^2-m}\sqrt{n(n-1)(n-2)}. \tag{10}$$

This perturbation theory result is indicated as a solid black line in Fig. 2. The two different problems that we have examined give very similar results for the indirect coupling matrix elements, and these results are in good agreement with the results from perturbation theory.

3.4. Decoupling of one basis state

One of the nearly degenerate states is decoupled from the others in this model. Consider the basis state

$$\Phi \;=\; |S,S,n_0\rangle. \tag{11}$$

in which all of the two-level systems are excited, and in which there are no excess oscillator quanta. This state has non-vanishing coupling matrix elements only to

$$|S,S-1,n_0\pm 1\rangle. \tag{12}$$

The energy of these states is below the cut-off energy in this model. Such states are presumed to be very lossy, and hence have a zero occupation probability in the infinite loss model. If so, then $|S,S,n_0\rangle$ becomes decoupled from the other states.

In Fig. 3, we show the lowest loss path in this case in a perturbation theory scheme. Two of the intermediate states have basis energies that are lower than that of the initial state, and which can decay. For comparison, we show the

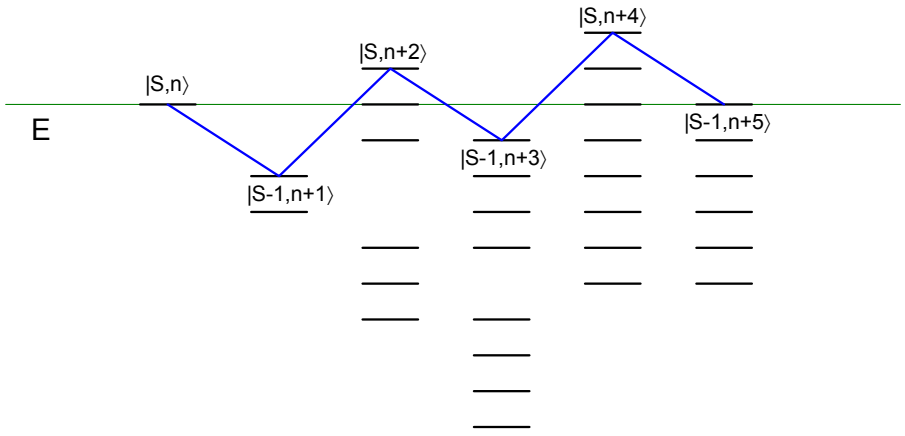

Figure 3. Levels and transitions for lowest loss pathway in perturbation theory starting from $|S, S, n\rangle = |S, n\rangle$, in the case of $\Delta E = 5\hbar\omega_0$.

lowest loss path in the general case in Fig. 4. In this case, none of the intermediate states have basis energies below that of the initial state, so that decay processes are minimized.

Coupling from this state in finite loss models would by necessity involve coupling through a lossy intermediate state. This is the first time in the present discussion that we come across this issue. When we consider more complicated models in papers that follow, we will find that this effect occurs generally in models of interest to us. We will eventually connect this effect with the low-level emission of energetic particles that is seen in some Fleischmann–Pons experiments.

3.5. Discussion

The specific problem that we selected to focus on in this section appears now to be very simple to understand. The second-order Hamiltonian leads to basis state energies that are very close to parabolic in m under conditions where perturbation theory is valid. The coupling between neighboring nearly degenerate states is dominant, and closely matches the result from perturbation theory.

In order for the associated system to exchange energy between the two degrees of freedom efficiently, all that we need is for the coupling matrix element between neighboring states to be as large as the splitting between neighboring states or greater. In this model, it seems clear how to do it. The more two-level systems that we have, the smaller the interaction we choose (in the scaling outlined above), so the smaller the difference between neighboring states. The coupling between neighboring states is strongest when about half of the two-level systems are excited, and is approximately constant with the number of two-level systems when scaled as above. Hence, as there are more two-level systems, we are able to maintain coherence over a larger fraction of the Dicke states.

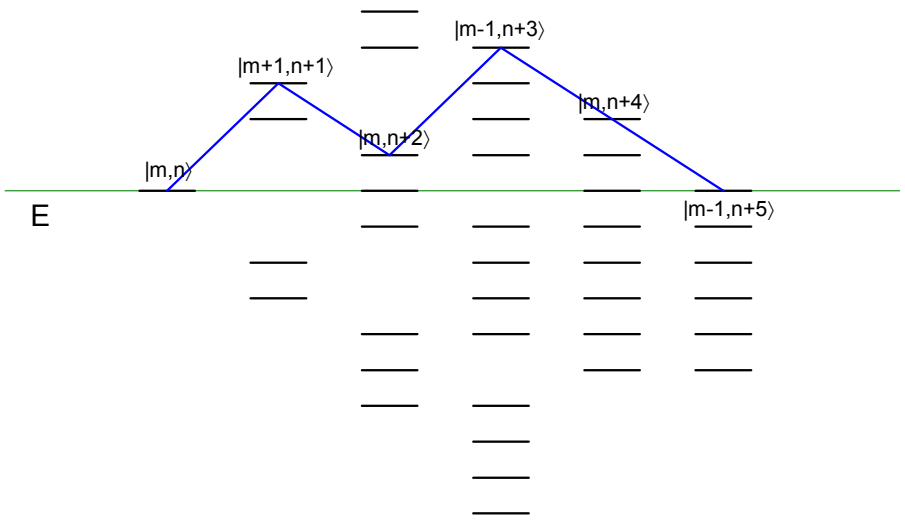

Figure 4. Levels and transitions for lowest loss pathway in perturbation theory starting from $|S, m, n\rangle = |m, n\rangle$, in the case of $\Delta E = 5\hbar\omega_0$.

4. Practical Issues

The isolation of a set of nearly degenerate states as outlined above is a very useful way to think about the problem, and provides a way to compute the important parameters of the model. However, as we start to go further in this direction, new issues arise. There is a practical computational issue concerning how to determine the energy eigenvalue self-consistently, since it appears in the second-order Hamiltonian. The self-energy shift tends to split the nearly degenerate states, so that we would like to understand under what conditions energy exchange can occur. The self-energy shift in addition impacts our selection of basis states, which motivates us to consider a restricted basis approximation.

4.1. Solving the second-order eigenvalue problem

If the dimensionless coupling strength is small, then the self-energy is also small, which means that one can obtain solutions to the second-order eigenvalue equation

$$E\mathbf{c} \;=\; \mathbf{H}_a \cdot \mathbf{c} + \mathbf{V}_{ab} \cdot (E - \mathbf{H}_b)^{-1} \cdot \mathbf{V}_{ba} \cdot \mathbf{c} \tag{13}$$

by using the unperturbed basis state energy on the right hand side. When the self-energy begins to become significant, then the accuracy of the energy eigenvalues computed this way is degraded. We can obtain accurate results by solving for the energy eigenvalue self-consistently, as discussed in Appendix B.

Unfortunately, it quickly becomes inconvenient to obtain numerical solutions using this approach as the number of quanta exchanged becomes larger, and when the dimensionless coupling strength is near or above unity. This will motivate us to pursue an approximate solution to the problem, which we will consider below.

4.2. Constraint for maintaining coherence

From the results in the previous section, we have seen that models with the same maximum dimensionless coupling coefficient g are very similar in terms of their self-energy and indirect coupling matrix elements. We can think of a family of models where the maximum dimensionless coupling constant is held fixed, and the number of two-level systems is varied (assuming that n is kept constant and large). For this family of models, the self-energy and indirect coupling matrix elements as a function of M/S are nearly the same. However, if the states were initially degenerate, then the splitting of the states is reduced when we have more two-level systems.

When we considered the dynamics resulting from the coupling between nearly degenerate states, we found that the problem was simplest in the case of degenerate basis states. If there is a splitting between the states, then this can alter the dynamics. In order for energy exchange to proceed at rates close to that for the degenerate version of the problem, we require that the splitting be less that the indirect coupling

$$|E_{m+1} - E_m| \; < \; |V_{m+\frac{1}{2}}| \tag{14}$$

in the notation of the previous paper. If the basis states are initially degenerate, then the splitting of interest for this constraint will be due to the self-energy shift. In this case, as we increase the number of two-level systems, the splitting will decrease, and more of the nearly degenerate states will be able to participate in the dynamics.

4.3. Constraint for three-quantum exchange

We can develop an approximate version of the constraint in the special case of three quantum exchange that we discussed above. The self-energy shift for small g is approximately

$$E_m \; = \; -0.0237\,(\max\{g\})^2 \left[1 - \left(\frac{m}{S}\right)^2\right] \Delta E \tag{15}$$

so that

$$|E_{m+1} - E_m| \; = \; 0.0237\,(\max\{g\})^2 \left(\frac{2|m|}{S^2}\right) \Delta E. \tag{16}$$

The matrix element for indirect coupling from perturbation theory is approximately

$$V_{\rm eff} \; = \; \frac{9}{8}(\max\{g\})^3 \left[1 - \left(\frac{m}{S}\right)^2\right]^{3/2} \Delta E \tag{17}$$

in the limit that S and n are large. We can combine these estimates to obtain

$$\frac{\left|\frac{m}{S}\right|}{\left[1 - \left(\frac{m}{S}\right)^2\right]^{3/2}} \; < \; 23.7\,\max\{g\}S. \tag{18}$$

This constraint is illustrated in Fig. 5.

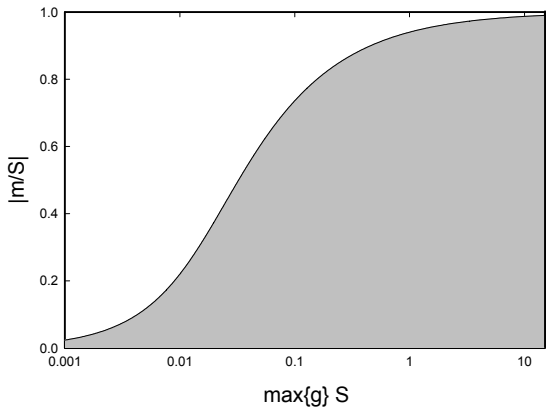

Figure 5. Evaluation of the constraint (18) in the case of three quantum exchange. The region in gray is where the level splitting is less than the indirect coupling matrix element.

4.4. Self-energy as potential energy of the coupled system

When the self-energy becomes large, there can be a significant shift of the energy levels. For example, when the coupling is near unity, the self-energy can be on the order of ΔE. Since this self-energy seems to be large, we need to think some about what it means, and what the implications are for our approximation.

The self-energy comes about due to the interactions in the model that produces the coupling between the states. Perhaps it is best to think of it as a binding energy or equivalently, a potential energy, for the coupled systems. If so, then it may be best to think of it on a per two-level system basis, especially if n is very large. For large g the self-energy becomes linear in g, so that this point of view will be helpful much later on when we consider models which seek to describe the Fleischmann–Pons excess power effect. Under the conditions that we have encountered so far, this self-energy per two-level system is small compared to the transition energy ΔE. It can be substantial compared to the oscillator energy, especially when a large number of oscillator quanta are exchanged.

4.5. Fixed basis state model

In the lossy spin-boson model with infinite loss, we proposed that all states with an energy less than E were to be assumed to have infinite loss. If the self-energy is small, then the basis state energy will not be so different from the diagonal energy in the second-order $\mathbf{H}(E)$ matrix. Hence, in this limit the choice of which states to keep and which to omit is clear.

However, if we include the self-energy, then things become more complicated. If we omit all states with an energy less than some energy E, and then calculate the diagonal energies for the $\mathbf{H}(E)$ matrix, we will find that many of the resulting states have an energy less than the energy E which we selected as a cut-off due to the contribution of the self-energy. If the dimensionless coupling constant g is close to unity, this contribution can be very large.

One approach to this problem is to go back and revise the list of included and omitted states so as to be self consistent with a cut-off energy. Another approach to the problem is to fix the basis initially, and keep it throughout the calculation. This latter approach is much more convenient for numerical calculations. In the limit that there are many oscillator quanta exchanged for each two-level transition, then this kind of model will lead to minor errors locally in the list of

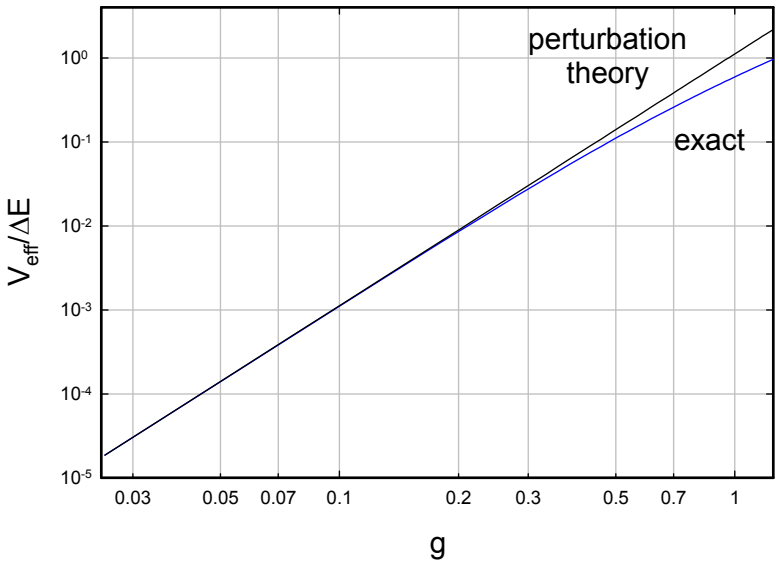

Figure 6. Largest normalized effective indirect coupling matrix element $V_{\rm eff}/\Delta E$ as a function of g computed using $S = 19$ (blue); perturbation theory result (black). The number of oscillator quanta used in this calculation is 10^{12}.

states that are retained (it will keep too many). We would not expect this to lead to significant changes in the model parameters or dynamics, but we have not pursued this issue in our work.

In Fig. 6, we show results from such a computation for the largest indirect coupling matrix element as a function of g. In most of the calculations that will follow in this and in following papers, we will work with this kind of model.

5. Discussion and Conclusions

In a previous paper of this set [17], we introduced the lossy spin-boson model and showed that it was capable of greatly enhanced coherent energy exchange (as compared to the lossless spin-boson model) when many oscillator quanta are exchanged for a two-level system quantum. In this we are pleased that the new model is capable of such efficient coherent energy exchange, since it is the basic effect that in our view is needed to account for excess heat in the Fleischmann–Pons experiment.

However, it is clear that we are going to need much stronger analytical tools to obtain results in a relevant regime. Perturbation theory is helpful when the coupling is weak, but we are going to need the model to work in a very strong coupling limit in order to convert a single two-level system quantum into 10^8 oscillator quanta. As a result, we need to develop models and approximations which are useful in the strong coupling limit.

The second-order formulation that we introduced above allows us to extend our modeling well beyond the weak coupling limit. We can use it directly to analyze the lossy spin-boson model when a relatively small number of oscillator quanta are exchanged. This is useful since it allows us to discuss scaling for this model, and also to introduce the dimensionless coupling constant g.

We cannot use the second-order formulation presented here for direct calculations of models in which millions of

quanta are exchanged for each two-level system transition, since the approach does not scale well as a computational problem. What is important here is the notion that we can isolate the nearly degenerate states, and that the self-energy and the matrix elements for indirect coupling between nearest neighbors obey scaling laws. For example, even though we are not able to perform a computation with 10^{10} two-level systems, we would have no trouble developing accurate estimates for the self-energy and indirect coupling between nearest neighbors for weak and moderately strong coupling in the case of 3 or 5 quantum exchange because of the scaling law. We still need to develop a scaling law that governs the self-energy and indirect coupling matrix element in the limit where a large number of oscillator quanta are exchanged.

In a paper that follows, we will present an approximation scheme which is based on the formulation presented here that will allow us to perform calculations for models where a much larger number of oscillator quanta are exchanged. Based on these results we will be able to deduce a scaling law that is useful generally when the number of oscillator quanta exchanged is large.

Appendix A. Numerical issues

The algebraic problem as outlined in Section 2 seems completely straightforward, but there are significant issues that remain. Some of these concern numerical issues which we must face when implementing the approximation. We will provide a brief discussion of a simple numerical approach in the subsections that follow.

Appendix A.1. Selection of basis states

We first consider the selection of basis states. We have the parity selection rule that states with positive parity $(-1)^{n+m}$ do not couple with states with negative $(-1)^{n+m}$. So, we have chosen to work with positive parity states here.

Next, we note that the number of Dicke states associated with the two-level systems alone is $2S+1$, since all of the two-level systems can be in the ground state ($m=-S$) and all of them can be in the excited state ($m=S$). The line for equal energy is defined according to

$$E \;=\; \Delta E m + \hbar\omega_0 n. \tag{A.1}$$

It seems reasonable to keep states up to some fixed energy above the threshold energy, which we define here has being

$$E_0 \;=\; \Delta E S + \hbar\omega_0 n_0. \tag{A.2}$$

At this energy, all of the two-level systems are excited, and the oscillator has nominal excitation n_0.

Appendix A.2. Banded Cholesky decomposition

In the algebraic equation above, we need to compute the inverse of a matrix. While this seems straightforward, not all numerical algorithms will result in a symmetric inverse. Consequently, we need to pay some attention to how this is carried out.

To proceed, we define

$$\mathbf{A} \;=\; \mathbf{A}(E) \;=\; \mathbf{H}_b - E. \tag{A.3}$$

Since $\mathbf{A}$ is symmetric, LU decomposition can be carried out using

$$\mathbf{A} \;=\; \mathbf{L}\cdot\mathbf{L}^{\mathrm{T}}, \tag{A.4}$$

where **L** is lower triangular.

We can use Cholesky decomposition in order to decompose **A**. This algorithm seems to work pretty well for this problem. We are aided by the fact that **A** is banded, which speeds the computation of **L**, and leads to a banded matrix **L**. Even for a very large problem, we are able to compute **L** by Cholesky decomposition conveniently.

Appendix A.3. Matrix inverse of the lower triangular matrix

For the solution linear systems, Cholesky decomposition is the time-consuming part of the algorithm in the case of symmetric matrices. Determination of the solution is done by back substitution. We have tried various algorithms based on back substitution, however, it seemed useful along the way to carry out an explicit construction of the inverse, and we subsequently kept it.

The construction of the inverse of a lower triangular matrix can be done reasonably efficiently in the case of a banded matrix. The algorithm that we have used works as follows. We assume that the inverse is also a lower triangular matrix **B**, so that

$$\mathbf{B}\cdot\mathbf{L} \;=\; \mathbf{I}. \tag{A.5}$$

To understand the associated algorithm for determining **B**, it is useful to write this equation out explicitly in the case of 3×3 matrices. We may write

$$\begin{pmatrix} B_{11} & 0 & 0 \\ B_{21} & B_{22} & 0 \\ B_{31} & B_{32} & B_{33} \end{pmatrix}\cdot\begin{pmatrix} L_{11} & 0 & 0 \\ L_{21} & L_{22} & 0 \\ L_{31} & L_{32} & L_{33} \end{pmatrix} \;=\; \begin{pmatrix} B_{11}L_{11} & 0 & 0 \\ B_{21}L_{11}+B_{22}L_{21} & B_{22}L_{22} & 0 \\ B_{31}L_{11}+B_{32}L21+B_{33}L_{31} & B_{32}L_{22}+B_{33}L_{32} & B_{33}L_{33} \end{pmatrix}. \tag{A.6}$$

It seems clear that we can solve for diagonal terms directly using

$$B_{ii} \;=\; \frac{1}{L_{ii}}. \tag{A.7}$$

If we go off of the diagonal by one, we end up with equations of the form

$$B_{i,i-1}L_{i-1,i-1}+B_{ii}L_{i,i-1} \;=\; 0. \tag{A.8}$$

We can solve this using

$$B_{i,i-1} \;=\; -\frac{B_{ii}L_{i,i-1}}{L_{i-1,i-1}}. \tag{A.9}$$

It is possible to continue the algorithm to determine the different B_{ij} values based on a knowledge of known L and previously determined B matrix elements.

Appendix A.4. Construction of the second-order matrix

The second-order matrix can be written as

$$\mathbf{H}(E) \;=\; \mathbf{H}_a - \mathbf{V}_{ab} \cdot \mathbf{A}^{-1}(E) \cdot \mathbf{V}_{ba}. \tag{A.10}$$

This can be written in terms of $\mathbf{L}$ as

$$\mathbf{H}(E) \;=\; \mathbf{H}_a - \mathbf{V}_{ab} \cdot (\mathbf{L} \cdot \mathbf{L}^{\mathrm{T}})^{-1} \cdot \mathbf{V}_{ba} \;=\; \mathbf{H}_a - \mathbf{V}_{ab} \cdot (\mathbf{L}^{\mathrm{T}})^{-1} \cdot \mathbf{L}^{-1} \cdot \mathbf{V}_{ba}. \tag{A.11}$$

We can recast this as

$$\mathbf{H}(E) \;=\; \mathbf{H}_a - (\mathbf{L}^{-1} \cdot \mathbf{V}_{ba})^{\mathrm{T}} \cdot (\mathbf{L}^{-1} \cdot \mathbf{V}_{ba}). \tag{A.12}$$

In this form, the resulting second-order matrix is explicitly real and symmetric, which was one of the goals of our construction.

Appendix B. Self-consistent computation of the energy

The Schrödinger equation in the case of the second-order Hamiltonian can be written as

$$E\mathbf{c} \;=\; \mathbf{H}_a \cdot \mathbf{c} + \mathbf{V}_{ab} \cdot (E - \mathbf{H}_b)^{-1} \cdot \mathbf{V}_{ba} \cdot \mathbf{c}. \tag{B.1}$$

We see that the energy eigenvalue appears both on the right-hand side (RHS) and on the left-hand side (LHS) of this equation. If the self-energy shift is small, then we can approximate the energy on the RHS with the basis state energy and obtain good results. If the self-energy shift is large, then a self-consistent calculation is needed.

Appendix B.1. Simple iteration

Iterative schemes can be used to obtain a self-consistent solution. The simplest iterative scheme can be written as

$$E^{(k+1)}\mathbf{c} \;=\; \mathbf{H}_a \cdot \mathbf{c} + \mathbf{V}_{ab} \cdot (E_j^{(k)} - \mathbf{H}_b)^{-1} \cdot \mathbf{V}_{ba} \cdot \mathbf{c}. \tag{B.2}$$

On the LHS, we have the energy eigenvalue in general $E^{(k+1)}$ for the $k+1$ iteration; on the RHS we have one particular basis state energy E_j^k determined on the previous iteration. If the scheme converges, then it can be stopped when the change in the energy eigenvalue of the state of interest doesn't change any more

$$|E_j^{(k+1)} - E_j^{(k)}| \;<\; \epsilon. \tag{B.3}$$

The iterations can be started by taking the initial energy equal to the initial basis state energy.

Appendix B.2. Iterations with relaxation

We have found that the iterations described above do not converge when the dimensionless coupling coefficient approaches unity. In this case, we have been able to converge using a modification of the scheme with relaxation based on

$$E^{(k+1)}\mathbf{c} \;=\; \mathbf{H}_a \cdot \mathbf{c} + \mathbf{V}_{ab} \cdot (F_j^{(k)} - \mathbf{H}_b)^{-1} \cdot \mathbf{V}_{ba} \cdot \mathbf{c}, \tag{B.4}$$

where

$$F_j^{(k)} \;=\; aE_j^{(k)} + (1-a)E_j^{(k-1)} \tag{B.5}$$

with a taken to be near 0.2.

References

[1] P.L. Hagelstein, A unified model for anomalies in metal deuterides, *Proc. ICCF9*, 2002, p. 121.
[2] P.L. Hagelstein and I.U. Chaudhary, Progress on phonon exchange models for excess heat in metal deuterides, *Proc. 13th Int. Conf. Cold Fusion*, 2007, p. 590.
[3] P.L. Hagelstein and I.U. Chaudhary, Models relevant to excess heat production in Fleischmann–Pons experiments, *Low-energy nuclear reactions sourcebook*, ACS Symposium Series 998, 2008, p. 249.
[4] P.L. Hagelstein and I.U. Chaudhary, Excitation transfer and energy exchange processes for modeling the Fleischmann–Pons excess heat effect, *Proc. 14th Int. Conf. Cold Fusion*, 2008, p. 579.
[5] M. Fleischmann, S. Pons and M. Hawkins, *J. Electroanal Chem.* **201** (1989) 301; errata **263** (1990) 187.
[6] M. Fleischmann, S. Pons, M.W. Anderson, L.J. Li and M. Hawkins, *J. Electroanal. Chem.* **287** (1990) 293.
[7] M.C.H. McKubre, S. Crouch-Baker, R.C. Rocha-Filho, S.I. Smedley, F.L. Tanzella, T.O. Passell, J. Santucci, *J. Electroanal. Chem.* **368** (1994) 55.
[8] E. Storms, *Science of Low Energy Nuclear Reaction: A comprehensive compilation of evidence and explanations about cold fusion*, World Scientific, Singapore, 2007.
[9] M.H. Miles, R.A. Hollins, B.F. Bush, J.J. Lagowski, R.E. Miles, *J. Electroanal. Chem.* **346** (1993) 99.
[10] M. H. Miles, B. F. Bush, and J. J. Lagowski, *Fusion Technology* **25** (1994) 478.
[11] M.H. Miles, Correlation of excess enthalpy and helium-4 production: A review, *Proc. 10th Int. Conf. Cold Fusion*, 2003, p. 123.
[12] P.L. Hagelstein, *Naturwissenschaften* **97** (2010) 345.
[13] P L. Hagelstein, M.C.H. McKubre, D.J. Nagel, T.A. Chubb, R.J. Hekman, New physical effects in metal deuterides, *Proc. 11th Int. Conf. Cold Fusion*, 2005, p. 23.
[14] F. Bloch and A. Siegert, *Phys. Rev.* **57** (1940) 522.
[15] J. Shirley, *Phys. Rev.* **138** (1965) B979.
[16] C. Cohen-Tannoudji, J. Dupont-Roc and C. Fabre, *J. Phys. B: Atom. Molec. Phys.* **6** (1973) L214.
[17] P.L. Hagelstein and I.U. Chaudhary, Energy exchange in the lossy spin-boson model, *J. Cond. Mat. Nucl. Sci.* **5** (2011) 52.
[18] P.L. Hagelstein and I.U. Chaudhary, Dynamics in the case of coupled degenerate states, *J. Cond. Mat. Nucl. Sci.* **5** (2011) 72.
[19] P.L. Hagelstein and I.U. Chaudhary, *J. Phys. B: Atom. Molec. Phys.* **41** (2008) 035601.
[20] P.L. Hagelstein and I.U. Chaudhary, *J. Phys. B: Atom. Molec. Phys.* **41** (2008) 035602.

J. Condensed Matter Nucl. Sci. 5 (2011) 102–115

Research Article

Local Approximation for the Lossy Spin–boson Model

Peter L. Hagelstein *

Research Laboratory of Electronics, Massachusetts Institute of Technology, Cambridge, MA 02139, USA

Irfan U. Chaudhary

Department of Computer Science and Engineering, University of Engineering and Technology. Lahore, Pakistan

Abstract

We are interested in the problem of coherent energy exchange in the spin-boson model augmented with loss, in the limit of infinite loss. This model is interesting because it predicts rapid coherent energy exchange under conditions when the transition energy of the two-level systems is much greater than the characteristic energy of the oscillator. Here we introduce the local approximation, in which we assume that the matrix elements change little when an energy exchange event occurs. This approximation results in a periodic system when a resonance condition is satisfied, which is much easier to solve than the original problem. We consider a model problem where we analyze the self-energy and indirect coupling matrix elements numerically and in the local approximation, with good agreement. Systematic results from the local approximation are obtained for the self-energy and indirect coupling matrix elements in models where 3, 5, 7, 9, and 11 quanta are exchanged.
© 2011 ISCMNS. All rights reserved.

Keywords: Coherent energy exchange, Excess heat, Fleischmann–Pons experiment, Lossy spin-boson model, Theory

1. Introduction

There have been a great many experiments which indicate that excess energy is produced in the Fleischmann–Pons experiment [1,2] and its variants. The amount of energy observed in some of these experiments is prodigious, with no obvious commensurate chemical processes observed. Since there has been measured ^{4}He in amounts proportional to the energy produced [3–5], with an associated Q-value near 24 MeV [6], one possible conclusion is that there is some kind of new nuclear reaction process occurring. The conundrum that arises in such a proposal is that known exothermic nuclear reactions put the reaction energy into energetic nuclear particles. In the Fleischmann–Pons experiment, there simply aren't energetic nuclear particles in amounts commensurate with the energy produced [7]. Consequently, conventional

*E-mail: plh@mit.edu

© 2011 ISCMNS. All rights reserved.

nuclear reactions that appear in the nuclear physics literature in general cannot be candidates to account for the excess heat effect.

If so, then the question arises as to what reactions or new physical processes can be consistent with these experimental observations? It seems the outstanding theoretical problem which must be faced involves the conversion of a very large MeV-level nuclear quantum of energy into a very large number of eV-level or meV-level quanta.

If we adopt such a point of view, then the recent results from two-laser experiments [8,9] perhaps begin to make sense. Excess power is observed when the cathode is stimulated by two weak laser beams, and the response depends on the frequency difference between the two laser frequencies. Two of the frequencies at which strong responses are observed correspond to the Γ-point (8 THz) and L-point (15 THz) of the optical phonon mode dispersion curve of PdD. The excess power in these experiments is seen in many cases to persist when the lasers are turned off. Some power is put into one of the these modes by the lasers, which initially stimulates excess power production. If excess power continues when the lasers are turned off, we might infer that some of the energy which is being produced in the reaction is going into the mode that has been stimulated. This could be verified by Raman measurements, but such experiments have not yet been attempted.

From experiment, a picture seems to emerge in which a new kind of nuclear reaction process occurs, in which the reaction energy is communicated to the optical phonon modes. Such an effect is unprecedented, which makes the theoretical problem of model development that much harder. Nevertheless, we have managed to construct new models based on two-level systems coupled to an oscillator, which exhibit a much accelerated coherent energy exchange effect involving the fractionation of a large energy quantum into a great many low energy quanta.

The simplest version of the model is the spin-boson model augmented with loss, which we have introduced in earlier publications. We have demonstrated the new coherent energy exchange effect using perturbation theory [10], and we have also presented a second-order formulation of the model [11] which allows us to think about the model in terms of a set of ordered nearly degenerate states with nearest neighbor coupling. In these papers, we have begun the analysis of the model, introducing tools that help us understand and analyze important properties. Our goal ultimately is to understand how coherent energy exchange works in a regime relevant to the Fleischmann–Pons experiment, and in this work we take a big step in that direction. In this paper, we introduce the local approximation, which provides us with a powerful tool to analyze coherent energy exchange when the coupling is strong, and also when a larger number of oscillator quanta are exchanged.

2. Local Approximation for the Lossy Spin-boson Model

As we have discussed in earlier works, the lossy spin-boson model is described by the Hamiltonian [10]

$$\hat{H} \;=\; \Delta E\frac{\hat{S}_z}{\hbar} + \hbar\omega_0\hat{a}^\dagger\hat{a} + V(\hat{a}^\dagger+\hat{a})\frac{2\hat{S}_x}{\hbar} - i\frac{\hbar}{2}\hat{\Gamma}(E), \tag{1}$$

where ΔE is the transition energy of the two-level systems, where $\hbar\omega_0$ is the oscillator energy, and where V is the coupling strength. Loss is included through the second-order $-i\hbar\hat{\Gamma}(E)/2$ term that comes from a Brillouin–Wigner formulation (see [10]). Eigenfunctions of the coupled two-level systems and oscillator can be found from the solution of the eigenvalue problem

$$E\Psi \;=\; \hat{H}\Psi. \tag{2}$$

2.1. Finite basis approximation

We can make use of a finite basis approximation for the associated wave function in terms of product basis states according to

$$\Psi \;=\; \sum_m \sum_n c_{m,n} |S,m\rangle |n\rangle. \tag{3}$$

We can use this to develop the above eigenvalue equation in terms of the expansion coefficients according to

$$\begin{aligned} E c_{m,n} \;=& \left(\Delta E m + \hbar\omega_0 n - i\frac{\hbar}{2}\Gamma(E) \right) c_{m,n} + V\sqrt{n+1}\sqrt{(S-m)(S+m+1)}\, c_{m+1,n+1} \\ &+ V\sqrt{n}\sqrt{(S-m)(S+m+1)}\, c_{m+1,n-1} + V\sqrt{n+1}\sqrt{(S+m)(S-m+1)}\, c_{m-1,n+1} \\ &+ V\sqrt{n}\sqrt{(S+m)(S-m+1)}\, c_{m-1,n-1}. \end{aligned} \tag{4}$$

2.2. Limit of many oscillator quanta and two-level systems

In the event that n is very large, then

$$\sqrt{n+1} \;\approx\; \sqrt{n}. \tag{5}$$

If S is very large, and if m is not close to $\pm S$, then

$$\sqrt{(S-m)(S+m+1)} \;\approx\; \sqrt{S^2-m^2}, \qquad \sqrt{(S+m)(S-m+1)} \;\approx\; \sqrt{S^2-m^2} \tag{6}$$

Under these approximations, the coupling coefficients to the nearby states are the same, so that the eigenvalue equation for the expansion coefficients is approximately

$$\begin{aligned} E c_{m,n} \;=& \left[\Delta E m + \hbar\omega_0 n - i\frac{\hbar}{2}\Gamma(E) \right] c_{m,n} \\ &+ V\sqrt{n}\sqrt{S^2-m^2} \left(c_{m+1,n+1} + c_{m+1,n-1} + c_{m-1,n+1} + c_{m-1,n-1} \right). \end{aligned} \tag{7}$$

2.3. Local approximation in terms of g

We recall that the dimensionless coupling constant g is given by

$$g \;=\; \frac{V\sqrt{n}\sqrt{S^2-m^2}}{\Delta E}. \tag{8}$$

The approximate eigenvalue equation can be written in terms of the dimensionless coupling constant as

$$\begin{aligned} \frac{E}{\Delta E} c_{m,n} \;=& \left(1 + \frac{\hbar\omega_0}{\Delta E} - i\frac{\hbar\Gamma(E)}{2\Delta E} \right) c_{m,n} \\ &+ g \left(c_{m+1,n+1} + c_{m+1,n-1} + c_{m-1,n+1} + c_{m-1,n-1} \right). \end{aligned} \tag{9}$$

Although g is dependent on m, we can simplify the problem significantly if we consider it to be a constant. The eigenvalue equation that results constitutes a local approximation, allowing us to obtain approximate basis state energies and indirect coupling coefficients.

2.4. Hamiltonian associated with the local approximation

We can write down a Hamiltonian for this local approximation as

$$\hat{H} \;=\; \Delta E \frac{\hat{S}_z}{\hbar} + \hbar\omega_0 \hat{a}^\dagger \hat{a} + g\Delta E \left(\hat{\delta}_+^n + \hat{\delta}_-^n\right)\left(\hat{\delta}_+^m + \hat{\delta}_-^m\right) - i\frac{\hbar}{2}\hat{\Gamma}(E), \tag{10}$$

where the $\hat{\delta}$ operators satisfy

$$\hat{\delta}_\pm^n |n\rangle \;=\; |n \pm 1\rangle, \tag{11}$$

$$\hat{\delta}_\pm^m |S, m\rangle \;=\; |S, m \pm 1\rangle. \tag{12}$$

3. Periodicity

An important feature of the Hamiltonian in the local approximation is that it is invariant under translations of the form

$$\hat{T}_\pm |S, m\rangle |n\rangle \;=\; |S, m \pm 1\rangle |n \mp \Delta n\rangle, \tag{13}$$

when the resonance condition holds

$$\Delta E \;=\; \Delta n\, \hbar\omega_0 \tag{14}$$

for odd Δn.

3.1. Bloch's theorem

The Hamiltonian is invariant under the energy-preserving translations of the $\hat{T}_\pm$ operators, so we know that Bloch's theorem applies. The eigenfunctions $\Phi_{m,n}$ of the local Hamiltonian satisfy the time-independent Schrödinger equation

$$\hat{H}\Phi_{m,n} \;=\; E\Phi_{m,n}. \tag{15}$$

In the local approximation with odd integer Δn, the Hamiltonian commutes with the translation operators

$$[\hat{T}_\pm, \hat{H}] \;=\; 0. \tag{16}$$

Hence it is possible to find solutions which are eigenfunctions of both operators

$$\hat{H}\Phi_{m,n} \;=\; E\Phi_{m,n}, \tag{17}$$

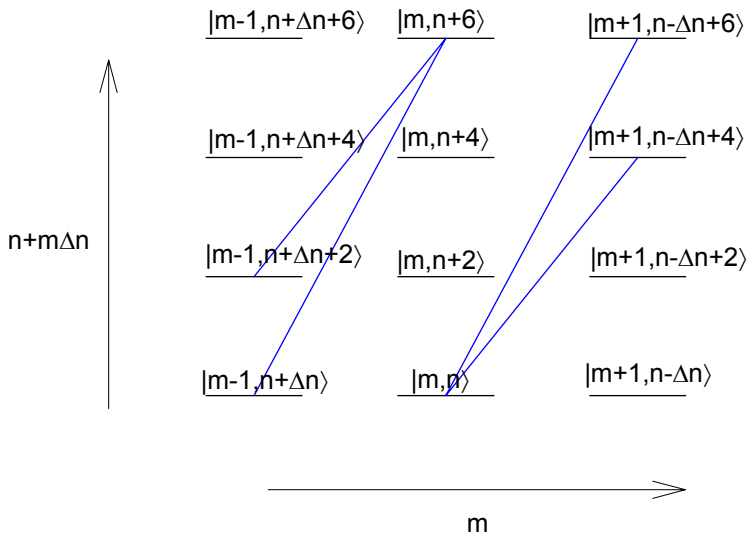

Figure 1. Levels and selected couplings in m and $n + m\Delta n$ basis with $\Delta n = 5$, plotted using m and $n + m\Delta n$ (proportional to the energy) axes. State $|m, n + 6\rangle$ is coupled to higher energy states $|m + 1, n + 6 \pm 1\rangle$, although this coupling is not shown.

$$\hat{T}_+ \Phi_{m,n} \;=\; C\,\Phi_{m,n}. \tag{18}$$

These solutions can be written in the form

$$\Phi_{m,n} \;=\; \mathrm{e}^{im\phi} u_{m,n}, \tag{19}$$

where the $u_{m,n}$ are periodic in m. As a result, the energy eigenvalues can be described as a set of bands in ϕ from the eigenvalue equation

$$E(\phi)\mathrm{e}^{im\phi} u_{m,n} \;=\; \hat{H}\mathrm{e}^{im\phi} u_{m,n}. \tag{20}$$

3.2. Reduced problem and boundary conditions

Since the problem is periodic under the local Hamiltonian, we can reduce the problem by working with a single column of states such as plotted in Fig. 1. We need only include the states $|m, n\rangle$, $|m, n + 2\rangle, \cdots$ explicitly. The phase factors that result in the Bloch solution relate the phase of a basis state with one value of m to the phase of the basis state at the same energy at a neighboring value of m. So, a Bloch state solution can be developed from a set of expansion coefficients associated with the basis states in a single column, knowing that the expansion coefficients for the basis states in neighboring columns differ only by a single phase factor for each column.

4. Product solution

The discussion above suggests that a convenient product solution can be constructed using

$$\Psi \;=\; \sum_m \sum_n d_m v_{n+m\Delta n} |S, m\rangle |n + m\Delta n\rangle \tag{21}$$

assuming large S with m away from $\pm S$, and large n. Since the index of the v coefficients is proportional to the basis state energy, it is unaffected by $\hat{T}_\pm$ translations. Hence we can implement the phase factors associated with the Bloch states in the d_m coefficients by taking

$$d_m \;=\; \mathrm{e}^{im\phi}. \tag{22}$$

The local Hamiltonian couples states with m and n indices that differ by one unit; however, when we line the states up according to their energy (which is useful in the local approximation), then this coupling appears to connect relatively distant states as indicated in Fig. 1.

4.1. Self-energy

Starting with the basis expansion above, we can isolate the v coefficients by taking advantage of orthogonality

$$\langle m', n' | m, n\rangle \;=\; \delta_{m',m}\delta_{n',n}. \tag{23}$$

The eigenvalue equation associated with the expansion coefficients can be written as

$$\begin{aligned} E(\phi) d_m v_{n+m\Delta n} \;=\; & \left[\Delta E m + n\hbar\omega_0 - i\frac{\hbar}{2}\hat{\Gamma}(E)\right] d_m v_{n+m\Delta n} \\ & + g\Delta E\Big[d_{m+1}(v_{n+1+(m+1)\Delta n} + v_{n-1+(m+1)\Delta n}) \\ & + d_{m-1}(v_{n+1+(m-1)\Delta n} + v_{n-1+(m-1)\Delta n})\Big]. \end{aligned} \tag{24}$$

If we focus on the coefficients corresponding to the column with $m = 0$ and use $d_m = \exp(im\phi)$, we obtain

$$\begin{aligned} E(\phi) v_n \;=\; & \left[n\hbar\omega_0 - i\frac{\hbar}{2}\hat{\Gamma}(E)\right] v_n \\ & + g\Delta E\Big[\mathrm{e}^{i\phi}(v_{n+\Delta n+1} + v_{n+\Delta n-1}) + \mathrm{e}^{-i\phi}(v_{n-\Delta n+1} + v_{n-\Delta n-1})\Big]. \end{aligned} \tag{25}$$

The lowest energy solution of this eigenvalue equation gives the self-energy in the local approximation.

4.2. Indirect coupling matrix element

Under conditions that are of interest to us in the development of models relevant to the excess heat effect in the Fleischmann–Pons experiment, the indirect coupling between nearly degenerate states is weak. In the local approximation, a second-order formulation that isolates the nearly degenerate states would result in degenerate states when Δn is an odd integer. The associated eigenvalue equation is of the form

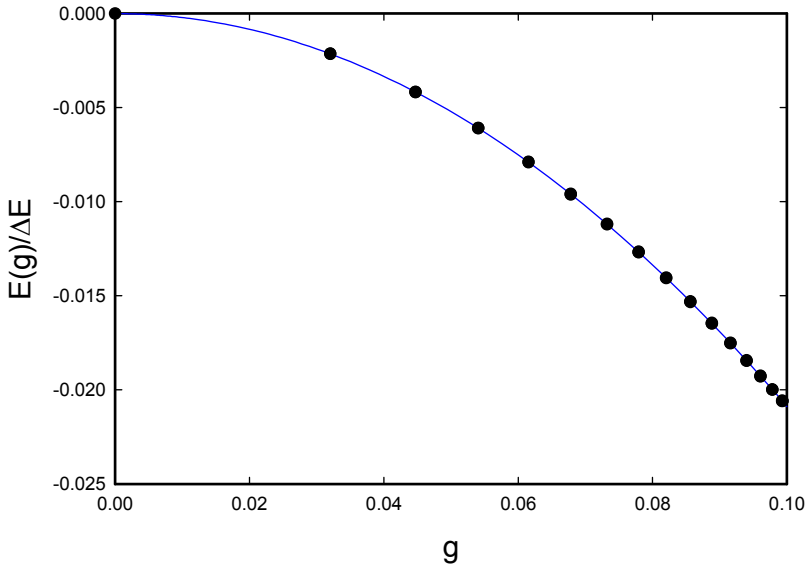

Figure 2. Self-energies for the nearly degenerate basis states of the test problem (black circles) and for the local approximation (blue line).

$$Ed_m \;=\; E_0 d_m + V_{\rm eff}(d_{m-1} + d_{m+1}). \tag{26}$$

It is possible to obtain a useful version of such an equation from the model under consideration above (but this will be of more interest in a later paper, so we defer the associated discussion).

We can solve this equation using

$$d_m \;=\; {\rm e}^{im\phi} \tag{27}$$

consistent with the phase factor that we used above from Bloch's theorem. The associated energy eigenvalue is

$$E(\phi) \;=\; E_0 + 2V_{\rm eff}\,\cos\phi. \tag{28}$$

As a result, if we were to solve the eigenvalue equation in the local approximation for two values of ϕ, then we could determine the indirect coupling coefficient in the weak coupling approximation. For example, if we take ϕ values of 0 and π, then we obtain

$$E(0) - E(\pi) \;=\; 4V_{\rm eff}. \tag{29}$$

We have used this to obtain numerical estimates for the indirect coupling matrix element for the restricted basis version of the infinite loss model with success.

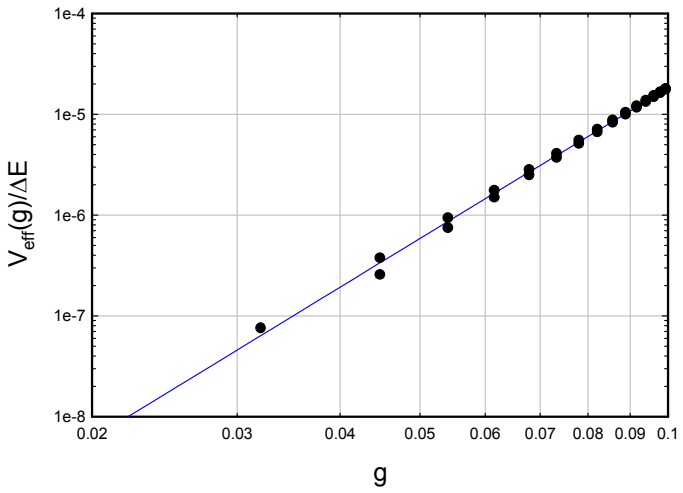

Figure 3. Indirect coupling matrix elements for the nearly degenerate basis states of the test problem (black circles) and for the local approximation (blue line).

5. Model Problem

The local approximation described above allows us to develop approximate results for the self-energy and indirect coupling matrix elements for the lossy spin-boson model. Since it is an approximation, we are interested in whether it can give good results. To explore this, we developed a model problem in which we can compare the approximate results with exact numerical results.

5.1. Problem specification

For the test problem, we chose

$$\frac{\Delta E}{\hbar\omega_0} = 5 \tag{30}$$

with

$$S = 19.5, \tag{31}$$

which corresponds to 39 two-level systems. We took the coupling strength V to satisfy

$$\frac{V\sqrt{n}S}{\Delta E} = 0.1 \tag{32}$$

for which the maximum dimensionless coupling strength g is close to 0.10. We have taken the lossy spin-boson model in the limit of infinite loss, using a restricted basis approximation [11].

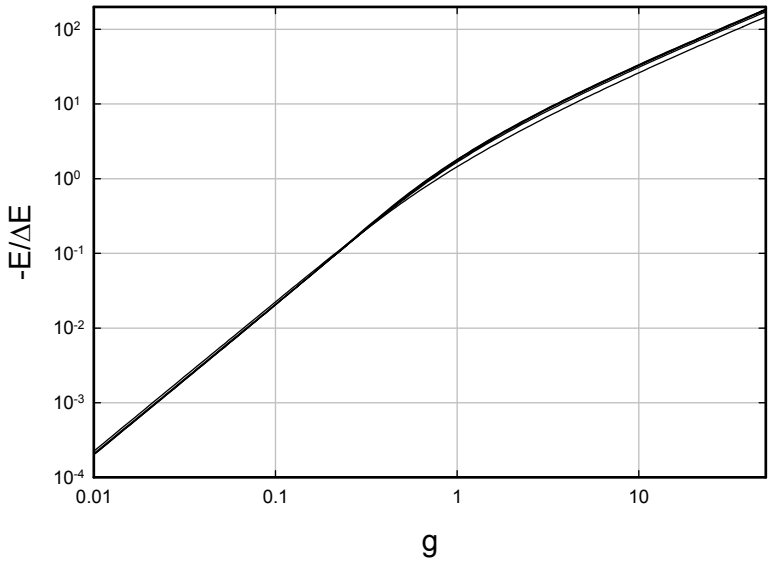

Figure 4. Self-energy as a function of g for $\Delta n = 3,5,7,9,11$ ($n = 3$ is the bottom curve, and $n = 11$ is the top).

5.2. Second-order formulation

In a previous paper we described a second-order formulation for the lossy spin-boson problem [11]. The advantage of this formulation is that we are able to reduce the original complicated Hamiltonian into a conceptually simpler one that focuses on a set of nearly degenerate states that are coupled indirectly. This formulation can be represented through the second-order Hamiltonian

$$\mathbf{H}(E) \;=\; \mathbf{H}_a + \mathbf{V}_{ab} \cdot (E - \mathbf{H}_b)^{-1} \cdot \mathbf{V}_{ba}, \tag{33}$$

which we can evaluate numerically to determine the self-energies and indirect matrix elements.

For this calculation, we took 50 energy points for the energy in the denominator and evaluated the self-energies and indirect coupling matrix elements between nearest neighbors. Then we interpolated for self-consistency for each state to get the self-energies. Based on this interpolation we obtained accurate values for the indirect coupling matrix elements.

5.3. Comparison of the self-energy

To compare the results from the two models, we needed to develop an estimate for the local coupling strength. Our procedure was to sum the coupling matrix elements out of one of the initial degenerate basis states of the original full Hamiltonian, and then divide by the product of ΔE and the number of couplings. This produces an approximate local g defined by

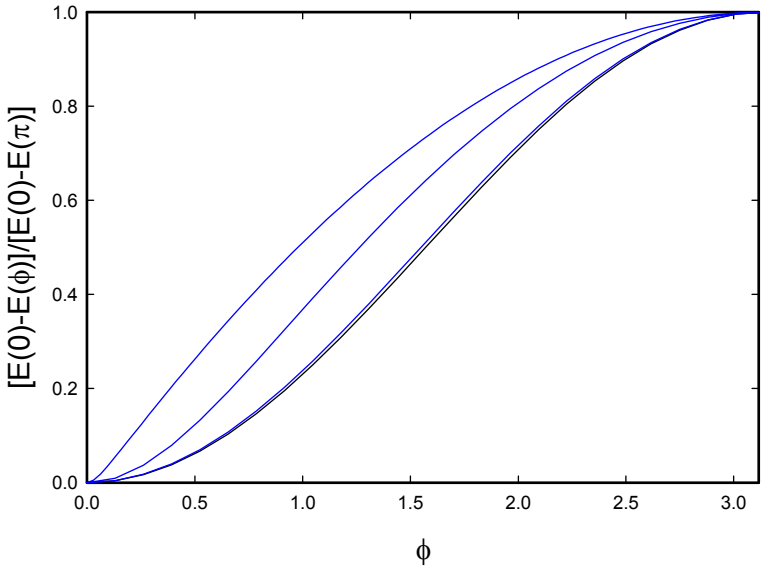

Figure 5. Relative self-energy as a function of phase angle ϕ for $\Delta n = 5$. Weak coupling limit is the lower curve in black; results from bottom to top in blue are for $g = 0.3, 1, 10$.

$$g_i = \frac{\sum_j H_{ij}}{\sum_j \Delta E}, \tag{34}$$

where the summation over j includes only states with non-zero coupling matrix elements from i. We plotted the self-energy for each state versus the approximate state g_i as points in Fig. 2, and we also plotted results for the self-energy as a function of g in the local approximation as a line. As can be seen, the agreement is excellent for all of the nearly-degenerate basis states.

5.4. Comparison of the indirect coupling matrix elements

In Fig. 3, we plotted the indirect matrix elements from each state as for each dimensionless coupling strength g_i as points, and results from the associated local approximation as a line. One sees good agreement for the larger values of g, which corresponds to the part of the problem where the different g_i values vary slowly (where we would expect the local approximation to be best). The agreement is not quite as good for the smaller g_i values. This is because the coupling matrix elements of the original Hamiltonian are most rapidly varying in this regime.

5.5. Discussion

We see from this comparison that the local approximation does very well in estimating the self-energy, which varies relatively slowly with g. The indirect coupling matrix element is a much stronger function of g, so the local approximation does not do quite as well. The underlying approximation that the coupling matrix elements of the original

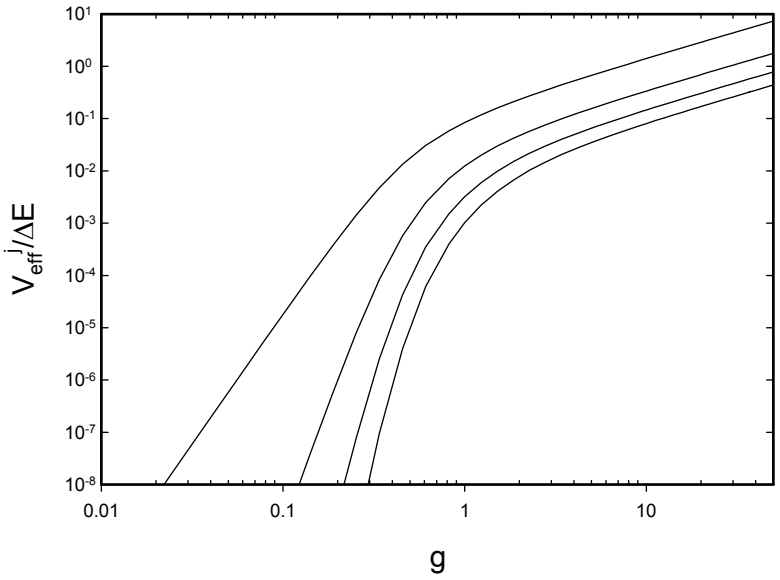

Figure 6. Indirect coupling matrix elements between nearest neighbors (upper curve); second, third and fourth nearest neighbors (lower curves in descending order).

Hamiltonian are all the same begins to break down for small g. In this regime, the indirect matrix elements which couple to states where the local coupling is stronger becomes larger, while the indirect matrix elements which couple to states with weaker local coupling become smaller. In this regime, we see a splitting of the matrix elements for the two different directions (see Fig. 3). When this occurs, the indirect matrix elements from the local approximation lie between them.

In this model problem, the number of two-level systems is not particularly large. As a result, we end up seeing a weak departure between the numerically exact results from the second-order formulation and the results from the local approximation. In problems where the number of two-level systems is much larger, we would expect the local approximation to be much better, since the associated coupling matrix elements of the original problem generally will have smaller differences locally.

6. Local Approximation Results

One advantage of the local approximation is that we are able to carry out computations systematically for a wide range of dimensionless coupling constants g when the number of oscillator quanta exchanged is modest.

6.1. Self-energies

In Fig. 4, we show the self-energies as a function of g for the local approximation for different values of Δn. One sees that for larger values of Δn, the different self-energies quickly approach a large Δn limit. For small g the self energy is quadratic in g; and for large g the self-energy is linear in g.

6.2. Energy as a function of angle

We expect the self-energy to be dependent on the phase angle ϕ, with a simple sinusoidal dependence when the coupling is weak as discussed above. In Fig. 5, we show results for the relative self-energy in the case of five quantum exchange for different values of the dimensionless coupling constant g. When the coupling is very weak, nearest neighbor coupling is dominant, and

$$\frac{E(0)-E(\phi)}{E(0)-E(\pi)} \;\rightarrow\; 1-\cos\phi. \tag{35}$$

We see that when $g = 0.3$ that the the relative self-energy is a good match, and that nearest neighbor coupling is dominant. For the larger values of the dimensionless coupling constant, there is some deviation from the cosine function, which indicates that coupling to second and higher neighbors contributes.

It is possible to extract from the angle-dependent self energy curves the coupling parameters for the different neighbors systematically. We have done this for the results shown in Fig. 5 to obtain the indirect coupling coefficients for the different neighbors in Fig. 6. From these results we see that nearest-neighbor coupling dominates, and that as the magnitude of the splitting gets larger the contributions from other neighbors increases.

6.3. Level splittings

Results for the normalized level splittings for different local approximation models as a function of g are shown in Fig. 7. In the event that the indirect coupling is weak, this normalized level splitting approaches the indirect coupling matrix element

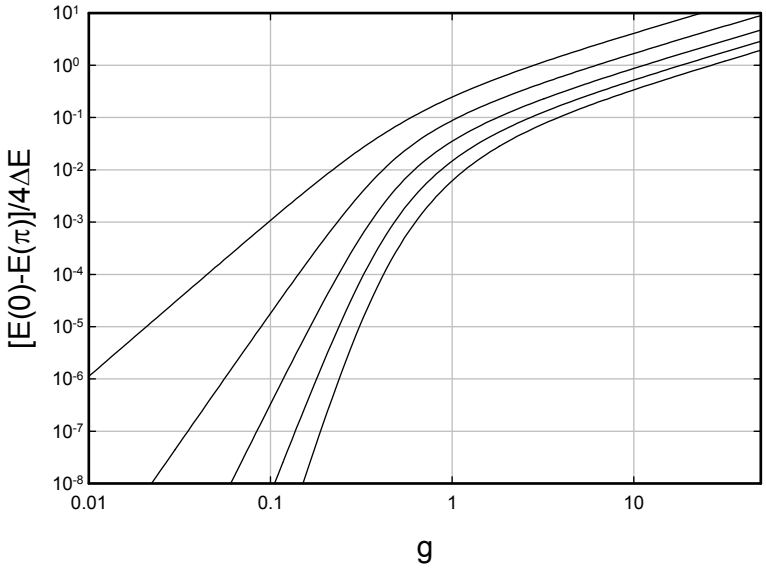

Figure 7. Normalized level splitting as a function of g for $\Delta n = 3, 5, 7, 9, 11$ ($n = 3$ is the top curve, and $n = 11$ is the bottom).

$$\frac{E(0) - E(\pi)}{4} \rightarrow V_{\rm eff} \tag{36}$$

It is easiest to carry out systematic computations for the level splitting, without isolating the contributions of indirect coupling between the different nearly degenerate neighbors.

In general, we see that the level splitting in the lossy spin-boson model decreases with the exchange of more oscillator quanta, and that the curves become sharper with a threshold at increasing g as Δn increases.

7. Discussion and Conclusions

In previous papers we have provided a systematic presentation of the lossy spin-boson model, which we have been interested in because of it is capable of fast coherent multi-quantum energy exchange between two-level systems and an oscillator. Although the model Hamiltonian is relatively simple in form, the analysis of coherent energy transfer between the two-level systems and the oscillator in the multi-quantum regime is not straightforward. In earlier work we have explored coherent energy exchange using perturbation theory, and a formulation that is based on a second-order Hamiltonian. Using these tools, we can study coherent energy exchange when a few quanta are exchanged under conditions where the coupling is weak to moderate. Here we introduced the local approximation, which greatly extends our ability to quantify coherent energy exchange in the model.

In the local approximation, we assume that the system is essentially unchanged when a single two-level system gains or loses excitation, such that the underlying coupling matrix elements do not change. The assumption leads to a problem that is periodic when the resonance condition is satisfied, and the resulting periodic problem is much easier to solve. We considered a model problem in order to see how good the local approximation does when compared to results obtained from the second-order Hamiltonian. The results from the local approximation were found to be very good under conditions where we would expect the local approximation to be good (large S, $S^2 - m^2 >> 0$).

Within the framework of the local approximation, we define a local value of the dimensionless coupling constant g, and the self-energy and indirect coupling matrix elements become unique functions of this g. We analyze the lossy spin-boson model in the limit of infinite loss, and the result of the analysis then is a determination of the associated self-energy and indirect matrix element functions versus g for a particular value of Δn. In practice, it is simpler to compute the level splitting $E(0) - E(\pi)$ than the indirect coupling matrix elements. This is useful since we know that nearest neighbor coupling dominates when the splitting is smaller than ΔE.

We have given results for the self-energy and level splitting for different values of Δn between 3 and 11 here. These results allow us to see the general trends that emerge. For example, the self-energy is quadratic at low g and linear when g is large. As the number of quanta exchanged becomes large, the self-energy curve approaches a large Δn limit. The level splitting (and coherent energy exchange rate) becomes smaller when more quanta are exchanged, as we might expect since intuitively we would expect the corresponding physical system to have more trouble breaking up a big quantum into smaller pieces.

What remains is for us to extend our analysis even further to understand what happens when Δn becomes large. From the results obtained so far, we would expect that g is going to have to become large in order to obtain a finite rate for coherent energy exchange. As we shall see, the local approximation presented in this paper is going to be of great help in analyzing this limit; however, we are going to need additional tools in order to extract quantitative results from the local approximation in this limit. (which we will discuss in a subsequent paper).

References

[1] M. Fleischmann, S. Pons and M. Hawkins, *J. Electroanal Chem.*, **201** (1989) 301; errata, **263** (1990) 187.

[2] M. Fleischmann, S. Pons, M.W. Anderson, L.J. Li and M. Hawkins, *J. Electroanal. Chem.*, **287** (1990) 293.
[3] M.H. Miles, R.A. Hollins, B.F. Bush, J.J. Lagowski, R.E. Miles, *J. Electroanal. Chem.* **346** (1993) 99.
[4] M.H. Miles, B.F. Bush, and J.J. Lagowski, *Fusion Technol.* **25** (1994) 478.
[5] M.H. Miles, Correlation of excess enthalpy and helium-4 production: A review, *Proc. ICCF10*, 2004, p. 123.
[6] P.L. Hagelstein, M.C.H. McKubre, D.J. Nagel, T.A. Chubb, R.J. Hekman, New physical effects in metal deuterides, *Proc. ICCF11*, 2005, p. 23.
[7] P.L. Hagelstein, *Naturwissenschaften* **97** (2010) 345.
[8] D. Letts, D. Cravens and P.L. Hagelstein, Dual laser stimulation and optical phonons in palladium deuteride, in low-energy nuclear reactions and new energy technologies, *Low-Energy Nuclear Reactions Sourcebook*, Vol. 2, American Chemical Society, Washington, DC, 2009, p. 81.
[9] P.L. Hagelstein, D. Letts and D. Cravens, Terahertz difference frequency response of PdD in two-laser experiments, *J. Cond. Mat. Nucl. Sci.* **3** (2010) 59.
[10] P.L. Hagelstein and I.U. Chaudhary, Energy exchange in the lossy spin-boson model, *J. Cond. Mat. Nucl. Sci.* **5** (2011) 52.
[11] P.L. Hagelstein and I.U. Chaudhary, Second-order formulation and scaling in the lossy spin-boson model, *J. Cond. Mat. Nucl. Sci.* **5** (2011) 87.

J. Condensed Matter Nucl. Sci. 5 (2011) 116–139

Research Article

Coherent Energy Exchange in the Strong Coupling Limit of the Lossy Spin-Boson Model

Peter L. Hagelstein *

Research Laboratory of Electronics, Massachusetts Institute of Technology, Cambridge, MA 02139, USA

Irfan U. Chaudhary

Department of Computer Science and Engineering, University of Engineering and Technology. Lahore, Pakistan

Abstract

We focus on the lossy spin-boson model since it is capable of efficient energy exchange between two-level systems and an oscillator under conditions where the characteristic energy of the oscillator is small compared to the transition energy of the two-level systems. We are considering this model as the essential component for a theoretical understanding of the excess heat effect in the Fleischmann–Pons experiment. We introduce an iterative algorithm that allows the numerical calculation of eigenfunctions and eigenvalues of the coefficient eigenvalue equation that arises in the local approximation. From systematic calculations in the strong coupling limit we establish scaling laws for the self-energy and for the indirect coupling matrix element in the local approximation. These results are used to study the system dynamics for simple strong coupling models.
© 2011 ISCMNS. All rights reserved.

Keywords: Coherent energy exchange, Excess heat, Fleischmann–Pons experiment, Lossy spin-boson model, Theory

1. Introduction

In this work we continue our studies of coherent energy exchange between a set of two-level systems and an oscillator, under conditions where the transition energy of the two-level systems is much greater than the characteristic energy of the oscillator. Our interest in this problem is motivated by a great many experiments in which positive results have been reported on measurements of excess heat in the Fleischmann–Pons effect [1,2]. In these experiments a very large amount of energy is sometimes produced, with no sign of chemical or material changes commensurate with the energy produced. Fleischmann and Pons conjectured that the origin of the energy was nuclear; however, known exothermic nuclear reactions that produce energy do so through energetic particles, and there are no commensurate energetic

*E-mail: plh@mit.edu

© 2011 ISCMNS. All rights reserved.

particles in the Fleischmann–Pons experiment. Helium has been observed correlated with the energy [3–5], and the ratio of energy produced to helium observed is near 24 MeV [6]. This is significant since it is consistent with the mass difference between two deuterons and a ^{4}He nucleus.

Hence, experiment suggests that the energy is probably nuclear in origin, and that perhaps deuterons are somehow reacting to make ^{4}He. The big problem with such a statement is that there are no previous examples in nuclear physics of nuclear reactions making energy without commensurate energetic particles [7]. So, whatever process that is responsible for the effect is one that hasn't been seen before. There are no previous relevant models in the nuclear physics or condensed matter physics literature, and most scientists believe the literature that does exist rules out any possibility of such an effect.

This situation would change radically if there were a known mechanism which could take a large nuclear scale MeV quantum and convert it efficiently into a large number of optical phonons. Such a scenario would be consistent with recent two-laser experiments [8,9], where two weak lasers incident on the cathode surface initiate an excess heat event when the beat frequency is matched to zero-group velocity point of the optical phonons, and the excess heat persists after the lasers are turned off. The excess heat effect initiated with a single laser does not persist. The picture which has been proposed to account for this is one in which the two lasers provide an initial excitation of the optical phonon modes which the new process requires; then, when the lasers are turned off, the new process channels energy into the same modes which sustains the effect.

To make progress given such a picture, we need to understand the conditions under which a large nuclear energy quantum can be converted into a large number of optical phonons. Once again, there is no precedent for this; however, it does seem to be what is going on in these experiments, and this motivates us to explore theoretical models which exhibit such an effect. Coherent energy exchange as a physical effect under conditions where are large quantum is divided into many smaller quantum is known in NMR and in atomic physics; it is predicted in the spin-boson model. However, the effect in the spin-boson model is weak, and we need a much stronger version of it to make progress with the excess heat effect in the Fleischmann–Pons effect.

When we augment the spin-boson model with loss, we see that the coherent energy exchange process improves dramatically [10]. In perturbation theory we see that this comes about through the removal of destructive interference, which drastically hinders the effect in the basic spin-boson model. In a set of recent papers [10–13], we have been discussing the model, and building up tools and results to try to understand coherent energy exchange when the coupling is stronger and when more quanta are exchanged. In the preceding paper [13], we introduced the local approximation for the lossy spin-boson model, which provides us with a powerful tool with which to address the strong coupling regime.

In this work, we continue the analysis by first introducing a numerical algorithm which allows us to obtain eigenfunctions, self-energies, and indirect coupling matrix elements in the strong coupling regime. As will be discussed, once we began assembling the results from systematic calculations we noticed that the system appeared to obey scaling laws in the strong coupling regime. This is interesting because after establishing the scaling laws, we can use them to predict the dynamics of the model under conditions of extremely strong coupling, which is where we need to go in order to convert a nuclear-scale quantum into a very large number of atomic scale quanta. Our primary goal then in what follows in this paper is to discuss the scaling laws for self-energy and for the indirect coupling matrix element in the strong coupling regime.

2. Eigenvalue Equation for the Coefficients

We are interested in coherent energy exchange in the lossy spin-boson model under conditions where the coupling is strong, and where a great many oscillator quanta are exchanged for each two-level system transition. In our earlier discussions of the problem, we have introduced a number of models and approximations which allow us to make

progress on what would otherwise be a difficult theoretical problem. For example, if we assume that the loss is infinite for states below a certain energy and adopt a restricted basis approximation, then we obtain a reduced version of the problem that has fewer states and leads to a real Hamiltonian and real solutions. In the local approximation, we assume that the matrix elements change little when the number of excited two-level systems is increased or decreased. When the resonance conditions is met, then the Hamiltonian becomes invariant under translation, and by Bloch's theorem the solutions are periodic in one dimension. This further simplifies things, and allows us here to analyze the system in regimes closer to those of interest for understanding excess heat in the Fleischmann–Pons effect.

2.1. Local approximation eigenvalue equation

We begin with the eigenvalue equation for the expansion coefficients that was developed previously [13] for the local approximation

$$E(\phi)v_n = \left[n\hbar\omega_0 - i\frac{\hbar}{2}\hat{\Gamma}(E)\right]v_n + g\Delta E\left[e^{i\phi}(v_{n+\Delta n+1} + v_{n+\Delta n-1}) + e^{-i\phi}(v_{n-\Delta n+1} + v_{n-\Delta n-1})\right]. \quad (1)$$

In this equation, ΔE is the transition energy of the two-level systems, $\hbar\omega_0$ is the characteristic oscillator energy, g is the dimensionless coupling constant, and ϕ is the phase associated with the Bloch solutions of the periodic problem that results when the resonance condition

$$\frac{\Delta E}{\hbar\omega_0} = \Delta n \quad (2)$$

is satisfied for odd integer Δn. Loss is included in general in this model through the second-order loss operator $i\hbar\hat{\Gamma}(E)/2$. In this paper our focus will be on the infinite loss model (in a restricted basis approximation), so that we will take v_0 to be to lowest expansion coefficient that is finite. As in our previous work, we assume that the oscillator is very highly excited, so that the oscillator index n is incremental. The number of oscillator quanta to be associated with v_0 is n_0, which we assume is very large; the total number of oscillator quanta in general associated with v_n is then $n_0 + n$.

2.2. Focus on the $\phi = 0$ and $\phi = \pi$ problems

We are interested in the self-energy and in the indirect coupling matrix element. As discussed in [13] it is easier to compute the level splitting, from which we can estimate the nearest neighbor indirect coupling matrix element. For this, we need two eigenvalues $E(0)$ and $E(\pi)$. The corresponding eigenvalue equations can be written as

$$\epsilon_0 v_n = \frac{n}{\Delta n}v_n + g\left[(v_{n+\Delta n+1} + v_{n+\Delta n-1}) + (v_{n-\Delta n+1} + v_{n-\Delta n-1})\right], \quad (3)$$

$$\epsilon_\pi v_n = \frac{n}{\Delta n}v_n - g\left[(v_{n+\Delta n+1} + v_{n+\Delta n-1}) + (v_{n-\Delta n+1} + v_{n-\Delta n-1})\right], \quad (4)$$

where

$$\epsilon_0 \;=\; \frac{E(0)}{\Delta E}, \qquad \epsilon_\pi \;=\; \frac{E(\pi)}{\Delta E}. \tag{5}$$

3. Solutions for Moderately Large Δn

To extend our results significantly beyond what was done in our earlier papers we require new numerical and analytical tools. In this section we present an iterative numerical approach which allows us to develop solutions to the eigenvalue equations under conditions where a direct solution is impractical. This allows us study coherent energy exchange when a two-level system quantum is split into a moderately large number of oscillator quanta. The results of such calculations are interesting since we find that the indirect coupling matrix element appears to obey a useful scaling law.

3.1. Matrix eigenvalue problem

When the resonance condition is satisfied in the local approximation, we obtain an eigenvalue equation for the expansion coefficients of the form

$$\epsilon_0 v_n \;=\; \frac{n}{\Delta n} v_n + g\Big[(v_{n+\Delta n+1} + v_{n+\Delta n-1}) + (v_{n-\Delta n+1} + v_{n-\Delta n-1}) \Big]. \tag{6}$$

In the restricted basis approximation of the lossy spin-boson model with infinite loss, we assume that the expansion coefficients with n negative are zero due to loss effects. Here Δn is an odd integer, which is the number of quanta exchanged on resonance, and g is the dimensionless coupling constant.

This eigenvalue equation for the expansion coefficients can be thought of as a matrix eigenvalue equation of the form

$$\epsilon \mathbf{v} \;=\; \mathbf{H} \cdot \mathbf{v}. \tag{7}$$

3.2. Iterative numerical scheme

When the vector $\mathbf{v}$ has more than 1000 elements, the matrix eigenvalue problem that results becomes computationally expensive for a direct calculation. As a result, we seek an iterative numerical scheme that is faster, which will allow us to extend our computations to examples with larger Δn and strong coupling.

We have found that the computations can be improved considerable with the use of Newton's method with an inequivalent Jacobian. Although the method in general was developed to handle nonlinear problems, it is possible to use it on a linear problem. We begin by assuming that the exact solution can be obtained by adding a small correction to a current guess, such that

$$\mathbf{v}_{\text{exact}} \;=\; \mathbf{v} + \delta\mathbf{v}. \tag{8}$$

If so, then we can develop an exact equation for the correction $\delta\mathbf{v}$ of the form

$$(\mathbf{H} - \epsilon) \cdot \delta\mathbf{v} \;=\; -(\mathbf{H} - \epsilon) \cdot \mathbf{v}. \tag{9}$$

The term on the RHS we recognize as a residual for this problem, which we define as

$$\mathbf{r} \;=\; (\epsilon - \mathbf{H}) \cdot \mathbf{v}. \tag{10}$$

This vector keeps track of how far away from the exact solution the current guess is. We see that the residual goes to zero when we have an exact solution for ϵ and $\mathbf{v}$. The correction $\delta\mathbf{v}$ then satisfies

$$(\mathbf{H} - \epsilon) \cdot \delta\mathbf{v} \;=\; \mathbf{r}. \tag{11}$$

Unfortunately, the amount of work required to evaluate the correction $\delta\mathbf{v}$ is considerable as written. However, we can gain an advantage if we can find an approximate version of $\mathbf{H}$ that we can solve more efficiently. Suppose that this approximate matrix is defined to be $\mathbf{A}$, and that

$$\mathbf{A} \;\approx\; \mathbf{H} \tag{12}$$

in some computationally useful sense. Then the correction $\delta\mathbf{v}$ will no longer be exact, but it may still improve $\mathbf{v}$ anyway. This leads to the following iterative scheme

$$[\mathbf{A} - \epsilon^{(m)}] \cdot \delta\mathbf{v}^{(m)} \;=\; \mathbf{r}^{(m)}, \tag{13}$$

$$\mathbf{v}^{(m+1)} \;=\; \mathbf{v}^{(m)} + \beta\delta\mathbf{v}^{(m)}, \tag{14}$$

$$\epsilon^{(m+1)} \;=\; \frac{(\mathbf{v} \cdot \mathbf{H} \cdot \mathbf{v})^{(m+1)}}{(\mathbf{v} \cdot \mathbf{v})^{(m+1)}}, \tag{15}$$

where β is an under-relaxation parameter.

We have found that corrections can be made with an approximate Hamiltonian that corresponds to

$$\epsilon\delta v_n \;=\; \frac{n}{\Delta n}\delta v_n - \alpha g(\delta v_{n+2} + \delta v_{n-2}) - r_n. \tag{16}$$

We have used the parameter values

$$\alpha \;=\; 0.5, \quad \beta \;=\; 0.5. \tag{17}$$

3.3. Selected results

We have computed results for two examples with $\Delta n = 91$ and with $\Delta n = 151$. These examples are instructive in that the number of oscillator quanta exchanged now is significantly larger than what we have presented previously, and the results already appear to show the presence of nontrivial scaling laws. We show the self-energy in Fig. 1. The two curves are very close to each other, and are roughly linear in g. For large g the curves approach

$$\frac{E(g)}{\Delta E} \;\rightarrow\; -4g. \tag{18}$$

We recall that when the indirect coupling is weak that the indirect matrix element $V_{\rm eff}$ is related to the level splitting through

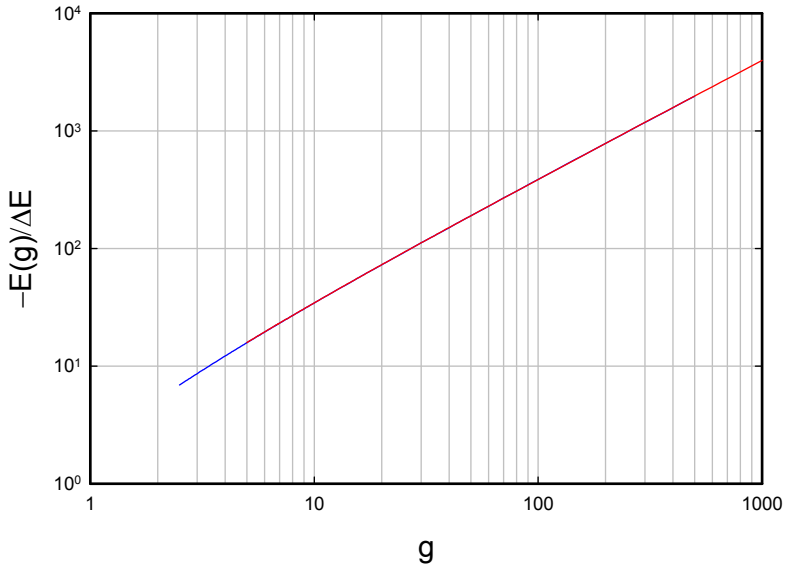

Figure 1. Self-energy as a function of the dimensionless coupling strength g for $\Delta n = 91$ (blue) and $\Delta n = 151$ (red).

$$V_{\rm eff} \;\rightarrow\; \frac{E(0) - E(\pi)}{4}. \tag{19}$$

We have computed the level splitting for the two examples for different values of g, and we have found that the results approximately line up if we plot $\Delta n^2 V_{\rm eff}/4g\Delta E$ (which is a scaled version of $V_{\rm eff}$) as a function of $g/\Delta n^2$ (which is a scaled version of g). The results are shown in Fig 2. This is our first indication so far that the solutions obey an important scaling law in this regime.

The expansion coefficients v_n are shown in Fig. 3 for models with different values of g, for the case where $\phi = 0$. We see peaks with an alternating sign that appear every $\Delta n = 91$ in n, with amplitudes that decrease at large n. The coupling present in the Hamiltonian results in phase coherence that extends over a large range of n. When the coupling is stronger we see that more expansion coefficients contribute to the solution. Expansion coefficients for $\phi = \pi$ are shown in Fig. 4 for the same set of g values. We see very similar results except that the peaks all have the same phase.

4. Continuum Model

Our ability to calculate solutions to the eigenvalue is limited, even with the iterative algorithm discussed above, since we require even more expansion coefficients when g and Δn are large. From the results of the previous section, we see that the solutions do not change suddenly between different values of n, which suggests that we might be able to develop a continuum model. If so, then we would be able to extend the range over which we could obtain results even further.

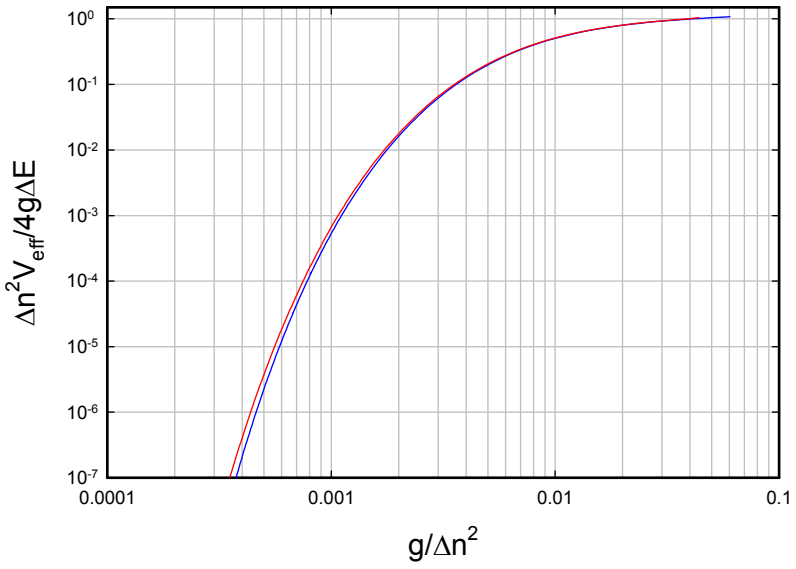

Figure 2. Scaled indirect coupling matrix element (derived from the level splitting) as a function of the $g/\Delta n^2$ for $\Delta n = 91$ (blue) and $\Delta n = 151$ (red).

4.1. Eigenvalue equation

To proceed, we define a continuous version of the index n according to

$$z = \frac{n}{\Delta n}. \tag{20}$$

The expansion coefficients v_n in the continuum approximation is then related to a continuous function $v(z)$ through

$$v_n = v\left(\frac{n}{\Delta n}\right). \tag{21}$$

The eigenvalue equation for $\phi = 0$ becomes

$$\begin{aligned}\epsilon_0 v(z) = {} & z v(z) + g\Bigg[v\left(z+1+\frac{1}{\Delta n}\right) + v\left(z+1-\frac{1}{\Delta n}\right) \\ & + v\left(z-1+\frac{1}{\Delta n}\right) + v\left(z-1-\frac{1}{\Delta n}\right)\Bigg].\end{aligned} \tag{22}$$

4.2. Approximate differential eigenvalue equation

Since the expansion coefficients vary slowly with n, we would expect reasonable results from assuming that $v(z)$ is locally continuous. For example, we can use a Taylor series expansion to write

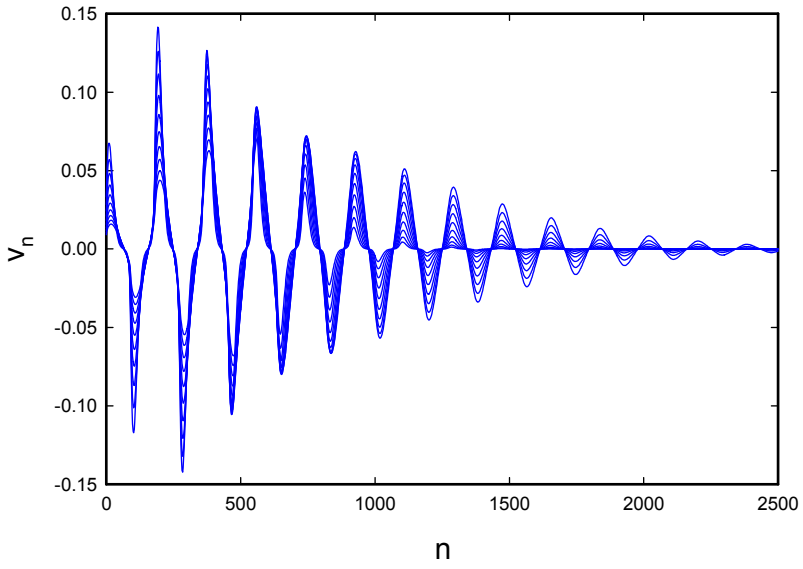

Figure 3. Results for the $\phi = 0$ expansion coefficients v_n for 10 values of g logarithmically spaced between $g = 10$ and $g = 100$. Results for $g = 10$ have the biggest magnitude for small n and the smallest magnitude for large n.

$$v\left(z + \frac{1}{\Delta n}\right) = v(z) + \frac{1}{\Delta n}\frac{\mathrm{d}v}{\mathrm{d}z} + \frac{1}{2\Delta n^2}\frac{\mathrm{d}^2 v}{\mathrm{d}z^2}, \tag{23}$$

$$v\left(z - \frac{1}{\Delta n}\right) = v(z) - \frac{1}{\Delta n}\frac{\mathrm{d}v}{\mathrm{d}z} + \frac{1}{2\Delta n^2}\frac{\mathrm{d}^2 v}{\mathrm{d}z^2}. \tag{24}$$

We can use these approximations to obtain an approximate difference-differential eigenvalue equation

$$\epsilon_0 v(z) = zv(z) + 2g[v(z+1) + v(z-1)] + \frac{g}{\Delta n^2}\frac{\mathrm{d}^2 v}{\mathrm{d}z^2}\bigg|_{z+1} + \frac{g}{\Delta n^2}\frac{\mathrm{d}^2 v}{\mathrm{d}z^2}\bigg|_{z-1}. \tag{25}$$

4.3. Discretization

To make progress, we would like to discretize the equation in order to obtain numerical solutions. Simple 3-point discretization results in

$$\begin{aligned}\epsilon_0 v_j &= z_j v_j + 2g[v_{j+N} + v_{j-N}] + \frac{g}{\Delta n^2}\frac{v_{j+N+1} - 2v_{j+N} + v_{j+N-1}}{\Delta z^2} \\ &\quad + \frac{g}{\Delta n^2}\frac{v_{j-N+1} - 2v_{j-N} + v_{j-N-1}}{\Delta z^2}.\end{aligned} \tag{26}$$

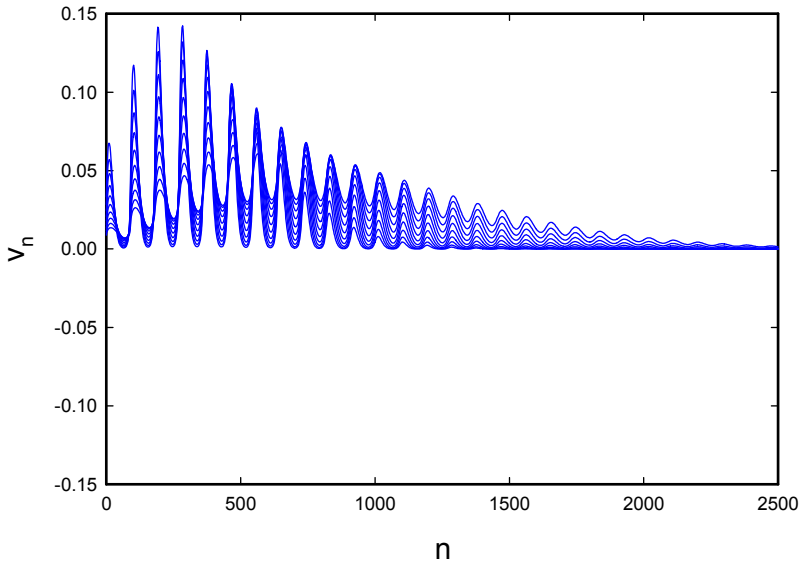

Figure 4. Results for the $\phi = \pi$ expansion coefficients v_n for 10 values of g logarithmically spaced between $g = 10$ and $g = 100$. Results for $g = 10$ have the biggest magnitude for small n and the smallest magnitude for large n.

The number of points used within a cycle N must satisfy

$$N \leq \Delta n \tag{27}$$

in order to obtain numerical solutions that correspond to the solutions of the original Hamiltonian.

4.4. Iterative solution

We have had some success using an iterative algorithm very similar to that discussed above to solve it. The correction equation that we used is

$$\epsilon \delta v_j = (z_j - 4\alpha_1 g)\delta v_j - \alpha_2 \frac{2g}{\Delta n^2}\left(\frac{\delta v_{j+1} - 2\delta v_j + \delta v_{j-1}}{\Delta z^2}\right) - r_j \tag{28}$$

with

$$\begin{aligned} r_j &= (z_j - \epsilon_0)v_j + 2g[v_{j+N} + v_{j-N}] + \frac{g}{\Delta n^2}\frac{v_{j+N+1} - 2v_{j+N} + v_{j+N-1}}{\Delta z^2} \\ &\quad + \frac{g}{\Delta n^2}\frac{v_{j-N+1} - 2v_{j-N} + v_{j-N-1}}{\Delta z^2}, \end{aligned} \tag{29}$$

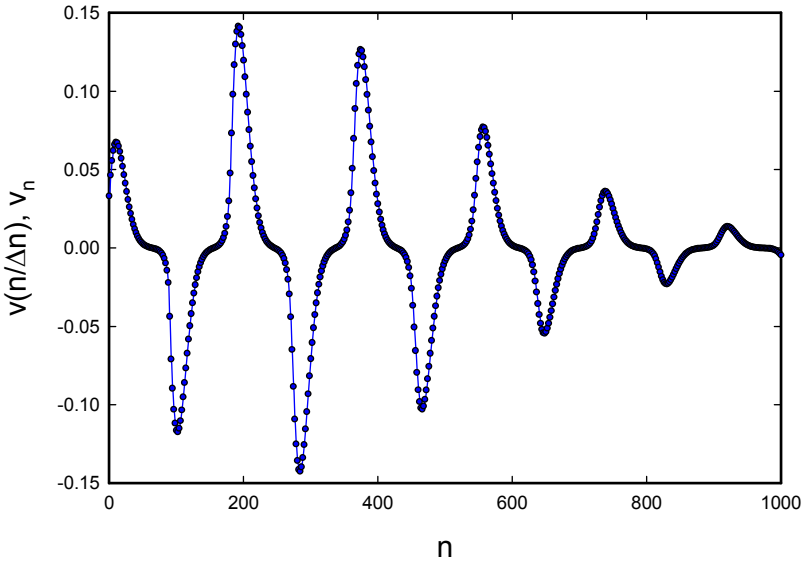

Figure 5. Results for the $\phi = 0$ expansion coefficients v_n computed for $g = 10$ using the periodic local model (black circles), and using the continuum approximation (blue line).

$$\alpha_1 = \frac{1}{2}, \quad \alpha_2 = 1 \tag{30}$$

and

$$v_j^{(m+1)} = v_j^{(m)} + \beta \delta v_j^{(m)} \tag{31}$$

with

$$\beta = 0.45. \tag{32}$$

The convergence rate is not great, but we are able to obtain solutions using this approach.

4.5. Numerical example

Of primary interest here is whether the solutions to the continuum model give a reasonable approximation to the solutions of the original problem. The issue here is that even though we now have more powerful tools to analyze the models, the number of coefficients involved in the solution grows in proportion to the product of g and Δn, so that we will end up needing to rely on a combination of analytic and numerical tools when Δn becomes large.

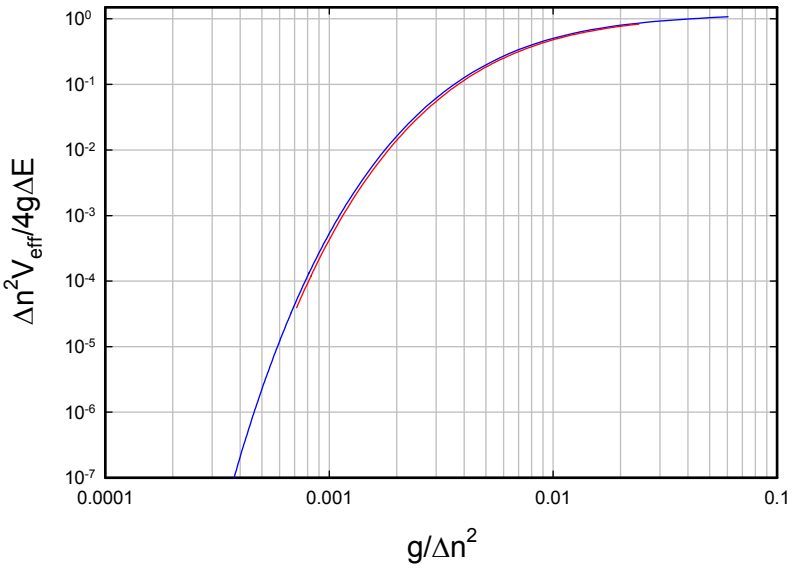

Figure 6. Scaled level splitting for $\Delta n = 91$ expressed as a scaled indirect matrix element from the periodic local model (blue line), and from the continuum approximation (red line).

In Fig. 5, we show the result from the continuum model (blue line) compared with the exact numerical coefficients from the periodic local model (black circles). The agreement is good, although there is a small offset associated with the continuum solution. The self-energy for the "exact" local periodic solution is

$$E(0) \;=\; -\,34.4370\;\Delta E. \tag{33}$$

The result from 3-pt differencing of the continuum approximation with 91 points is

$$E(0) \;=\; -\,34.4312\;\Delta E \;\; (3-\text{pt discretization}). \tag{34}$$

We can correct this self-energy by including the contribution of the lowest-order discretization error to obtain

$$E(0) \;=\; -\,34.4316\;\Delta E \;\; (\text{corrected } 3-\text{pt discretization}). \tag{35}$$

We conclude that the continuum model itself as an approximation is responsible for most of the energy difference.

The level splitting from the continuum model is shown in red in Fig. 6, compared with the periodic model result in blue. We see that the continuum model result is very close to the periodic model result. We conclude from these calculations that we should be able to make use of the continuum model for self-energy and for level splitting calculations and get good results.

5. Strong-coupling Limit

Direct numerical computations with the models described above becomes increasingly slow for larger values of g. This is because the solutions that make up the expansion coefficients include a large number of peaks, which involves a large number of points. An additional difficulty is that the iterative algorithm discussed converges more slowly as more points are used. It is possible to make use of the models outlined above to obtain systematic results for large g, by taking advantage of the presence of a large number of peaks. Since the peaks have nearly the same shape from one cycle to the next it becomes possible to develop strong coupling approximations.

5.1. Large g approximation for the periodic model

We see in Fig. 5 that the $\phi = 0$ solutions are made up of peaks that alternate in sign, and that for large g we might expect that the peak amplitudes will become uniform. In this case we would write

$$v_{n+\Delta n} \;=\; -\,v_n \;(\phi = 0). \tag{36}$$

The eigenvalue equation for the expansion coefficients in this limit reduces to

$$\epsilon_0 v_n \;=\; \frac{n}{\Delta n} v_n - 2g(v_{n+1} + v_{n-1}). \tag{37}$$

In the case of $\phi = \pi$, the different peaks have the same sign, so that we would expect

$$v_{n+\Delta n} \;=\; v_n \;(\phi = \pi). \tag{38}$$

The corresponding eigenvalue equation in this large g limit is essentially the same

$$\epsilon_\pi v_n \;=\; \frac{n}{\Delta n} v_n - 2g(v_{n+1} + v_{n-1}). \tag{39}$$

We show the result of computations for $\Delta n = 91$ for the level splitting as a function of g in Fig. 7 for this strong coupling approximation (red) compared with exact numerical results from the periodic model (blue). We see that the strong coupling approximation approaches the exact solution at large g, and that it deviates some at low g. This is consistent with our expectations, since when g is small only a few peaks make up the solution, in which case the assumption that the peaks are uniform (or linear) becomes poor.

5.2. Large g version of the continuum approximation

We can make a similar approximation in the case of the continuum approximation in the large g limit where there are many peaks, and where the shapes and amplitudes are similar in the different peaks. The resulting large g approximation is

$$\epsilon v(z) \;=\; z v(z) - 4g v(z) - \frac{2g}{\Delta n^2} \frac{\mathrm{d}^2 v}{\mathrm{d}z^2} \tag{40}$$

for both $\phi = 0$ and $\phi = \pi$.

This strong coupling continuum approximation is interesting because it predicts that the level splitting depends on the ratio $g/\Delta n^2$, but not on g independently. We can see this be recasting the eigenvalue equation as

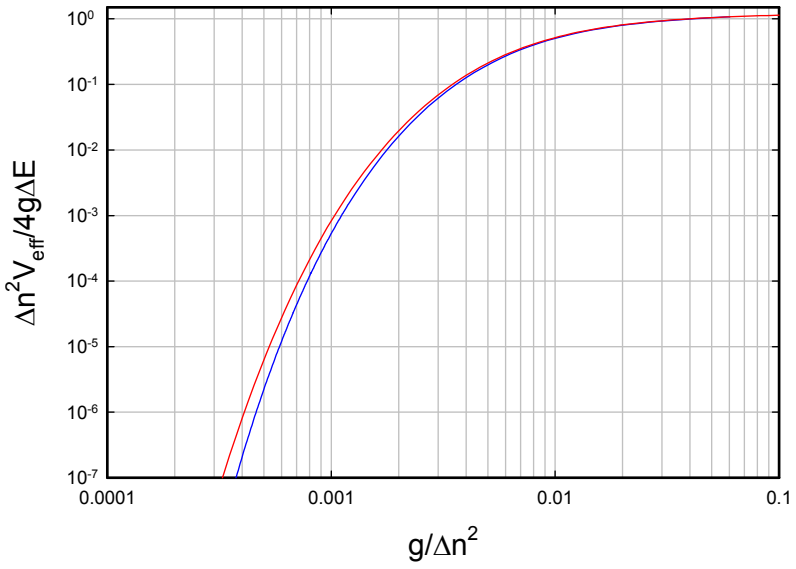

Figure 7. Scaled level splitting for $\Delta n = 91$ expressed as a scaled indirect matrix element from the periodic local model (blue line), and from the strong coupling approximation (red line).

$$\epsilon' v(z) \;=\; z v(z) - \frac{2g}{\Delta n^2}\frac{\mathrm{d}^2 v}{\mathrm{d}z^2}, \tag{41}$$

where

$$\epsilon' \;=\; \epsilon + 4g. \tag{42}$$

We noticed in our calculations that the discrete strong coupling approximation above gave very nearly the same level splittings as a function of $g/\Delta n^2$ for different large values of Δn. We see now that such behavior is expected, since when g is very large, it is only $g/\Delta n^2$ that matters in determining the level splitting.

The calculated level splitting in this model is very close to the large g approximation result in Fig. 7.

5.3. Scaling law for indirect coupling matrix element

From the strong coupling results, we see that the indirect coupling matrix element obeys a scaling law of the form

$$\frac{V_{\mathrm{eff}}}{\Delta E} \;=\; 4\frac{g}{\Delta n^2}\Phi\left(\frac{g}{\Delta n^2}\right). \tag{43}$$

For ease of use, we have fit the function $\Phi(x)$ according to

$$\Phi(x) \;=\; \exp\left\{a + b\ln x + c(\ln x)^2 + d(\ln x)^3 + e(\ln x)^4\right\} \tag{44}$$

using data in the range

$$0.00020 \;<\; x \;<\; 0.12. \tag{45}$$

The fitting parameters that result are

$$a \;=\; -1.11722, \quad b \;=\; -1.61939, \quad c \;=\; -0.780116, \quad d \;=\; -0.171302, \quad e \;=\; -0.0159906. \tag{46}$$

5.4. Analytic model for the large g continuum model

We can solve the differential equation for the strong coupling continuum model using a solution of the form

$$v(z) \;=\; \mathrm{Ai}\left[\left(\frac{\Delta n^2}{2g}\right)^{1/3}(z - z_0)\right], \tag{47}$$

$$\epsilon \;=\; -4g + z_0, \tag{48}$$

where Ai is an Airy function. A scaled version of this analytic result is shown in Fig. 8 compared with results from exact numerical calculations with the local periodic model. We see that the agreement over most of the cycle is very good. Deviations between the analytic solution and the exact solution on the small n side are due to the fact that the coefficients at $n - \Delta n$ are zero in the exact model (the analytic model here does not know about the cut-off at $n = 0$).

5.5. Peak amplitudes

If we assume that the different peaks have approximately the same shape, then it is possible to develop a model for the peak amplitudes. To proceed, we assume that the expansion coefficients for the $\phi = 0$ case can be approximated by

$$v_n \;=\; \sum_m (-1)^m a_m u_{n-m\Delta n}, \tag{49}$$

where a_m is the amplitude, and where u_n describes a single peak. For $\phi = 0$, the eigenvalue equation is

$$\epsilon_0 v_n \;=\; \frac{n}{\Delta n}v_n + g\Big[(v_{n+\Delta n+1} + v_{n+\Delta n-1}) + (v_{n-\Delta n+1} + v_{n-\Delta n-1})\Big], \tag{50}$$

we can develop an equation for the amplitudes of the form

$$\begin{aligned}\epsilon_0\langle u_n|u_n\rangle a_m \;=\; &\langle u_n|\frac{n}{\Delta n}|u_n\rangle - g\langle u_n|u_{n+1}\rangle a_{m+1} - g\langle u_n|u_{n-1}\rangle a_{m+1} \\ &-g\langle u_n|u_{n+1}\rangle a_{m-1} - g\langle u_n|u_{n-1}\rangle a_{m-1},\end{aligned} \tag{51}$$

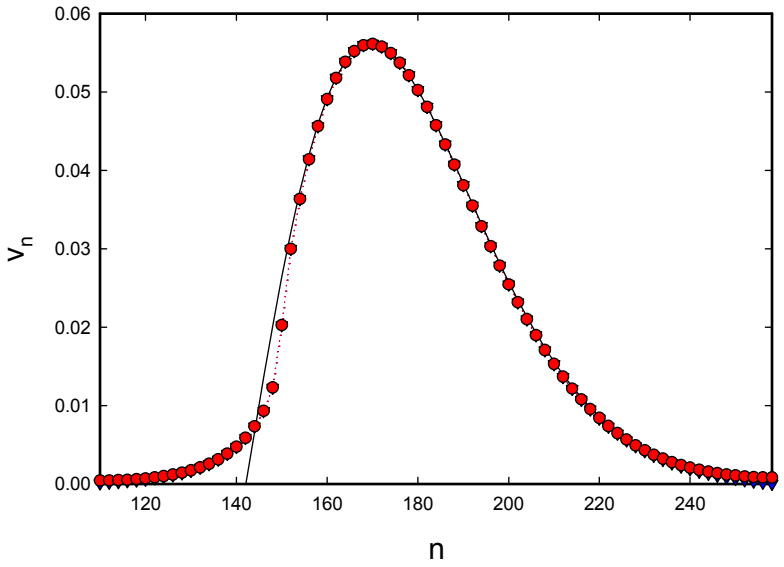

Figure 8. Expansion coefficients for $g = 30$ and $\Delta n = 151$; $\phi = 0$ (blue triangles); $\phi = \pi$ (red circles); and Airy function analytic model (black line).

When g is large we may approximate

$$\frac{\langle u_n | u_{n+1} \rangle}{\langle u_n | u_n \rangle} \rightarrow 1. \tag{52}$$

We require an estimate the expectation value $\langle n/\Delta n \rangle$. Since each successive peak occurs at a position Δn units past the previous one, we would expect that the expectation value would be equal to m plus an offset that depends on the width (which depends on $g/\Delta n^2$). From the results of numerical calculations, the following approximation seems reasonable

$$\left\langle \frac{n}{\Delta n} \right\rangle = m + \delta n \left(\frac{g}{\Delta n^2} \right). \tag{53}$$

We can then reduce the amplitude equation to

$$\left[\epsilon_0 - \delta n \left(\frac{g}{\Delta n^2} \right) \right] a_m = m a_m - 2g(a_{m-1} + a_{m+1}). \tag{54}$$

This equation can be solved analytically using a solution of the form

$$a_m = J_{m+m_0}(4g), \tag{55}$$

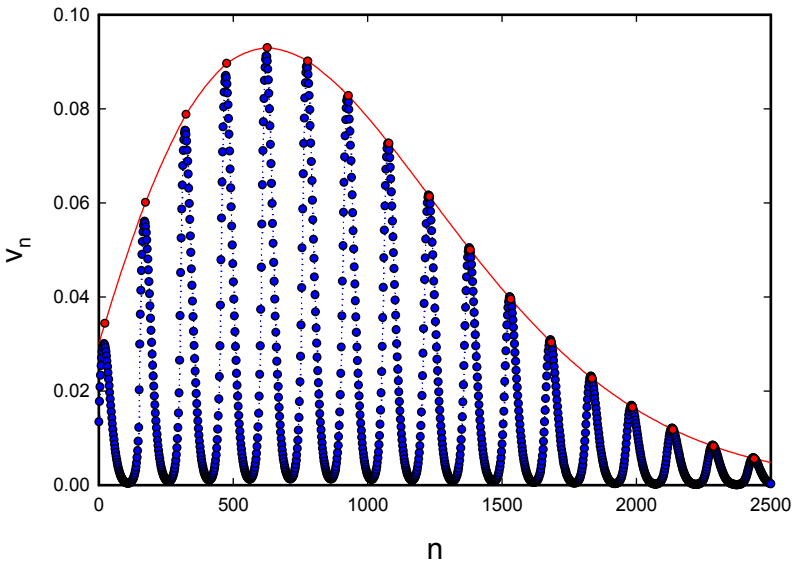

Figure 9. Expansion coefficients for $g = 30$, $\Delta n = 151$, and $\phi = \pi$ (blue); and results from the peak amplitude model (red).

where m_0 is chosen so that the first zero of the Bessel function is matched to the boundary condition near $n = 0$. We illustrate in Fig. 9 an example where we have chosen the $\phi = \pi$ version of the problem (in which the peaks all have the same sign, so that it is easier to compare). In this case, we have used $\Delta n = 151$ and $g = 30$, and we have scaled the amplitudes to approximately match the peak amplitude. We see that this model for the amplitudes is in reasonable agreement with the exact numerical calculation.

5.6. Continuum approximation for the peak amplitudes

When g becomes large there occur a great many peaks. In this case, we can adopt a continuum approximation

$$a_m \;\rightarrow\; a(m) \tag{56}$$

with

$$a_{m+1} \;\rightarrow\; a(m) + \frac{\mathrm{d}a}{\mathrm{d}m} + \frac{1}{2}\frac{\mathrm{d}^2 a}{\mathrm{d}m^2} \tag{57}$$

$$a_{m-1} \;\rightarrow\; a(m) - \frac{\mathrm{d}a}{\mathrm{d}m} + \frac{1}{2}\frac{\mathrm{d}^2 a}{\mathrm{d}m^2}. \tag{58}$$

The eigenvalue equation becomes

$$\left[\epsilon_0 + 4g - \delta n\left(\frac{g}{\Delta n^2}\right)\right] a(m) \;=\; ma(m) - 2g\frac{\mathrm{d}^2 a}{\mathrm{d}m^2}. \tag{59}$$

This is solved using

$$a(m) \;=\; \mathrm{Ai}\left[\left(\frac{1}{2g}\right)^{1/3}(m - \delta m)\right]. \tag{60}$$

Here δm is chosen to match the boundary condition.

6. Dynamics for Strong Coupling

Since the indirect coupling matrix element obeys a scaling law in the strong coupling limit, it is possible to examine coherent energy exchange under conditions where a large number of oscillator quanta are converted. From previous work the dynamics is governed by

$$\frac{\mathrm{d}^2}{\mathrm{d}t^2}m \;=\; \frac{2}{\hbar^2}\frac{\mathrm{d}}{\mathrm{d}m}V^2(m). \tag{61}$$

We assume in writing this that there are enough two-level systems present so that the nearly-degenerate set of indirectly coupled states can be treated as degenerate. To proceed, we recall that

$$g \;=\; \frac{V\sqrt{n}\sqrt{S^2 - m^2}}{\Delta E}. \tag{62}$$

In what follows we will simplify things by assuming that n does contribute to the dynamics. This would be the case if a large n were imposed such that the energy exchange gives rise to only a small change in oscillator excitation. This limit might also be of interest if conventional oscillator loss limited the maximum excitation of the oscillator.

6.1. Scaled Dicke number

In what follows, it will be convenient to work with a scaled version of m; hence, we define y according to

$$y \;=\; \frac{m}{S}. \tag{63}$$

The equation of motion can then be written as

$$\frac{\mathrm{d}^2}{\mathrm{d}t^2}y(t) \;=\; \frac{2}{\hbar^2 S^2}\frac{\mathrm{d}}{\mathrm{d}y}\left[4\Delta E\frac{g}{\Delta n^2}\Phi\left(\frac{g}{\Delta n^2}\right)\right]^2. \tag{64}$$

We can simplify the subsequent algebra if we introduce g_{max} which we define as

$$g_{\mathrm{max}} \;=\; \frac{V\sqrt{n}S}{\Delta E}. \tag{65}$$

This allows us to write

$$\frac{\mathrm{d}^2}{\mathrm{d}t^2}y(t) \;=\; \frac{32}{S^2}\left(\frac{\Delta E}{\hbar}\right)^2 \frac{\mathrm{d}}{\mathrm{d}y}\left[\left(\frac{g_{\max}}{\Delta n^2}\right)^2 (1-y^2)\Phi^2\left(\frac{g_{\max}}{\Delta n^2}\sqrt{1-y^2}\right)\right]. \tag{66}$$

6.2. Characteristic frequency

The scaling law here involves y appearing in the same way in the different terms. We can extract the physical parameters by introducing the scaled variable

$$\xi \;=\; \frac{g_{\max}}{\Delta n^2}\sqrt{1-y^2}. \tag{67}$$

This allows us to write

$$\frac{\mathrm{d}^2}{\mathrm{d}t^2}y(t) \;=\; \frac{32}{S^2}\left(\frac{\Delta E}{\hbar}\right)^2 \frac{\mathrm{d}}{\mathrm{d}y}\left[\xi^2\Phi^2(\xi)\right] \;=\; \frac{32}{S^2}\left(\frac{\Delta E}{\hbar}\right)^2 \frac{\mathrm{d}\xi}{\mathrm{d}y}\frac{\mathrm{d}}{\mathrm{d}\xi}\left[\xi^2\Phi^2(\xi)\right]. \tag{68}$$

We can evaluate the derivative in y to obtain

$$\frac{\mathrm{d}\xi}{\mathrm{d}y} \;=\; -\frac{g_{\max}}{\Delta n^2}\frac{y}{\sqrt{1-y^2}}. \tag{69}$$

This leads to

$$\frac{\mathrm{d}^2}{\mathrm{d}t^2}y(t) \;=\; -\frac{32}{S^2}\left(\frac{\Delta E}{\hbar}\right)^2 \left(\frac{g_{\max}}{\Delta n^2}\right)^2 y\left(\frac{1}{\xi}\frac{\mathrm{d}}{\mathrm{d}\xi}\left[\xi^2\Phi^2(\xi)\right]\right). \tag{70}$$

We can define a characteristic frequency Ω_0 for this model to satisfy

$$\Omega_0^2 \;=\; \frac{1}{S^2}\left(\frac{\Delta E}{\hbar}\right)^2 \left(\frac{g_{\max}}{\Delta n^2}\right)^2. \tag{71}$$

This can be recast as

$$\Omega_0^2 \;=\; \frac{1}{\Delta n^4}\left(\frac{V\sqrt{n}}{\hbar}\right)^2. \tag{72}$$

The characteristic frequency Ω_0 can then be written in the two equivalent forms

$$\Omega_0 \;=\; \frac{1}{S}\left(\frac{\Delta E}{\hbar}\right)\left(\frac{g_{\max}}{\Delta n^2}\right) \;=\; \frac{1}{\Delta n^2}\left(\frac{V\sqrt{n}}{\hbar}\right). \tag{73}$$

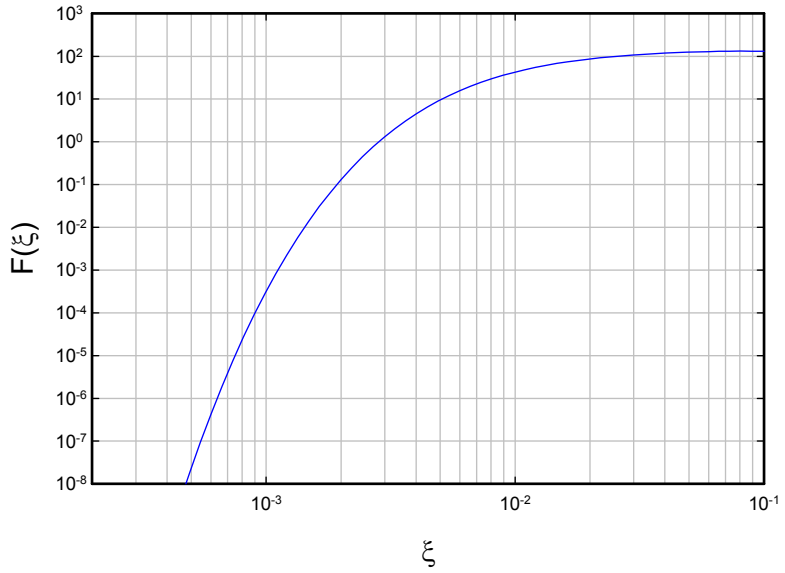

Figure 10. Function $F(\xi)$ discussed in the text plotted as a function of ξ.

6.3. Nonlinearity

Ultimately we end up with the dynamics of a nonlinear oscillator which can be expressed as

$$\frac{\mathrm{d}^2}{\mathrm{d}t^2}y(t) \;=\; -\,\Omega_0^2 y\left(\frac{32}{\xi}\frac{\mathrm{d}}{\mathrm{d}\xi}\left[\xi^2\Phi^2\left(\xi\right)\right]\right). \tag{74}$$

To compute the dynamics of this system, it is convenient to define

$$F(\xi) \;=\; \frac{32}{\xi}\frac{\mathrm{d}}{\mathrm{d}\xi}\left[\xi^2\Phi^2\left(\xi\right)\right]. \tag{75}$$

We have evaluated this function (see Fig. 10), and fit it to the form

$$F(\xi) \;=\; \exp\left\{a + b\ln\xi + c(\ln\xi)^2 + d(\ln\xi)^3 + e(\ln\xi)^4\right\} \tag{76}$$

with

$$a \;=\; 2.46013,\;\; b \;=\; -\,3.22909,\;\; c \;=\; -\,1.60184,\;\; d \;=\; -\,0.362187,\;\; e \;=\; -\,0.0332753. \tag{77}$$

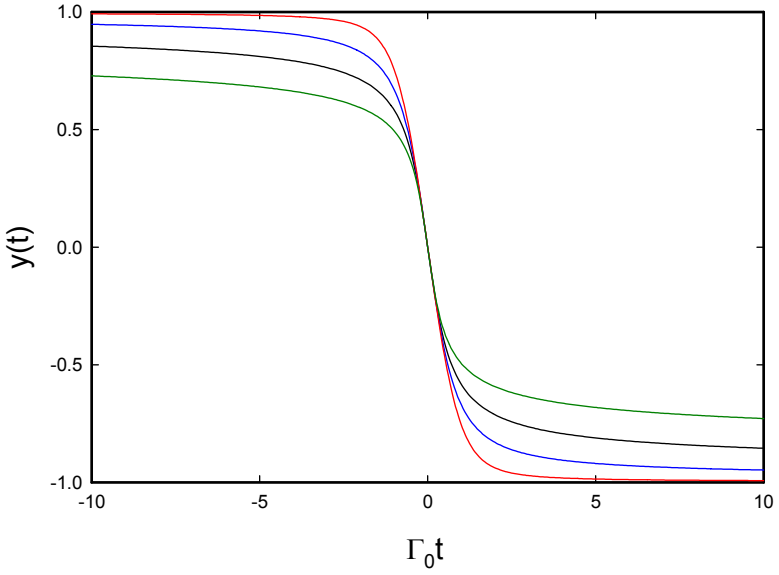

Figure 11. Non-periodic solutions for $y(t)$ as a function of scaled time for $g_{\max}/\Delta n^2$ values of 0.0003 (green), 0.001, 0.003, 0.01 (red). The time scaling uses $\tau^{-1} = |y'(0)|$.

6.4. Solutions

Using this function we may write for the evolution equation

$$\frac{\mathrm{d}^2}{\mathrm{d}t^2} y(t) \;=\; -\,\Omega_0^2 y F\left(\frac{g_{\max}}{\Delta n^2}\sqrt{1-y^2}\right). \tag{78}$$

In Fig. 11, we show non-periodic solutions that we computed for different values of $g_{\max}/\Delta n^2$. We scaled the time axis of the different solutions by the maximum rate for the different cases in order to compare them. To do this, we start with the maximum reaction velocity

$$\left|\frac{\mathrm{d}m}{\mathrm{d}t}\right|_{\max} \;=\; \frac{2}{\hbar}\max\{V_{\mathrm{eff}}\} \;=\; 8\left(\frac{\Delta E}{\hbar}\right)\left(\frac{g_{\max}}{\Delta n^2}\right)\Phi\left(\frac{g_{\max}}{\Delta n^2}\right). \tag{79}$$

The maximum rate for the normalized version of m can be written as

$$\Gamma_0 \;=\; \frac{1}{S}\left|\frac{\mathrm{d}m}{\mathrm{d}t}\right|_{\max} \;=\; \frac{8}{S}\left(\frac{\Delta E}{\hbar}\right)\left(\frac{g_{\max}}{\Delta n^2}\right)\Phi\left(\frac{g_{\max}}{\Delta n^2}\right) \;=\; \sqrt{2}\Omega_0\Phi\left(\frac{g_{\max}}{\Delta n^2}\right). \tag{80}$$

6.5. Connection between the maximum rate and the coupling

One of the key questions that relates to these models concerns determining how large the coupling matrix element must be in order for coherent energy exchange to occur at a given rate. In the large Δn scaling that we have considered in this section, we can determine the maximum reaction rate from the coupling matrix element by expressing Ω_0 in terms of V in the expression above to obtain

$$\Gamma_0 \;=\; \sqrt{2}\frac{1}{(\Delta n)^2}\frac{V\sqrt{n}}{\hbar}\Phi\left(\frac{g_{\max}}{(\Delta n)^2}\right). \tag{81}$$

The coupling matrix element in this model is $V\sqrt{n}$, so it is natural to expect $V\sqrt{n}/\hbar$ as providing the underlying rate scale. The maximum rate is then smaller by a factor of $(\Delta n)^2$, which is essentially the penalty in this model for fractionating the large two-level system quantum ΔE into a large number of oscillator quanta with energy $\hbar\omega_0$. The function Φ is shown in Fig. 7, and we might regard this factor as an additional penalty factor required for insufficiently strong coupling. Finally, we need to arrange for $g_{\max}/(\Delta n)^2$ to be sufficiently large so that our penalty Φ is not too great, which we can interpret as a constraint on the number of two-level systems required to fractionate the large quantum.

7. Discussion and Conclusions

The lossy spin-boson model is interesting in that it exhibits a strong coherent energy exchange effect between a set of two-level systems and an oscillator under conditions where the large energy quantum of the two-level systems is divided into a large number of oscillator quanta. In previous papers, we have examined this using perturbation theory [10], and using a second-order formulation [12]. Our interest in the problem stems from seeking models for the excess heat effect in the Fleischmann–Pons experiment, where we interpret the experimental results as splitting a large nuclear quantum of energy into a very large number of atomic scale quanta associated with phonon modes of the lattice. We are interested in this paper in the question of whether the lossy spin-boson model is capable coherent energy exchange under such conditions.

In a previous paper we introduced the periodic local approximation [13], which is a powerful tool which allows us to reduce a large and difficult two-dimensional (m and n) problem into a much smaller and easier one-dimensional (n) problem when a resonance condition is satisfied. In this paper we have exploited the local approximation to compute eigenfunctions, self-energies, and indirect coupling matrix elements for examples when the dimensionless coupling constant is reasonably large and when many oscillator quanta are exchanged. After a number of such calculations, we have found that the system appears to obey a scaling law for the self-energy, and a scaling law for the indirect coupling matrix element. The is interesting in its own right, since we had no reason *a priori* to expect such behavior. Also interesting is that the self-energy and indirect matrix elements show convergence to the strong coupling limit result in a regime where we can perform calculations directly, enabling us to verify the behavior of the system independently.

With the aid of the scaling law for the indirect coupling matrix element, we are able to carry out computations of the resulting system dynamics in the strong coupling regime where coherent energy exchange occurs with a very large number of oscillator quanta. In the end, we see that this lossy spin-boson model is able to exchange energy efficiently even when the two-level system transition energy is very much less than the characteristic energy of the oscillator. For this to work, the system must be in a very strong coupling regime, which can be done by simply increasing the number of two-level systems. The price to be paid for such a large mismatch is a reduction in the coherent energy transfer rate. In the large n model, the rate Γ_0 scales as $(\Delta n)^{-2}$ when Δn is increased and $g_{\max}/\Delta n^2$ is held fixed. Such scaling is relatively gentle, which encourages us in exploring it for application to excess heat in the Fleischmann–Pons experiment. The coherent energy transfer rate in the finite n model discussed in the Appendix is much faster.

In looking forward, much work remains to develop a usable theory for the Fleischmann–Pons experiment. We will need to generalize the model to describe donor and receiver two-level (as well as n-level) systems. Our computations in this paper were carried out in an infinite loss approximation, and we will need to develop models with finite oscillator loss at ΔE in order to connect with experiment. In our computations in the strong coupling limit in this work, a characteristic feature of the solutions is that a very large number of different oscillator n-states are occupied when g is large. In the physical system the oscillator sees loss at ω_0, so that one would expect the results to depend on this loss. We would like to examine models which shed light on this. We will also need to connect this simple two-level system and oscillator models to the physical system, which will require a derivation of the model as well as an evaluation of the coupling matrix elements.

Appendix A. A Finite n Model

We chose the simple model discussed in the previous subsections in part because it was simple and informative. However, the restriction that the number of oscillator quanta is not changed by the dynamics is a strong one, and we are interested here in the generalization to the case where the change in the number of oscillator quanta is significant.

Appendix A.1. Energy conservation

In this case, the number of oscillator quanta n would depend explicitly on m. If we assume that the oscillator loss at ω_0 can be neglected, then we may use energy conservation to write

$$n_0 \;=\; n + \Delta n(S+m). \tag{A.1}$$

In this model the number of oscillator quanta decreases when the number of excited two-level systems increases.

Appendix A.2. Evolution equation

The relation between the local g and m is modified to read

$$g \;=\; \frac{V\sqrt{n_0-\Delta n(S+m)}\sqrt{S^2-m^2}}{\Delta E}. \tag{A.2}$$

We use this to generalized the definition of ξ to

$$\xi \;=\; \frac{g}{\Delta n^2} \;=\; \frac{VS\sqrt{n_0-\Delta nS(1+y)}\sqrt{1-y^2}}{\Delta E\Delta n^2}. \tag{A.3}$$

We then compute

$$\frac{\mathrm{d}\xi}{\mathrm{d}y} \;=\; -\frac{g}{\Delta n^2}\left[\frac{y}{1-y^2}+\frac{S\Delta n}{2n}\right], \tag{A.4}$$

where we note that g and n both depend on y.

The evolution equation in general can be written as

$$\frac{\mathrm{d}^2}{\mathrm{d}t^2}y(t) \;=\; \frac{32}{S^2}\left(\frac{\Delta E}{\hbar}\right)^2\frac{\mathrm{d}\xi}{\mathrm{d}y}\frac{\mathrm{d}}{\mathrm{d}\xi}\left[\xi^2\Phi^2\left(\xi\right)\right]. \tag{A.5}$$

Using the expression above for the derivative $d\xi/dy$, we obtain

$$\frac{d^2}{dt^2}y(t) \;=\; -\frac{V^2 n}{\hbar^2 \Delta n^4}\left[y + \frac{S\Delta n}{2n}(1-y^2)\right]F(\xi). \tag{A.6}$$

Note that n and ξ depend explicitly on y in this evolution equation.

Appendix A.3. Steady-state condition

If all of the two-level systems are initialized in the ground state, and if the oscillator is initialized in an excited state, we would expect that some of the two-level systems would become excited. We can determine how many are excited in the steady state by solving

$$y + \frac{S\Delta n}{2n}(1-y^2) \;=\; 0. \tag{A.7}$$

We use

$$n \;=\; n_0 - \Delta n S(1+y) \tag{A.8}$$

to obtain the constraint

$$3y^2 + 2\left(1 - \frac{n_0}{\Delta n S}\right) - 1 \;=\; 0. \tag{A.9}$$

We assume that the amount of excitation is small, and obtain the approximate result

$$y \;=\; -1 + \frac{n_0}{2\Delta n S}. \tag{A.10}$$

The number of excited two-level systems in this case is

$$m + S \;=\; \frac{1}{2}\frac{n_0}{\Delta n} \;=\; \frac{n}{\Delta n}. \tag{A.11}$$

This is the condition at which the contributions that increase the indirect matrix elements are the same for the two-level systems as for the oscillator.

Appendix A.4. Discussion

In the large n model described in Section 6, if the oscillator is initially excited and the two-level systems are in the ground state, then the model predicts that in time all of the two-level systems would be excited. One of the reasons for going to a finite n model is that now the matrix elements increase when the number of oscillator quanta increases, so that the two-level systems in such a model want to give up their energy to the oscillator. In this new model, the rate at which the two-level systems give up their energy is increased by roughly $S\Delta n/n$ over that of the large n limit, a factor which can be very large.

If the two-level systems are initially in the ground state, then we would expect that they can be excited if the oscillator is highly excited. The evolution equation for this model gives this result. The large n model and this energy

conserving finite n model exhibit two different limits for coherent energy exchange. Unfortunately, there are issues with both models in connection with modeling excess heat in the Fleischmann—Pons experiment. If we are interested in coupling energy to optical phonon modes, it can never be the case that the system can reach a large n limit, because the associated thermal power would be so high as to be physically unreasonable (since the thermalization time of these phonon modes is so short). Since optical phonon modes are so lossy, a model which enforces energy conservation without optical phonon loss also seems not so realistic. To do better, we will need to include phonon loss.

References

[1] M. Fleischmann, S. Pons and M. Hawkins, *J. Electroanal Chem.* **201** (1989) 301; errata, **263** (1990) 187.
[2] M. Fleischmann, S. Pons, M.W. Anderson, L.J. Li and M. Hawkins, *J. Electroanal. Chem.* **287** (1990) 293.
[3] M.H. Miles, R.A. Hollins, B.F. Bush, J.J. Lagowski and R.E. Miles, *J. Electroanal. Chem.* **346** (1993) 99.
[4] M.H. Miles, B.F. Bush and J.J. Lagowski, *Fusion Technol.* **25** (1994) 478.
[5] M.H. Miles, Correlation of excess enthalpy and helium-4 production: A review, *Proc. ICCF10*, 2004, p. 123.
[6] P.L. Hagelstein, M.C.H. McKubre, D.J. Nagel, T.A. Chubb and R.J. Hekman, New physical effects in metal deuterides, *Proc. ICCF11*, 2005, p. 23.
[7] P.L. Hagelstein, *Naturwissenschaften* **97** (2010) 345.
[8] D. Letts, D. Cravens and P.L. Hagelstein, Dual laser stimulation and optical phonons in palladium deuteride, in low-energy nuclear reactions and new energy technologies, *Low-Energy Nuclear Reactions Sourcebook*, Vol. 2, American Chemical Society, Washington, DC, 2009, p. 81.
[9] P.L. Hagelstein, D. Letts and D. Cravens, Terahertz difference frequency response of PdD in two-laser experiments, *J. Cond. Mat. Nucl. Sci.* **3** (2010) 59.
[10] P.L. Hagelstein and I.U. Chaudhary, Energy exchange in the lossy spin-boson model, *J. Cond. Mat. Nucl. Sci.* **5** (2011) 52.
[11] P.L. Hagelstein and I.U. Chaudhary, Dynamics in the case of coupled degenerate states, *J. Cond. Mat. Nucl. Sci.* **5** (2011) 72.
[12] P.L. Hagelstein and I.U. Chaudhary, Second-order formulation and scaling in the lossy spin-boson model, *J. Cond. Mat. Nucl. Sci.* **5** (2011) 87.
[13] P.L. Hagelstein and I.U. Chaudhary, Local approximation for the lossy spin-boson model, *J. Cond. Mat. Nucl. Sci.* **5** (2011) 102.

J. Condensed Matter Nucl. Sci. 5 (2011) 140–154

Research Article

Generalization of the Lossy Spin–Boson Model to Donor and Receiver Systems

Peter L. Hagelstein *

Research Laboratory of Electronics, Massachusetts Institute of Technology, Cambridge, MA 02139, USA

Irfan U. Chaudhary

Department of Computer Science and Engineering, University of Engineering and Technology. Lahore, Pakistan

Abstract

Energy in the Fleischmann–Pons experiment is produced without commensurate energetic particles, and ^{4}He is seen in amounts proportional to the energy produced (with a ratio of energy to number near 24 MeV). Correspondingly we focus on the $D_2/^4$He transition as a two-level system coupled to an oscillator, in order to make a connection with the lossy spin–boson model considered in previous work. Because of the strong Coulomb repulsion between the deuterons, the associated coupling matrix element is very small, and there is no possibility of converting the transition energy to oscillator quanta within a simple lossy spin–boson model. This motivates us to generalize to more complicated model that includes a set of (donor) two-level systems for the $D_2/^4$He transition, and a set of (receiver) two-level systems that are strongly coupled to the oscillator. We analyze the resulting model in the limit that the receiver system is very strongly coupled. Within this formulation, the associated dynamics can be interpreted in terms of a transition from D_2 to ^{4}He with direct conversion (and fractionation) of the large energy quantum to the oscillator, once the coupling with the receiver system is sufficiently strong.
© 2011 ISCMNS. All rights reserved.

Keywords: Coherent Fusion, Donor–receiver Model, Excitation Transfer, Theory Excess Heat in the Fleischmann–Pons Experiment

1. Introduction

In the previous papers, we introduced the lossy spin–boson model, and we studied the ability of the model to describe the fractionation of a large quantum [1–5]. Our goal in these studies has been to develop new models relevant to excess heat production in the Fleischmann–Pons experiment [6], where a large amount of energy is made [7], ^{4}He is observed

*E-mail: plh@mit.edu

© 2011 ISCMNS. All rights reserved.

in amounts commensurate with the energy produced [8,9], and where no commensurate energetic particles are observed [10].

The fundamental question that was the focus of our earlier work is whether a large nuclear-scale quanta can be fractionated into a large number of much smaller quanta relevant to condensed matter degrees of freedom. Our approach in this study was to focus on equivalent two-level systems and an oscillator, in an effort to simplify the problem as much as possible (since the associated models and coherent dynamics are much more complicated than for incoherent reactions). As a result, it was not important to specify precisely which levels were involved. Had our ultimate conclusion been otherwise (that fractionating a large quantum was impossible), then there would have been no need to examine specific cases.

1.1. General mathematical models versus specific physical models

Our results suggest that a large quantum can be fractionated, and we have explicit models which show the effect and which we can analyze quantitatively. This now opens the door to trying to connect the general model to specific examples of models of this type for evaluation. This new problem that we face now must be viewed as a significant problem in its own right. One new task is to identify upper and lower levels of the two-level systems with specific nuclear states, and another is to associate specific condensed matter oscillatory modes to the harmonic oscillator in the model.

Ideally, we would like for experiment to provide an unambiguous positive identification for us the states that are involved, and to make perfectly clear which oscillator is relevant. Unfortunately, in the experiments that have been done so far, and we generally lack the experimental clarity that would result in unambiguous choices. Consequently, there is not agreement within the community of scientist working on the problem as to what states should be focused on, and at this point some discussion of the problem is worth while. In the remainder of this Introduction, we summarize briefly some of the discussion that has occurred within our group over the years.

1.2. Lossy spin–boson model for the D_2 to ^{4}He transition

If we select molecular D_2 (keeping in mind that there are a number of such states) for the upper state of the two-level system, and ^{4}He for the lower state, then the resulting model would predict a ratio of excess energy to the number of ^{4}He atoms to be 23.85 MeV, which is consistent with the two experiments that measure the ratio under conditions where an attempt was made to recover the helium retained in the cathode [11,12].

Unfortunately, the associated coupling matrix element is exceedingly small because of Coulomb repulsion. If we model the system using a lossy spin–boson model, then we quickly conclude that it is impossible to fractionate the large quantum with these states alone since the associated coupling matrix element is so small.

1.3. Generalization of the model and excitation transfer

Because of this, we decided (many years ago) to generalize the model in order to have a more complicated system in which the D_2/^{4}He transition would supply the large energy quantum, and another transition would be involved in the fractionation of the quantum.

For this to work, we require a new fundamental mechanism that takes the energy associated with a transition at one site, and transfers it to another site. There is precedence for such a physical effect in biophysics, in which an excited molecule is observed to transfer its excitation (through a Coulomb interaction) to another molecule. In this case, the effect is termed “resonance energy transfer”, or “Förster effect” (in honor of the physicist who first gave a quantitative model for the effect [13,14]). There is no reason to believe that a nuclear version of the Förster effect should not be

able to exist for nuclei, but from calculation we know that a version of the effect that depends on Coulomb interactions alone cannot do what we require (because the Coulomb dipole–dipole interaction is of short range).

For us, the solution to this problem was to focus on phonon exchange instead of Coulomb exchange, since we found that a much longer range for the effect could work in the case of phonon exchange with a highly excited phonon mode. This is very closely connected with the kinds of models we discussed earlier. For example, one can establish the effect using perturbation theory in a model with two different two-level systems each coupled linearly to an oscillator. As a result, this new excitation transfer mechanism comes into the problem in a natural way in the generalization of our model from one set of two-level systems to two sets of two-level systems, both coupled to a common oscillator.

1.4. But what transition would fractionate the large quantum?

From the beginning of our research on this generalization, we have faced the issue of specifying a second set of two-level systems which would fractionate the large quantum, and convert the energy to a condensed matter mode. Models with different choices have been studied, and from these studies we have begun to understand what the relevant issues are.

In the early days of our work, we thought that the most important issue in the selection of the second set of two-level systems was the degree of resonance with the $D_2/^4He$ transition energy. As a result, it seemed natural to consider transitions between ^4He as the ground state, and whatever two-deuteron states were available near the initial transition energy (23.85 MeV), since we would come closest to obtaining a resonance.

Once we began to understand phonon exchange in association with nuclear transitions better, and when we also understood the coherent models better, it became clear that the Pd isotopes should be considered as candidates. Arguing for this approach is that Pd is the primary constituent of the host lattice, so that we might expect it to be numerically dominant.

We focused at one point on transitions to excited states, composed of a neutral plus daughter, that seemed to be favored in exchanging phonons; one such example was the $^{110}Pd/^{106}Pd+^4n$ transition. This transition is probably not such a close match in energy to the $D_2/^4He$ transition, so the issue of energy exchange in connection with excitation transfer becomes important.

Recently, we undertook a systematic effort to see whether we could identify candidate transitions that would be able to serve as receivers in the donor-receiver model under discussion in this work. The general approach that we used was to derive constraints directly from our model, and we examined several hundred nuclear and atomic transitions to see how closely the constraints could be satisfied. It quickly came clear from this analysis that no physical transition can stand in for the receiver-side of this model, since we ask for too much. Perhaps the biggest issue in this study is that we require a large coupling matrix from the ground state, and also a long lifetime so that coherence can be preserved; yet generally a large coupling matrix element implies a short radiative lifetime.

Because of this, we have adopted a revised point of view concerning this simple donor-receiver model, with two sets of two-level systems coupled to an oscillator, and augmented with loss. Certainly it is the simplest model that demonstrates the basic physical effects we require: the ability to exhange energy coherently under conditions where a large quantum is fractionated, and the ability to transfer excitation from one two-level system to another. But since the receiver system doesn't correspond to a simple physical transition, we view it as a likely idealization of a more complicated receiver system that involves three or more levels. But the two-level systems of the donor side of the model appears relevant to the $D_2/^4He$ transition, allowing us to study the donor dynamics in the presence of an idealized receiver system.

1.5. But what about the oscillator?

The oscillator in the general two-level system and oscillator models can in principle represent any condensed matter oscillatory mode, and the question at issue is what modes are involved. The candidates in principle include acoustic

phonon modes, optical phonon modes (with compressional modes at the Γ-point and L-point apparently preferred in the two-laser experiment), and plasmon modes (which we expect to be mixed with optical phonon modes, and which are implicated in single laser experiments). There is no reason to exclude any of these modes in the basic Fleischmann–Pons experiment, based on measurements done so far. In the single laser experiment, probably a plasmon mode is involved. In the two-laser experiment [15,16] specific optical phonon modes are involved. In what follows our focus will be on optical phonon modes, primarily since the resulting model seems "cleanest" to us (optical phonon modes couple well with the $D_2/^4$He transition).

2. Generalization of the Lossy Spin–Boson Model

Based on the above discussion, we generalize the lossy spin–boson model to include two different sets of two-level systems

$$\hat{H} = \Delta E_1 \frac{\hat{S}_z^{(1)}}{\hbar} + \Delta E_2 \frac{\hat{S}_z^{(2)}}{\hbar} + \hbar\omega_0 \hat{a}^\dagger \hat{a} + V_1 e^{-G}(\hat{a}^\dagger + \hat{a}) \frac{2\hat{S}_x^{(1)}}{\hbar} + V_2(\hat{a}^\dagger + \hat{a}) \frac{2\hat{S}_x^{(2)}}{\hbar} - i\frac{\hbar}{2}\hat{\Gamma}(E). \tag{1}$$

The first set of two-level systems will have transition energy ΔE_1, and will be considered to be the "donor" system within the model (in the sense that excitation is transferred from this system); the second set of two-level systems (the "receiver" system) in general has a different transition energy ΔE_2. The oscillator has a characteristic energy $\hbar\omega_0$. We include linear coupling terms between the oscillator and each of the two sets of two-level systems, with the coupling constant $V_1 e^{-G}$ for coupling from the first set of two-level systems (where e^{-G} accounts for transitions from the first set of two-level systems being hindered by the tunneling factor associated with tunneling through the Coulomb barrier), and V_2 for coupling with the second set of two-level systems. Loss is included through a Brillouin–Wigner type of loss operator as we have discussed previously.

3. Local Approximation for the Generalized Lossy Spin–Boson Model

We are interested ultimately in a regime in which the coupling between the receiver system and the oscillator is very strong. In our previous work on coherent energy exchange, we found that the system could be understood by taking advantage of the local approximation, since direct calculations when the coupling is very strong are computationally expensive. For the generalized lossy spin–boson model we would like to make use of the local approximation for our analysis.

3.1. Eigenvalue equation for the expansion coefficients

To proceed, we begin with a finite basis expansion for this more complicated system in the form

$$\Psi = \sum_{m_1} \sum_{m_2} \sum_{n} c_{m_1,m_2,n} |S_1, m_1\rangle |S_2, m_2\rangle |n\rangle. \tag{2}$$

For the wave function Ψ to satisfy the time-independent Schrödinger equation, the expansion coefficients $c_{m_1,m_2,n}$ satisfy

$$
\begin{aligned}
Ec_{m_1,m_2,n} \;=& \left[\Delta E_1 m_1 + \Delta E_2 m_2 + \hbar\omega_0 n - i\frac{\hbar}{2}\Gamma(E)\right] c_{m_1,m_2,n} \\
&+ V_1 \mathrm{e}^{-G}\sqrt{n+1}\sqrt{(S_1-m_1)(S_1+m_1+1)}\, c_{m_1+1,m_2,n+1} \\
&+ V_1 \mathrm{e}^{-G}\sqrt{n}\sqrt{(S_1-m_1)(S_1+m_1+1)}\, c_{m_1+1,m_2,n-1} \\
&+ V_1 \mathrm{e}^{-G}\sqrt{n+1}\sqrt{(S_1+m_1)(S_1-m_1+1)}\, c_{m_1-1,m_2,n+1} \\
&+ V_1 \mathrm{e}^{-G}\sqrt{n}\sqrt{(S_1+m_1)(S_1-m_1+1)}\, c_{m_1-1,m_2,n-1} \\
&+ V_2 \sqrt{n+1}\sqrt{(S_2-m_2)(S_2+m_2+1)}\, c_{m_1,m_2+1,n+1} \\
&+ V_2 \sqrt{n}\sqrt{(S_2-m_2)(S_2+m_2+1)}\, c_{m_1,m_2+1,n-1} \\
&+ V_2 \sqrt{n+1}\sqrt{(S_2+m_2)(S_2-m_2+1)}\, c_{m_1,m_2-1,n+1} \\
&+ V_2 \sqrt{n}\sqrt{(S_2+m_2)(S_2-m_2+1)}\, c_{m_1,m_2-1,n-1}. \qquad (3)
\end{aligned}
$$

3.2. Limit of many oscillator quanta and two-level systems

Previously we used large n and large S approximations to develop a local approximation. Here we need to do the same. We assume that n is large to write

$$\sqrt{n+1} \;\approx\; \sqrt{n}. \qquad (4)$$

For the different two-level systems, we make the approximation

$$\sqrt{(S_j-m_j)(S_j+m_j+1)} \;\approx\; \sqrt{S_j^2-m_j^2}, \qquad (5)$$

$$\sqrt{(S_j+m_j)(S_j-m_j+1)} \;\approx\; \sqrt{S_j^2-m_j^2}. \qquad (6)$$

If each S_j is very large, and if each m_j is not close to $\pm S_j$, then these approximations should be good ones.

3.3. Local approximation

The coupling coefficients become the same to different states when we make this approximation, which leads directly to a local approximation for this model

$$
\begin{aligned}
Ec_{m_1,m_2,n} \;=& \left[\Delta E_1 m_1 + \Delta E_2 m_2 + \hbar\omega_0 n - i\frac{\hbar}{2}\Gamma(E)\right] c_{m_1,m_2,n} \\
&+ V_1 \mathrm{e}^{-G}\sqrt{n}\sqrt{S_1^2-m_1^2}\,\left(c_{m_1+1,m_2,n+1} + c_{m_1+1,m_2,n-1} + c_{m_1-1,m_2,n+1} + c_{m_1-1,m_2,n-1}\right) \\
&+ V_2 \sqrt{n}\sqrt{S_2^2-m_2^2}\,\left(c_{m_1,m_2+1,n+1} + c_{m_1,m_2+1,n-1} + c_{m_1,m_2-1,n+1} + c_{m_1,m_2-1,n-1}\right). \qquad (7)
\end{aligned}
$$

It is convenient to define two dimensionless coupling constants according to

$$g_1 = \frac{V_1\sqrt{n}\sqrt{S_1^2 - m_1^2}}{\Delta E_1}, \tag{8}$$

$$g_2 = \frac{V_2\sqrt{n}\sqrt{S_2^2 - m_2^2}}{\Delta E_2}. \tag{9}$$

We can rewrite the eigenvalue equation for the expansion coefficients as

$$\begin{aligned} Ec_{m_1,m_2,n} = & \left[\Delta E_1 m_1 + \Delta E_2 m_2 + \hbar\omega_0 n - i\frac{\hbar}{2}\Gamma(E)\right]c_{m_1,m_2,n} \\ & + \Delta E_1 g_1 \mathrm{e}^{-G}\left(c_{m_1+1,m_2,n+1} + c_{m_1+1,m_2,n-1} + c_{m_1-1,m_2,n+1} + c_{m_1-1,m_2,n-1}\right) \\ & + \Delta E_2 g_2\left(c_{m_1,m_2+1,n+1} + c_{m_1,m_2+1,n-1} + c_{m_1,m_2-1,n+1} + c_{m_1,m_2-1,n-1}\right). \end{aligned} \tag{10}$$

This is consistent with a local configuration space Hamiltonian of the form

$$\begin{aligned} \hat{H} = & \Delta E_1 m_1 + \Delta E_2 m_2 + \hbar\omega_0 n - i\frac{\hbar}{2}\Gamma(E) \\ & + \Delta E_1 g_1 \mathrm{e}^{-G}(\hat{\delta}_+^n + \hat{\delta}_-^n)(\hat{\delta}_+^{m_1} + \hat{\delta}_-^{m_1}) \\ & + \Delta E_2 g_2\,(\hat{\delta}_+^n + \hat{\delta}_-^n)(\hat{\delta}_+^{m_2} + \hat{\delta}_-^{m_2}). \end{aligned} \tag{11}$$

4. Periodic Donor and Receiver Models

In the strong coupling limit direct calculations of eigenfunctions, eigenvalues, and indirect coupling matrix elements becomes increasingly difficult the stronger the coupling. In the periodic model the problem simplifies, allowing us to make use of numerical and analytic approaches. We use this approach here to analyze donor–receiver models under conditions where the coupling between the oscillator and the receiver two-level systems is very strong.

4.1. Periodic approximation and resonance condition

One of the most important tools that we have for analyzing coherent energy exchange in the strong coupling regime is the periodic approximation. Since we would like to understand the generalized lossy spin–boson model when Δn is very large for the receiver system, it seems reasonable to once again make use of the period version of the problem. Since there are two sets of two-level systems, we are going to require two distinct resonance conditions. For coherent energy exchange between the receiver system and oscillator, we require

$$\Delta E_2 = \Delta n_2 \hbar\omega_0. \tag{12}$$

For excitation transfer transitions, we require

$$\Delta E_1 = \Delta E_2 + \Delta n_{12}\hbar\omega_0. \tag{13}$$

Even though we do not expect direct coherent energy exchange between the donor two-level systems and the oscillator, it is useful to define Δn_1 to satisfy

$$\Delta E_1 \;=\; \Delta n_1 \hbar\omega_0. \tag{14}$$

4.2. Periodic solution

When the above resonance condition is satisfied, we can construct a locally periodic solution of the form

$$\Psi \;=\; \sum_{m_1}\sum_{m_2}\sum_{n} d_{m_1,m_2} u_{n+m_1\Delta n_1+m_2\Delta n_2} |S_1, m_1\rangle |S_2, m_2\rangle |n + m_1\Delta n_1 + m_2\Delta n_2\rangle. \tag{15}$$

It is possible to develop eigenfunction solutions for the local Hamiltonian using

$$d_{m_1,m_2} \;=\; \mathrm{e}^{i(m_1\phi_1+m_2\phi_2)}. \tag{16}$$

4.3. Eigenvalue equation

We assume that the wavefunction satisfies the time-independent Schrödinger equation, and then we use orthogonality to obtain an eigenvalue equation for the expansion coefficients

$$\begin{aligned} E d_{m_1,m_2} u_{n+m_1\Delta n_1+m_2\Delta n_2} &\\ &= \left[\Delta E_1 m_1 + \Delta E_2 m_2 + n\hbar\omega_0 - i\frac{\hbar}{2}\hat{\Gamma}(E)\right] d_{m_1,m_2} u_{n+m_1\Delta n_1+m_2\Delta n_2} \\ &\quad + g_1 \mathrm{e}^{-G} \Delta E_1 [d_{m_1+1,m_2}(u_{n+1+(m_1+1)\Delta n_1+m_2\Delta n_2} + u_{n-1+(m_1+1)\Delta n_1+m_2\Delta n_2}) \\ &\quad + d_{m-1,m_2}(u_{n+1+(m_1-1)\Delta n_1+m_2\Delta n_2} + u_{n-1+(m_1-1)\Delta n_1+m_2\Delta n_2})] \\ &\quad + g_2 \Delta E_2 [d_{m_1,m_2+1}(u_{n+1+m_1\Delta n_1+(m_2+1)\Delta n_2} + u_{n-1+m_1\Delta n_1+(m_2+1)\Delta n_2}) \\ &\quad + d_{m_1,m_2-1}(u_{n+1+m_1\Delta n_1+(m_2-1)\Delta n_2} + u_{n-1+m_1\Delta n_1+(m_2-1)\Delta n_2})]. \end{aligned} \tag{17}$$

If we make use of Eq. (16), then this can be simplified to

$$\begin{aligned} E(\phi_1,\phi_2) u_n \;&=\; \left[n\hbar\omega_0 - i\frac{\hbar}{2}\hat{\Gamma}(E)\right] u_n \\ &\quad + g_1 \mathrm{e}^{-G} \Delta E_1 [\mathrm{e}^{i\phi_1}(u_{n+1+\Delta n_1} + u_{n-1+\Delta n_1}) + \mathrm{e}^{-i\phi_1}(u_{n+1-\Delta n_1} + u_{n-1-\Delta n_1})] \\ &\quad + g_2 \Delta E_2 [\mathrm{e}^{i\phi_2}(u_{n+1+\Delta n_2} + u_{n-1+\Delta n_2}) + \mathrm{e}^{-i\phi_2}(u_{n+1-\Delta n_2} + u_{n-1-\Delta n_2})], \end{aligned} \tag{18}$$

where we have focused as before on the special case of m_1 and m_2 equal to zero.

4.4. Solution for the second set of two-level systems

In this problem, the first set of two-level systems is weakly coupled to the oscillator, while the second set of two-level systems is strongly coupled. As a result, we would expect that the strong coupling associated with the second set of

two-level systems would dominate the problem. We have considered such a problem previously. It is possible to adapt it here by first taking

$$g_1 e^{-G} \rightarrow 0 \tag{19}$$

and writing

$$\begin{aligned} E_2(\phi_2)v_n(\phi_2) &= \left[n\hbar\omega_0 - i\frac{\hbar}{2}\hat{\Gamma}(E)\right]v_n(\phi_2) \\ &+ g_2\Delta E_2[e^{i\phi_2}(v_{n+1+\Delta n_2}(\phi_2) + v_{n-1+\Delta n_2}(\phi_2)) \\ &+ e^{-i\phi_2}(v_{n+1-\Delta n_2}(\phi_2) + v_{n-1-\Delta n_2}(\phi_2))], \end{aligned} \tag{20}$$

where the $v_n(\phi_2)$ are the same coefficients that we studied previously in Ref. [5], and where $E_2(\phi_2)$ is the associated energy eigenvalue. We found previously that this energy eigenvalue in the strong coupling regime with large Δn_2 is approximately

$$E_2(\phi_2) \rightarrow \Sigma_2(g_2) + 2V_2^{\rm eff}\cos\phi_2, \tag{21}$$

where Σ_2 is the self-energy which we found previously in the strong coupling limit to be

$$\Sigma_2(g_2) \rightarrow -4g_2 \tag{22}$$

and where $V_2^{\rm eff}$ is [5]

$$V_2^{\rm eff} \rightarrow \frac{4g_2}{\Delta n_2^2}\Delta E_2 \Phi\left(\frac{g_2}{\Delta n_2^2}\right). \tag{23}$$

4.5. Perturbation theory estimate for the energy eigenvalue

We can use this as a starting point to estimate the energy eigenvalue. We can use perturbation theory to write

$$\begin{aligned} E(\phi_1,\phi_2) \approx E_2(\phi_2) + \Big\langle v_n(\phi_2)\Big| g_1 e^{-G}\Delta E_1\Big[e^{i\phi_1}\big[v_{n+1+\Delta n_1}(\phi_2) + v_{n-1+\Delta n_1}(\phi_2)\big] \\ + e^{-i\phi_1}\big[v_{n+1-\Delta n_1}(\phi_2) + v_{n-1-\Delta n_1}(\phi_2)\big]\Big]\Big\rangle. \end{aligned} \tag{24}$$

We saw from earlier work that the expansion coefficients are slowly varying in the strong coupling limit, so that

$$v_{n+1-\Delta n_1}(\phi_2) \approx v_{n-\Delta n_1}(\phi_2). \tag{25}$$

Hence, we may write

$$\begin{aligned} E(\phi_1,\phi_2) &\approx E_2(\phi_2) \\ &+ 2g_1 e^{-G}\Delta E_1[e^{i\phi_1}\langle v_n(\phi_2)|v_{n+\Delta n_1}(\phi_2)\rangle + e^{-i\phi_1}\langle v_n(\phi_2)|v_{n-\Delta n_1}(\phi_2)\rangle]. \end{aligned} \tag{26}$$

The bra and kets here denote summations over the different n, and we may write

$$\langle v_n(\phi_2)|v_{n+\Delta n_1}(\phi_2)\rangle \;=\; \langle v_n(\phi_2)|v_{n-\Delta n_1}(\phi_2)\rangle^*. \tag{27}$$

Hence

$$E(\phi_1,\phi_2) \;\approx\; E_2(\phi_2) + 4g_1\, \mathrm{e}^{-G}\Delta E_1 \mathrm{Re}\{\mathrm{e}^{i\phi_1}\langle v_n(\phi_2)|v_{n+\Delta n_1}(\phi_2)\rangle\}. \tag{28}$$

5. Dynamics of the Donor System

Our attention is first drawn to the dynamics of the donor system. Instead of dealing with the more complicated problem associated with both the donor and receiver systems, we wish to first study the donor dynamics independently. Aside from the fact that it greatly simplifies the problem, this study will emphasize a key feature of how this coupled system works. We will see that under some conditions it becomes possible for the transition energy of the donor system to be converted directly to the oscillator, as a result of the oscillator being strongly coupled with the other two-level system.

5.1. Dynamical equations for the expansion coefficients

We begin with a wave function definition of the form

$$\Psi \;=\; \sum_{m_1}\sum_{m_2}\sum_{n} d_{m_1}(t)\mathrm{e}^{im_2\phi_2}u_{n+m_1\Delta n_1+m_2\Delta n_2}|S_1,m_1\rangle|S_2,m_2\rangle|n+m_1\Delta n_1+m_2\Delta n_2\rangle. \tag{29}$$

The associated evolution equation becomes

$$\begin{aligned}
i\hbar\frac{\mathrm{d}}{\mathrm{d}t}&d_{m_1}(t)\mathrm{e}^{im_2\phi_2}u_{n+m_1\Delta n_1+m_2\Delta n_2}\\
&= \left[\Delta E_1 m_1 + \Delta E_2 m_2 + n\hbar\omega_0 - i\frac{\hbar}{2}\hat{\Gamma}(E)\right] d_{m_1}(t)\mathrm{e}^{im_2}u_{n+m_1\Delta n_1+m_2\Delta n_2}\\
&\quad + g_1\mathrm{e}^{-G}\Delta E_1[d_{m_1+1}(t)\mathrm{e}^{im_2\phi_2}(u_{n+1+(m_1+1)\Delta n_1+m_2\Delta n_2} + u_{n-1+(m_1+1)\Delta n_1+m_2\Delta n_2})\\
&\quad + d_{m-1}(t)\mathrm{e}^{im_2\phi_2}(u_{n+1+(m_1-1)\Delta n_1+m_2\Delta n_2} + u_{n-1+(m_1-1)\Delta n_1+m_2\Delta n_2})]\\
&\quad + g_2\Delta E_2[d_{m_1}(t)\mathrm{e}^{i(m_2+1)\phi_2}(u_{n+1+m_1\Delta n_1+(m_2+1)\Delta n_2} + u_{n-1+m_1\Delta n_1+(m_2+1)\Delta n_2})\\
&\quad + d_{m_1}(t)\mathrm{e}^{i(m_2-1)\phi_2}(u_{n+1+m_1\Delta n_1+(m_2-1)\Delta n_2} + u_{n-1+m_1\Delta n_1+(m_2-1)\Delta n_2})].
\end{aligned} \tag{30}$$

We first simplify the phases to write

$$
\begin{aligned}
i\hbar\frac{\mathrm{d}}{\mathrm{d}t}d_{m_1}(t)u_{n+m_1\Delta n_1+m_2\Delta n_2}
&= \left[\Delta E_1 m_1 + \Delta E_2 m_2 + n\hbar\omega_0 - i\frac{\hbar}{2}\hat{\Gamma}(E)\right] d_{m_1}(t)u_{n+m_1\Delta n_1+m_2\Delta n_2} \\
&+ g_1 \mathrm{e}^{-G}\Delta E_1[d_{m_1+1}(t)(u_{n+1+(m_1+1)\Delta n_1+m_2\Delta n_2} + u_{n-1+(m_1+1)\Delta n_1+m_2\Delta n_2}) \\
&+ d_{m-1}(t)(u_{n+1+(m_1-1)\Delta n_1+m_2\Delta n_2} + u_{n-1+(m_1-1)\Delta n_1+m_2\Delta n_2})] \\
&+ g_2\Delta E_2[\mathrm{e}^{i\phi_2}(u_{n+1+m_1\Delta n_1+(m_2+1)\Delta n_2} + u_{n-1+m_1\Delta n_1+(m_2+1)\Delta n_2}) \\
&+ \mathrm{e}^{-i\phi_2}(u_{n+1+m_1\Delta n_1+(m_2-1)\Delta n_2} + u_{n-1+m_1\Delta n_1+(m_2-1)\Delta n_2})]d_{m_1}(t). \qquad (31)
\end{aligned}
$$

We then approximate

$$
u_n \;\rightarrow\; v_n(\phi_2) \qquad (32)
$$

and obtain

$$
\begin{aligned}
i\hbar\frac{\mathrm{d}}{\mathrm{d}t}d_{m_1}(t) \;&\approx E_2(\phi_2)d_{m_1}(t) \\
&+ 2g_1\mathrm{e}^{-G}\Delta E_1[d_{m_1+1}(t)\langle v_{n+m_1\Delta n_1+m_2\Delta n_2}|v_{n+(m_1+1)\Delta n_1+m_2\Delta n_2}\rangle \\
&+ d_{m-1}(t)\langle v_{n+m_1\Delta n_1+m_2\Delta n_2}|v_{n+(m_1-1)\Delta n_1+m_2\Delta n_2}\rangle], \qquad (33)
\end{aligned}
$$

where we have used a reference energy offset based on $m_1 = 0$ and $m_2 = 0$. This can be denoted more simply as

$$
\begin{aligned}
i\hbar\frac{\mathrm{d}}{\mathrm{d}t}d_{m_1}(t) \;&\approx E_2(\phi_2)d_{m_1}(t) \\
&+ 2g_1\mathrm{e}^{-G}\Delta E_1[d_{m_1+1}(t)\langle v_n(\phi_2)|v_{n+\Delta n_1}(\phi_2)\rangle + d_{m-1}(t)\langle v_n(\phi_2)|v_{n-\Delta n_1}(\phi_2)\rangle]. \qquad (34)
\end{aligned}
$$

5.2. Interpretation

In the solution Ψ that we adopted, the basis states are presumed degenerate as an ansatz of the model. As a result, we expected to obtain evolution equations with indirect coupling between distant expansion coefficient of degenerate states (distant in n, but nearest neighbors in m_1), and this corresponds to our result of Eq. (34). However, this result deserves some consideration in its own right in terms of the associated physical mechanism that has come out of the model we proposed. In previous work we considered models in which the donor system would transfer excitation to the receiver system, and then the receiver system would convert it to oscillator energy.

However, what we have found using this formulation in the strong coupling limit is qualitatively different, and much simpler. In essence, once there is sufficient coupling between the oscillator and receiver system, then the oscillator states become spread, allowing the donor transition energy to be accepted directly by the oscillator. This differs qualitative from our earlier proposals and models.

The overlap integral $\langle v_n(\phi_2)|v_{n+\Delta n_1}(\phi_2)\rangle$ is a function of the dimensionless coupling of the receiver system g_2, even though we have not denoted this dependence explicitly. When the coupling between the receiver system and oscillator is too weak, then the overlap integral becomes vanishingly small. When the coupling is strong, and the donor transition energy is approximately matched to a multiple of the receiver system transition energy, then the overlap approaches unity.

5.3. Evolution equations for expectation values

We may write for the evolution equation for the expansion coefficients an equivalent dynamical equation of the form

$$i\hbar \frac{\mathrm{d}}{\mathrm{d}t} d_{m_1} \;=\; V_{m_1+\frac{1}{2}} d_{m_1+1} + V_{m_1-\frac{1}{2}} d_{m_1-1}, \tag{35}$$

where we have discarded the unimportant constant energy offset. In the event that ϕ_2 is 0 or π, then the coupling coefficients are real; otherwise they can be complex. In such cases we may write

$$V_{m_1+\frac{1}{2}} \;=\; |V_{m_1+\frac{1}{2}}| \mathrm{e}^{i\theta}, \tag{36}$$

$$V_{m_1-\frac{1}{2}} \;=\; |V_{m_1-\frac{1}{2}}| \mathrm{e}^{-i\theta}. \tag{37}$$

If we define scaled expansion coefficients according to

$$e_{m_1} \;=\; d_{m_1} \mathrm{e}^{i m_1 \theta} \tag{38}$$

then the associated evolution equation is

$$i\hbar \frac{\mathrm{d}}{\mathrm{d}t} e_{m_1} \;=\; |V_{m_1+\frac{1}{2}}| e_{m_1+1} + |V_{m_1-\frac{1}{2}}| e_{m_1-1}. \tag{39}$$

We define the expectation value of the Dicke number m_1 as

$$\langle m_1 \rangle \;=\; \sum_{m_1} m_1 |e_{m_1}|^2. \tag{40}$$

The associated evolution equations are

$$\frac{\mathrm{d}}{\mathrm{d}t} \langle m_1 \rangle \;=\; \langle \hat{v}_1 \rangle, \tag{41}$$

$$\frac{\mathrm{d}}{\mathrm{d}t} \langle \hat{v}_1 \rangle \;=\; \frac{2}{\hbar^2} \sum_{m_1} |e_{m_1}|^2 \big(|V_{m_1+\frac{1}{2}}|^2 - |V_{m_1-\frac{1}{2}}|^2 \big). \tag{42}$$

5.4. Classical limit

In the classical limit we may write

$$\frac{\mathrm{d}^2}{\mathrm{d}t^2} m_1(t) \;=\; \frac{2}{\hbar^2} \frac{\mathrm{d}}{\mathrm{d}m_1} [V_1^{\mathrm{eff}}]^2 \tag{43}$$

using

$$V_1^{\rm eff} \;=\; 2g_1 {\rm e}^{-G} \Delta E_1 |\langle v_n(\phi_2)|v_{n+\Delta n_1}(\phi_2)\rangle|. \tag{44}$$

Most of the factors that make up the indirect coupling coefficient for the donor system $V_1^{\rm eff}$ do not depend on m_1; the overlap matrix element depends on parameters associated with the receiver system, but not the donor system. As a result, we may write

$$\begin{aligned}
\frac{{\rm d}^2}{{\rm d}t^2} m_1(t) \;&=\; \frac{2}{\hbar^2} 4{\rm e}^{-2G} (\Delta E_1)^2 |\langle v_n(\phi_2)|v_{n+\Delta n_1}(\phi_2)\rangle|^2 \frac{\rm d}{{\rm d}m_1} g_1^2 \\
&=\; \frac{2}{\hbar^2} 4{\rm e}^{-2G} V_1^2 n |\langle v_n(\phi_2)|v_{n+\Delta n_1}(\phi_2)\rangle|^2 \frac{\rm d}{{\rm d}m_1} (S_1^2 - m_1^2) \\
&=\; -\left[\frac{16 V_1^2 n}{\hbar^2} {\rm e}^{-2G} |\langle v_n(\phi_2)|v_{n+\Delta n_1}(\phi_2)\rangle|^2 \right] m_1(t).
\end{aligned} \tag{45}$$

It may be most useful to write this as

$$\frac{{\rm d}^2}{{\rm d}t^2} m_1(t) \;=\; -\left[\Omega_1(g_2, \phi_2)\right]^2 m_1(t) \tag{46}$$

with

$$\Omega_1(g_2, \phi_2) \;=\; 4 \left(\frac{V_1 \sqrt{n}}{\hbar} {\rm e}^{-G} \right) |\langle v_n(\phi_2)|v_{n+\Delta n_1}(\phi_2)\rangle|. \tag{47}$$

The characteristic frequency associated with the donor system is seen to be four times the coupling matrix element (including the Gamow factor) divided by $\hbar$, times a hindrance factor (magnitude of the overlap matrix element) that depends on the receiver system.

5.5. Analytic solution when the receiver system is static

In the event that we impose (mathematically) a condition of steady state on the receiver system, the associated dynamics of the donor system will be oscillatory. As an example, if all of the two-level systems of the donor system are initially excited, then the relevant classical solution is

$$m_1(t) \;=\; S_1 \cos(\Omega_1 t). \tag{48}$$

We see that the dynamics are determined by the characteristic frequency.

6. Discussion and Conclusions

Since the coupling is so weak in the case of the $D_2/^4$He transition, we have generalized the lossy spin–boson model to the present donor-receiver model that includes two sets of two-level systems coupled to an oscillator. We recognize this model as an simplification of a more complicated model, as the two-level system of the receiver side is an idealization of a system involving more levels.

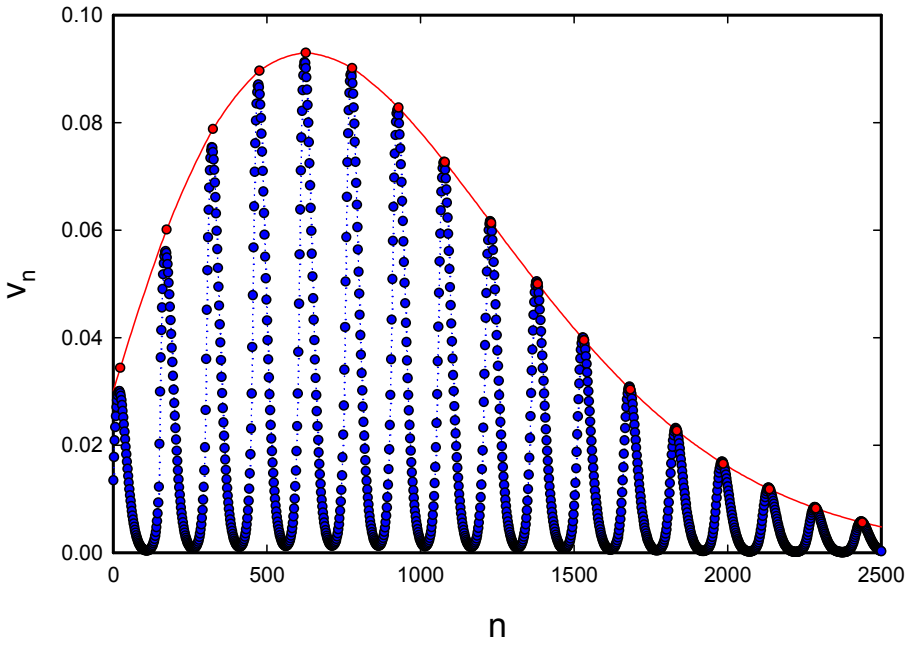

Figure 1. Expansion coefficients for $g = 30$, $\Delta n = 151$, and $\phi = \pi$ (*blue*); and results from the peak amplitude model (*red*).

We have made use of the tools and analysis that we presented earlier in our discussions of the lossy spin–boson model to analyze the donor-receiver model in the local and periodic approximation, under conditions where the coupling between the receiver two-level systems and the oscillator is strong. We find that in this limit the dynamics of the donor system in our formalism appears to execute simple sinusoidal dynamics, including coherent energy exchange with the lattice where the large donor quantum is fractionated by the receiver system. We anticipate that in a more sophisticated version of the model, the addition of loss at ω_0 in the oscillator model with prevent reverse reactions (in which energy from the oscillator results in splitting of ^{4}He to D_2).

We note that the dynamics in this model are coherent, so that the rate at which D_2 make transitions to ^{4}He states is linear in the matrix element. The Gamow factor due to tunneling through the Coulomb barrier which hinders the matrix element then appears as e^{-G} in the rate, in contrast to the incoherent case which is typical in hot fusion where the reaction rate is proportional to e^{-2G}.

Because the donor dynamics are determined by the donor-side coupling matrix element in the limit that the receiver system is strongly coupled (and also resonant), this donor-receiver model seems already to have some applicability for comparing experimental results with candidate models for D_2 inventory, screening energy, and reaction rate.

There is more to be gleaned from this donor-receiver model from an examination of the overlap matrix element $\langle v_n(\phi_2)|v_{n+\Delta n_1}(\phi_2)\rangle$. For simplicity, we show expansion coefficients $v_n(\pi)$ for a model with $\Delta n_2 = 151$ and $g = 30$ in Fig. 1 along with the associated overlap matrix element (Fig. 2). In the event that the donor and receiver transitions are assumed resonant, then we would look at Fig. 2 to see how big the overlap is when $\Delta n_1 = 151$. In this case,

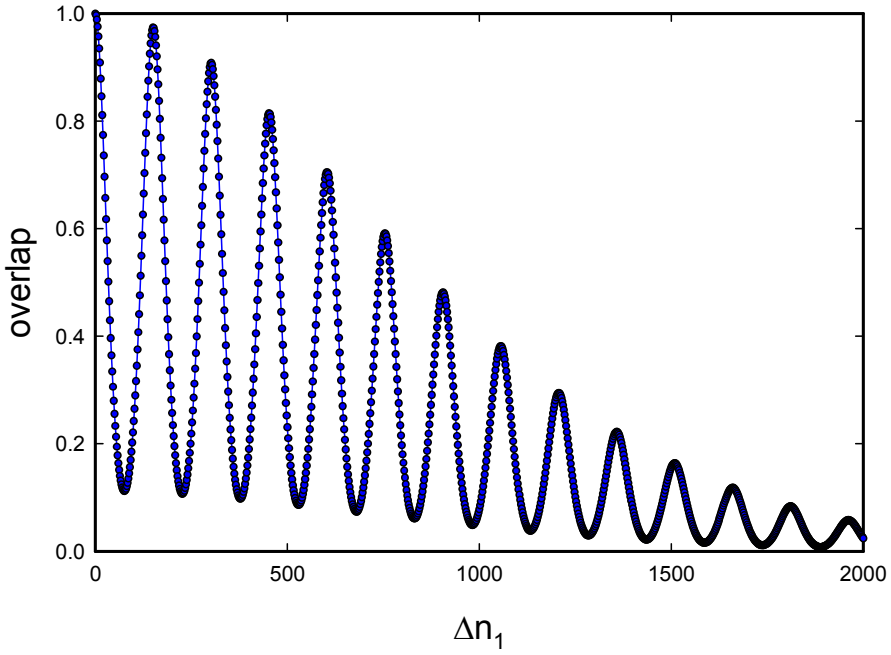

Figure 2. Overlap integral for $g_2 = 30$, $\Delta n_2 = 151$, and $\phi_{=}\pi$ as a function of Δn_1.

the overlap integral is close to unity, in which case the donor dynamics would be determined nearly completely by the strength of the donor coupling matrix element.

However, there are other peaks present in Fig. 2 which attract our attention. Suppose that the transition energy of the donor system were twice as large as the transition energy of the receiver system, then we would look to see how big the overlap matrix element is near $\Delta n_1 = 302$. We see that a peak occurs there, and that the overlap matrix element is near 0.9. In this case, the resonance appears because the donor energy is twice the receiver energy, and we can think of the system responding as if we first converted the donor excitation into the excitation of two receiver systems, and then subsequently fractionated.

This is interesting because we know from our earlier studies of the lossy spin–boson model that the larger the quantum is, the harder it is to fractionate. If we can break up the donor quantum into many smaller receiver quanta, then it is much easier to fractionate the smaller receiver quanta. The overlap integral in this example is showing us qualitatively how this subdivision works. We also see that the subdivision resonance need not be perfect, because the receiver system is able to make up a mismatch in the resonance.

So, even though the simple donor-receiver model is idealized in the sense that our two-level receiver does not correspond directly to a physical transition, we are able to get some guidance as to how to make a better model. To maintain coherence, we probably want to make use of long-lived metastable states which have a transition energy that is close to an integer subdivision of the donor transition energy. But such a long-lived metastable state will have essentially no coupling with the ground state (since it is metastable). This tells us that we need to include in a more

realistic receiver model the intermediate strong transitions that take us from the ground state to the metastable state. We are at present exploring such models as candidates to account for the excess heat effect in the Fleischmann–Pons experiment.

References

[1] P.L. Hagelstein and I.U. Chaudhary, Energy exchange in the lossy spin–boson model, *J. Cond. Mat. Nucl. Sci.* **5** (2011) 52.
[2] P.L. Hagelstein and I.U. Chaudhary, Dynamics in the case of coupled degenerate states, *J. Cond. Mat. Nucl. Sci.* **5** (2011) 92.
[3] P.L. Hagelstein and I.U. Chaudhary, Second-order formulation and scaling in the lossy spin–boson model, *J. Cond. Mat. Nucl. Sci.* **5** (2011) 87.
[4] P.L. Hagelstein and I.U. Chaudhary, Local approximation for the lossy spin–boson model, *J. Cond. Mat. Nucl. Sci.* **5** (2011) 102.
[5] P.L. Hagelstein and I.U. Chaudhary, Coherent energy exchange in the strong coupling limit of the lossy spin–boson model, *J. Cond. Mat. Nucl. Sci.* **5** (2011) 116.
[6] M. Fleischmann, S. Pons and M. Hawkins, *J. Electroanal. Chem.* **261** (1989) 301; errata **263** (1990) 187.
[7] M. Fleischmann, S. Pons, M.W. Anderson, L.J. Li and M. Hawkins, *J. Electroanal. Chem.* **287** (1990) 287.
[8] M.H. Miles, R.A. Hollins, B.F. Bush, J.J. Lagowski, R.E. Miles, *J. Electroanal. Chem.* **346** (1993) 99.
[9] M.H. Miles, Correlation of excess enthalpy and helium-4 production: A review, *Proc. ICCF10*, 2003, pp. 123.
[10] P.L. Hagelstein, *Naturwissenschaften* **97** (2010) 345.
[11] P.L. Hagelstein, M.C.H. McKubre, D.J. Nagel, T.A. Chubb, R.J. Hekman, New physical effects in metal deuterides, *Proc. ICCF11*, 2005, pp. 23–59.
[12] M. Appicella, E. Castanga, L. Capobianco, L. D'Aulerio, G. Mazzitelli, F. Sarto, A. Rosada, E. Santoro, V. Violante, M. McKubre, F. Tanzella and C. Sibilia, *Proc. ICCF12* 117 (2005). An effort was made to scrub out retained helium in the experiment denoted Laser-3 in this paper.
[13] T. Förster, *Naturwissenschaften* **33** (1946) 166–175.
[14] T. Förster, *Ann. Phys. (New York)* **2** (1948) 55–75.
[15] D. Letts, D. Cravens and P.L. Hagelstein, Dual laser stimulation of optical phonons in palladium deuteride, *Low-energy Nuclear Reactions Sourcebook, ACS Symposium Series* **998** (2008) 337.
[16] P.L. Hagelstein, D. Letts and D. Cravens, Terahertz difference frequency response of PdD in two-laser experiments, *J. Cond. Mat. Nucl. Sci.* **3** (2010) 59.